Advanced Diagnostics and Inspection of Common Foundation Elements in Hong Kong using Ultrasonic Non-Destructive Testing and Evaluation Techniques

Chan Wan Yin, Fiona

M.Phil.

The Hong Kong Polytechnic University

2004

Advanced Diagnostics and Inspection of Common Foundation Elements in Hong Kong using Ultrasonic Non-Destructive Testing and Evaluation Techniques

by

Chan Wan Yin, Fiona

A thesis submitted in partial fulfillment of the requirements
for the Degree of Master of Philosophy.

at the Department of Building and Real Estate
The Hong Kong Polytechnic University

March 2004

CERTIFICATE OF ORGINIALITY

I hereby declare that this thesis is my own work and that, to the best of my knowledge and belief, it reproduces no material previously published or written nor material which has been accepted for the award of any other degree or diploma, except where due acknowledgement has been made in the text.

Chan Wan Yin, Fiona

List of Publications

1. Chan, W. Y. & Tsang, W. F. "Earth echo sounding technique for quality control of drilled shaft foundations". *BINDT Insight*, Vol. 46, No.1, p.p.17-22 (2004).
2. Tsang, W. F., Chan, W. Y. & Scott, D. "Quality assurance of in-situ cast concrete foundation elements using an ultrasonic evaluation technique". *Journal of Construction and Building Materials* (manuscript).
3. Tsang, W. F., Chan, W. Y. & Scott, D. "Calibration Technique Applicable to Ultrasonic Earth Echo Bore-hole Sounding and Profiling of submerged drilled pile shafts". *ASTM Geotechnical Testing Journal* (manuscript).
4. Chan, W. Y. & Tsang, W. F. "A prototype of the multi-channel sonic logging for evaluation of deep foundation concrete elements". *ASCE Journal of Engineering Mechanics* (manuscript).
5. Chan, W. Y. & Tsang, W. F. "Application of Ultrasonic Wave Propagation for Identification of Soil Strata". *ASCE Journal of Materials in Civil Engineering* (manuscript).
6. Chan, W. Y. & Tsang, W. F. "Effects of different sonic access tube materials on the signal strength of ultrasonic waves in the Cross-hole Sonic Logging Technique". *Journal of Hong Kong Institution of Engineers* (manuscript).

List of Presentations

1. Chan, W. Y. (Feb 2001). "Pile Diagnostics & Inspection (PDI) Technical Forum 2001", the Hong Kong Polytechnic University & Earth Products China Limited, Hong Kong.
2. Chan, W. Y. (May 2002). "Seminar on Advanced Diagnostics of Inspection of concrete structures including both substructure and superstructure in Hong Kong using ultrasonic evaluation technique", Hong Kong Institute of Construction Managers (HKICE), Hong Kong.
3. Chan, W. Y. (Sep 2003). "The application of an in-house Multiple Referencing System (MRS) for evaluation of concrete foundation elements", British Institute of Non-Destructive Testing (BINDT), United Kingdom.

ABSTRACT

Non-Destructive Evaluation (NDE) is essential in modern foundation testing. The advantages of NDE are no need to destroy what has been constructed and change the integrity (i.e. material properties) of foundation elements. This study aims to evaluate and inspect common foundation elements in Hong Kong using the ultrasonic NDE techniques. This aim was achieved by the applications of two ultrasonic-based non-destructive testing techniques (i.e. the Ultrasonic Echo Sounding (UES) technique and the Cross-hole Sonic Logging (CSL) technique). The scopes of this study are shown as follows:

- Establishment of the in-house developed calibration and verification procedures to verify the real performance and behavior of UES equipment
- Investigation of the effects of different sonic access tube materials on the signal strength of ultrasonic wave transmission
- Demonstration of the applicability of the UES and CSL testing techniques by performing extensive field investigations
- Development of an in-house multi-channel ultrasonic data acquisition prototype to provide an efficient means of performing sonic tests
- Assessment of concrete specimens with sonic-tube-installation by the in-house developed prototype
- Identification of soil strata by the in-house developed prototype

An extensive literature review was performed at the beginning stage of the study to acquire background knowledge about the ultrasonic stress wave propagation principles and the basis (including the theoretical basis, testing procedures and methodologies, data interpretation techniques and limitations) of UES and CSL. Literature review was also performed in the area of ultrasonic wave propagation in soil related to this study.

Following the comprehensive review, the in-house calibration and verification procedures were established to ascertain the real performance and behavior of the UES equipment under different testing conditions, as no report regarding the determination of the working performance of UES equipment has yet been published.

The calibration work detailed an account of the efforts in the *range and depth* concerns that shed some lights on the performance of the UES equipment in different working situations. With the expression of calibration uncertainties, the reliability of different measurement techniques was assessed. By the experimental results in the *depth* calibration, the measuring tape approach was more accurate than the theodolites approach in terms of the value of the calibration uncertainty obtained. In the verification work, the effects of bentonite/slurry solutions, angles of reflection (i.e. simulation of 'bell-out' at a shaft toe) and roughness of reflecting surfaces on the measured ranges (obtained from UES profiles) of a shaft were quantified.

By carrying out the extensive tests within the HKSAR territories in this research, UES was proven as a reliable and useful technique to provide an early stage diagnosis and inspection of bentonite/slurry or water-filled shafts (including shaft verticality, shaft diameter, shaft depth, and geometry and dimension of 'bell-out' at a shaft toe) before the concreting stage. Examples of acceptable/slanted-drilled shafts were reported. The application of the UES technique identifies the suspected drilled shafts which can be taken into remediation works at an early stage of construction. The benefits and results are clear improvements in the costs incurred and time taken during the construction project.

The need to check deep foundations before and after the concreting stage is equally important. Another focus of this research was placed on the Cross-hole Sonic Logging (CSL) technique. It was developed in the late 1960's and has been used extensively to inspect the integrity of in-situ cast concrete foundation elements after the concreting stage. The applications of UES and CSL provide a better picture regarding to the quality assurance of deep foundation concrete elements since UES and CSL are conducted on foundation elements respectively before and after the concreting stage.

A series of tests were conducted to determine the effects of different sonic access tube materials (including polyvinyl chloride (PVC) and steel) on the signal strength of ultrasonic waves. With the development of the in-house developed prototype, the *apparent transmission velocity* and signal strength of the acquired waveforms were determined by the use of different sonic access tubes. A

set of experimental results showed that the signal strength when using PVC sonic access tubes are clearly larger than that when using steel tubes due to the smaller difference in the acoustic impedance value between PVC and water.

The success of the applicability of CSL was achieved by the results obtained from the extensive tests carried out (within the HKSAR territories) and examples also shown in this thesis. The results showed that CSL provides the precious information/feedback regarding the construction process of the final finished products (i.e. foundation elements). Questionable/suspected defects (like honeycombing, voids or foreign materials embedded in concrete elements) found were reported and discussed thoroughly and classified into several categories of defects.

An adaptive, versatile and relatively low cost prototype was developed and constructed especially for deep foundation concrete elements after installation. This prototype was labelled the 'Multiple Referencing System' (MRS) which was developed based on National Instruments hardware and a LabVIEW (Laboratory Virtual Instrument Engineering Workbench) environment. This prototype is capable of acquiring two or more channels of signals simultaneously in performing a sonic test in a bored pile with sonic-tube-arrangement to save time and cost.

A purpose-developed analysis graphical programming (based on the digital *virtual instrument*) of the in-house prototype MRS was constructed to

analyze the signals in different parameters (i.e. signal strength in a time domain and spectral energy content in a frequency domain) in addition to a traditional parameter of *first-arrival-time/apparent transmission velocity* in order to increase the reliability of the testing method in evaluating test materials.

The successful application of the in-house developed MRS in the concrete assessment was demonstrated by carrying out a sonic test in the testing concrete block with artificial defects. The signals acquired in two channels were displayed simultaneously during the measurement. The ultrasonic parameters (including *first-arrival-time*, transmission velocity, signal strength and spectral energy content of the signals) were investigated and found to be correlated to the properties of the materials.

In addition to the concrete assessment, the in-house developed prototype MRS was transferred as a geophysical technique to identify different soil strata. Variation of ultrasonic transmission velocity with degree of saturation and surcharge pressure were analyzed. A 'novel' method, the *'X-factor'* technique, was developed to classify soil strata. According to the experimental results, it was found that the *'X-factor'* technique has a potential of identifying soil strata and the value of *'X-factor'* is correlated to the attenuation of test materials.

Summary and conclusions of this research, fulfillment of the research objectives, contributions to the knowledge of NDE foundation testing, and recommendations for future research were presented.

ACKNOWLEDGEMENTS

The author wishes to thank Dr. Steven W.F. Tsang, Chief Supervisor, for his guidance, encourage and support throughout the project. Grateful thanks also go to Co-supervisor Prof. David Scott for giving his valuable time in providing his valuable comments and suggestions.

This research would not have been completed without ETS-Testconsult Limited as the Teaching Company, who provided the author with an excellent opportunity for conducting a research project in a real industrial environment. Gratitude is also extended to Mr. J.A. Fraser (Managing Director), Dr. Peter Lai (General Manager), Mr. Henry Yeung (Assistant Project Manager) for coordinating the works and resources that were crucial to this research. Thanks are extended to all members in ETS-Testconsult Limited, their help and suggestions are greatly acknowledged.

The author would like to thank the laboratory technicians of the Department of Building and Real Estate, Mr. I.K. Chan and Mr. Kenneth Lai, the staff of the Industrial Center for generously providing valuable assistance with the specimen preparation associated with this project.

Thanks to other research students (including Mr. Wallace Lai and Mr. Louis Chu) and all the fellow students in BTM-3 (2000), BTM-3 (2001), BEM-3 (2002) and BEM-3 (2003) especially Miss Mei Choi, Mr. Colin Tang and Miss

Janet Shum. They all helped construct the test specimens and share a lot of valuable experiences with the author.

Special gratitude are expressed to the Department of Building and Real Estate, Industrial Support Fund and ETS-Testconsult Limited for the assistantship and scholarship provided which made it possible for the author to continue the research work and to finish the dissertation.

Finally, the author would also like to thank her parents and Mr. Edward Ho for giving continuous support.

TABLE OF CONTENTS

APPENDICES

List of Abbreviations

CSL	Cross-hole Sonic Logging
CPRH	Concrete Piles Reinforced with a H-beam
CT	Crosshole Tomography
FAT	*First-arrival-time*
HOKLAS	Hong Kong Laboratory Accreditation Scheme
MRS	Multiple Referencing System
NDE	Non-Destructive Evaluation
NDT	Non-Destructive Testing
PIT	Pile Integrity Testing
PVC	Polyvinyl chloride
SSL	Single-hole Sonic Logging
UES	Ultrasonic Echo Sounding

List of Symbols

ν	Poisson's ratio
ρ	Density of the material
$\alpha_1, \alpha_2, \beta_1, \beta_2$	Theodolite readings in the *depth* calibration
θ	Incident angle of waves
β	Refraction angle of waves
C_p	Velocity of P-waves
C_r	Velocity of R-waves
C_s	Velocity of S-waves
d	Diameter of an old wheel of the UES equipment
D	Diameter of a brand new wheel of the UES equipment
E	Dynamic elastic modulus of the material
G	Shear modulus of elasticity
h_1, h_2	Height of the theodolites T1 & T2 from the ground level in the *depth* calibration
h	Height difference between two theodolites T1 & T2 in the *depth* calibration
H	Length of the cable in the *depth* calibration
ℓ	Length of the travel of the sensor head
L	Distance between two steel plates which is measured by a calibrated measuring tape
Ĺ	Converted range value (i.e. r*S) of the UES technique
r	Measured value on trace by a calibrated caliper
R	Reflection coefficient
s	Steel plate projection (i.e. Distance the edge of the steel plates and the surface of the steel block)
S	Scaling factor (to convert r into Ĺ) which is provided by the manufacturer
T	Transmission coefficient
V	Verticality of a drilled shaft
X	Horizontal difference between two theodolites in the *depth* calibration
Y	Horizontal difference between theodolite T2 and the cable in the *depth* calibration
Z	Acoustic impedance

List of Tables

List of Figures

1.1. Problem Statement

Quality assurance of foundations, particularly large bored piled foundations, plays an important role in their installation process to ensure that they are good and transfer the applied loads to the surrounding soil or/and rock. Traditionally, the only effective way to verify the loading capacity of a foundation element was by a static loading test in which a pile was required to withstand up to two times its designed loading capacity to meet the acceptance criterion. However, the time and expense involved in this procedure can only be justified for a small number of foundation elements that were not necessarily representative of all. Drilling or coring was sometimes applied to evaluate the integrity of deep foundation concrete elements. Again, tests of a small number of foundation elements were justified because of high costs and long operation time causing delays to subsequent work. Also, only limited fractions of foundation elements were covered in the coring process.

Technology has advanced recently so as to allow various kinds of Non-Destructive Evaluation (NDE) techniques to be carried on foundation elements. NDE of deep foundation elements (such as the Impact/Sonic Echo technique, the Impulse Response technique and the Cross-hole Sonic Logging (CSL) technique) are good quality control tools that help evaluate, inspect and survey the integrity of concrete in bored piled foundations. These techniques are designed to inspect finished foundation elements while ignoring a critical phase in the formation of drilled shafts. If drilled shafts are not in the first place

constructed properly (i.e. do not meet the design requirement) in terms of alignment, geometry and dimensions of 'bell-out' at the toe of shafts, subsequent finished piles may not be structurally adequate. So there is a pressing need to check foundation shafts before the concreting stage.

The 'Ultrasonic Echo Sounding' (UES) technique is designed to inspect the construction of bentonite/slurry- or water-filled shafts before concreting the shafts. This advanced technique is effective to provide an early stage diagnosis and inspection of shafts characteristics such as shaft verticality, shaft diameter, shaft depth, and geometry and dimension of 'bell-out' at a shaft toe. Early detection of deviations from design allows timely correction of problems, minimization of construction time and reduction of overall construction cost.

The need to check deep foundations before and after the concreting stage is equally important. The applications of two ultrasonic-based NDE techniques (i.e. UES and CSL) provide a better picture regarding the quality assurance of deep foundation concrete elements since UES and CSL are conducted respectively before and after the concreting stage.

CSL was developed in the late 1960's and has been used extensively to inspect the integrity of in-situ cast concrete foundation elements after the concreting stage. In the last forty years, many studies have been conducted to verify the capability of the CSL method. These studies were performed either on a small-scale with a large sample or on a large-scale with a small sample. Few

real-case field investigations have yet been done (i.e. large in both scale and sample).

The traditional instrumentation of the CSL technique involves a transmission probe and a reception probe used simultaneously to record the propagation time for ultrasonic signals traveling through concrete. However, for some cases of sonic-tube-arrangement (i.e. more sonic tubes), this traditional CSL system (i.e. a pair of probes) may be inadequate, and a more efficient instrumentation may be required to acquire several signals simultaneously in order to save time and cost. To provide a more efficient way to conduct a CSL test, an in-house developed multi-channel ultrasonic data acquisition prototype called the 'Multiple Referencing System' (MRS) is designed, constructed and developed by the researcher in this study. The MRS is capable of acquiring two or more channels of signals simultaneously by using one transmission probe and several receiving probes to save time and cost.

Analysis of ultrasonic signals is typically limited to measurement of the value of *first-arrival-time* (FAT)/*apparent transmission velocity*. However, ultrasonic waveforms contain considerably more information regarding the characteristics of test materials. A purpose-developed analysis graphical programming in a Laboratory Virtual Instrument Engineering Workbench (LabVIEW) environment is constructed to analyze the acquired waveforms in different parameters (i.e. signal strength in a time domain and spectral energy content in a frequency domain) in addition to the traditional parameter of

FAT/*apparent transmission velocity* in order to increase the reliability of the testing method in evaluating test materials.

Soils are common foundation materials in addition to foundation concrete elements. To obtain geological information of the site, drilling at a specific location is conducted, and laboratory tests using drilling cores are subsequently carried out. However, the information obtained at a particular drilling location is only the information at a specific point in the site. The NDE testing methods provides fast and useful approaches to characterize in-situ soils without changing the states of soils. The in-house prototype MRS developed in this research, as a geophysical technique, is applied to identify different soil strata.

1.2. Goals and Objectives

Specific objectives of this research are as follows:

- To advance the ultrasonic-based NDE techniques, particularly the Ultrasonic Echo Sounding (UES) and the Cross-hole Sonic Logging (CSL) testing techniques, on inspection of common foundation elements by performing field investigations. UES provides at an early stage (i.e. before the concreting stage) diagnosis and inspection of drilled shafts characteristics (including shaft verticality, shaft diameter, shaft depth, and geometry and dimensions of 'bell-out' at a shaft toe), whereas, CSL is used to assess the integrity of finished deep foundation concrete elements (i.e. after the concreting stage).

- To establish the in-house developed calibration and verification procedures to ascertain the real performance and behavior of UES equipment in different working conditions.
- To investigate the effects of different sonic access tube materials (i.e. polyvinyl chloride (PVC) and steel) on the signal strength of ultrasonic wave transmission.
- To provide a more efficient way to conduct CSL tests, an adaptive and versatile multi-channel ultrasonic data acquisition prototype is constructed and developed.
- To obtain more information of test materials, a purpose-developed analysis graphical programming based on digital *virtual instrument* platform is constructed to analyze the acquired ultrasonic waveforms in different approaches (i.e. signal strength in a domain and spectral energy content in a frequency domain) in addition to the traditional one (i.e. FAT/*apparent transmission velocity*).
- To demonstrate the successful applications of the in-house developed prototype in assessing concrete elements (with sonic-tube-installation) and identifying different soil strata.

1.3. Outline of the Thesis

This dissertation encompasses ten chapters. CHAPTER 2 reviews literature pertinent to the UES and the CSL testing techniques and presents the background information necessary to appreciate the application of these

techniques to foundation elements. For each method, the theoretical basis, testing procedures and methodologies, instrumentation, data interpretation techniques and limitations are presented.

In CHAPTER 3, the in-house calibration and verification procedures are described to determine the real performance and behavior of the UES equipment. The calibration work covers *range and depth* measured by the UES equipment. The uncertainties in the calibration work as required by the ISO 17025 Standard have also been determined together with a detailed uncertainty analysis as well. The verification work quantifies the effects of density of bentonite/slurry solutions, angles of reflection and roughness of reflecting surface on the measured ranges (obtained from UES profiles) of a shaft.

CHAPTER 4 describes the effects of different sonic access tube materials (i.e. PVC and steel) on the signal strength of ultrasonic wave transmission.

CHAPTERS 5 and 6 summarize the results of the extensive field investigations using the UES and the CSL testing techniques respectively. Over 200 foundation elements were tested from various Hong Kong construction sites under the author's leadership. Examples of typical results and the identified possible causes of the defects found by the corresponding testing techniques are also discussed.

CHAPTER 7 describes the construction and development of the software and hardware of an in-house developed multi-channel ultrasonic data acquisition prototype named the 'Multiple Referencing System' (MRS). This prototype is capable of acquiring two or more channels of ultrasonic signals from several receiving probes simultaneously. The performance of the MRS has also been verified (in terms of transmission velocity and possible transmission path of the pulses generated from the in-house developed ultrasound generator in the MRS).

The test results of the study of the application of the in-house developed prototype MRS for concrete assessment are presented in CHAPTER 8. A specimen concrete block with built-in defects (including voids and pieces of polystyrene) was constructed and tested by the MRS. The test results involving different parameters (including FAT, transmission velocity, temporal signal strength and spectral energy content) are presented and discussed.

The application of the in-house developed prototype MRS, as a geophysical technique, to identify different soil strata is studied in CHAPTER 9. The effects on ultrasonic velocity as due to different degree of saturation and surcharge pressure were analyzed, and the effects of soil types on temporal ultrasonic signal response were also investigated.

In the summary and conclusions, an overall evaluation of two ultrasonic-based testing techniques (i.e. UES and CSL) and the applicability of the in-house developed prototype MRS in concrete assessment and soil identification

are given and summarized, and the contributions of this research to the knowledge of NDE foundation testing are discussed and presented in CHAPTER 10. A number of valid conclusions are then drawn and recommendations for future work are also outlined.

2.1. Introduction to the Literature Review and Background

Non-Destructive Evaluation (NDE) techniques have been used for a number of years as quality control tools in the evaluation of foundation elements. The foundation elements are examined by measuring their response to indirect physical scanning techniques such as those using acoustic or mechanical vibration waves, electrical impulses, nuclear radiation etc. (Turner 1997).

The Non-Destructive Testing (NDT) techniques such as the Cross-Hole Sonic Logging (CSL) and the Pile Integrity Testing (PIT) are widely used to assess the integrity of the constructed deep foundation elements. However, these techniques are devoted to the finished foundation elements. If the construction of a drilled shaft does not meet the requirement (such as shaft verticality, shaft diameter, shaft depth, geometry and dimensions of the 'bell-out' at a shaft toe), subsequently a finished foundation element may not be structurally adequate. Checking the drilled shafts at an early stage (i.e. before the concreting stage) eliminates the need for correction of faulty piles and reduces overall construction cost.

The 'Ultrasonic Echo Sounding' (UES) testing technique is designed to perform an UES test to bentonite/slurry- or water-filled shafts before concreting the shafts. This advanced technique is effective in providing information at an early stage on drilled shafts characteristics. UES is based on measuring the

propagation time of an ultrasonic pulse taken for a reflection off the sidewalls (such as steel casing, bedrock, soil layer etc.) of shaft foundations to be detected.

The applications of two ultrasonic-based NDE testing techniques (including those applied before and after the concreting stage) offer a better picture regarding the quality control to ascertain the condition of foundation elements.

The Cross-hole Sonic Logging (CSL) technique was developed in the late 1960's and has been used extensively to inspect the integrity of deep foundation concrete elements. CSL is based on measuring the propagation time of a sonic/ultrasonic signal between two vertical sonic access tubes, usually steel tubes, cast into the foundation concrete elements during construction. Changes in propagation time are caused by irregularities/anomalies in concrete. Several other NDE testing methods exist in practice today, including sonic echo, impulse response, gamma-gamma logging, resistivity and ground radar, but they were not considered in this study.

This chapter reviews two ultrasonic-based NDE methods and provides the background information necessary to understand the application of these two methods to deep foundation concrete elements. The basic principles of stress wave propagation are first reviewed, including a presentation of the piezoelectric effect, a description of the various types of waves and a discussion of the characteristics of these waves in real materials. Finally, both the UES and the CSL testing

methods are described, focusing on the basis, testing procedures, interpretation of test results and limitations of each method.

2.2. Stress Wave Propagation Principles

2.2.1. Ultrasound

The term ultrasound means vibrations of a material medium which are similar to sound waves, but which have frequencies that are too high to be detected by an average human ear (Szilard 1982). Ultrasound is an acoustic wave in the range of 20kHz to 500MHz, which satisfies the wave equation as it is propagated. The acoustic frequency scale was well defined by Stephens (1975).

2.2.2. Ultrasonic transducers

Ultrasound is usually generated by piezoelectric transducers. Piezoelectricity, discovered by the Curie brothers in 1880, is such a phenomenon that some materials, when they are under some external mechanical stresses, develop an internal electric field with charges of opposite sign appearing on opposite surfaces as shown in Figure 2.2.1.

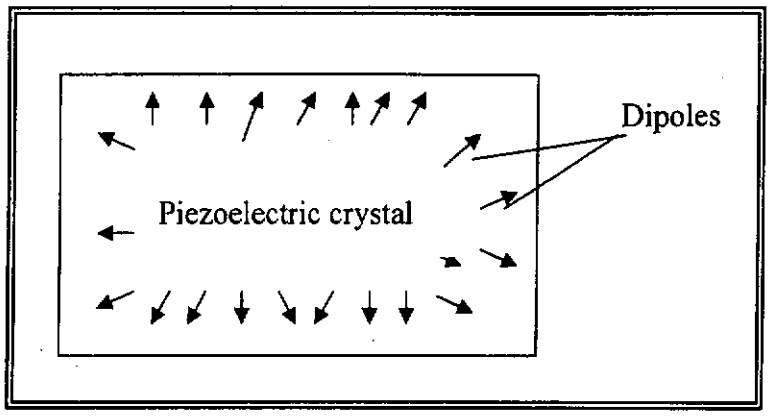

Figure 2.2.1. When a voltage is applied, piezoelectric materials change their shape.

In the following year Lippmann predicted the inverse effect namely the appearance of mechanical deformation of certain materials in external electric fields. This effect makes piezoelectric transducers act as either a generator and/or a detector of ultrasound (Wooh 1989). Of many piezoelectric materials, lead zirconate-titanate (PZT), barium titanate ($BaTiO_3$), lead metaniobate ($PbNb_2O_6$), lithium sulfate ($LiSo_4$), quartz (SiO_2), and lithium niobate ($LiNbO_3$) are the most widely used ones for NDE of materials. In concrete testing, ceramic transducers are normally chosen in this study because of their mechanical impedance close to that of concrete (Finno et al. 1997).

Ultrasound transducers use piezoelectric materials that produce a voltage when deformed by an applied pressure. A piezoelectric material subjected to an electric field will change dimension suddenly, and then gradually 'ring down' to its initial state. Figure 2.2.2 summarizes the ultrasound production by the piezoelectric effect.

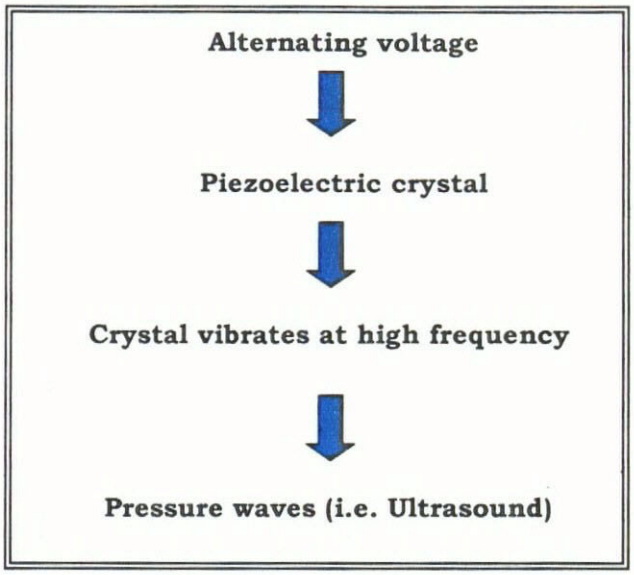

Figure 2.2.2. Summary of ultrasound production by the piezoelectric effect

Higher frequencies permit more accurate detection of a defect, but the signal absorption will be higher as well (Mor 1991). Relatively low frequencies are used to keep the wavelength greater than the aggregate size in case of testing concrete. Waves traveling at 4000m/s with a frequency of 50kHz produce a wavelength of 80mm. Wavelengths from 80 to 400mm are larger than typical aggregate sizes, and thus are used in the concrete testing in order to minimize the ultrasonic attenuation (Finno et al. 1997).

2.2.3. Wave propagation

When a stress is applied suddenly to a solid, the disturbance generated travels through the solid as stress waves. There are three primary modes of stress wave propagation through isotropic and elastic media: longitudinal, shear and Rayleigh waves (Sansalone et al. 1991). Longitudinal and shear waves are commonly referred to P-waves and S-waves. They are characterized by the

direction of particle motion respect to the direction of the wavefront. In a P-wave, the particles of the medium are displaced along the direction of propagation; while in a S-wave, the particles are displaced perpendicular to the direction of propagation.

P-waves can propagate in all types of media while S-waves can propagate only in media with shear stiffness, i.e. in solids. Rayleigh waves, or R-waves, propagate along the surface of a solid. The particular motión in an R-wave near the surface is retrograde elliptical (Sansalone 1991).

In most applications of stress wave propagation, the input is a pulse of finite duration and the resulting disturbance propagates through the solid as transient waves. The propagation of transient stress waves through a heterogeneous bounded solid, such as a structural concrete member, is a complex phenomenon. However, a basic understanding of the relationship between the physical properties of a material and the wave speed can be acquired from the theory of wave propagation in isotropic elastic media (Timoshenko 1970).

In finite elastic solids, the P-waves speed, C_P, is a function of Young's modulus of elasticity, E, the mass density, ρ, and Poisson's ratio, ν :

$$C_p = \sqrt{\frac{E(1-\nu)}{\rho(1+\nu)(1-2\nu)}} \qquad \text{(unit = km/s)} \qquad \text{---} \qquad \text{(Equation 2.2.1)}$$

In bounded solids, such as thin plates or long rods, the P-waves speed can vary depending on the dimensions of the solid relative to the component

wavelength(s) of the propagating waves. For rod-like structures, such as piles, the P-waves speed is independent of Poisson's ratio if the rod diameter is much less than the wavelength(s) of the propagating waves (Banks 1962). In this case, C_p is given by the following equation:

$$C_p = \sqrt{\frac{E}{\rho}} \qquad \text{(unit = km/s)} \qquad \text{---} \qquad \text{(Equation 2.2.2)}$$

The S-waves speed, C_s, in an infinite solid is given by the following equation:

$$C_s = \sqrt{\frac{G}{\rho}} \qquad \text{(unit = km/s)} \qquad \text{---} \qquad \text{(Equation 2.2.3)}$$

where G = shear modulus of elasticity = $\frac{E}{2(1-\nu)}$

The character of S-waves is further determined by the direction of the particle displacements. When particle displacements are horizontal, the waves are called SH-waves. SV-waves, on the other hand, are characterized by vertical motion. A general S-wave may be decomposed into its SV and SH components.

A useful parameter is the ratio, ϕ, of the S- to P-wave speeds:

$$\phi = \frac{C_s}{C_p} = \sqrt{\frac{(1-2\nu)}{2(1-\nu)}} \qquad \text{---} \qquad \text{(Equation 2.2.4)}$$

R-waves propagate at a speed, C_R, which can be determined from the following approximate formula (Banks 1962):

$$C_R = \frac{0.87+1.12\nu}{1+\nu} C_s \qquad (\text{unit} = \text{km/s}) \qquad \text{---} \qquad \text{(Equation 2.2.5)}$$

Waves radiate from the point of application of the load. As the distance from this point increases, the waves may be assumed to travel as a plane front. All material particles then move in this plane (S-waves) or perpendicular to it (P-waves). This assumption leads to substantial simplification in the mathematical treatment. If we denote the particle displacement by ψ, then the propagation of the plane waves is governed by the following differential equation:

$$\frac{\partial^2 \psi}{\partial t^2} = C^2 \frac{\partial^2 \psi}{\partial x^2} \qquad \text{---} \qquad \text{(Equation 2.2.6)}$$

in which $C_s^2 = \frac{E}{2\rho(1+\nu)}$ for S-waves and $C_p^2 = \frac{E}{\rho} x \frac{(1-\nu)}{(1+\nu)(1-2\nu)}$ for P-waves. C, as usual, is the wave propagation velocity. For Poisson's ratio ρ = 0.25, the velocity ratio $\frac{C_p}{C_s}$ is equal to $\sqrt{3}$, which means that P-waves propagate much faster than S-waves.

2.2.4. Attenuation and mode conversion

The equations presented above were derived on the assumption that the waves travel in a perfectly elastic medium. In real life, however, such solids are non-existent, and real materials also exhibit viscous and frictional behavior. As the ultrasound beam proceeds through the media, the amplitude of particle vibration is reduced, thus the intensity of the beam is decreased. This loss of the intensity termed as attenuation.

Attenuation is a factor that describes the decrease in ultrasound intensity with distance. Normally expressed in decibels per unit length (ASTM E664, 1993). The equation is shown as follows:

$$dB = 20\log\left(\frac{A}{A_0}\right) \qquad \text{--- (Equation 2.2.7)}$$

where A = amplitude of beam at any point;
A_0 = initial amplitude of beam.

A negative sign in Equation 2.2.7 indicates a loss of intensity as the beam passes through the media.

The six different interactions that are responsible for attenuation in the ultrasound beam are absorption, scattering, diffraction, interference, reflection and refraction. Absorption involves the conversion of ultrasound to other forms of energy, whereas in the case of scattering, diffraction, interference, reflection and refraction the ultrasound is simply redirected to some other directions. In other

words, the absorption depends only on the nature of the medium, while the other attenuations are caused by the geometry as well as the physical properties of the material (McDicken 1991).

❖ *Absorption*

Absorption of the ultrasound is a result of internal friction forces that oppose the vibration of molecules in the media. The friction caused by particle movement converts the ultrasound energy into heat. Absorption generally increases with the frequency of oscillation (Stephenson 1968). Absorption is the only process that directly removes energy from the ultrasound beam. The other interactions decrease the beam intensity by redirecting waveform.

❖ *Scattering*

Scattering is an attenuation process in which the ultrasound beam interacts with interfaces (i.e. smaller than the wavelength of the beam) causing the ultrasound energy to be dispersed in all directions (McDicken 1991). Figure 2.2.3 indicates the scattering of an ultrasound beam by small objects such as gas bubbles, matrix cracks and inclusions. Scattering can also be caused by rough or irregular surfaces.

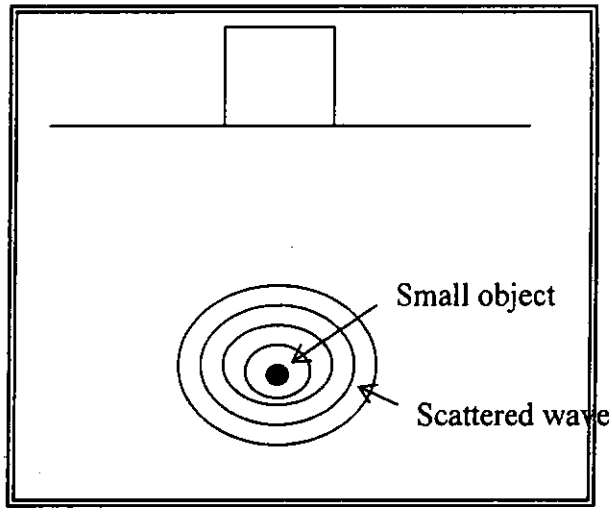

Figure 2.2.3. Scattering of ultrasound beam by a small object (from McDicken 1991)

❖ *Diffraction*

Diffraction is the spreading of the ultrasound beam as it moves further from the sound source as shown in Figure 2.2.4a. The degree of diffraction is related to the size of the source. A small sound source results in large diffraction. As shown in Figure 2.2.4b, diffraction also occurs after the beam passes through a small opening. The aperture acts as a small source of sound, and the beam diffracts rapidly. Increased diffraction results in increased attenuation (McDicken 1991).

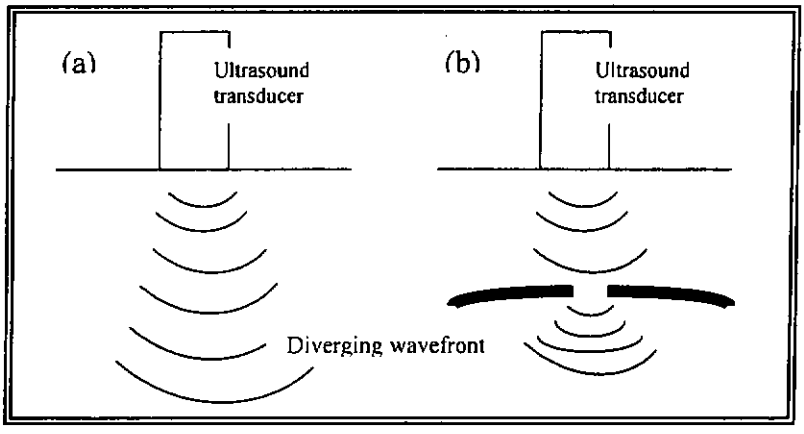

Figure 2.2.4. Diffraction of ultrasound beam (a) with distance and (b) by a small aperture (from McDicken 1991)

❖ *Interference*

Ultrasound waves undergo constructive interference if they are in phase. They will add together by algebraic summation to give increased amplitude. If the waves are out-of-phase, they undergo destructive interference. Every combination from complete constructive to complete destructive interference can occur in ultrasound. If the frequencies are similar, interference can produce the beat frequencies used in Doppler ultrasound. Wave interference is useful in transducer design since interference affects the uniformity of the beam intensity (McDicken 1991).

❖ *Reflection & Refraction*

In dealing with wave propagation, a medium is defined as non-homogeneous where the characteristic impedance is not the same throughout. In such media, whenever a wave enters a region with different acoustic properties, its propagation pattern will change at the interface. Here two cases are distinguished:

a. Normal incidence: If an ultrasonic beam is sent perpendicular to an interface, it will be partially transmitted across the interface and partially reflected back towards the source due to the difference in acoustic impedances (i.e. $Z_A \neq Z_B$) as illustrated in Figure 2.2.5.

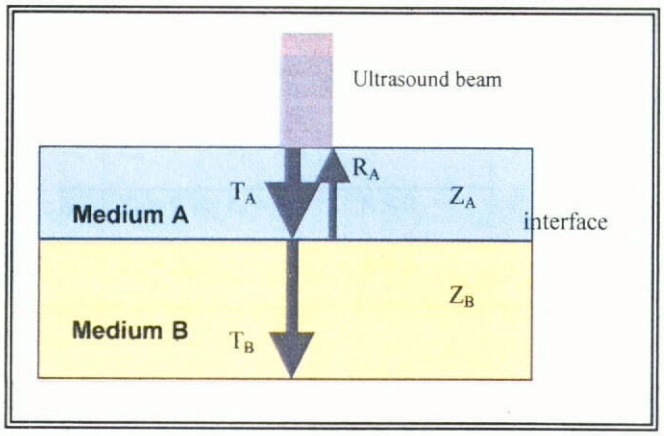

Figure 2.2.5. Plane wave traveling through medium A to the second medium B with the wave transmitted perpendicular to the interface.

The reflection and transmission coefficients (R, T) are governed by the respective acoustic impedance, Z, of each medium as shown in the following equations:

$$R = \frac{Z_B - Z_A}{Z_B + Z_A} \quad \text{--- (Equation 2.2.8)}$$

$$T = \frac{2Z_B}{Z_B + Z_A} \quad \text{--- (Equation 2.2.9)}$$

The amplitude of the reflected wave is large when the difference of acoustic impedances is large. The material, which has higher acoustic impedance, is called acoustically harder/stronger than the one with lower acoustic impedance. Five different scenarios warrant special considerations in Table 2.2.1:

Table 2.2.1. The variation of the reflection and transmission coefficients in relation to the acoustic impedances

Case i,	$Z_A > Z_B > 0$;	$R < 0$	$T > 1$
Case ii,	$Z_B > Z_A > 0$;	$R > 0$	$T > 1$
Case iii,	$Z_A = 0$ & $Z_B > 0$;	$R = 1$	$T = 2$
Case iv,	$Z_B = 0$ & $Z_A > 0$;	$R < 0$	$T = 0$
Case v,	$Z_A = Z_B$;	$R = 0$	$T = 1$

If Z_A is greater than Z_B, then R is negative, indicating that the reflected wave will have the opposite sign, i.e. a phase change occurs as in case i. For example, if the incident P-wave is a compressive stress-wave, then the stress-wave in the reflection is a tensile P-wave. If Z_B is greater than Z_A, no phase change occurs and the transmitted wave is amplified in amplitude as in case ii. When the second medium wave has a very low acoustic impedance (air for instance), then the reflected stress-wave is a total reflection of the interface as in case iv. Two media with equal impedance are said to be acoustically matched and no reflection occurs as in case v.

b. Oblique Incidence

When a wave strikes the interface at an angle θ to the normal, it will create four new waves: two of them reflections and two refractions, as shown in Figure 2.2.6.

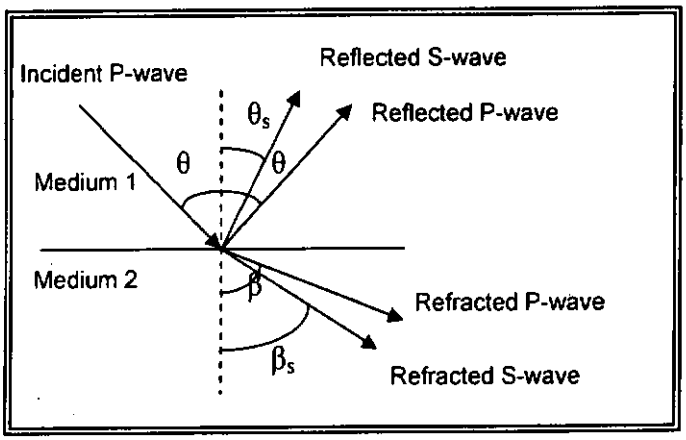

Figure 2.2.6. The behavior of a P-wave incident upon an interface between two dissimilar media results in mode conversion

The Snell's law as depicted in Equation 2.2.10 shows the relationship amongst the reflections and refractions near the interface:

$$\frac{\sin\theta}{C_{P1}} = \frac{\sin\beta}{C_{P2}} = \frac{\sin\theta_S}{C_{S1}} = \frac{\sin\beta_S}{C_{S2}} \qquad \text{---} \qquad \text{(Equation 2.2.10)}$$

where θ = incident angle/reflection angle of P-waves
θ_S = reflection angle of S-waves
ß = refraction angle of P-waves
$ß_S$ = refraction angle of S-waves
C_{P1} = velocity of P-waves in medium 1
C_{P2} = velocity of P-waves in medium 2
C_{S1} = velocity of S-waves in medium 1
C_{S2} = velocity of S-waves in medium 2

2.3. The Ultrasonic Echo Sounding Technique

2.3.1. Past research works on the Ultrasonic Echo Sounding technique

Before the transfer of Ultrasonic Technology into the civil engineering field, the conditions of boreholes including a hole diameter, depth, verticality, thickness of the settlement and the location of reinforcement cage were usually checked by divers prior to the concreting stage. But more people became increasingly concerned with the safety of this method. A major concern was for the safety of divers who could be fatally trapped in boreholes during the checking process.

Ultrasonic Technology was used in locating target objects situated on the sea, under the sea or under the ground. In the 60's, this technique was applied to produce the profiles of a seabed. Koden then transferred this technique from marine to foundation work. Two companies called 'Koden Techno-Info-Co. Ltd.' and 'Kaijo Corporation' in Japan developed advanced Ultrasonic equipment for checking the construction of shaft foundations in the 70's. The equipment measures the time taken for a reflection off the sidewalls of a shaft foundation to be detected using ultrasonic wave propagation. This testing technique has commonly been known as the 'Koden' test/ 'Ultrasonic Echo Sounding' (UES) test.

The UES testing technique was described fully by Lau (1995), who

reported that when ultrasonic pulses pass through a longer path and high-density muddy water, transmission time is longer and attenuation is respectively larger. The results depended on the transmission path and density of the muddy water. In high-density muddy water, UES equipment should be set in a higher sensitive setting (i.e. a larger signal-to-noise ratio) in order to receive the clear reflected signals from the back wall surfaces. Transmission time, transmission speed, attenuation amplitude and waveform change are all parameters used to evaluate the construction of shaft foundations. The study also introduced the UES equipment 'Koden DM-686 II' (see Figure 2.3.1) which measures the verticality and profiles of the boreholes. Figure 2.3.2 shows the operation of the equipment 'Koden DM-686 II'.

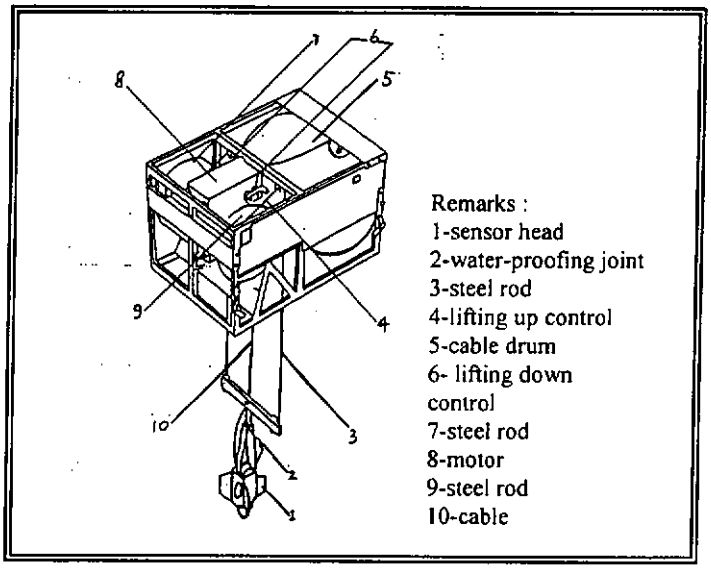

Figure 2.3.1. Schematic drawing of the UES equipment 'Koden DM-686 II'

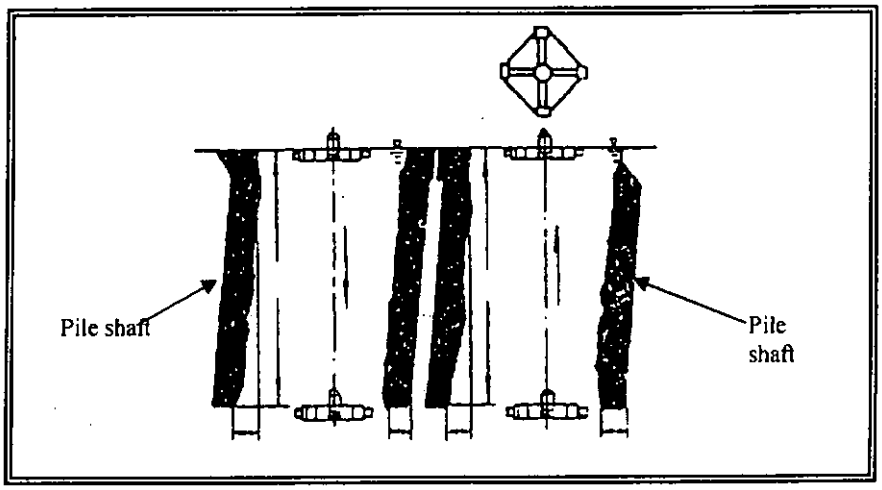

Figure 2.3.2. Operation of the UES equipment 'Koden DM-686 II'

Figure 2.3.3 shows another equipment for the borehole size measurement. Four testing legs were installed into the equipment. The legs can be contracted and lengthened that depend on the diameter of boreholes. The signals were recorded and the diameter reading of a drilling shaft was electronically calculated.

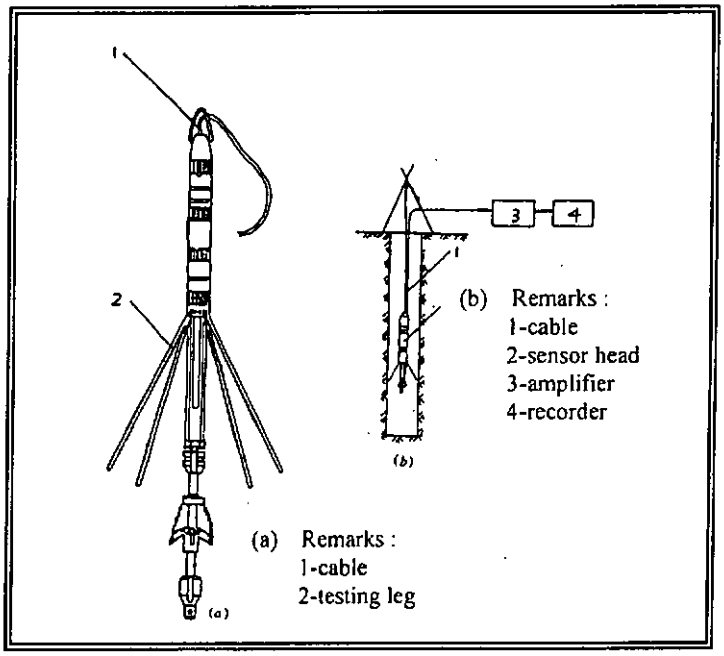

Figure 2.3.3. Diameter measurement equipment (b) with enlargement of diameter measurement sensor in (a).

The UES equipment applied in this research work is similar to the 'Koden DM686 II'. In performing an UES test, a sensor head is lowered from the top of a drilled shaft to the toe and simultaneously measures the time taken for a reflection off the sidewalls of a drilled shaft to be detected using ultrasonic wave propagation (Section 2.3.3).

The quality control of drilled shafts using UES was studied in Taiwan (Lin and Hoe 1998). Their report briefly described the basic theoretical background of UES and indicated that UES is an effective quality control tool of drilled shafts before the concreting stage. The construction of shaft foundations (including shaft verticality, shaft diameter, shaft depth, geometry and dimensions of the 'bell-out' at a shaft toe) is measured prior to the concreting stage. So that the failure of drilled shafts initially in alignment, geometry and 'bell-out' dimensions is detected at an early stage, and immediate remedies should be undertaken. Otherwise the consequences are extremely expensive to handle the failure-finished foundation elements. UES is undoubtedly an efficient technique for shaft foundations testing rather than using a method where human divers are involved in carrying out the assessment of shaft foundations. This method was frequently used in the past but now it is superseded by the UES testing technique.

Early detection of deviation from design allows timely correction of problems, elimination of construction time and reduction of overall construction cost. However, no document regarding to the determination of the real performance and behavior of UES testing equipment has yet been published.

In this research, the in-house calibration and verification procedures were developed to ascertain the real performance and behavior of UES equipment in different testing situations (Sections 3.2 and 3.3). The calibration work covers the *range and depth* parameters, while the verification work quantifies the effects of different densities of bentonite/slurry solutions, different angles of reflections (i.e. simulation of 'bell-out' at a shaft toe) and different roughness of reflecting surfaces on the measured ranges (obtained from UES profiles) of a shaft.

These calibration and verification procedures are a pioneering task in investigating the real performance of UES equipment, and have been adopted to the Hong Kong Laboratory Accreditation Scheme (HOKLAS) as a basis for accreditation of commercial laboratories specializing UES tests.

The study of the field investigation using UES is inadequate in the past work. In this research, an extensive field investigation using UES testing technique were carried out in various Hong Kong construction sites under the author's leadership. Examples of the acceptable and slanted-drilled shafts, and the remedial works for the unacceptable drilled shafts are discussed in Section 5.3.

2.3.2. Principles of the Ultrasonic Echo Sounding technique

UES is based on measuring the propagation time of an ultrasonic pulse for a reflection off the sidewalls (such as steel casing, bedrock and soil layer) of a drilled shaft. It is important to fill the drilled shafts with water (to obtain a good

coupling effect) for ultrasonic wave propagation. In the case of diaphragm walls, steel casings do not reach the bedrock as shown in Figure 2.3.4. For the prevention of soil collapse from an uncased excavation, a drilled shaft is very often filled with bentonite/slurry solution rather than only water. Bentonite/slurry solutions can provide a supportive pressure to the surrounding soil within an uncased region and also act as a medium for ultrasonic wave propagation.

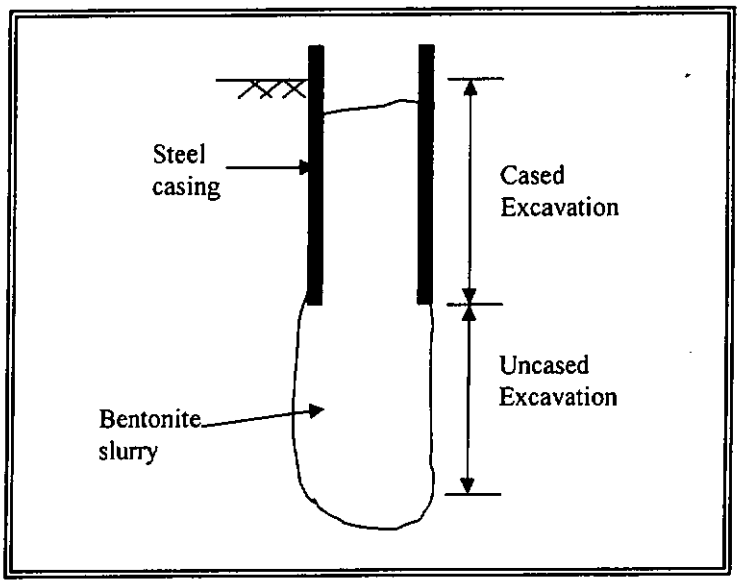

Figure 2.3.4. Schematic diagram showing a partly cased excavation filling with bentonite/slurry solution in a diaphragm wall.

The UES equipment applied in this research (i.e. Kaijo KE-200 model) consists of a sensor head with four transmitters and four receivers in two directions (i.e. *X-X' direction & Y-Y' direction*). For example in *X-X' direction*, the ultrasonic waves are transmitted from the transmitters (i.e. T1 & T2) as shown in Figure 2.3.5 and reflected off the sidewalls of an excavated shaft and then received by the receivers (i.e. R1 & R2 in Figure 2.3.5).

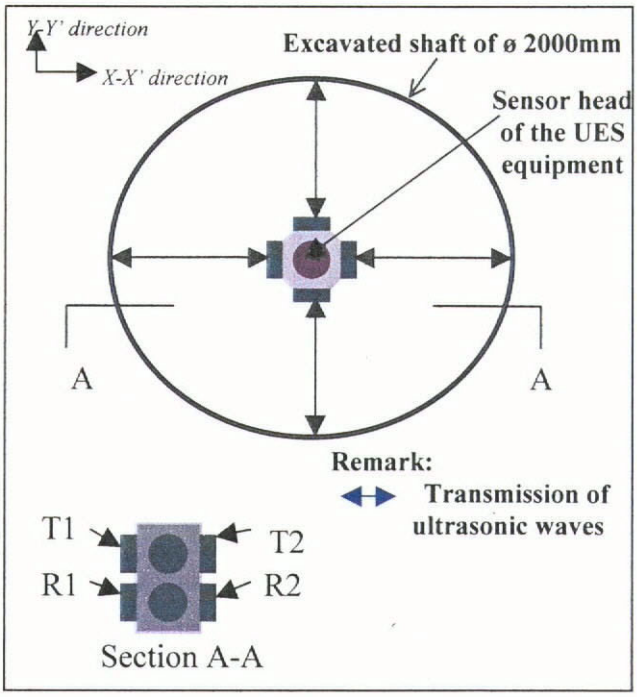

Figure 2.3.5. Schematic drawing showing the sensor head of the UES equipment

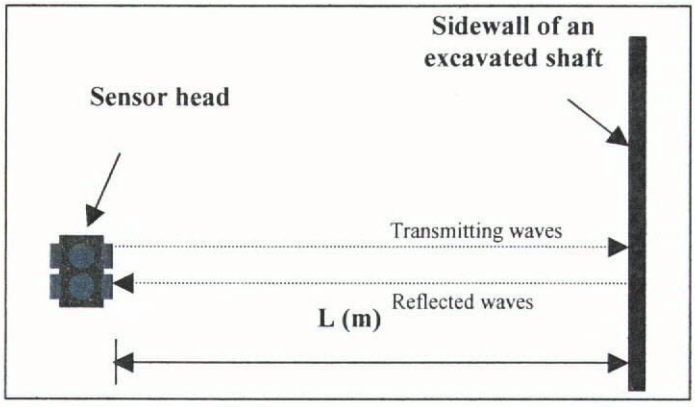

Figure 2.3.6. Schematic drawing showing the propagation path measurement reflected from the sidewall of an excavated shaft

As shown in Figure 2.3.6, the value of the propagation path is simply calculated by the following equation:

$$L = \frac{1}{2}ST \qquad \text{(unit: m)} \qquad \text{---} \qquad \text{Equation (2.3.1)}$$

where L is the distance between the sensor head of the UES equipment and the surface wall of an excavated shaft (unit: m);
S is the propagation speed of ultrasonic waves in clear water or bentonite/slurry solution (unit: m/s);
T is the time for the ultrasonic waves reflected from the surface wall of an excavated shaft and then received by the receiver (unit: s).

Equation 2.3.1 shows the propagation path calculation in relation to the propagation speed of ultrasonic pulses in a traveling medium and the required time for the ultrasonic pulses reflected off the sidewalls of an excavated shaft. In fact, the transmitted ultrasonic pulses are reflected as a result of changes of the acoustic impedance at different material boundaries. The flow paths of such transmission are as follows:

A transmitter ⇨ Water/ Bentonite/slurry solution ⇨ Reflected off steel casing/ bedrock/ soil layer/ other obstacles ⇨ Water/ Bentonite/slurry solution ⇨ A receiver

Each interface of two different materials (i.e. difference in acoustic impedance, Z) will produce partial reflection (i.e. receiving signals) and transmission to occur at a normal incidence, and even make the receiving signals variable (Sections 5.3.1 and 5.3.2).

If the excavation shafts do not meet the design requirement (i.e. in vertical alignment), then a steel reinforcement cage may not be fitted properly into a drilling hole as shown in Figure 2.3.7, and the structural adequacy of the completed foundations may also be in question.

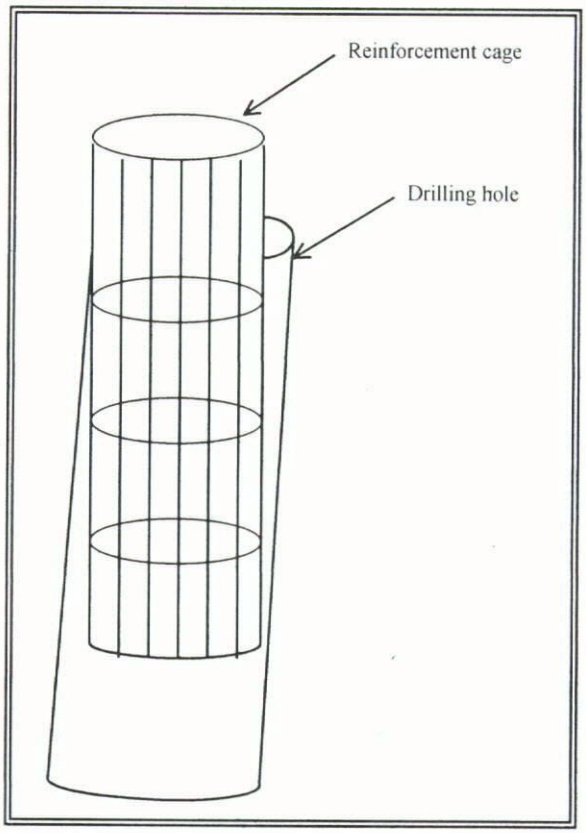

Figure 2.3.7. Problem of inserting a steel reinforcement cage into a slanted drilling hole

2.3.3. Implementation of the Ultrasonic Echo Sounding technique

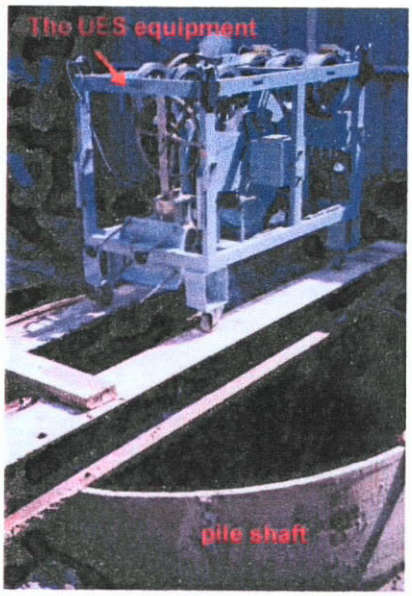

Figure 2.3.8. Experimental set-up in which the UES equipment, being supported by two H-steel beams, was put on a test drilled shaft.

Figure 2.3.8 shows the experimental set up of performing an UES test, in which two H-steel beams were put on a drilled shaft and act as supporters for the UES equipment to carry out an UES test.

In performing a typical UES test, a sensor head of the UES equipment is lowered to a bentonite/slurry- or water-filled excavation hole/shaft (as shown in Figures 2.3.9 and 2.3.10) to produce a 'so-called' UES profile (see Figure 2.3.11).

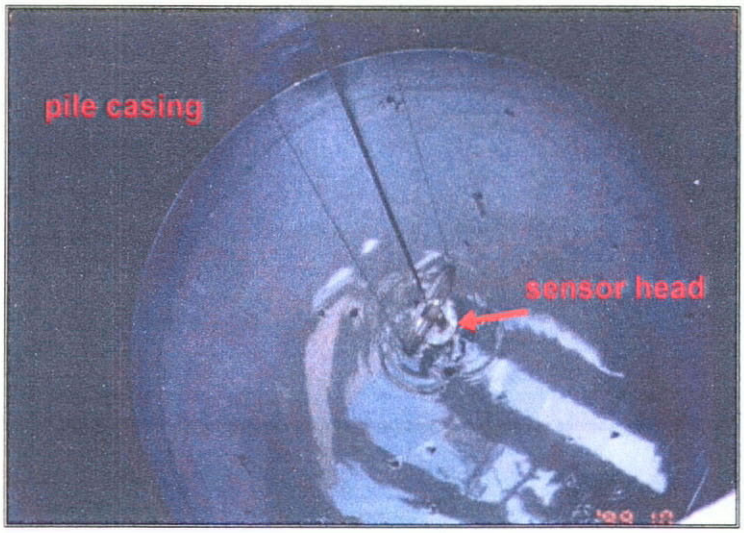

Figure 2.3.9. Lowering the sensor head of the UES equipment into a water-filled shaft

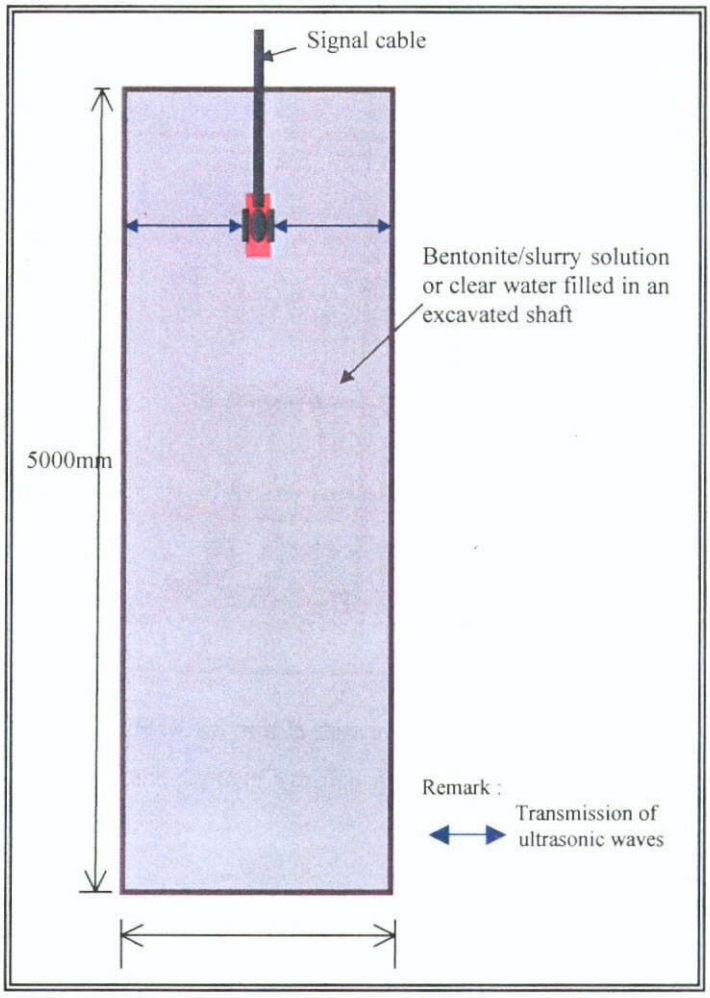

Figure 2.3.10. Schematic drawing showing an UES test in an excavated shaft

2.3.4. Interpretation of the Ultrasonic Echo Sounding test results

Figure 2.3.11 shows a typical UES test result of a drilled shaft, in which the ranges (i.e. shaft diameter and 'bell-out' at a shaft toe) of a drilled shaft are obtained. The corresponding depths of the drilled shaft are shown in the center of the UES profile, which can be an alternative method of checking the depth of a drilled shaft instead of using a measuring tape.

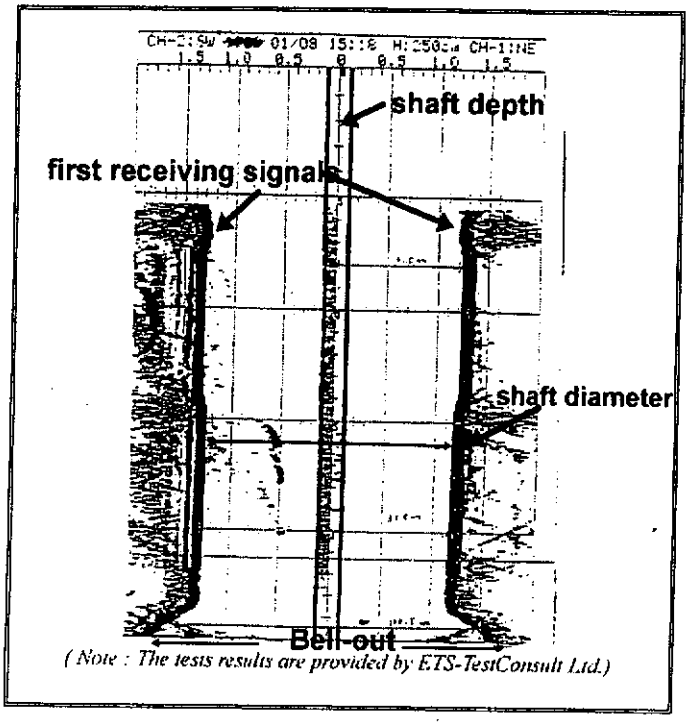

Figure 2.3.11. Example of the UES profile showing the ranges (i.e. shaft diameter and 'bell-out' at a shaft toe) and depth of a drilled shaft

UES simultaneously measures, displays and records the ranges of the sidewalls of an excavated shaft in either one or both of the two orthogonal directions (depends on the design of the instrumentation of UES equipment) at any one time. It also records test information such as date and time of the test carried out, and depth of a drilled shaft. This test information is particularly useful from a regulatory control perspective, as it is the only available instantaneous records/evidence. The incomplete or falsified records are sometimes found in the reported 'short piling' scandals. From the technical perspective, this test information can uncover potential problems such as defective works and procedures during and after drilling, and forming of the 'bell-out' at a shaft toe.

2.3.5. Limitations of the Ultrasonic Echo Sounding technique

Due to the design of the instrumentation of the UES equipment, only two directions (i.e. *X-X' direction* and *Y-Y' direction*) can be measured at any one time. The testing area is limited to two directions and the conditions of drilled shafts in other elevations are not covered.

In performing an UES test, the sensor head of the UES equipment is found to be required in the center of a drilled shaft to produce reliable UES profiles at an optimal position. However, for slanted shafts, a number of measurements should be carried out to obtain an actual picture of the construction of these slanted shafts (see Section 5.3.3).

The travel medium is sometimes bentonite/slurry solutions in a diaphragm wall. However, the UES equipment cannot measure the sidewalls in muddy water (Lau 1995). For the UES equipment applied in this study, it is found to be operated properly in bentonite/slurry solutions with density not higher than 1026kg/m^3 (Section 3.3.1). This is due to the high attenuation (including scattering, absorption and reflection) of ultrasonic waves in a muddy solution. As a result, clear reflecting signals cannot be obtained on UES profiles even though the UES equipment is in a high signal-to-noise ratio (SNR) setting.

2.4. The Cross-hole Sonic Logging Technique

2.4.1. Past research works on the Cross-hole Sonic Logging technique

The Cross-hole Sonic Logging (CSL) technique is one of the common NDT methods to determine the integrity of deep foundation concrete elements. CSL was first developed in France by the Experimental Center for Research and Studies in Building and Public Works (CEBTP) in the late 1960's (Finno et al. 1997). This method was first introduced into the United Kingdom in 1969, when the Greater London Council (GLC) arranged for a series of tests to be carried out on specially constructed piles to examine the possibilities of the method. This work was reported on by Levy (1970) and Bobrowski et al. (1970). The trials were undertaken because of the concern within the GLC's statutory building control departments regarding the quality of construction of large-diameter bored piles. Single piles, capable of carrying loads in the region of 1000 tones, were becoming more common at that time, but there was no accepted method of investigating their integrity (Turner 1997).

Later, the CEBTP compared the polyvinyl chloride (PVC) and metallic tubes applied in CSL (CEBTP 1969). The results showed very little signal deviation by obstructions, the signals were fairly well damped and no resonant interference appeared when using PVC tubes. However, the external surface of these tubes is often very difficult to wet, carrying the risk of poor bonding with the concrete, while good bonding of the concrete to the metallic tubes can

strengthen the reinforcement. However few studies have been conducted to investigate in detail the effects of different sonic access tube materials on signal strength of ultrasonic wave transmission. In this research a series of experimental tests were carried out to study this issue.

The interpretation of CSL results is based on the comparison of known irregularities with those registered on a series of piles with known typical defects. In these conditions, it was necessary to test piles with classical defects in order to judge whether CSL was able to detect them and, by comparison, to allow a better interpretation of the results obtained. A number of studies in the past have been conducted to interpret CSL profiles by constructing piles with built-in defects.

A series of ten test piles prepared by Hertlein in 1965 was constructed at Saint-Rémy-les-Chevreuse in France. The irregularities in these piles were representative of the defects normally encountered in certain in-situ piles. Figure 2.4.1 shows the details of the built-in defects inside the ten test piles at Saint-Rémy-les-Chevreuse, where four tubes were used and arranged with two tubes diagonally opposed. With the tubes arranged in this way, six profiles were obtained for each pile. The irregularities in these piles varied in their nature and in their importance. They varied in nature because of inclusions consisting of gravel, topsoil, and marl. The inclusion of gravel also simulated the case of concrete washed out by circulating water. They varied in their importance because of defects covering a small area or whole section. A pile was also included with silting at the bottom, which was a typical defect of concreting under bentonite.

Analysis of the different profiles led to the conclusions that, (1) important defects occupying more than a quarter of the cross-section were all detected, (2) the detection was clearer when the defect surrounded one of the tubes, (3) the defects located off the profiles between tubes were not always located.

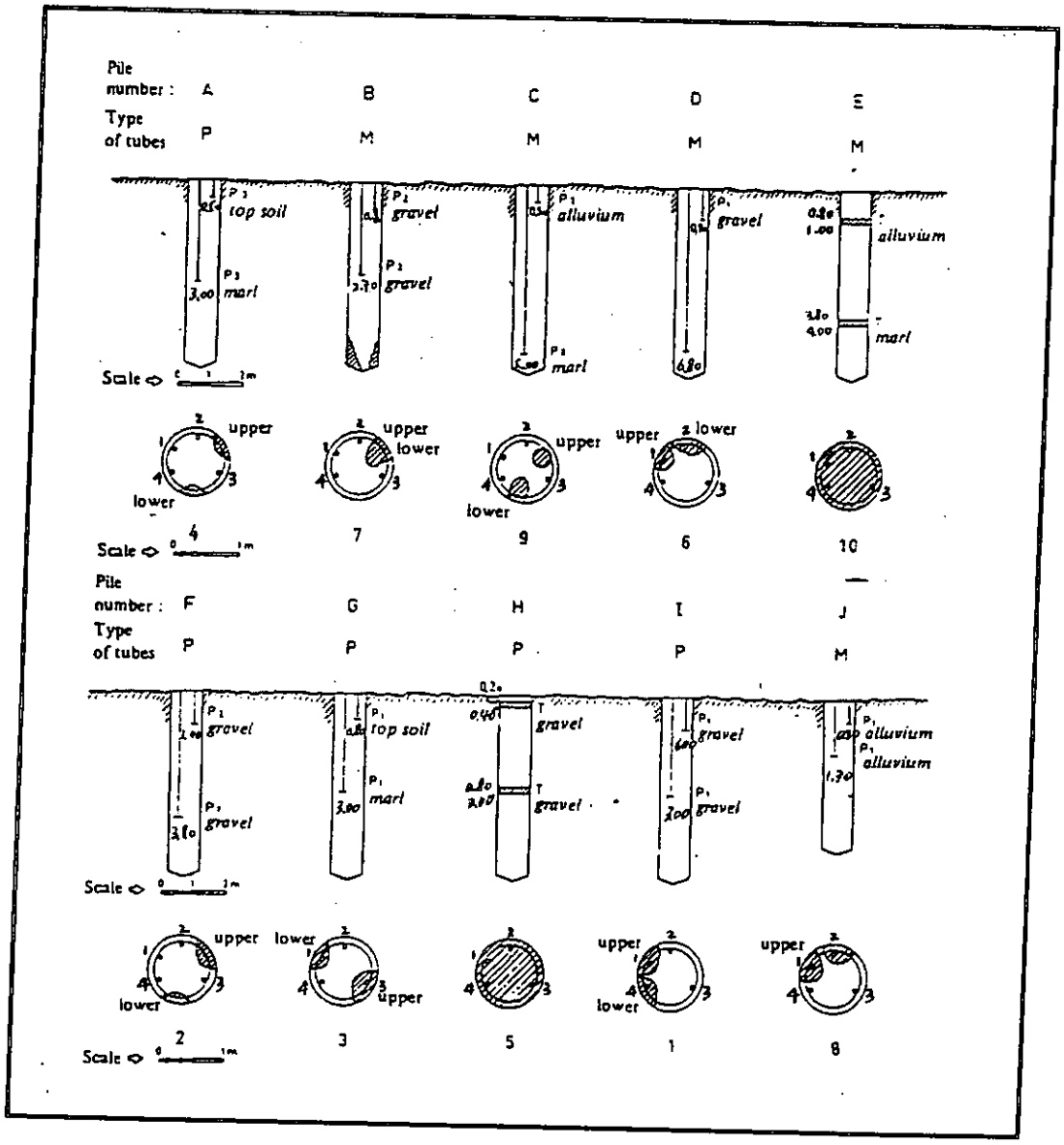

Figure 2.4.1. The built-in defects at Saint-Rémy-les-Chevreuses (from Hertlein 1965)

Paquet and Briard (1975) did similar work. A number of trial shafts with known included anomalies was reported. Four cases were followed, one from a

S.E.R.C. research project and three from UK Construction sites. A diaphragm wall panel was constructed in Kent where the sonic profile between the front face of the panel and the back of the fin showed increases in transmission time (see Figure 2.4.2).

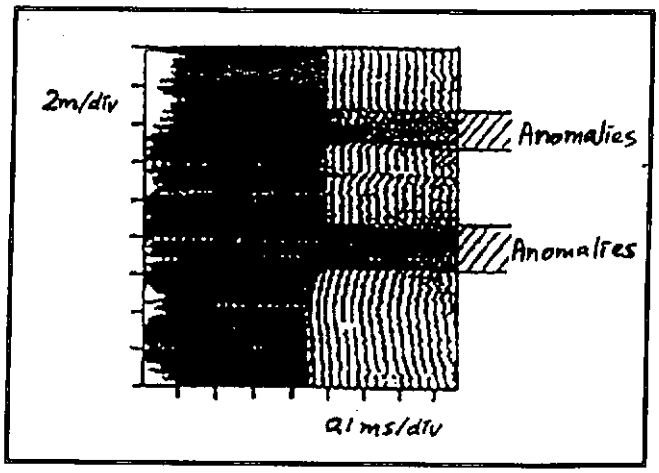

Figure 2.4.2. The sonic profile in Kent (from Paquet and Briard 1975)

In another test, a large number of shafts were constructed in a water-filled dock in Hull, the upper portion of shaft being permanently cased to 1m above the water level. Concrete was placed by tremie pumping under water. Figure 2.4.3 shows the upper section of a sonic profile of one shaft. The signal anomaly, 1.0m from the shaft top, was investigated by cutting two inspection holes in the casing. The material at this level was found to be very weak cement grout. The increase in transit time was similar to that in the laboratory test in weak grout.

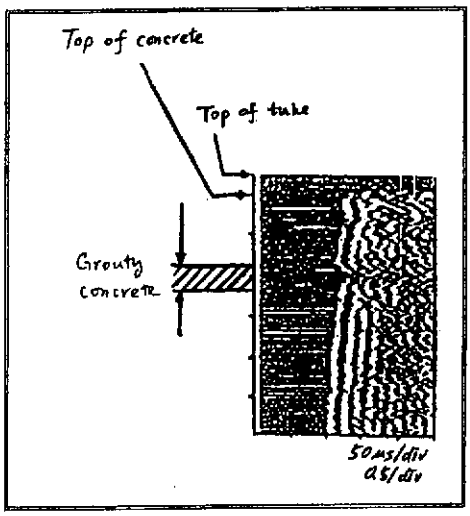

Figure 2.4.3. The sonic profile in Hull (from Paquet and Briard 1975)

On the same site in Hull, tests were carried out on a bored pile prior to the concreting stage. With the reinforcing cage in piece and the bore full of water, gravel was tipped down the shaft to cover the lower 2m. CSL tests were carried out and the results are shown in Figure 2.4.4. Three separate signal types are visible (1) signals traveling through water, (2) signals traveling from tube to tube around the reinforcing cage hoops, (3) signals traveling through waterlogged gravel. For gravel and water, the apparent transmission velocities were consistent with those found in the laboratory trial panels.

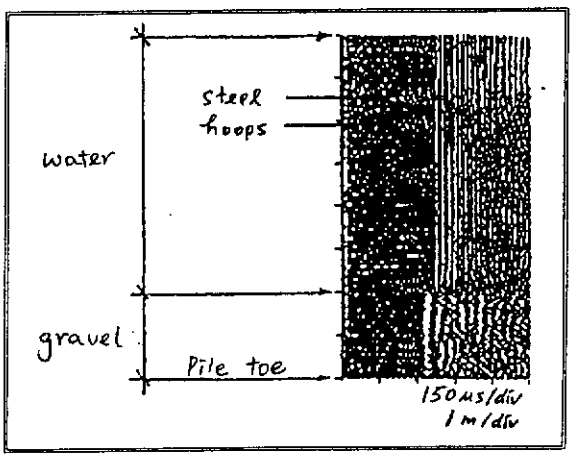

Figure 2.4.4. The sonic profile in the gravel-filled sore (from Paquet and Briard 1975)

Newcastle University, as part of an S.E.R.C. research project, installed a number of bored shafts at Blyth in Northumberland. Many of these had carefully included anomalies, one of which is shown in Figure 2.4.5. The results of the CSL test are shown alongside. The polystyrene annuli through which the access tubes passed were clearly visible, as was the signal 'skipping' effect.

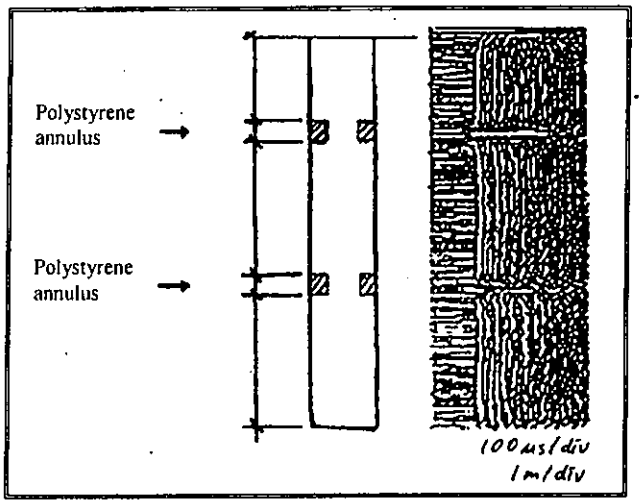

Figure 2.4.5. The pile in Blyth S.E.R.C. Project (from Paquet and Briard 1975)

The profiles in Figures 2.4.3 and 2.4.5 clearly showed ultrasonic pulses passing through different materials leading to different transmission times. A longer pulse transmission time was necessary in passing through weak grouty concrete and polystyrene annulus. These four cases, and the ten test piles at Saint-Rémy-les-Chevreuse, highlight the successful application of the CSL testing technique and form a good foundation for other researchers to carry out further relevant studies.

A more detailed experiment was done, by the CEBTP, again where a special pile was constructed at a construction site in Westminster, London (CEBTP 1982). The special pile with built-in discontinuities at different levels is shown in Figure 2.4.6.

The pile size was 30 inches and the length was 30 feet. Three metal tubes were installed with the reinforcement cage prior to the concreting stage. Three sonic profiles were measured in a three-tube arrangement. The materials were varied at different depths of the pile, for example polythene sheeting was put on the top of the pile, and additional lightweight concrete, low slump concrete, brown sand and gravel were put within the body of the pile. A void made by a 5-gallon sealed empty drum was placed inside the pile at a depth of 25 ft. The profiles clearly showed the zone of built-in anomalies.

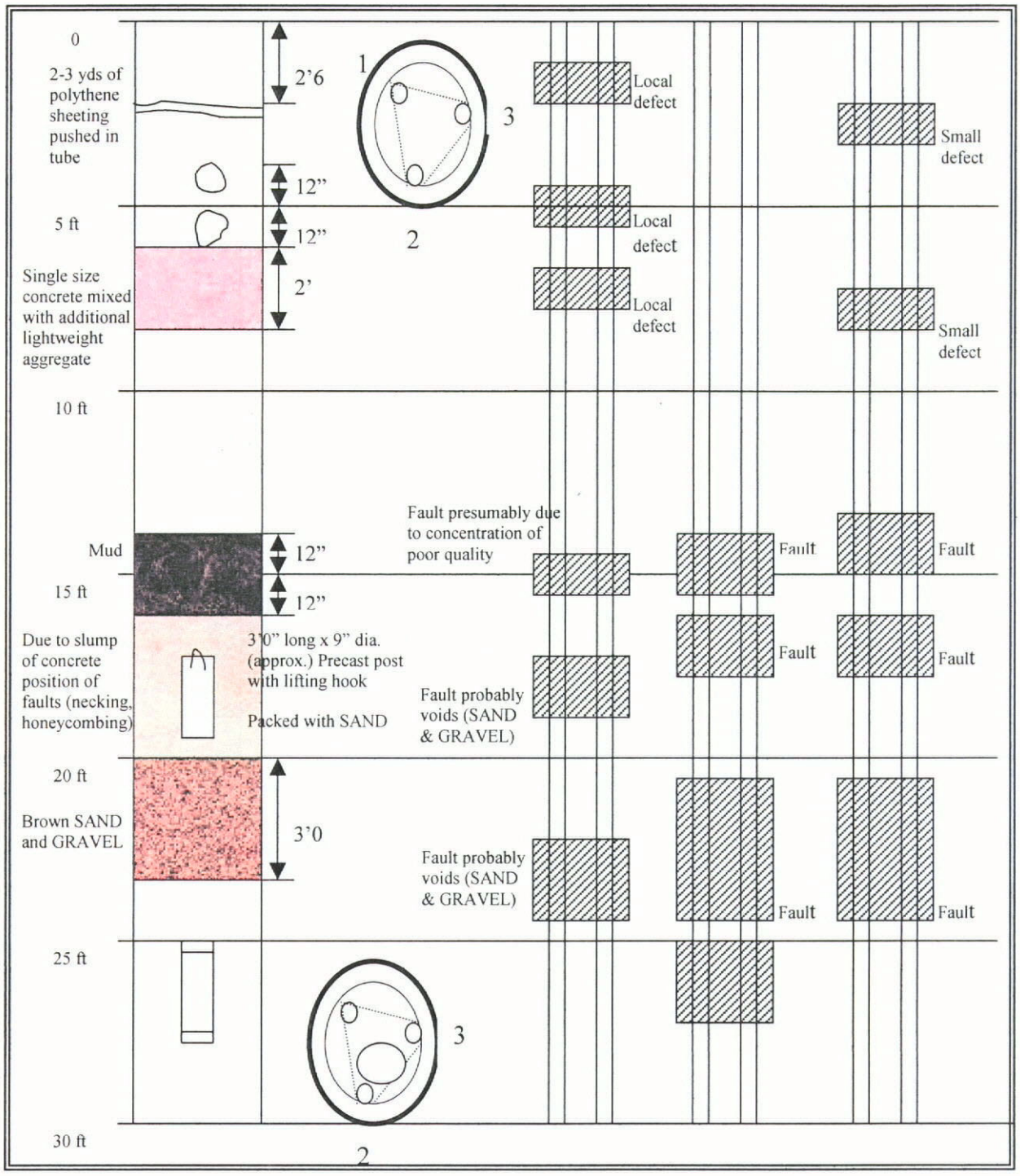

Figure 2.4.6. The special test pile (30 inches diameter) with built-in discontinuities (from CEBTP 1982)

Similar results were obtained by Williams & Stain (1987). A series of piles with artificial defects was constructed as part of a research project in northern London. One pile, nominally 750mm in diameter and 10m in length, was

constructed with neck defects at 2.4m and 6.9m respectively. A section of the pile and the CSL results are illustrated in Figure 2.4.7. The test profile clearly showed the locations of necks inside the pile. In comparison, an impulse response test performed on this pile identified a defect at 2.7m, but then totally missed the second neck.

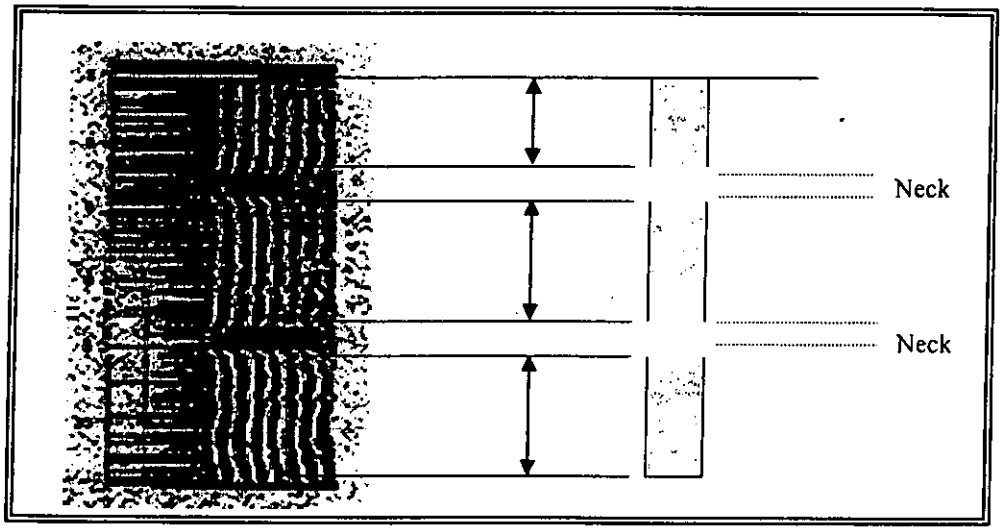

Figure 2.4.7. The sonic profile and the pile section (from Williams and Stain 1987)

The effects of different components (including weak concrete, weak grout, bentonite, gravel and soil) on sonic signals were further investigated in a laboratory research project described by Stain and Williams again in 1991. A number of small concrete panels was constructed, as shown in Figure 2.4.8. All panels were of the same dimensions and some had voids of various sizes to allow for the later addition of materials such as sand, gravel, water and bentonite.

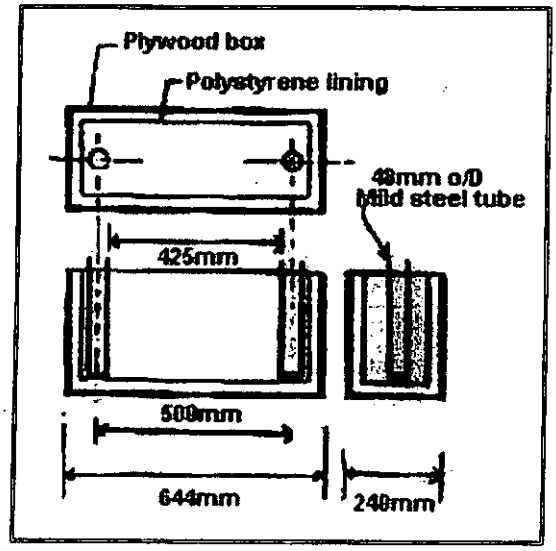

Figure 2.4.8. Panel dimensions (from Williams and Stain 1991)

The results showed that very little or no effect on signal transit time occurred when testing weak concrete (20N/mm^2) but that weak grout (2000 psi or 14N/mm^2) increased signal arrival time by 20%. Using thin wall plastic tubes is essentially the same as using mild steel tubes for obtaining CSL results. Signals passing through water-filled voids were very strong but at a much-reduced velocity of 1500m/s. The composite velocity through water and concrete reduced accordingly. Concrete contaminated with 30% bentonite attenuated the high frequency components of the signals and caused a significant increase in transit time. Bentonite-filled voids rapidly attenuated the signals. No signal was visible through bentonite. Voids filled with wet sand caused severe signal attenuation so that only a faint response was visible. In gravel-filled voids, the signal characteristics varied according to the condition of the gravel: (1) total effective attenuation in dry gravel, (2) severe signal attenuation in wet unwashed gravel, (3) attenuation similar to that in water in wet washed gravel.

The work done by Stain and Williams in 1991 provides a good insight for this research. A more detailed study of the variation of ultrasonic velocity with water content in various soils was carried out. Soil specimens were prepared at water contents ranging from dry to a maximum degree of saturation. Ultrasound was transmitted into soil specimens from a transmitting probe. The resulting signals were received by a receiving probe and digitized by an in-house multi-channel ultrasonic data acquisition prototype named the 'Multiple Referencing System' (MRS).

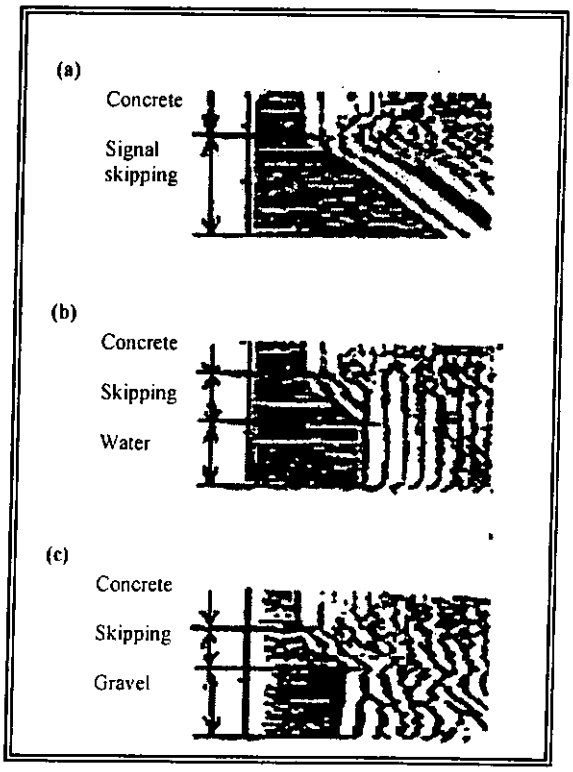

Figure 2.4.9. Signal skipping effects (from Stain and Williams 1991)

Stain and Williams (1991) also investigated signal-skipping effects. Signal skipping was reflected by a linear increase in travel time over a given depth of concrete. In the case of a void, the signals travelled down the transmitter tube across the concrete and up the receiver tube. Signal transit time increased linearly

through these areas (see Figure 2.4.9a). In the case of a water-filled void, signal skipping occurred as the probe entered the void area until the probe reached a point where the direct transit time through water was equal to the skipping time, in which case the transit time becomed constant (see Figure 2.4.9b). In the case of saturated and washed gravel, the results were similar to those in the water-filled void case (see Figure 2.4.9c).

Stain and Williams (1991) did work related to staggered testing; in which signal anomalies down a shaft were investigated by staggering the probes. The staggered tests enabled the horizontal extent of the anomaly to be determined, or at least limited to a certain zone, as shown in Figure 2.4.10.

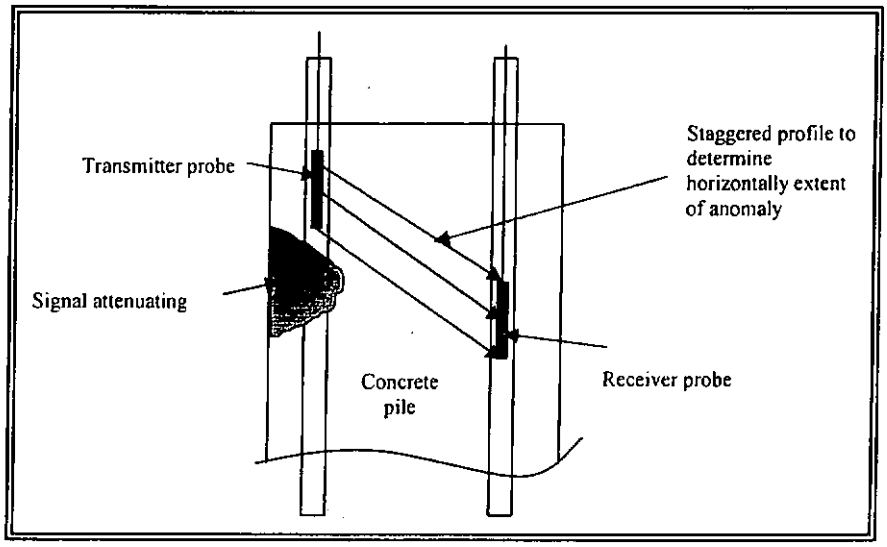

Figure 2.4.10. Staggered testing (from Stain & Williams 1991)

The laboratory work was concentrated on examining the effect of base anomalies on sonic profiles including anomalies around one tube in case 1 and anomalies around two tubes in case 2, as shown in Figure 2.4.11. Figure 2.4.12

shows the theoretical transit time in the form of a sonic profile.

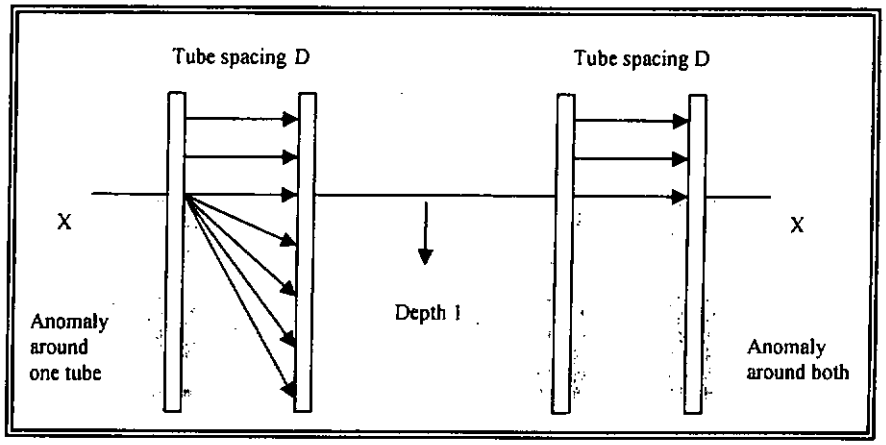

Figure 2.4.11. Expected paths around anomalies (from Stain & Williams 1991)

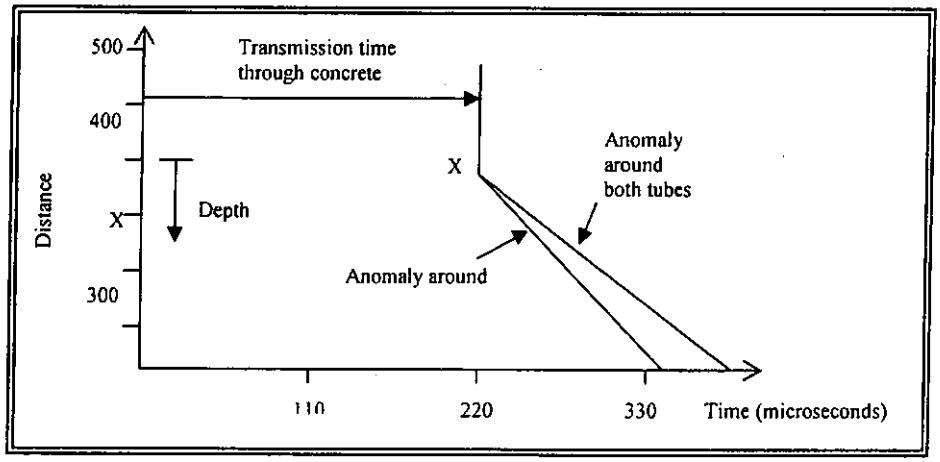

Figure 2.4.12. The theoretical profile (from Stain & Williams 1991)

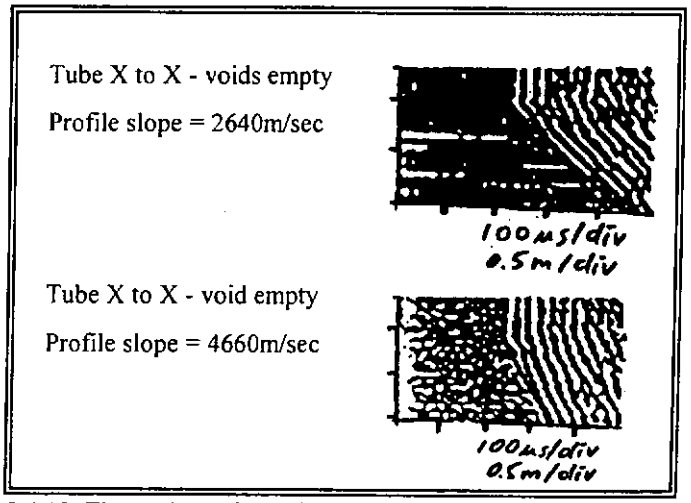

Figure 2.4.13. The sonic profiles of the trial panel with base anomalies (from Stain & Williams 1991)

In the first profile in Figure 2.4.13, voids around both tubes produced a slope of 2640m/sec, being approximately equal to half the propagation velocity of signals traveling vertically in the tubes. While in the second profile, a void around only one tube produced a slope of 4660m/sec. This showed that anomalies around both tubes led to more attenuation of sonic signals.

Normally, a pair of probes is kept at the same elevation/level to create a horizontal travel path between a transmitter and a receiver. Consequently a defect with a significant vertical 'foot-print' can normally be intercepted/detected, whereas a thin horizontal-running crack may not be detected because the signal can go around this defect through neighboring sound concrete or water without any significant change in *first arrival time* (FAT) and/or received signal strength (CEBTP 1969). However, a staggered test is performed in which the pair of probes is placed at different elevations/levels so that a straight line joining the two probes will intercept the 'foot-print' of the crack. Once a defect is located, more local tests (i.e. staggered tests) can be performed to locate the defect's horizontal position more accurately (Stain 1982). The work conducted by Stain and Williams (1991) provides a good foundation for the application of staggered testing in piles.

It is not, however, sufficient to concentrate on the bodies of foundation concrete piles, the integrity at their bases is also a concern. Without a good and firm base, the buildings on these faulty piles are not safe structurally. In this research, a number of on-site 'fan-shaped' tests was carried out to investigate pile toe/rock interfaces. The details of performing a 'fan-shaped' test are described in

Section 2.4.3.

A recent report, prepared by Dr. Finno et al. of the Department of Civil Engineering of Northwestern University in the United States in September 1997, provided the most accurate picture of the state-of-the-art of the CSL testing method on drilled pile shafts. Two shafts with known defects were constructed at the National Geotechnical Experimental Site (NGES) at Northwestern University. A section of these two shafts is shown in Figure 2.4.14.

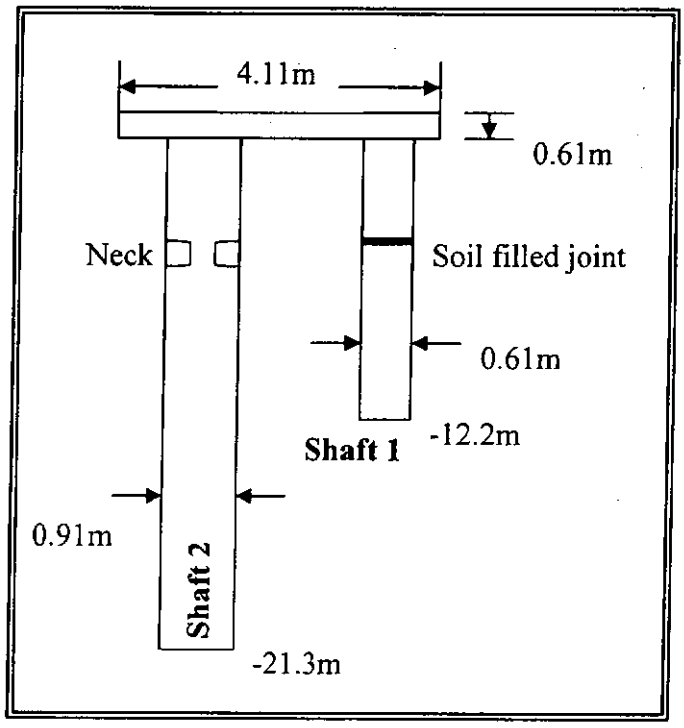

Figure 2.4.14. A section of two shafts in the NGES (Gassman 1997)

These shafts were each equipped with three PVC access tubes which were attached to the reinforcing cage to permit CSL. The soil-filled joint of shaft 1 was constructed by placing a layer of 254mm of clay at a depth of 4.96m. The necking of shaft 2 was built into the shaft by tying sandbags to the reinforcing

cage at depths between 3.76m and 4.47m.

CSL successfully determined the locations and extents of the built-in defects on shafts 1 and 2 at the NGES test site. The reliability of the test results seemed good, because the apparent velocities computed from the cross-hole sonic logging data fit the expected range of Ultrasonic Pulse Velocity obtained from laboratory tests. CSL tests performed at the NGES test site showed that results could be unreliable if such a test were performed within one week after construction. CSL analysed on shafts 1 and 2 performed at 7, 14, 28 and 1000 days after construction. The analysis of the effects of concrete age on the signals showed that one should wait between 7 and 14 days before performing a CSL test in order to obtain reliable data.

The above studies were all performed either on a small-scale with a large sample or on a large-scale with a small sample. Few real-case field investigations have yet been done (i.e. large in both scale and sample).

Real case studies

CSL was used extensively in 1993 and 1994 on the foundations of the world's tallest skyscrapers, the 1,482 ft tall Petronas Twin Towers in Kuala Lumpur, Malaysia (Brettmann et al. 1996a). The foundations consisted of 223 drilled shafts 5 ft in diameter and 208 barrettes with depths ranging from 130 to 310 ft. The drilled shafts and barrettes were sonically logged by Tesonic of

Selangor in Malaysia, using Fugro's TCP3 system. Some defects that required corrective measures were found using CSL.

A comprehensive quality assurance program (Olson et al. 1994) was carried out to non-destructively inspect the integrity of over 200 large diameter drilled shaft foundations which were constructed to support aerial structures of the El Segundo segment of the Los Angeles Metro Green Line rail transit project near Los Angeles International Airport. Each of the large diameter drilled shafts was tested by CSL in plastic tubes installed with the steel reinforcement cage. During the course of the investigation, 97.5% of the drilled shafts placed were identified as sound with no significant flaws. Of the remaining 2.5% with anomalies, the majority were minor defects that required no remediation due to their small sizes or locations in the shafts. Only one drilled shaft was identified as having a major flaw. This quality control program showed the efficiency of CSL. The 10-day testing schedule allowed for a greater economy of scale as the testing could be performed after several shafts had been completed. During the bulk of the testing, it was quite common to be able to test 10 or more shafts in a single day. Field-testing results indicating which shafts were sound or which were questionable were available by the end of the testing day.

Two buildings, the "Pot de Normandie" and Commerzbank II, in Frankfurt were executed by foundation engineers of the LFINGER + BERGER Bauaktiengesellschaft. The piles in both buildings were examined by ultrasonic technology to check the quality of the concrete (Gross et al. 1997). More than

6,800 piles for deep foundation of thermal power plants, electrical lines, bridges viaducts and residential buildings in Italy have been tested by CSL (Faiella et al. 1998). An adequate statistical analysis of the large amount of data has been collected allowing for the establishment of an interpretative criterion for an objective and homogenous classification of defects.

The above research work and successful applications in real situations ascertain the importance of quality control of deep foundation concrete elements using the CSL testing method. Several US state departments of transportation have specified CSL for the quality assurance of concrete placement in drilled shaft foundations, including Alabama, Arizona, California, Colorado, Georgia, Missouri, Nevada, New Mexico, Oregon and West Virginia (Brettmann et al. 1996a). In Hong Kong, all the piles in Hong Kong Housing Authority (HKHA) projects are to be tested by CSL prior to further construction. Not all, but most, piles in other projects like those of the Mass Transit Railway Corporation (MTRC), Kowloon Canton Railway Corporation (KCRC) and private projects have been advised to apply CSL testing as well.

In this research, an extensive field investigation was performed on over 100 foundation elements on various Hong Kong construction sites. Examples of typical results, and the possible causes of the defects found by CSL, are discussed in Section 6.3.

The Single-hole Sonic Logging Technique

CSL involves a pair of sonic probes in two parallel ducts. A combined acoustic transmitter/receiver unit was instrumented to perform a Single-hole Sonic Logging (SSL) test in the same hole to evaluate the test materials. Figure 2.4.15 shows a schematic drawing of performing a SSL test. The transmitter and receiver, mounted at the top and bottom of a single probe respectively, are separated by an acoustic isolator. The pulse energy from the transmitter travels through the surrounding concrete and part of the pulse energy is received by the receiver (Turner 1997).

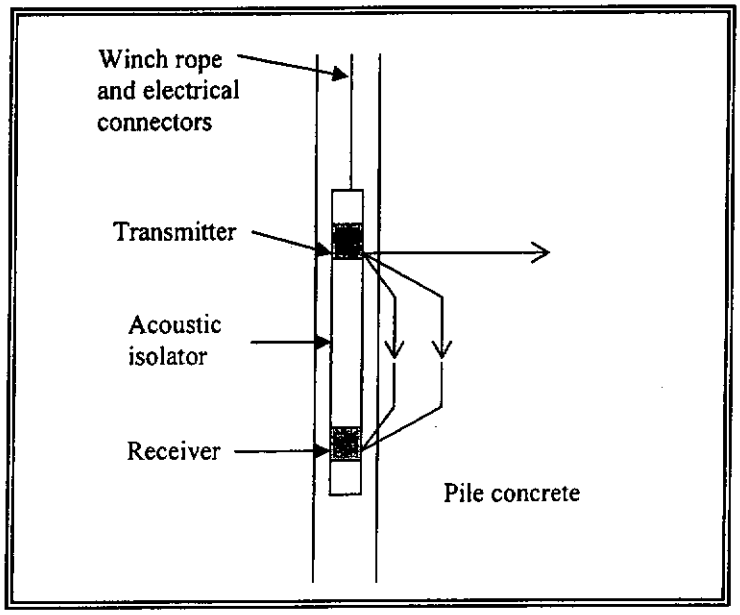

Figure 2.4.15. Schematic drawing of performing a Single-hole Sonic Logging technique

Brettmann and Frank (1996b) compared the conventional CSL and the SSL testing methods. Their study was conducted at Fugro's sonic integrity test pile site in Houston and at the National Geotechnical Experimentation Site (NGES) at the Texas A&M Riverside Campus. The test piles at both sites were

installed with various planned artificial and construction defects. The test results of the SSL method showed a good correlation with the results of the CSL method. The study showed that SSL was also faster than CSL because only one log was run per pile. The single access pipes led to fewer obstructions in the piles, and were less costly to purchase and install. Using PVC access pipes was recommended over using steel pipe for an SSL test in order to reduce the effect of interference from high-speed waves traveling directly along the pipes. However, the application of the SSL method is limited to small diameter concrete elements. Defects can appear vertically enlarged on SSL logs. CSL provides a better horizontal resolution of defects than those from SSL because multiple profiles around the perimeter and through the center of the piles are performed. SSL is especially beneficial for small diameter piles where installing multiple access tubes for CSL is not practical.

Signal Analysis

The traditional analog CSL instrumentations (i.e. a graph of FAT versus depth) have very limited signal-processing capabilities. The interest of past researchers in the field mostly focused on first arrival time or/and apparent pulse velocity to evaluate the concrete integrity of test piles. The received energy was totally disregarded in the evaluation. A new generation of ultrasonic logging equipment was developed in the 90's. In this equipment, the received ultrasonic signals were stored digitally and could be post-processed in different approaches so that the signal processing technique was improved.

Kissenpfennig et al. (1984) identified the signal intensity (attenuation) of the sonic signal as a more reliable indicator of concrete quality than P-wave velocity. Signal intensity was defined as the total energy measured by the receiver (i.e. area under the waveform) and could be calculated by a technique of root-mean-square (RMS) integration. A total of over 60 piles was tested by CSL, and a reliable correlation between concrete compressive strength and sonic signal intensity was developed. Figure 2.4.16 shows the nature of the correlation between the normalized signal intensity and the core compressive strengths in the integrity testing program.

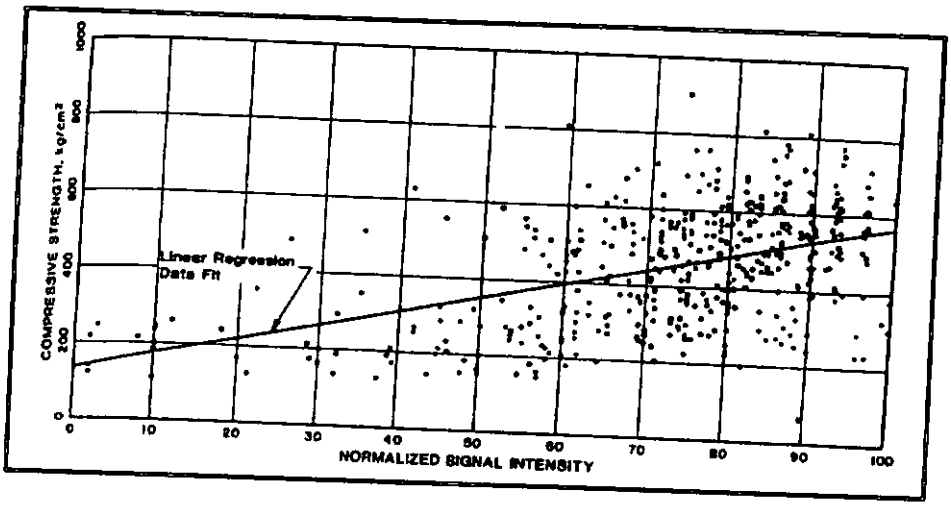

Figure 2.4.16. A plot of normalized signal intensity versus compressive strength (from Kissenpfennig et al. 1984)

A new generation of CSL instrumentation

New generations of ultrasonic testing systems, 'Cross Hole Ultrasonic Monitor (CHUM)' by Amir et al. (1998) and 'Pile Integrity Sonic Analyzer (PISA)' by Chernauskas et al. (2000), have been instrumented in recent years. Both systems can calculate both FAT and received energy of the arriving signals,

and carry out post-processing of data analysis.

The recent instrumentation development is a big forward step in signal processing, and also forms a good foundation for this project. In this research work, an in-house ultrasonic data acquisition prototype named the 'Multiple Referencing System' (MRS) was instrumented based on National Instruments (NI) hardware and a LabVIEW (Laboratory Virtual Instrument Engineering Workbench) environment. This prototype is capable of detecting two or more channels of signals simultaneously instead of only one channel of signals as in a traditional CSL instrumentation.

The in-house developed MRS was designed to allow pre-programmed data acquisition and processing. A purposely-developed graphical analysis programming in a LabVIEW environment was constructed to analyze the acquired waveforms in different parameters (i.e. signal strength in a time domain and spectral energy content in a frequency domain) in addition to the traditional parameter of FAT. This analysis is help to increase the reliability of the method in characterizing and evaluating test materials. The design and development of the MRS are described in Section 7.2.

Tomography

In addition to the data analysis for the evaluation of concrete integrity, a few studies have been carried out for the advanced presentation of CSL profiles.

Crosshole Tomography (CT), a technique of imaging, was discussed by Olson et al. (1998). The tomographic analysis was performed by using a simultaneous iterative reconstruction technique (SIRT) (Herman 1980), which was based on the analysis program developed as part of a research project, sponsored by the National Science Foundation, to image defects in structural concrete. The CT method used multiple CSL logs with varying receiver locations to produce a two-dimensional image of the defect, as shown in Figure 2.4.17. CT tests were performed on two drilled shaft foundations in California in 1994. Figure 2.4.18 shows the velocity tomogram between the tested tubes from one of the tested drilled shafts. The velocity tomogram identified the anomalous zone which was represented by the low-velocity area. This allowed engineers/contractors to determine if repairs were needed and where the repairs needed to be performed. However, the greater time to perform tomographic analysis made its popularity limited.

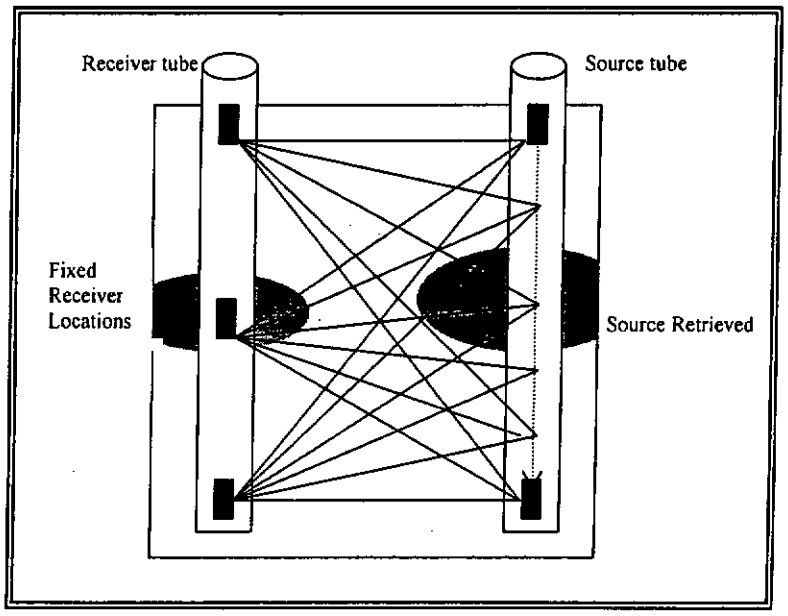

Figure 2.4.17. The Crosshole Tomography (CT) setup between two tubes of a drilled shaft (from Olson et al. 1998)

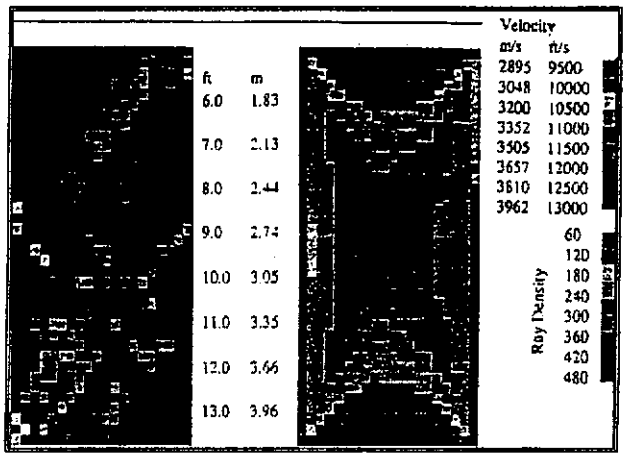

Figure 2.4.18. The velocity tomography from the first tested drilled shaft in California (from Olson et al. 1998)

Tomography is an analytical technique that uses an inversion procedure on the FAT data of compression or shear wave energy that can produce pulse-velocity-based images of a two-dimensional concrete zone inside a test member.

Other tomographic analysis techniques, Fuzzy-logic Tomography and Parametric Tomography, were introduced by Amir (1998). The shape of major anomalies can be shown in a two-dimensional presentation. A more advanced presentation of CSL profiles is recommended to produce a three-dimensional graphic by combining all the necessary CSL profiles, in which the deficient zone can be easily identified.

2.4.2. Principles of the Cross-hole Sonic Logging technique

CSL is based on measuring the propagation time of a sonic/ultrasonic pulse traveling through concrete between two vertical sonic access tubes. These tubes are usually steel/PVC cast inside the concrete. CSL is usually carried out some time after the concrete has set and cured (normally 7 days), These tubes are installed in various arrangements (one such arrangement is shown in Figure 2.4.19), the objective is to cover a large section of the foundation elements. And these tubes are typically cast into a shaft during construction, or attached to the reinforcing cage not more than 4m apart because the useful transmission distance is about 4m in good concrete for a 35kHz signal (Davis and Hertlein 1994). It is important to fill these tubes full of clear water (to obtain a good coupling effect) for ultrasonic pulse transmission.

A transmitter is lowered in one tube and a receiver in a neighboring tube. Pulses are triggered by a depth encoder wheel and generated typically at 20 to 50mm vertical intervals. The transmission time between the transmitter and the receiver is a function of the quality of the concrete between the tubes. A major defect (such as air voids and soil pockets, etc.) may affect the ultrasonic wave transmission at various degrees: from total blockage, absorption to partial scattering and attenuation. Thus record charts would show late arrival and/or low energy of ultrasonic received signals. This test has been successfully used on shafts of length up to 90m (Davis and Hertlein 1994).

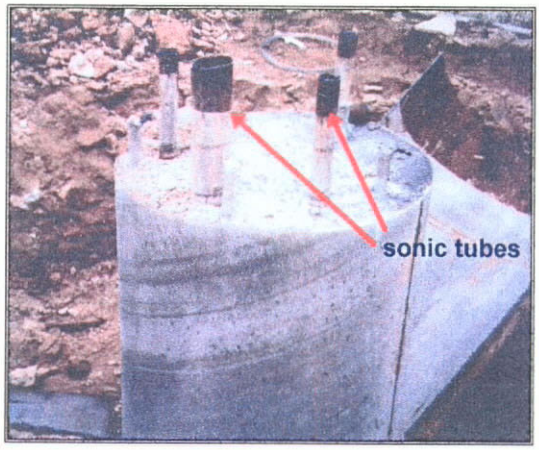

Figure 2.4.19. Four sonic access tubes were installed inside a pile prior to the concreting stage

From the basic wave theory, the propagation velocity of an ultrasonic wave/pulse through a known path length, L, across the main body of a foundation element is given by:

$$c = \frac{L}{t} \qquad \text{--- (Equation 2.4.1.)}$$

where t is the transmission time of the waves traversing the path length, L.

Transposing Equation 2.4.1, the transmission time, t, of such waves is given by :

$$t = \frac{L}{c} \qquad \text{--- (Equation 2.4.2.)}$$

The propagation velocity of an ultrasonic wave/pulse through an isotropic elastic medium is related to the elastic constants of the media (i.e. air, water, steel/plastic, concrete etc.) by the following expression

$$c = \sqrt{\frac{E(1-v)}{\rho(1+v)(1-2v)}} \qquad \text{--- (Equation 2.4.3.)}$$

where: E is the dynamic elastic modulus of the material (unit: GPa);
ρ is the density of the material(unit : kg/m^3);
v is the dynamic Poisson's ratio.

Hence substituting into Equation 2.4.3, the transit time, t, can be expressed as follows:

$$t = L\left[\frac{\rho(1+\nu)(1-2\nu)}{E(1-\nu)}\right]^{\frac{-1}{2}} \qquad \text{--- (Equation 2.4.4.)}$$

Thus, if the distance traveled by the wave/pulse is the same (as envisaged in the access tubes spatially installed) at different depths, the transmission time, t, is then a function of the properties of the media defined by E, ρ and ν.

Sonic logging utilizes the relationship of Equations 2.4.2 and 2.4.4 to deduce the interior properties of a foundation element, usually concrete, by measuring the transmission time of an ultrasonic wave/pulse traveling between two known points. Caution must be exercised, because this *apparent transmission velocity* includes the combined effects of transmission through water, access tube walls, concrete and/or other embedded materials. A typical flow path of such transmission is shown in Table 2.4.1. Each interface of two different materials (i.e. difference in acoustic impedance, Z) will produce partial reflection, refraction and transmission to occur.

Table 2.4.1. Transmission path in a typical CSL test

probes → water → access tube walls → concrete → anomalies (if defects present) → access tube walls → water → probes

The apparent transmission velocity obtained from Equation 2.4.3 is applicable to CSL because, for the frequencies used in the test, the wavelength produced is much smaller than the diameter of the shafts. Therefore wave propagation is three-dimensional, rather than one-dimensional as in the case of a long thin rod (Finno et al. 1997). The apparent transmission velocity is used as an indicator for evaluating the quality of concrete as illustrated in Table 2.4.2.

Table 2.4.2. Ultrasonic velocity ratings for concrete structures (after Bungey 1980)

Velocity (m/s)	Concrete condition
4575 and above	Excellent
3660 to 4575	Good
3050 to 3660	Questionable
2135 to 3050	Poor
Below 2135	Very poor

2.4.3. Implementation of the Cross-hole Sonic Logging technique

Figures 2.4.20 and 2.4.21 show the actual arrangement in the implementation of an on site CSL test. The probes are first lowered to the toe of a pile along two adjacent tubes and slowly raised in unison. The cables connecting the probes are then wound over the wheel of the depth encoder. The latter provides triggering pulses for synchronous range and depth measurement. The depth decoder generates a trigger pulse typically at 20 to 50mm vertical intervals.

Figure 2.4.20. Situation while measuring sonic speed

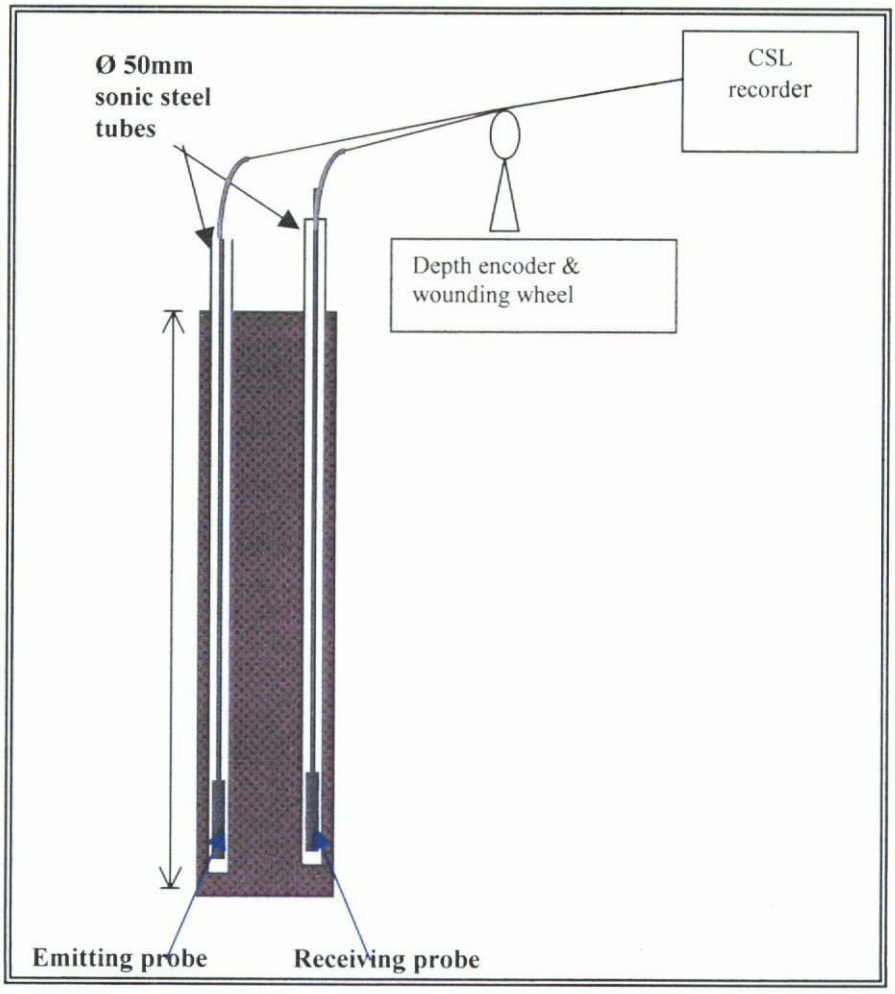

Figure 2.4.21. Schematic drawing of performing a CSL test

The pair of probes is usually kept at the same elevation/level to create a horizontal travel path between the transmitter and the receiver as shown in Figure 2.4.22. Consequently a defect with a significant vertical 'foot-print' can normally be intercepted/detected, whereas a thin horizontal-running crack as shown in Figure 2.4.23 may not able to be detected because the signals can go around this defect through neighboring sound concrete or water without any significantly changing of *first-arrival-time* (FAT) and/or received signal strength (CEBTP 1969). In this particular situation, the pair of probes should be arranged at different elevations/levels so that a straight line joining the two probes will intercept the 'foot-print' of the crack (see Figure 2.4.24).

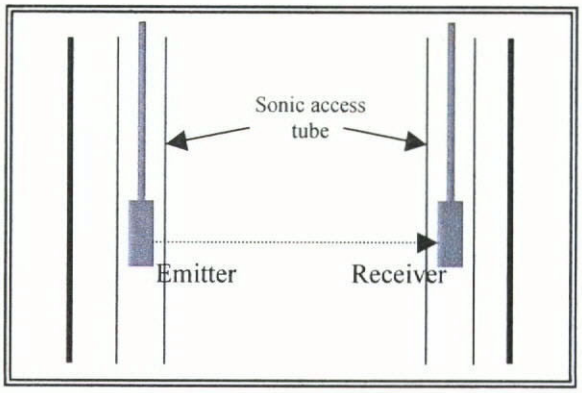

Figure 2.4.22. A 'straight-through' technique

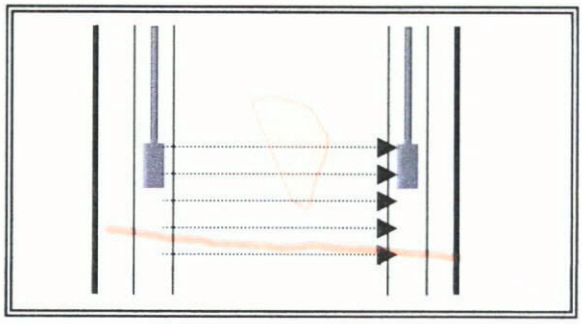

Figure 2.4.23. Horizontal and vertical defects

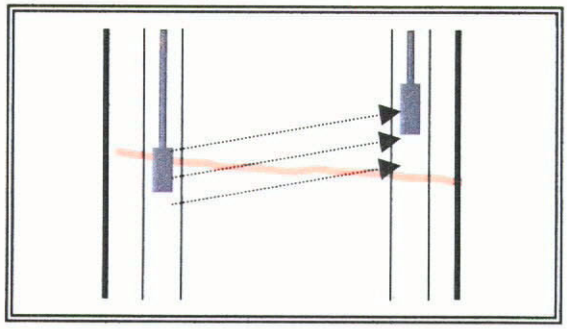

Figure 2.4.24. An 'oblique' evaluation technique

This 'oblique' evaluation technique is frequently used to check the pile toe/rock interface and called a 'fan-shaped' test in the foundation testing industry nowadays.

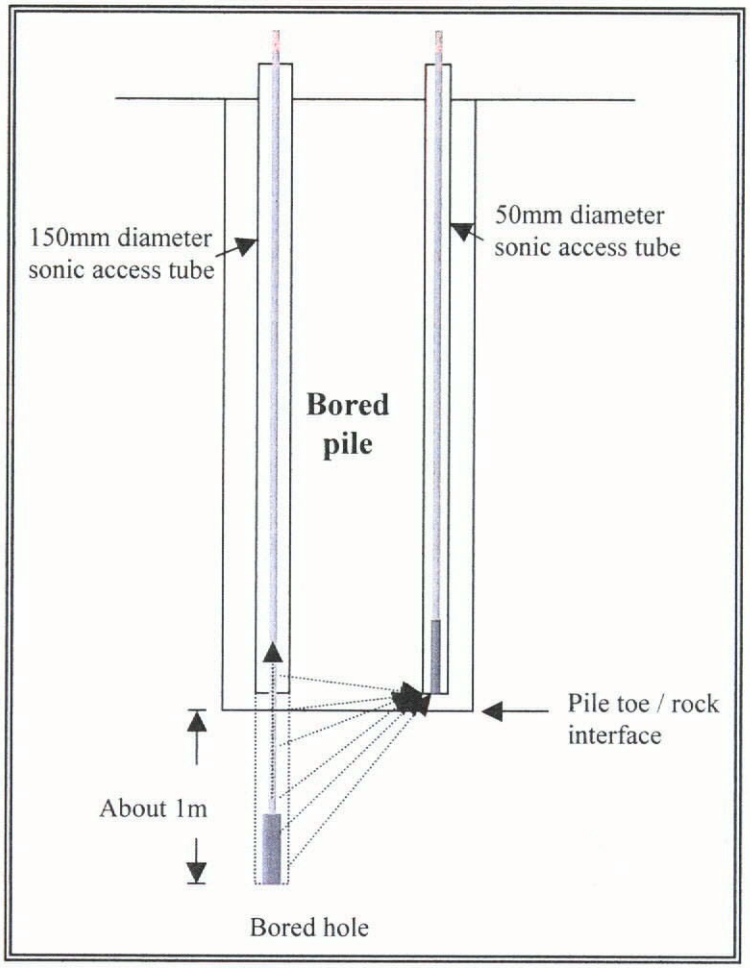

Figure 2.4.25. Schematic drawing showing the arrangement of the toe of a bored pile in performing a 'fan-shaped' test

Figure 2.4.25 shows a typical schematic drawing depicting the arrangement of the toe of a bored pile in performing a 'fan-shaped' test. As descried earlier, this 'oblique' arrangement will allow an ultrasonic evaluation of the horizontal running interface between a pile toe and rock.

One of the sonic access tubes in a pile to be of diameter about 150mm is allowed a drill rod to fit down the tube. An access hole is then drilled through the pile toe and into the bedrock to approximately 1m below the toe. The access tubes are also filled up with clean water. The two sonic probes are lowered respectively at the bottom of 50mm-diameter sonic access tube and the bored hole. The probe inside the bored hole is raised while the probe inside the 50mm-diameter sonic access tube is kept stationary. Horizontal extent of anomalies of the pile near the pile toe can be investigated based on the sonic logging profiles.

2.4.4. Provisions of sonic access tubes

The number of sonic access tubes can vary. For a circular in-situ cast concrete pile of 1 to 2m-diameter, the provision of four to six sonic access tubes would be typical. These tubes are usually metal owing to their greater rigidity and good bonding to concrete. PVC tubes have also been used but are not preferable owing to a number of practical problems encountered in their installation, such as the collapse of the tubes causing blockage to the passage of the probes. The sonic access tubes are tied securely to the reinforcement cage at a roughly equal spacing along the circumference of the pile. This permits greater coverage of the concrete

in the pile for the sonic logging evaluation exercise. To examine the conditions of the concrete/rock interface, a sonic access tube with a larger diameter (about 150mm) is installed to allow a coring machine to drill 1m across the interface to obtain a sample for visual evaluation.

The sonic access tubes should be made in steel of a specified diameter typically 50mm or 80mm etc. They should be free from defects and blockage to allow the free and unobstructed passage of the probes employed. The tubes, including any joints, should also be watertight and should be fitted with screw-on watertight shoes at both ends. The top end of each tube should project sufficiently above finishing concrete level for easy identification and access. Care should be taken not to damage the tubes during the concreting stage or subsequent trimming of excessive concrete. The sonic access tubes should also be filled with water to provide a good coupling medium needed when performing CSL.

For concrete barrette piles as well as diaphragm walls, the arrangement and details of the sonic access tubes for a circular bored pile described previously can also be applied with slight modification. Figures 2.4.26 and 2.4.27 show the staggered tube-arrangement along a concrete barrette pile/diaphragm wall panel.

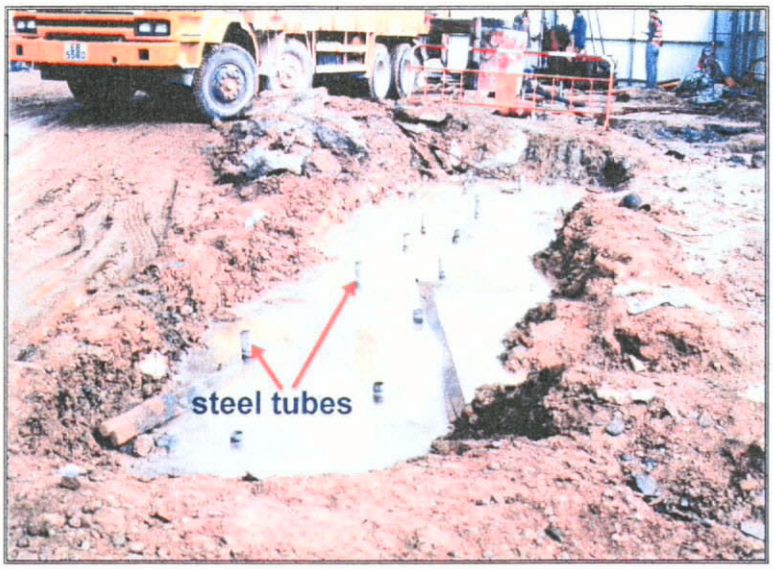

Figure 2.4.26. Staggered tube-arrangement in a concrete barrette pile

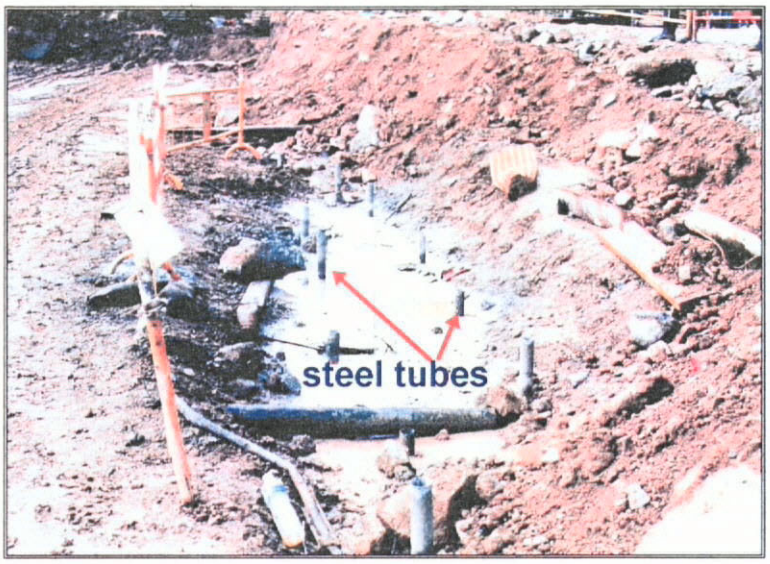

Figure 2.4.27. Staggered tube-arrangement in a diaphragm wall panel

2.4.5. Interpretation of the Cross-hole Sonic Logging test results

The ultrasonic pulse velocity in good concrete (i.e. free from any significant defects) is in the order of 4000 m/s, depending on its constitutions and compositions. Foundation concrete containing foreign materials (i.e. materials other than concrete such as soil inclusions, cobbles, bentonite cake or

honeycombing, etc.) has a much lower propagation velocity. Actually the pulse transmission time (i.e. often called FAT of the transmitted pulse) is the property measured in CSL. FAT is a function of the transmission velocity and distance traveled. For a given distance traveled, a longer transmission time and/or a higher signal attenuation (i.e. loss of energy) is a sign of encountering a poor quality concrete zone.

In performing a typical CSL, two probes are, first of all, lowered to the bottom of the respective sonic access tubes (i.e. near the pile toe) and then pulled simultaneously upwards to produce a 'so-called' CSL profile. The profile of a normal foundation element without defects is shown in Figure 2.4.28.

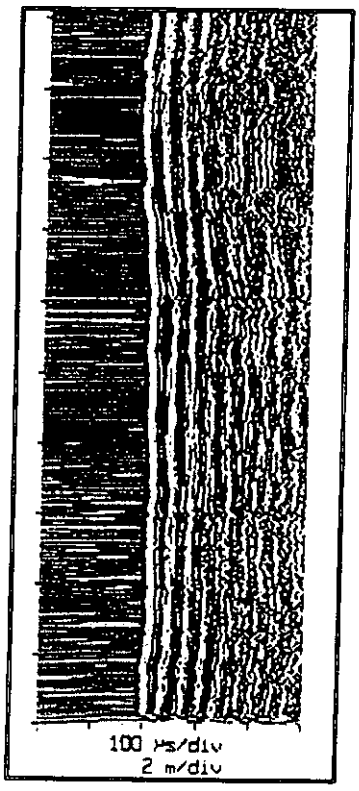

Figure 2.4.28. Typical CSL profile showing propagation time versus depth

In fact the profile is produced and visualized by stacking a series of time traces (obtained at different depths) one on top of the other. This technique produces a visual display of all the received signals. In interpreting these profiles, the first wavering dark strip signifies a significant variation of FAT (i.e. a significant difference in the quality of the concrete between the pair of the sonic access tubes). A straight black strip signifies otherwise. A gray scale-coding scheme is often applied to modulate signal amplitudes to an alternating sequence of dark and white strips as shown in Figures 2.4.29 and 2.4.30. A sudden change of FAT indicates a likely presence of a defect at the respective depth. By building up a continuous profile along the entire length of a pile, this graphical plot allows a fast and easy evaluation of the integrity of the concrete in the foundation elements.

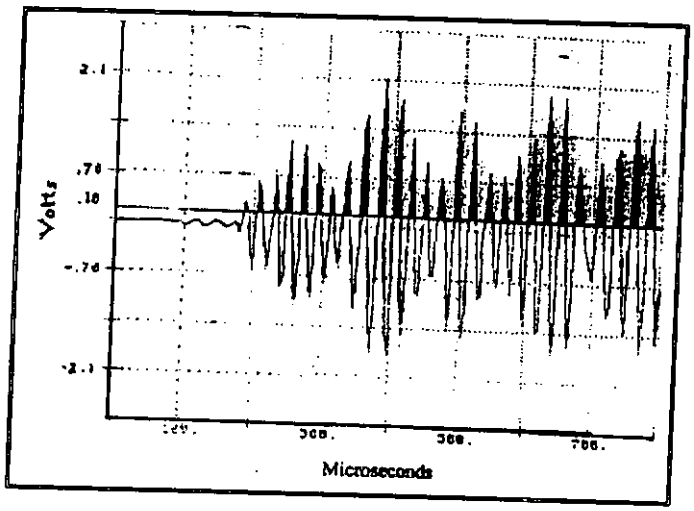

Figure 2.4.29. Typical signal recorded through concrete at one depth

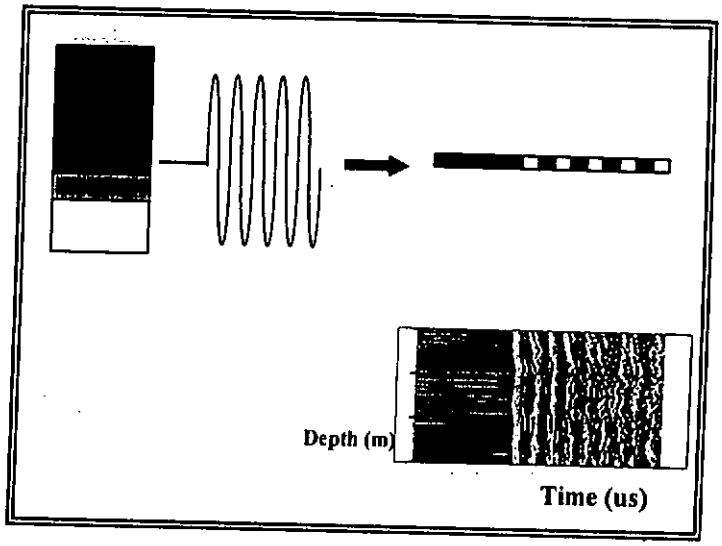

Figure 2.4.30. Modulated signals in CSL profiles

Electrical noise can be reduced or faint signals enhanced by changing the gain or sensitivity. The signal threshold is set at an arbitrary value, for example 0.1V, so that the signal amplitudes, larger than the threshold, are modulated to black strips and white strips if less than the threshold. Figure 2.4.31 shows a typical good result of a 'fan-shaped' test which a good cohesion is clear at the pile toe / rock interface.

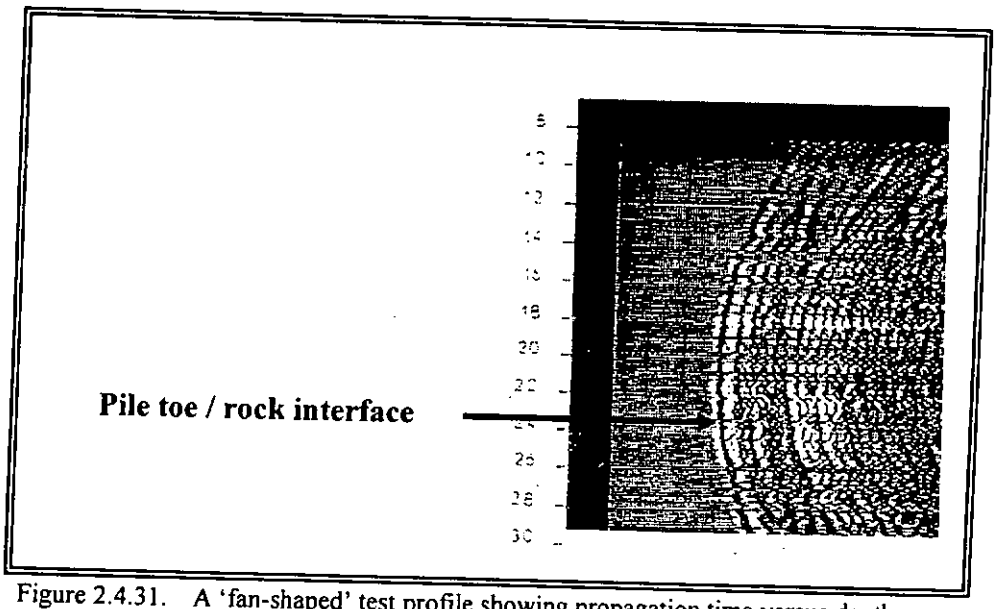

Figure 2.4.31. A 'fan-shaped' test profile showing propagation time versus depth

2.4.6. Limitations of the Cross-hole Sonic Logging technique

The main limitation of the test is that pre-selection of the foundations is necessary at the design stage in order to fix access tubes to a reinforcing cage at a roughly constant spacing. Extra time and cost are involved to fix access tubes to a reinforcing cage.

The method only detects those defects located along the path of the access tubes. If the defects present too near to the periphery of the reinforcing cage, they may not be sufficiently covered.

A negative effect induced by the presence of the tubes is that the reinforcing steel cage is harder to place due to the presence of access tubes. This reinforcing steel cage also diverts a portion of the signal and produces a shadow effect (Finno 1997).

The test yields no information on dynamic properties or piles/soil interaction. To allow this interaction to be examined, drilling out into the underlying stratum through the access tubes is usually suggested.

2.4.7. Test standards and specific requirements of the Cross-hole Sonic Logging technique

Various countries have their own CSL standards as shown in Table 2.4.3.

Table 2.4.3. Test standards for CSL in various countries/cities

Country/ City	Reference	Title
Australia	AS 2159-1995	Piling-Design and Installation
China	JGJ 94-94	Technical Code for Building Pile Foundation Chapter 9: Inspection and Acceptance of Pile Foundation Engineering 9.1: Quality Inspection of Pile Installation.
Hong Kong	ASTM D6760-02	Standard Test Method for Integrity Testing of Concrete Deep Foundations by Ultrasonic Crosshole Testing
	Association of Construction Materials Testing Laboratories Ltd.	Standard Test Method for Ultrasonic Logging Test (Cross-hole Method) for Integrity of Concrete Foundation Elements
	Hong Kong Laboratory Accreditation System (HOKLAS)	HOKLAS Supplementary Criteria No.16 – Construction Materials Test Category – Accreditation of Foundation Tests
France	NFP 94-160-1	Soil: Investigation and testing Auscultation of buried work Method by Sonic Core Test
UK	Institution of Civil Engineers (ICE)	Specification of Piling

2.5. Ultrasonic Wave Propagation in Soils

Destructive methods are used to determine the properties and the behavior of the soils (ASTM 1992, AASHTO 1997). Drilling at a specific location is first conducted for obtaining geological information of the site and then laboratory tests using drilling cores and in situ mechanical and/or hydrogeological tests follow. However, such information obtained at a drilling location is only the information at a specific point in the site. Non-destructive test methods can provide a fast and simple alternative approach to analyze soils. A variety of geophysical testing techniques (seismic refraction/ reflection, electrical resistivity, gravity and ground-penetrating radar) are used to obtain the properties of the soil strata. Relevant references for these geophysical testing techniques include Parasnis (1997), Robinson and Coruh (1988), and Milsom (2003). Ultrasonic testing was selected as the nondestructive test method for this study since it is simple and fast with significant experience in the evaluation of some materials like concrete and steel.

Sologyan (1990) provided a brief summary of applications of ultrasonic testing to determine density of soils in the field. The information provided was related to agricultural applications. It was suggested that ultrasonic testing was used effectively to determine density, water content, and micro-structural properties of soils. However, specific details were not provided.

An extensive investigation of the use of ultrasonic testing for compacted

soils was reported in an early study by Sheeran et al. (1967). Ultrasonic tests on laboratory compacted sandy, silty, and clayey soils were conducted to determine the relation between P-wave velocity, dry density, water content, and compactive effort. It was observed that for a particular compactive effort, P-wave velocity increased with increasing dry density, up to optimum water content. Then a sharp drop in velocity was observed at increasing dry densities. The peak velocity was obtained generally within 0.5% water content of the optimum water content for the soils. Velocity of the material increased with increasing compactive effort. Results also indicated that desiccation had significant effects on velocity, causing increases in the velocities up to peak velocities. However, water content below the shrinkage limit had little or no effect on the velocity variation.

Stephenson (1978) used P-wave and S-wave velocities determined by ultrasonic methods to obtain the dynamic elastic and shear moduli of low plasticity silty clay. Results indicated that velocity and Poisson's ratio decreased with an increase in void ratio for a given saturation. He also indicated that velocity increased with the degree of saturation.

Wang et al. (1991) conducted a simple study to determine the variation of ultrasonic velocity with water content and pressure for a silt loam compacted under static pressure. The velocity was used as an indicator to estimate the soil moisture content and compaction. The ultrasonic wave velocities increased with decreasing water content and increasing compaction pressure.

Cockaerts and De Cooman (1994) did similar works. They used ultrasonic methods on saturated artificial sand-clay mixtures in a drained triaxial setup. Maximum P-wave and S-wave velocities were obtained at a minimum porosity. It was stated that the clay mineralogy did not affect wave velocities of clayey sands.

A soil testing system for measuring wave propagation through soils using a pulse transmission method was developed by Nakagawa et al. (1996). The system can detect strongly attenuated waves traveling dry sand by mounting very sensitive P- and S-transducers in the cap and pedestal of a triaxial testing device. Velocities measured in the triaxial setup were in good agreement with the in situ velocities measured by suspension type S-wave logging. However, velocities determined with the resonant column for the soils were lower than the in situ measurements by up to 50% in clays.

Yesiller, et al. (2000) conducted the ultrasonic testing to evaluate stabilized soils. Ultrasonic velocity was measured on laboratory prepared stabilized soil samples. It was observed that P-wave velocities were higher for samples stabilized with cement compared with samples stabilized with lime and fly ash. In addition, velocities increased with curing time for all the stabilized mixes, and increased with the unconfined compressive strength of the samples increased. The P-wave velocities of the stabilized soils increased as the modulus of the soils increased. Also the variation of modulus with time was similar to the variation of velocity with time. The P-wave velocities increased as the densities of

the samples increased. In 2001, Yesiller also used ultrasonic methods to determine compaction characteristics of clayey soils. Effects of soil type and compaction conditions on velocity were investigated. It was observed that velocity increased with increasing compaction effort and decreasing plasticity and clay content.

The kinds of soil specimens involved in the past study were limited in quantity and the effects on ultrasonic signals of various kinds of soils have not been outlined. With the use of an in-house developed prototype MRS (Section 7.3), different kinds of soils (including very gravelly GRAVEL, very sandy SAND, silty clayey gravelly SAND, clayey gravelly very sandy SILT and very sandy GRAVEL) were characterized. These soil specimens were prepared at water contents ranging from dry to a maximum degree of saturation. Variations of ultrasonic velocity with degree of saturation and surcharge pressure were investigated (sections 9.6.1. and 9.6.2). A new technique was also developed to identify different soil strata (Section 9.6.3).

2.6. Summary of the Literature Review and Background

Two types of ultrasonic-based NDT methods for deep foundation quality control were presented, the Ultrasonic Echo Sounding (UES) test and the Cross-hole Sonic Logging (CSL) test. The past research work for each method was reviewed and a basic principle of stress wave propagation underlying the theory of the methods was described. The basis, the testing procedures, the data interpretation and the limitations of each method were presented. The combined applications of testing methods including those applied before (i.e. UES) and after (i.e. CSL) the concreting stage provide a better picture regarding the quality assurance of deep foundation concrete elements. In addition to the evaluation of concrete elements, soils were also involved in this study. The past research work for ultrasonic wave propagation in soils was reviewed.

3.1. Introduction to the Calibration and Verification Procedures of the Ultrasonic Echo Sounding Equipment

The Ultrasonic Echo Sounding (UES) testing method is able to provide effective diagnosis and inspection of drilled shafts characteristics (such as shaft verticality, shaft diameter, shaft depth, geometry and dimensions of the 'bell-out' at a shaft toe) at an early stage. Early detection of deviation from design allows timely correction of problems, elimination of construction time and reduction of overall construction cost. However, no document regarding the determination of the working performance of the UES equipment has been published.

In this research, the in-house developed calibration and verification procedures were developed to ascertain the real performance and behavior of UES equipment in different testing situations. The calibration work cover the *range and depth* parameters, while the verification work cover the effects of different densities of bentonite/slurry solutions, different angles of reflections (i.e. simulation of the 'bell-out' at a shaft toe) and different roughness of reflecting surfaces on the measured ranges (obtained from UES profiles) of a shaft.

In this chapter, the details of the in-house developed calibration and verification procedures of UES equipment are described. The analysis of uncertainties in the calibration work is outlined to provide a basis for the comparison among different measurement techniques.

3.2. Calibration Procedure of the Ultrasonic Echo Sounding Equipment

The purpose of the calibration work is to determine the real performance and accuracy of the UES equipment in terms of *range and depth* parameters. *Range* is the horizontal distance between the two ends of the surface walls of excavation shafts that can be measured by the distance between the two first received signals on UES profiles. *Depth* is the vertical distance that can represent the depth of excavation shafts.

3.2.1. *Range* Calibration

The reference steel tank (as shown in Figure 3.2.1) used in the *range* calibration and has a dimension of 4000mm (L along *X-X' direction/Y-Y' direction*) * 700mm * 600mm (H).

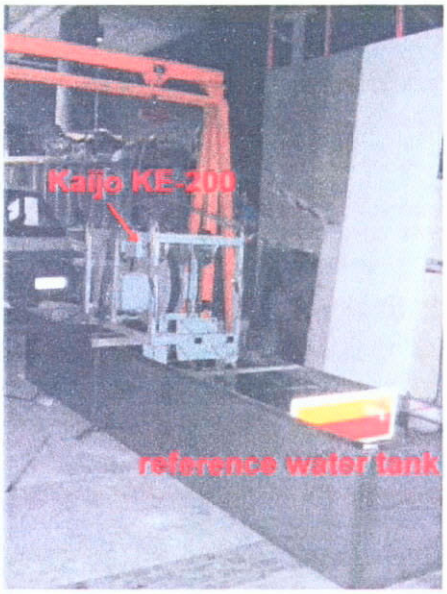

Figure 3.2.1. Photograph showing the reference steel tank in the *range* calibration

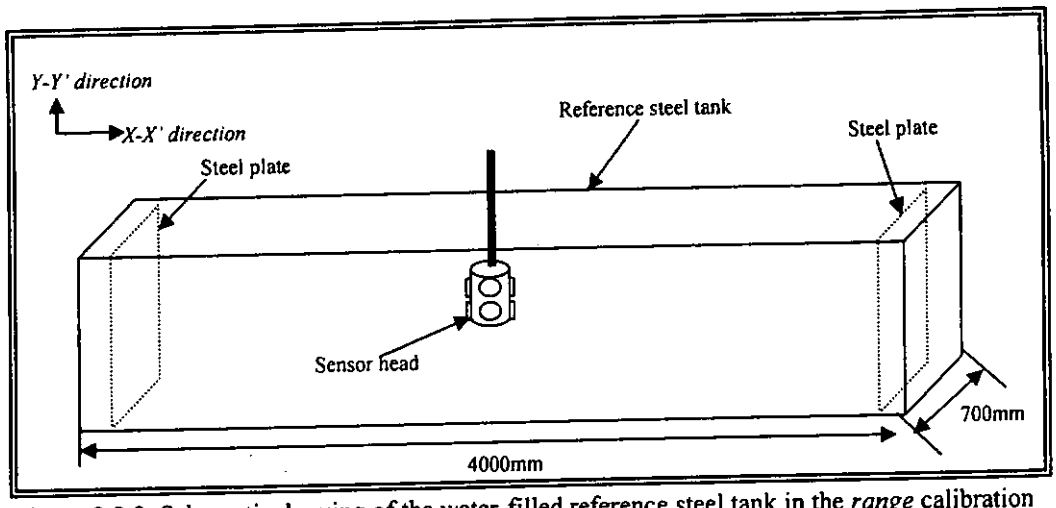

Figure 3.2.2. Schematic drawing of the water-filled reference steel tank in the *range* calibration

The *range* calibration was carried out at different horizontal dimensions ranging between 800mm and 3940mm at an interval of roughly 500mm. The reference steel tank was firstly filled with water to provide a propagation medium for ultrasonic wave transmission.

In Figure 3.2.2, the sensor head of the UES equipment was lowered into the water-filled reference steel tank until the whole sensor head was fully immersed in water. The sensor head was kept stationary at the calibration level. Two steel plates were put at each end of the tank to produce the first calibration range (i.e. 3940mm between the surfaces of the two steel plates). After the measurement at the first calibration range was obtained, the steel plates were moved towards the sensor head to produce the second one and so on until the measurement at the last calibration range (i.e. 800mm between the ends of the two steel plates) was obtained.

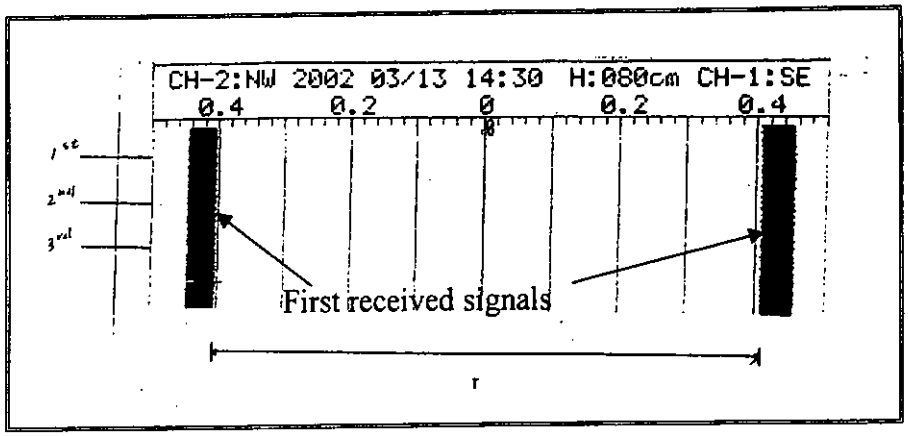

Figure 3.2.3. The UES profile (in *X-X' direction*) in the *range* calibration

Figure 3.2.3 shows the UES test result in the *range* calibration especially at the last calibration range. The two thick black lines are the first received signals reflected off the two steel plates put at each end of the tank. The horizontal distance between the two black lines is the *range* value r which also represents the horizontal distance between the surfaces of the two steel plates (i.e. the calibration range).

Three reading values of the *range* r were taken from each UES profile to get their average. The deviation/error was calculated by comparing the converted *range* value Ĺ with the independently measured dimension L of the reference steel tank (i.e. using an independent measuring tape) at each calibration range.

The sensor head of the UES equipment consists of the ultrasonic transmitters in two orthogonal directions (i.e. *X-X' direction* and *Y-Y' direction*) (Figure 2.3.5). After the measurements at all the calibration ranges in *X-X' direction* were obtained, the sensor head was turned to 90° to obtain that in *Y-Y' direction*.

Table 3.2.1 shows the average values of L (i.e. distance between two steel plates) and Ĺ (i.e. converted range value after the calculation of r*S), and the deviations/errors, derived by Equation 3.2.1, of the UES equipment at different calibration ranges in both *X-X' direction* and *Y-Y' direction*.

$$\text{Percentage of error} = \frac{(\acute{L} - L)}{L} * 100 \quad \text{(unit: \%)} \quad \text{--- (Equation 3.2.1)}$$

where $\acute{L} = r*S$ (unit: m)

Amongst the range of distances tested (i.e. 0.8 to 3.94m), the largest deviation/error of the UES equipment in both directions was found to be in the case of a calibration range (i.e. the separation between two steel plates) of 2m. The details of calculation and conversion in this *range* calibration exercise, and the UES profiles at different calibration ranges are given in Appendix A.

Table 3.2.1. Results in the *range* calibration

Distance of separation between two steel plates (±0.001m)	Scaling factor (S)	Test 1		Test 2		Test 3		Mean		Percentage of Error (%)
		L (m)	r (mm)	L (m)	r (mm)	L (m)	r (mm)	L (m)	Ĺ (m)	
		X-X' direction								
0.800	0.0074	0.81	109.8	0.80	109.8	0.81	109.8	0.807	0.81	0.73
1.000	0.0148	1.01	67.9	1.00	67.9	1.01	68.0	1.007	1.01	-0.12
1.500	0.0148	1.51	101.8	1.51	101.9	1.50	101.9	1.507	1.51	0.06
2.000	0.0296	2.00	68.4	2.01	68.3	2.01	68.3	2.007	2.02	0.80
2.500	0.0296	2.51	85.2	2.51	85.2	2.50	85.1	2.507	2.52	0.57
3.000	0.0296	3.00	101.6	3.01	101.7	3.00	101.7	3.003	3.01	0.20
3.500	0.0296	3.51	119.0	3.50	118.9	3.50	118.8	3.503	3.52	0.46
3.940	0.0592	3.94	67.1	3.95	67.0	3.94	67.0	3.943	3.97	0.63
Distance of separation between two steel plates (±0.001m)	Scaling factor (S)	*Y-Y' direction*								
0.800	0.0074	0.80	109.0	0.80	109.1	0.81	109.1	0.803	0.81	0.47
1.000	0.0148	1.01	68.0	1.01	68.1	1.00	68.0	1.007	1.01	0.02
1.500	0.0148	1.51	101.6	1.50	101.6	1.50	101.6	1.503	1.50	0.02
2.000	0.0296	2.00	68.3	2.01	68.4	2.01	68.4	2.007	2.02	0.85
2.500	0.0296	2.51	84.6	2.50	84.8	2.50	84.9	2.503	2.51	0.23
3.000	0.0296	3.01	102.1	3.00	102.0	3.01	102.0	3.007	3.02	0.45
3.500	0.0296	3.50	118.9	3.51	118.9	3.51	118.8	3.507	3.52	0.34
3.940	0.0592	3.94	67.2	3.94	67.1	3.94	67.0	3.940	3.97	0.82

Notes:
L = Distance between two steel plates which is measured by a calibrated measuring tape
r = Measured value on trace by a calibrated caliper
S = Scaling factor (to convert r into Ĺ) which is provided by the manufacturer
Ĺ = Converted range value (i.e. r*S)

3.2.2. *Depth* Calibration

The *depth* calibration includes a *theodolite approach* and a *measuring tape approach*. Two theodolites as shown in Figure 3.2.4 were used in the *depth* calibration. The steel hoisting cable (with the sensor head attached to one end and wound in a drum in the other end) was measured optically using the theodolites.

Figure 3.2.4. Two theodolites on the same plane in the *depth* calibration

The advantage of this technique is the elimination of the problem associated with any measurement technique involving tapes. The master/hoisting unit of the UES equipment was firstly hoisted to a high point by an overhead traveling crane (situated within The Hong Kong Polytechnic University campus) as shown in Figure 3.2.5. The cable was lowered from this top position to a series of predetermined depths. It was important to ensure that the hoisting cable and the two theodolites were aligned on the same plane (Figure 3.2.6)

Figure 3.2.5. The hoisting of the UES equipment to a high position within the campus of The Hong Kong Polytechnic University

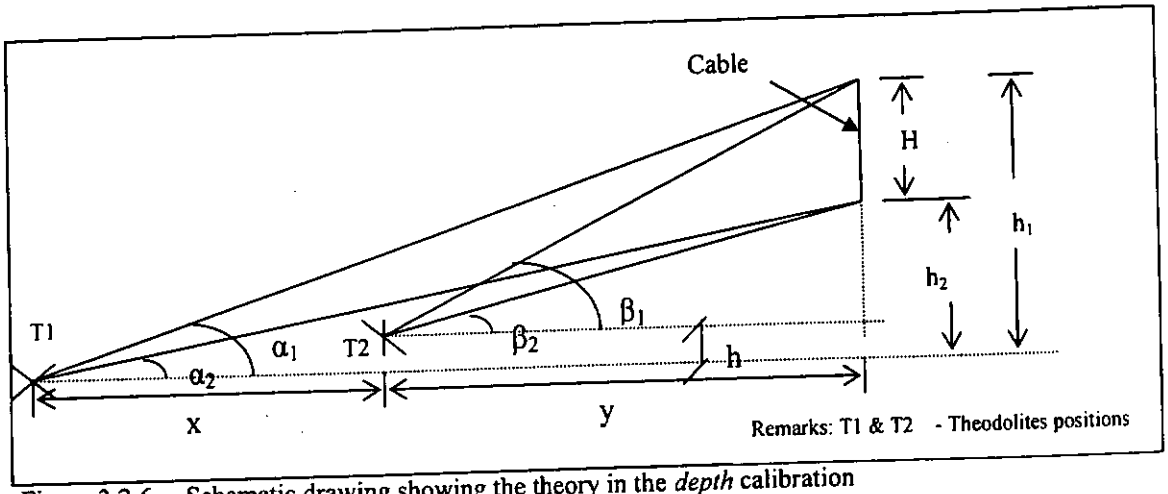

Figure 3.2.6. Schematic drawing showing the theory in the *depth* calibration

The theoretical principles underlying the hoisting (i.e. the theodolite approach) is explained by the followings:

$$h_1 = \frac{x\tan\alpha_1 \dfrac{h\tan\alpha_1}{\tan\beta_1}}{1-\dfrac{\tan\alpha_1}{\tan\beta_1}} \qquad \text{--- (Equation 3.2.2)}$$

$$h_2 = \frac{x\tan\alpha_2 \dfrac{h\tan\alpha_2}{\tan\beta_2}}{1-\dfrac{\tan\alpha_2}{\tan\beta_2}} \qquad \text{--- (Equation 3.2.3)}$$

$$H = h_1 - h_2 \qquad \text{--- (Equation 3.2.4)}$$

where $\alpha_1, \alpha_2, \beta_1, \beta_2$ are the theodolite readings ,
h_1 is the height of the theodolite T1 from the ground level,
h_2 is the height of the theodolite T2 from the ground level,
h is the height difference between two theodolites T1 & T2,
X is the horizontal difference between two theodolites,
Y is the horizontal difference between theodolite T2 and the cable,
H is the length of the cable.

Equation 3.2.4 calculates the length of the cable, denoted as H (as shown in Figure 3.2.6), which is then compared with the *display depth* (i.e. depth readings shown on

UES profiles). In addition to the *theodolite approach*, a separate measuring tape was also used to provide an auxiliary measure of the length of the cable (i.e. the *measuring tape approach*) as well.

Figures 3.2.7 and 3.2.8 show respectively the correlation between the *theoretical depth readings* (obtained in the *theodolite approach*) and *display depths*, and that between the *measuring tape readings* (obtained in the *measuring tape approach*) and *display depths*.

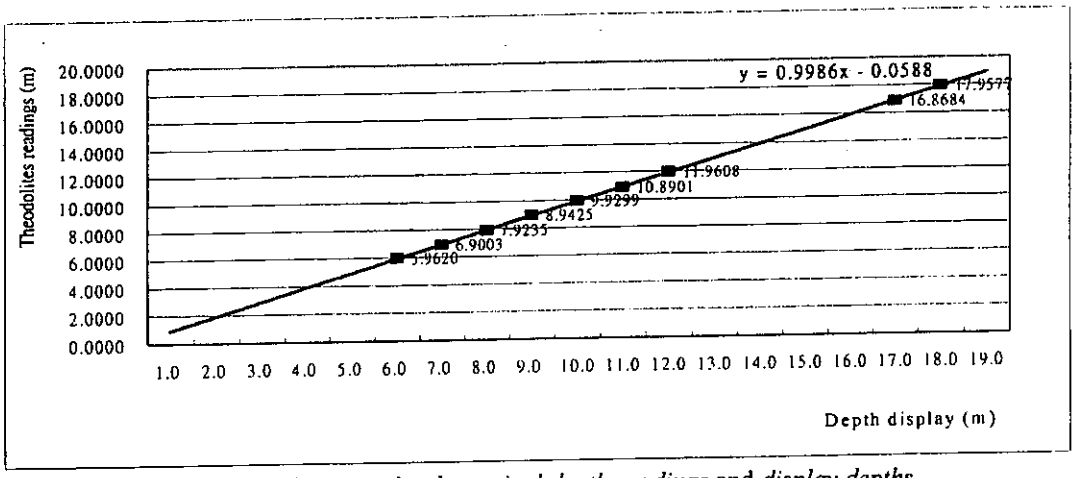

Figure 3.2.7. Correlation between the *theoretical depth readings* and *display depths*

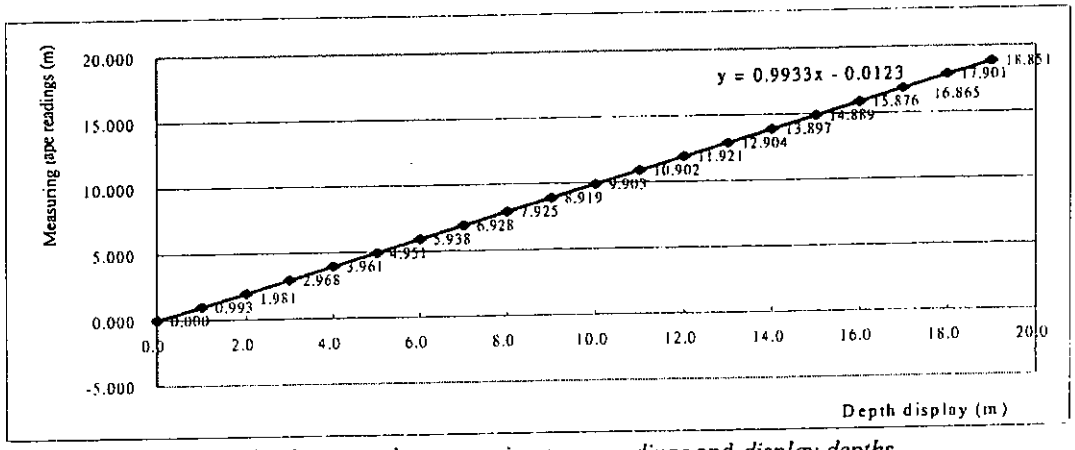

Figure 3.2.8. Correlation between the *measuring tape readings* and *display depths*

The *theoretical depth and measuring tape readings* are found to be different from the *display depths* (i.e. the depth readings shown on the UES profiles). This deviation suggests the *display depth* have to be corrected by a suitable correction factor. A possible reason for this depth deviation is properly due to the wearing out of the aluminum encoder wheel of the UES equipment. A theoretical treatment of this hypothesis is given as follows:

Let D be a brand new wheel diameter (at the first time of use) of the UES equipment;
an old worn wheel diameter of the UES equipment be $(D-\partial D)$ be d;
the length of the travel of the sensor head be ℓ.

After the cable has operated for a long time, the wheel is worn and its diameter becomes smaller (i.e. d which is smaller than D). Number of revolutions recorded by the recorder of the UES equipment should be

$$\frac{\ell}{\pi d}=n' \qquad \text{--- (Equation 3.2.5)}$$

However, the *display depth* is (by deriving Equation 3.2.5):

$$n'\pi D=\frac{\ell}{\pi d}(\pi D) \qquad \text{--- (Equation 3.2.6)}$$

Such that

$$\frac{\ell(\textit{theoretical reading})}{\ell(\textit{depth reading of the UES equipment})}$$

$$=\frac{\ell}{(\frac{\ell}{\pi d})(\pi D)} \qquad \text{--- (Equation 3.2.7)}$$

which is a constant.

From the theoretical derivation as shown above, the ratio of the 'true' depth (i.e. the actual up and down movement of the sensor head) to the *display depth* is a constant, denoted as C. C has the probable value of 0.99 as according to the results given in Figures 3.2.7 and 3.2.8. This is due to the problem of the wear-and-tear of the aluminum wheel of the UES equipment.

After prolong operation, the aluminum wheel of the UES equipment becomes smaller in diameter (i.e. the old worn wheel diameter). So, the number of results recorded by the UES equipment will produce a smaller value of D (i.e. a different D when a brand new wheel of a different diameter is used) in the depth computation. For this reason, the values of the *display depth* are always larger than the actual length comparing to the actual cable run.

3.2.3. Uncertainty analysis of the calibration

The calibration procedure in Sections 3.2.1 and 3.2.2 sets out the guidelines for determination of the real performance of the Ultrasonic Echo Sounding equipment (for the brand name 'Kaijo' or 'Koden'). Calibration is an important task, and the data presented in the measurement techniques therefore has to be accompanied by precision figures.

According to ISO Guide 17025, the estimation of calibration uncertainties is a requirement. The uncertainty analysis in this research work is based on "Guide to the Expression of Uncertainty in Measurement" (attached in

Appendix B) which is referred to in the following text as the ISO Guide.

The ISO Guide is seen as an appropriate chance to determine uncertainties as it was developed by a committee made up of experts from the Bureau International des Poids et Mesures (BIPM), the International Electrotechnical Commission (IEC), the International Organisation of Legal Metrology (OIML) and the International Standards Organisation (ISO). The ISO Guide is universal and presents a unified approach to uncertainty assessment in any kind of measurement.

The ISO Guide defines two categories of uncertainty components, Type A and Type B, which are distinguished by their methods of evaluation. Type A is evaluated by using standard statistical methods to analyze a set of measurements. Type B is evaluated by means other than the statistical analysis of series of observations. They include systematic errors that are due to inherent defects in the design, construction, or calibration of the devices or systems used. Some depend upon the environment, the observer or the measuring techniques. Both types of uncertainty components are characterized by an estimated variance or standard deviation, a mean value and a number of degrees of freedom.

Before the calculation of the uncertainty, a mathematical model has to be set up and the sources of the uncertainty components are required to be clearly identified. In the *range* calibration exercise, the major sources of uncertainty components lied with the uses of a caliper to measure the dimensions between two

first received signals on UES profiles, and a tape to measure the dimensions of the reference steel tank. It is worth pointing out that the measurement pertaining to the dimensions of the reference steel tank should be at the same water depth as the immersed sensor head. However, this requirement is difficult to achieve in practice.

Table 3.2.2. The uncertainty components in the *range* calibration

Source	Uncertainty components	Type	Unit	Semi-range (mm)	Standard uncertainty
L_{20}	Calibration uncertainty of measuring tape	B	m	0.002	0.001155
	Randomness	A	m	0.0058	0.004101
	Error of measuring tape	B	m	0.02	0.011547
	Resolution of measuring tape	B	m	0.0005	0.000289
r_{20}	Calibration uncertainty of caliper	B	mm	0.02	0.011547
	Randomness	A	mm	0.0889	0.062862
	Error of caliper	B	mm	0.02	0.011547
	Resolution of caliper	B	mm	0.005	0.002887

Table 3.2.2 shows the uncertainty components and the corresponding semi-range and standard uncertainty in the *range* calibration exercise. The details of this uncertainty analysis in the *range* calibration are given in Appendix C. The expanded uncertainty in the *range* calibration is determined after the calculations of the combined uncertainty and the effective degree of freedom as follows:

Combined uncertainty

$$= \sqrt{\begin{matrix}0.001155^2 + 0.004101^2 + 0.0011547^2 + 0.000289^2 + \\ (-0.0148)^2 * (2 * 0.011547^2 + 0.062862^2 + 0.002887^2)\end{matrix}} = 0.012349$$

Effective degree of freedom

$$= \frac{0.012349}{\left\{\frac{(0.01155+0.004101+0.0011547+0.000289)^4}{62.59} + \frac{(0.001547+0.062862+0.011547+0.002887}{4.58}\right\}}$$

$$= 63$$

With the use of the 'Student's distribution in statistics for 95% confidence' (attached in Appendix D), the coverage factor was 2.00 based on the effective degree of freedom value calculated previously. The expanded uncertainty in the range calibration is as follows:

$$= 2.00 * 0.012349$$

$$= 0.0247\text{m}$$

The expanded uncertainty in the *range* calibration was 0.0247m and also expressed in terms of percentages. These two values are used as a basis of comparison for better or worse performance when comparing different models of the UES equipment. The lower the two values, the higher the accuracy of the equipment is.

To perform the *depth* calibration, two approaches were applied. The method of determination of the expanded uncertainty in the *depth* calibration (i.e. for both approaches) is similar to those for the *range* calibration discussed previously.

For the *measuring tape approach*, the main source uncertainty

component arose from manually measuring with a tape. As for the *theodolite approach*, not only the measuring tape but also the theodolites played major roles in determining the uncertainty components. Appendices E and F respectively show the details of the uncertainty analysis in the *measuring tape approach* and the *theodolite approach*. Tables 3.2.3 and 3.2.4 define the uncertainty components for these two approaches.

Table 3.2.3. The uncertainty components in the *depth* calibration (the *measuring tape approach*)

Source	Uncertainty components	Type	Unit	Semi-range	Standard uncertainty
Re	Resolution of the depth indicator of the control logging unit	B	m	0.05	0.028868
	Randomness	A	m	0.05774	0.033336
M_{20}	Calibration uncertainty of measuring tape	B	m	0.001	0.000577
	Randomness	A	m	0.06	0.034641
	Error of measuring tape	B	m	0.04	0.023095
	Resolution of measuring tape	B	m	0.0005	0.000289

Table 3.2.3 shows the uncertainty components, the corresponding semi-range and standard uncertainty in the *depth* calibration (i.e. the measuring tape approach). The calculation of the expanded uncertainty in the *measuring tape approach* is as follows:

Combined uncertainty

$$= \sqrt{0.028868^2 + 0.033336^2 + 0.000577^2 + 0.034641^2 + 0.023095^2 + 0.000289^2} = 0.060650$$

Effective degree of freedom

$$= \frac{0.060650}{\left\{\frac{(0.028868+0.033336)^4}{6.01}+\frac{(0.000577+0.034641+0.023095+0.000289)}{4.14}\right\}} = 22$$

Again from the Student's distribution in statistics for 95% confidence, the coverage factor is 2.09 in this case. The expanded uncertainty is:

$2.09*0.060650 = 0.1268$m

Table 3.2.4 shows the uncertainty components, the corresponding semi-range and standard uncertainty in the *depth* calibration (i.e. the *theodolite approach*). The calculation of the expanded uncertainty in the *thedolite approach* is as follows:

Combined uncertainty

$$= \sqrt{\begin{matrix}0.000577^2+0.002615^2+0.023095^2+0.000289^2+0.000577^2+0.003343^2+0.023095^2+0.000289^2\\+2*(0.010046^2+0.030138^2+0.030254^2+0.005023^2)+0.010046^2+0.029849^2+0.030254^2\\+0.005023^2+0.010046^2+0.003926^2+0.030254^2+0.005023^2\end{matrix}}$$

$= 0.084118$

Effective degree of freedom

$$= \frac{0.084118}{\left\{\begin{matrix}\frac{(0.000577+0.002615+0.023095+0.000289)^4}{51.16}+\frac{(0.000577+0.003343+0.023095+0.000289)^4}{51.63}\\+\frac{(0.010046+0.030138+0.030254+0.005023)^4}{8.85}+\frac{(0.010046+0.030138+0.030254+0.005023)^4}{64.93}\\+\frac{(0.010046+0.029849+0.030254+0.005023)^4}{9.02}+\frac{(0.010046+0.003926+0.030254+0.005023)^4}{65.36}\end{matrix}\right\}}$$

$= 114$

From the Student's distribution in statistics for 95% confidence, the coverage factor is 1.98 in this case. The expanded uncertainty as follows:

$$1.98*0.084118 = 0.1666\text{m}$$

Table 3.2.4. The uncertainty components in the *depth* calibration (the *theodolite approach*)

Source	Uncertainty components	Type	Unit	Semi-range	Standard uncertainty
X	Calibration uncertainty of measuring tape	B	m	0.001	0.000577
	Randomness	A	m	0.00453	0.002615
	Error of measuring tape	B	m	0.04	0.023095
	Resolution of measuring tape	B	m	0.0005	0.000289
h	Calibration uncertainty of measuring tape	B	m	0.001	0.000577
	Randomness	A	m	0.00579	0.003343
	Error of measuring tape	B	m	0.04	0.023095
	Resolution of measuring tape	B	m	0.0005	0.000289
$\tan\alpha_1$	Calibration uncertainty of theodolites	B	-	0.0174	0.010046
	Randomness	A	-	0.0522	0.030138
	Error of theodolites	B	-	0.0524	0.030254
	Resolution of theodolites	B	-	0.0087	0.005023
$\tan\alpha_2$	Calibration uncertainty of theodolites	B	-	0.0174	0.010046
	Randomness	A	-	0.0054	0.030138
	Error of theodolites	B	-	0.0524	0.030254
	Resolution of theodolites	B	-	0.0087	0.005023
$\tan\beta_1$	Calibration uncertainty of theodolites	B	-	0.0174	0.010046
	Randomness	A	-	0.0517	0.029849
	Error of theodolites	B	-	0.0524	0.030254
	Resolution of theodolites	B	-	0.0087	0.005023
$\tan\beta_2$	Calibration uncertainty of theodolites	B	-	0.0174	0.010046
	Randomness	A	-	0.0068	0.003926
	Error of theodolites	B	-	0.0524	0.030254
	Resolution of theodolites	B	-	0.0087	0.005023

Based on the above calculations, the calibration uncertainties of the two approaches (the *measuring tape approach* and the *theodolite approach*) were determined and compared. The expanded uncertainty in the *measuring tape approach* is 0.1268m whereas 0.1666m in the *theodolite approach*. As a result, the *measuring tape approach* is more accurate because of its smaller expanded uncertainty value.

3.3. Verification Procedure of the Ultrasonic Echo Sounding Equipment

The verification aims to investigate the working performance of the UES equipment in different testing situations. The verification work quantifies the effects of different densities of bentonite/slurry solutions, different angles of reflections (i.e. simulation of the 'bell-out' at a shaft toe) and different extents of horizontal projections (i.e. simulation of rough reflecting surfaces of a drilled shaft) on the measured ranges (obtained from UES profiles) of a drilled shaft.

3.3.1. Simulation of bentonite/slurry solutions

In performing an UES test, a test drilled shaft is required to fill with water (to obtain good coupling) for ultrasonic wave propagation. In the case of diaphragm walls, bentonite/slurry solutions are sometimes filled in the shafts rather than only water. Bentonite/slurry solutions can provide a supportive pressure to the surrounding soil and also act as a medium for ultrasonic wave propagation (Section 2.3.2). There is a need to verify the behavior of the UES

equipment in different densities of bentonite/slurry solutions.

The range of bentonite/slurry density under investigation is between 1001 and 1032 kg/m^3 (close to pure water with density of 1000 kg/m^3). Normally, the concentration used in the field is circa 1000kg/m^3. The different densities of bentonite/slurry solutions used in the verification are known by using a hydrometer. In order to obtain more information of bentonite/slurry solutions involved, other independent checks (i.e. an electrical conductivity value and a pH value) on the bentonite/slurry solutions involved were carried out. The full range sensitivity settings (i.e. signal-to-noise ratio (SNR)) of the UES equipment were investigated in different densities of bentonite/slurry solutions.

Bentonite has the property of being hydrophilic, or water swelling, it is known that some clay can absorb as much as 5 times its own weight of water composition. Analysis of bentonite from various sources are found to vary from 54% to 69% silica, 13% to 18% alumina, 2% to 4% ferric oxide, 0.12% to 3.5% ferrous oxide, to 2.2% lime, 1.8% to 3.6% magnesia, 0.1% to 0.6% titania, 0.5% to 2% soda, and 0.14% to 0.46% potash. Soda (i.e. sodium hydroxide) and potash (potassium hydroxide) are known to be good conductors of the electric current and apply Ohm's law (E=IR). Na^+, K^+ and $0H^-$ are the main conductive ions in bentonite solutions. For those bentonite consists of high concentration of lime (i.e. more alkaline), higher bentonite powder is dissolved, and higher electrical conductivity and pH values are obtained. In the foundation industry, an Ultrameter and a pH-meter respectively are used for controlling and ascertaining

the correct concentration of bentonite/slurry solutions.

During the verification process, the sensor was kept stationary and the value of SNR was adjusted from the smallest one (i.e. 0.5) to the largest one (i.e. 8.0). By comparing the UES profiles (obtained at various SNR in each density of bentonite solution) with the actual dimension of the reference steel tank, the deviations were determined.

Table 3.3.1. Verification results in different concentration/densities of bentonite/slurry solutions

	Density of mixture (kg/m^3)	pH value	Conductivity (microsiemen /cm)	Proper sensitivity setting (SNR)
Mixture 1	1001-1002	9.30-9.52	300-399	1.0-4.0
Mixture 2	1004-1005	9.78-9.82	400-499	1.0-5.0
Mixture 3	1008-1009	10.00-10.06	500-599	1.0-5.0
Mixture 4	1014-1015	10.07-10.08	600-699	2.0-7.0
Mixture 5	1025-1026	10.13-10.16	700-799	6.0-8.0
Mixture 6	1031-1032	10.19-10.22	800-899	Signals obtained were too weak and noisy, therefore the proper sensitivity setting can't be determined.

Table 3.3.1 indicates that the UES equipment can work properly in a bentonite/slurry solution with density up to 1026(kg/m^3), and the corresponding proper sensitivity settings for each density of bentonite/slurry solutions were given. For bentonite solutions with higher density and conductivity (i.e. more than 1026(kg/m^3) and 800(microsiemens/cm) respectively), the use of the UES equipment was not recommended. Experience from these tests also shows that no significant change was found in pH and flow values in different densities of bentonite/slurry solutions. Therefore, it is difficult to evaluate quantities of

bentonite/slurry solutions using pH and flow measurements.

3.3.2. Simulation of 'bell-out' at a shaft toe

The UES equipment is designed especially for the 'bell-out' measurement at a shaft toe. Verification of the UES equipment in different angles of reflections determines its effectiveness in measuring a 'bell-out'. This is achieved using a pre-fabricated angle reflector (shown in Figure 3.3.1). The angle between two steel plates in the angle reflector can be adjusted, which simulates the 'bell-out' at a shaft toe. The performance of the UES sensors was verified at different angles (i.e. started from 75^{o} to 30^{o} with reference to the horizontal level) until the 'bell-out' shape could not be displayed clearly on UES profiles.

Figure 3.3.1. Photograph of the pre-fabricated angle reflector or simulation of 'bell-out' at a shaft toe

Table 3.3.2. Verification results in different angles of reflections

Angle of reflector (with reference to the horizontal level)	Receiver in Channel 1 (R_1)	Receiver in Channel 2 (R_2)	Receiver in Channel 3 (R_3)	Receiver in Channel 4 (R_4)
75°	Identified	Identified	Identified	Identified
60°	Identified	Identified	Identified	Identified
45°	Identified	Identified	Identified	Identified
30°	Identified	Identified	Identified	Identified
< 30°	Not identified	Not identified	Not identified	Not identified

Remarks: Identified – The UES equipment can identify the profile of a reflection angle.
Not identified – The UES equipment cannot identify the profile of a reflection angle.

Table 3.3.2 shows the verification results at different reflection angles (i.e. 75°, 60°, 45° and 30° with reference to the horizontal level) for all four sensors (ultrasonic receivers R_1 to R_4) in four channels (Figure 2.3.5). The ultrasonic receivers, R_1 to R_4, cannot identify shaft profiles for the reflection angles smaller than 30°. Figure 3.3.2 to 3.3.5 show examples of the verification results especially for the sensor R_1. The 'bell-out' shape appears clearly at the larger angles (for angles 75°, 60° and 45°) but is barely visible for smaller angles (i.e. less than 30°). Based on these experimental results, the effectiveness of the UES equipment for the 'bell-out' measurement is limited to angles larger than 30° with reference to the horizontal level. The results of other sensors, R_2 to R_4, are given in Appendix G.

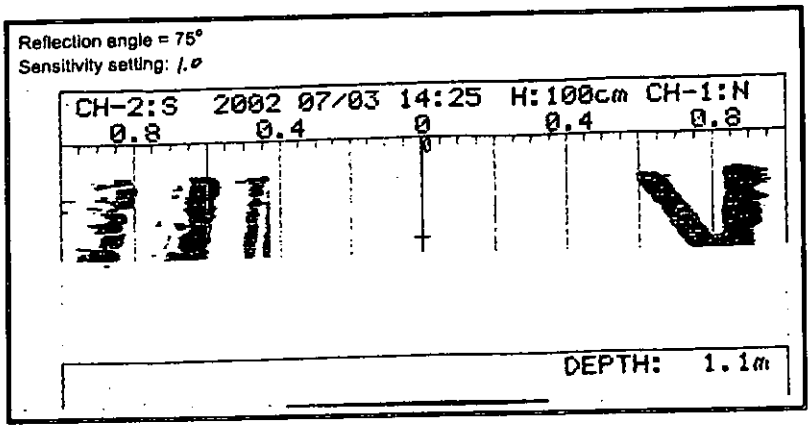

Figure 3.3.2. The UES profile at the reflection angle 75° in Channel 1

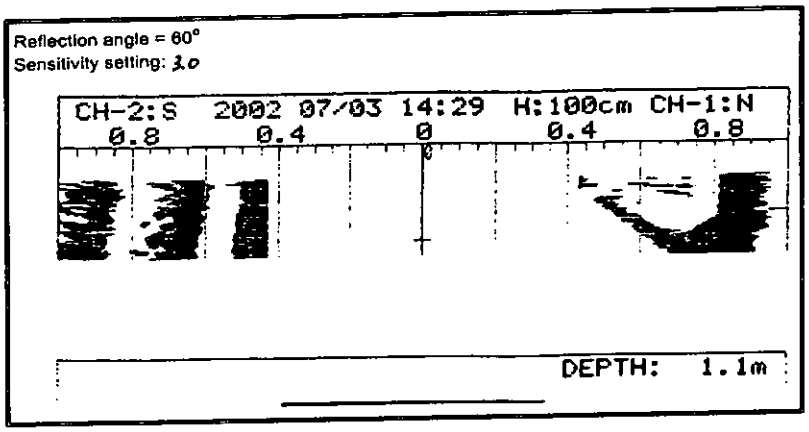

Figure 3.3.3. The UES profile at the reflection angle 60° in Channel 1

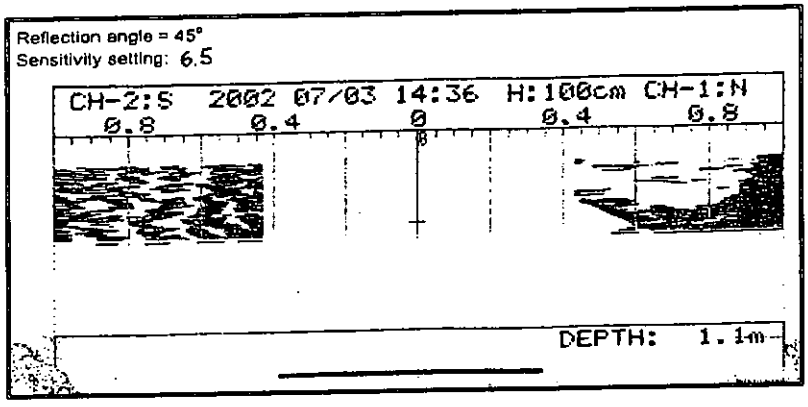

Figure 3.3.4. The UES profile at the reflection angle 45° in Channel 1

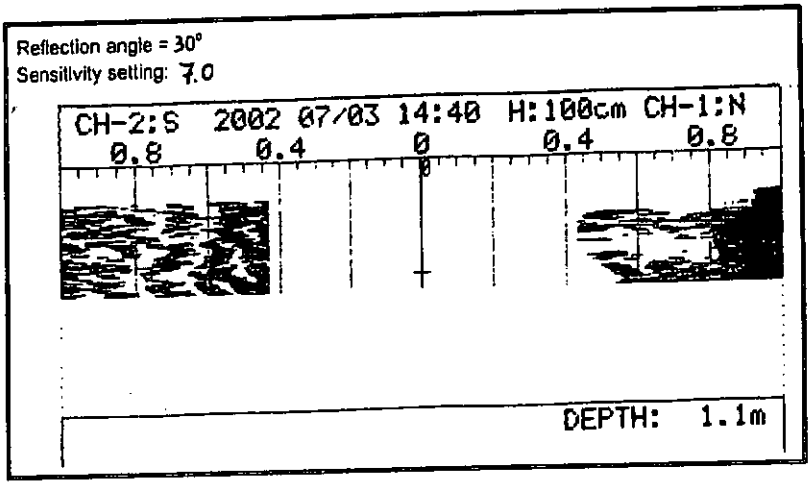

Figure 3.3.5. The UES profile at the reflection angle 30° in Channel 1

3.3.3. Simulation of roughness of reflecting surfaces

To determine the limitation of the UES equipment in the horizontal measurement, a pre-fabricated steel assembly (as shown in Figure 3.3.6) with adjustable projections was constructed to simulate profile variations of reflecting surfaces of a drilled shaft. Two rectangular steel plates (150mm*100mm) were fixed on the surface of a steel block and projected at different distances (i.e. 200mm, 150mm, 100mm, 50mm and 25mm from the surface of the steel block).

During the verification process, a sensor head of the UES equipment was lowered to a water-filled water tank with the prefabricated steel assembly inside. These tests were performed with different projection distances (i.e. ranging from 200mm to 25mm at an interval of 50mm/25mm).

Figure 3.3.6. Photograph of the prefabricated steel assembly for simulation of rough reflecting surfaces of a drilled shaft

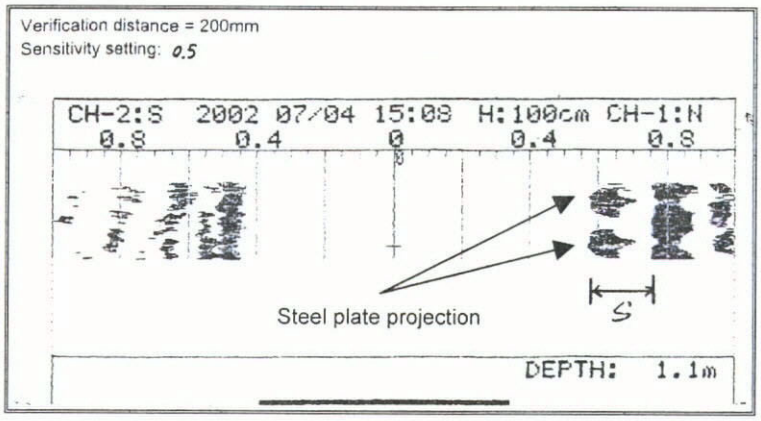

Figure 3.3.7. The UES profile showing the projection of the steel plates at 200mm from the surface of the steel block

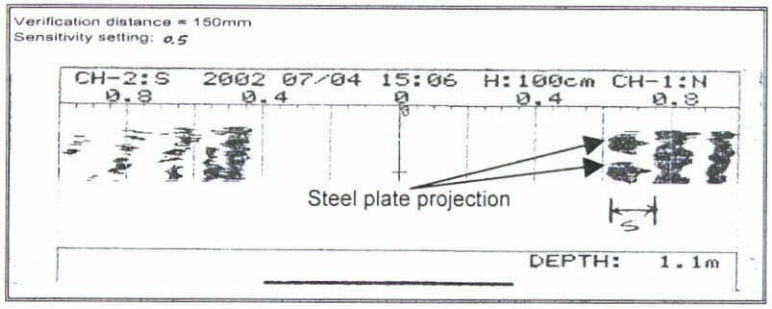

Figure 3.3.8. The UES profile showing the projection of the steel plates at 150mm from the surface of the steel block

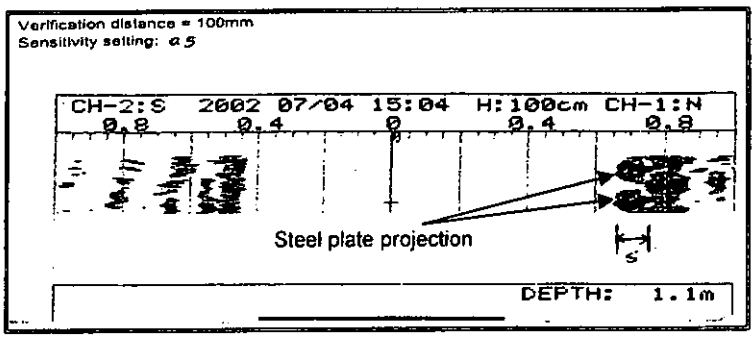

Figure 3.3.9. The UES profile showing the projection of the steel plates at 100mm from the surface of the steel block

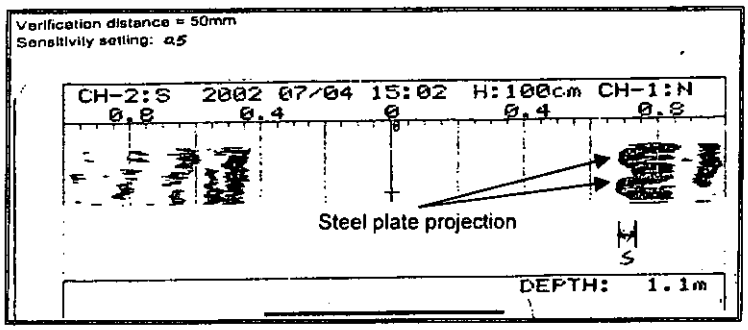

Figure 3.3.10. The UES profile showing the projection of the steel plates at 50mm from the surface of the steel block

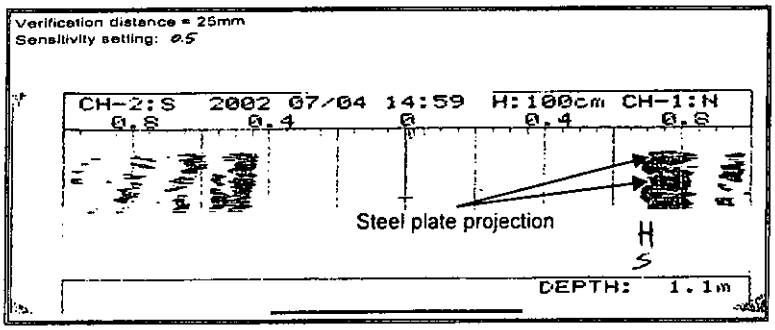

Figure 3.3.11. The UES profile showing the projection of the steel plates at 25mm from the surface of the steel block

Figures 3.3.7 to 3.3.11 show examples of the UES profiles (especially for the ultrasonic sensor in Channel 1) with different projections of the steel plates. The projections (i.e. the distance between the edge of the steel plates and the surface of the steel block) were measured on the UES profiles and denoted as s.

Table 3.3.3. The verification results in different projections for all the sensors

Projection (±1mm)	Ultrasonic sensor in Channel 1		Ultrasonic sensor in Channel 2		Ultrasonic sensor in Channel 3		Ultrasonic sensor in Channel 4	
	Measured value s (mm)	Error (mm)	Measured value s (mm)	Error (mm)	Measured value s (mm)	Error (mm)	Measured value s (mm)	Error (mm)
200	191.8	-8.2	184.6	-15.4	181.7	-18.3	184.4	-15.6
150	139.9	-10.1	143.4	-6.6	145.6	-4.4	137.1	-13.0
100	99.9	-0.1	94.3	-5.7	103.2	3.2	91.0	-9.0
50	55.6	5.6	55.9	5.9	53.4	3.4	50.8	0.8
25	26.3	1.3	30.3	5.3	27.5	2.5	21.8	-3.2
<25	Cannot be discerned by the sensors							

Note: s = converted projection value measured on the UES profiles

Table 3.3.3 summarizes the measured projection values s and the corresponding errors in different projections for all the sensors (from Channel 1 to Channel 4). All sensors are capable of identifying the projections of the steel plates until the projection is less than 25mm with reference to the horizontal level. The UES profiles in the other channels are given in Appendix H. As according to the experimental results, the horizontal resolution of the UES equipment is limited to 25mm.

3.4. Summary of the Calibration and Verification Procedures of the Ultrasonic Echo Sounding Equipment

The Ultrasonic Echo Sounding (UES) testing technique is used to assess the construction of drilled shaft foundations (including shaft verticality, shaft diameter, shaft depth, geometry and dimensions of 'bell-out' at a shaft toe) at an early stage. UES for quality control of bored piles will soon be recognized as an industry standard. But before that recognition becomes a reality, the work recorded here in calibrating and verifying UES equipment is considered instrumental and crucial.

This chapter describes the in-house developed calibration and verification procedures that shed some lights on the performance of the UES equipment in different working situations. *Range and depth* are the major concerns in the calibration work. *Range* is the horizontal distance between the two sides of the surface walls of excavation shafts that can be measured by the distance between the two first received signals on the UES profiles. *Depth* is the vertical distance that represents the depth of excavation shafts. With the expression of calibration uncertainties (in both the *range and depth* parameters), the reliability of different measurement techniques can be assessed and compared. For the *depth* calibration in this work, the *measuring tape approach* is more accurate than the *theodolite approach* in terms of the value of the calibration uncertainty calculated.

In the verification work, the effects of different densities of bentonite/slurry solutions, different angles of reflections (i.e. simulation of the 'bell-out' at a shaft toe) and different rough reflecting surfaces on the measured ranges (obtained from UES profiles) of a drilled shaft were investigated.

Based the experimental results, the UES equipment (applied in this research) work properly in the bentonite/slurry solutions (with density not higher than 1026(kg/m^3) or the electrical conductivity not higher than 800(microsiemens/cm)). The effectiveness of the 'bell-out' measurement of the UES equipment is limited to 30^o with reference to the horizontal level. And the horizontal measurement fineness of the UES equipment is limited to 25mm with reference to the horizontal level.

These calibration and verification procedures have been adopted by the Hong Kong Laboratory Accreditation Scheme (HOKLAS) as a basis for accreditation of the commercial laboratories specializing UES tests.

The successful application of the UES testing technique is demonstrated by carrying out the extensive investigation, and the results are presented in Section 5.3.

4.1. Introduction to the Effects of Different Sonic Access Tube Materials on Signal Strength

Proper installation of sonic access tubes (including the use of suitable materials, a good bonding to concrete surface, the use of sufficient numbers and a proper arrangement) is a key factor in performing a CSL test. Sonic access tubes provide the measurement accesses for ultrasonic probes to travel along a foundation concrete element, and also act as containers for water (i.e. a coupling medium) within them (Section 2.4.2).

The effects of different sonic access tube materials on the signal strength of ultrasonic waves were investigated by the use of the in-house developed multi-channel ultrasonic data acquisition prototype called the 'Multiple Referencing System' (MRS). The details of the construction and development of the in-house MRS is described in Section 7.2.

This chapter describes a series of experiments investigating the effects of different sonic access tube materials on the signal strength of ultrasonic waves. These experiments covered polyvinyl chloride (PVC) and steel sonic access tubes of different diameters and thickness, which are considered to have an effect on signal transmission.

4.2. Experimental Procedures and Signal Processing

The tests were conducted using a through-transmission test methodology

(i.e. a pair of probes kept at a distance and maintained at the same level). Figure 4.2.1 shows the experimental set-up in which one probe was located within a sonic access tube and the other was in direct contact with water inside a water tank. The ultrasonic waves emitted from the transmitting probe passed through the water (which acted as a coupling), then through the wall of the sonic access tube and were finally picked up by the receiving probe. Table 4.2.1 shows the physical properties of different sonic access tubes investigated in these experiments. Amongst these materials, three sonic access tubes were made of PVC and the others of steel of different diameters and wall thickness as depicted from Table 4.2.1.

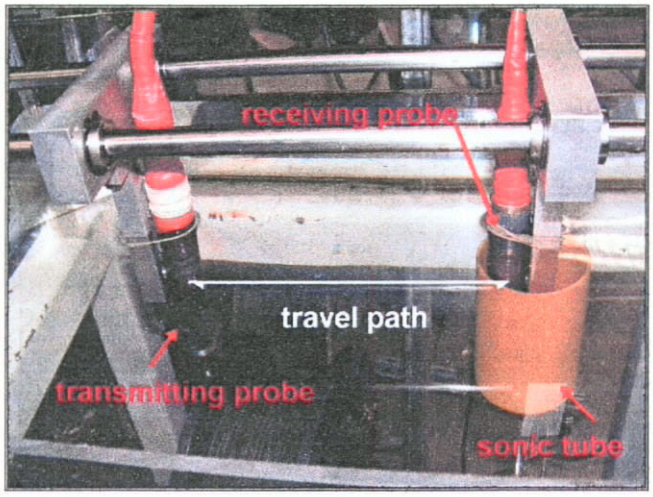

Figure 4.2.1. Photograph of the experimental set-up showing the transmitting probe in direct contact with water and the receiving probe inside the test sonic access tube in the water tank.

Table 4.2.1. Physical properties of the test sonic access tubes

Sonic access tube		Material	Transmission path (probe to probe, center to center)
External diameter (mm)	Internal diameter (mm)		
38	34	PVC	200mm
68	66		
110	102		
42	35	Steel	
60	50		
165	155		

The *travel time* for the ultrasonic waves to be picked up by the receiving probe was called the *first-arrival-time* (FAT). FAT was determined as the time difference between the time of initiation of the triggered pulse from the transmitting probe and the time of arrival of the first pulse at the receiving probe (as shown in Figure 7.2.10). The *apparent transmission velocity* of the ultrasonic waves was obtained as the ratio of the travel path (distance between two probes) to FAT.

For each experimental run, three sets of signal waveforms were recorded. The average of these three waveforms was then utilized for further processing. Based on a purpose-developed program under the LabVIEW environment (i.e. written on a *Virtual Instrument* platform), the FAT and signal strength of the signal waveforms were determined. Figure 4.2.2 shows a typical time trace of ultrasonic waveforms used for the calculation of signal strength by the successive summation of partial areas of an acquired waveform (Section 7.3). The signal strength calculated (i.e. area under the curve bounded by the curve and the x-axis in Figure 4.2.2) is the amount of the ultrasonic energy transmitted in a transmission medium and picked up by the receiving probe.

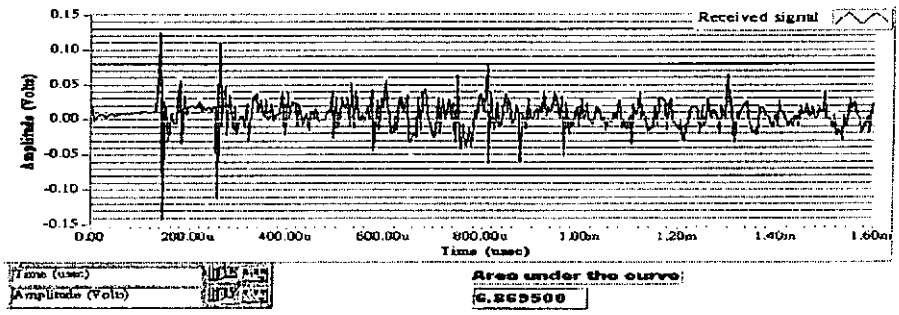

Figure 4.2.2. Diagram showing the time trace of a typical ultrasonic waveform used for the calculation of strength of the signal waveform.

4.3. Results and Discussion

Variation of transmission velocity with the use of different sonic access tubes is presented in Figure 4.3.1. According to the values depicted in this figure, the variation is found to be insignificant for all the sonic access tubes tested. The *apparent transmission velocities* determined in these experiments range from 1480 to 1600 m/s, which is in good agreement with the values for ultrasonic transmission in water (represented by a dotted line in Figure 4.3.1) (Sansalone et al. 1991).

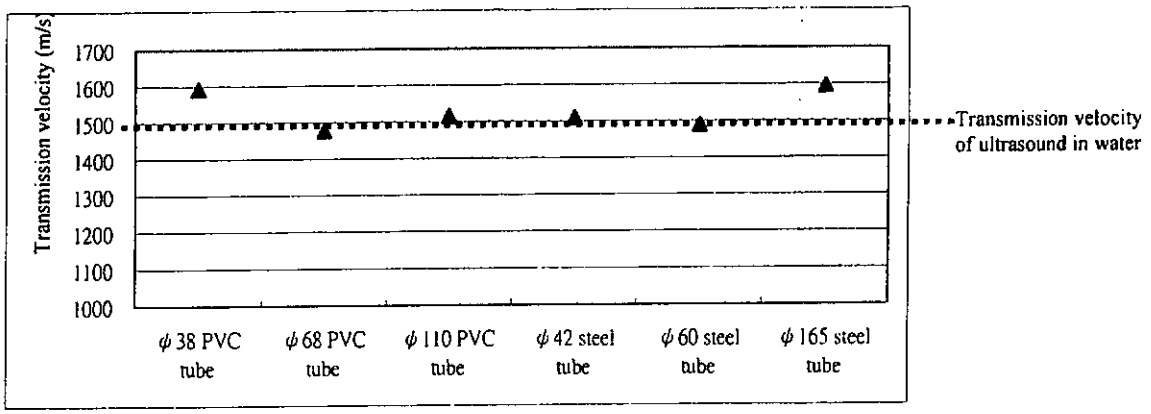

Figure 4.3.1. Variation of transmission velocity with the use of different sonic access tubes

In addition to the transmission velocity, the signal strength of the signal waveforms was also determined. Figure 4.3.2 shows the variation of signal strength with the use of different sonic access tubes. This variation is found to change considerably according to the materials used. Higher values of signal strength are obtained with PVC than with steel sonic access tubes. It is also found that the signal strength increases with increasing sonic access tube diameter for each of the materials tested (i.e. PVC and steel). This phenomenon is believed to

be attributable to the effect of the curved wall surface of the sonic access tubes, which act very much the same way as a convergent lens, as shown in Figure 4.3.3. In a larger-diameter sonic access tube, greater signal strength is collected by the larger surface wall of the tube.

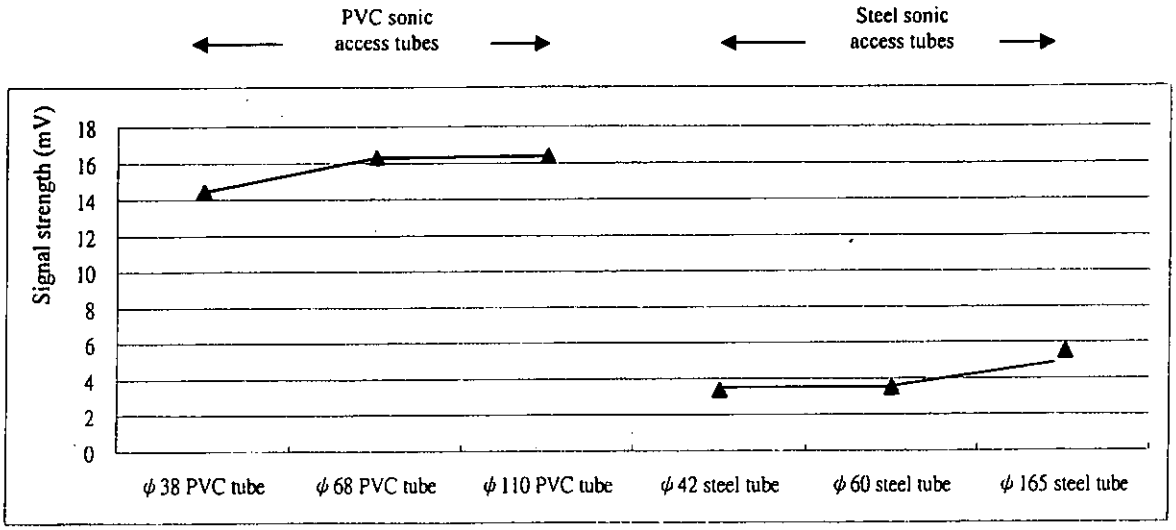

Figure 4.3.2. Variation of signal strength with the use of different sonic access tubes

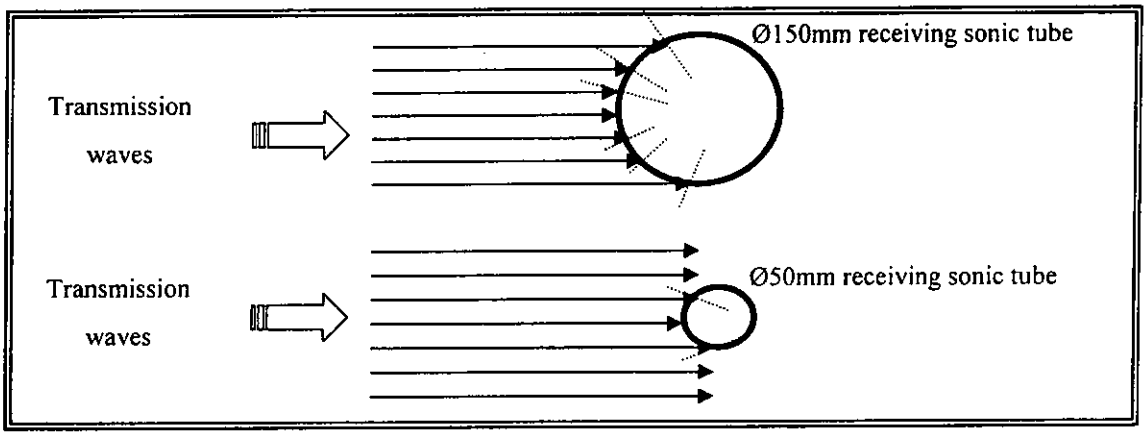

Figure 4.3.3. Effects of the curved wall surface of sonic access tubes

The signal strength obtained when using PVC sonic access tubes is obviously higher than those when using steel sonic access tubes. This phenomenon is explainable in terms of the difference in acoustic impedance across the water/PVC and water/steel interfaces. As a result of this difference, an

ultrasonic beam partially transmits across the interface and partially reflects back towards the source (as shown in Figure 2.2.5).

Table 4.3.1 shows the transmission factors at different material boundaries for a normally incident wave from medium 1 to medium 2. The acoustic impedance value of PVC (i.e. 2.5×10^6 kg/m^{2}s) is similar to that of water (i.e. 1.5×10^6 kg/m^{2}s), while steel has a higher acoustic impedance value (i.e. 46×10^6 kg/m^{2}s). Typical flow paths of ultrasonic wave transmission in the cases of PVC and steel sonic access tubes are shown in Figure 4.3.4.

Table 4.3.1. Theoretical transmission coefficients at different material boundaries for a normally incident wave from medium 1 to medium 2

	Material in medium 2 (Z_B)	**Steel**	**PVC**	**Water**
Material in medium 1 (Z_A)	**Acoustic impedance (x10^6 kg/m^{2}s)**	**46**	**2.5**	**1.5**
		Transmission coefficient		
Steel	**46**	*1*	*0.1*	*0.06*
PVC	**2.5**	*1.9*	*1*	*0.75*
Water	**1.5**	*1.94*	*1.25*	*1*

With PVC tubes:
Transmitting probe → water → PVC tube → water → Receiving probe

With steel tubes:
Transmitting probe → water → Steel tube → water → Receiving probe

Figure 4.3.4. Typical flow paths of the ultrasonic wave transmission

Based on the transmission coefficients at water and PVC boundaries as shown in Table 4.3.1, the overall transmission factor using PVC sonic tubes (T_P) is as follows (i.e. a smaller reflection):

$$T_P = 1.25 * 0.75 = 0.94 \quad \text{--- (Equation 4.3.1)}$$

On the other hand, the overall transmission coefficient when steel tubes (T_S) are used is comparatively lower and shown in the following (i.e. a larger reflection):

$$T_S = 1.94 * 0.06 = 0.12 \quad \text{--- (Equation 4.3.2)}$$

The calculations depicted in Equations 4.3.1 and 4.3.2 clearly show that the overall transmission coefficient using PVC sonic access tubes is higher due to the small difference in the value of acoustic impedance between PVC and water. However, the use of steel sonic access tubes is more common than that of PVC sonic access tubes because the external surface of PVC tubes is very smooth and difficult to wet. For this reason, there is a risk of poor bonding between PVC sonic access tubes and concrete, or a risk of delamination. As a result, gaps are produced between concrete and PVC sonic access tubes causing difficulties with the ultrasonic wave transmission. In contrast, steel tubes bond well to concrete, and can serve a similar function as main reinforcing bars (Finno 1997). Although the high value of the acoustic impedance of steel tubes leads to a larger reflection of signal than when PVC tubes are used, the steel tubes are still preferable.

The sonic profile in Figure 4.3.5 illustrates the effect of using a

larger-diameter (i.e. about 150mm diameter) sonic access tube in performing a CSL test, as the probes can move around inside it. This occurrence is usually identified by irregular zones of CSL profiles. (i.e. unclear and fuzzy successions of black and white stripes or even outright discontinuity) even though no artificial defect is presented inside the test bored pile.

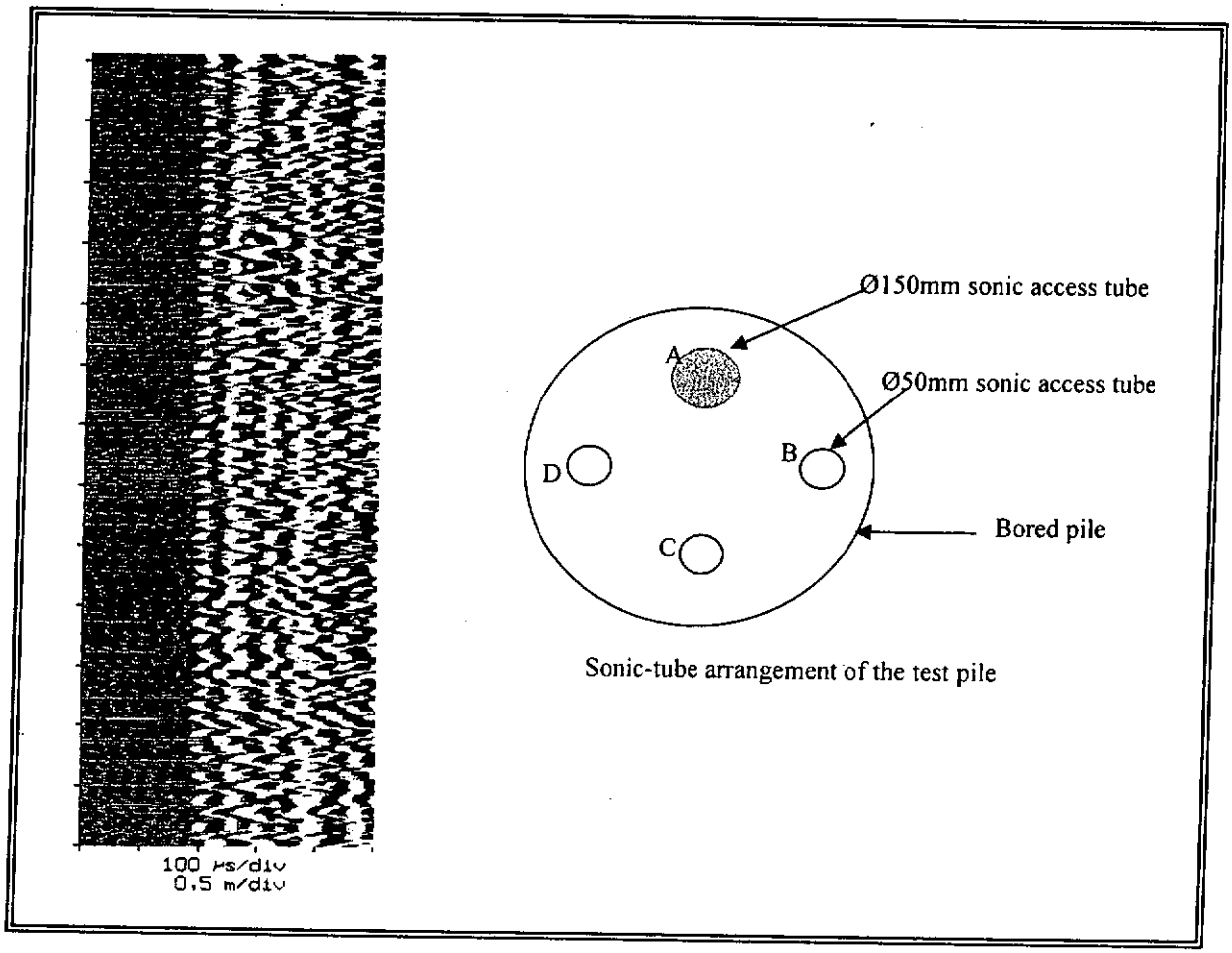

Figure 4.3.5. Sonic profile showing unclear and fuzzy successions of the white and black stripes

This phenomenon is explained by using the experimental set-up (in Figure 4.2.1) with a steel sonic access tube of 165mm-diameter. Three received waveforms were obtained at three different positions of the receiving probe as shown in Figures 4.3.6a to 4.3.6d.

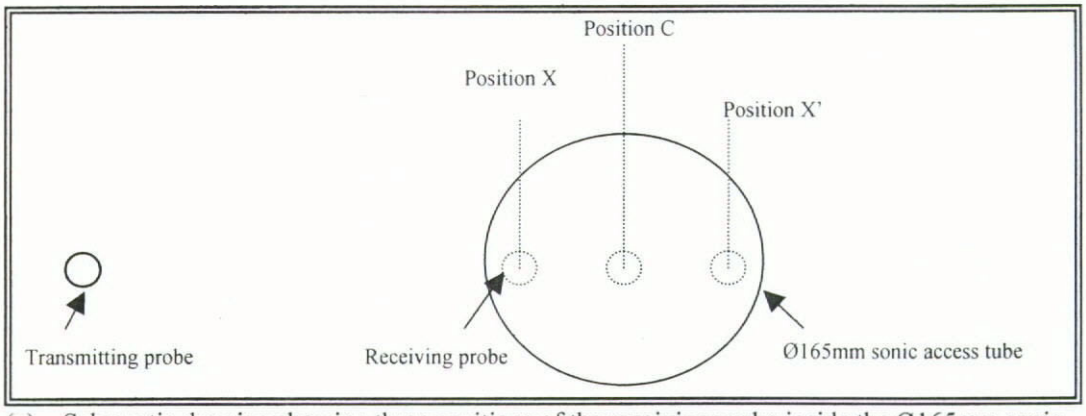

(a) Schematic drawing showing three positions of the receiving probe inside the Ø165mm sonic access tube

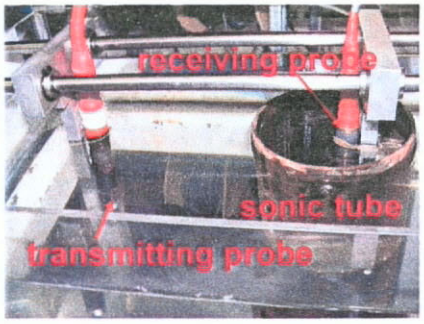

(b) The receiving probe at position C

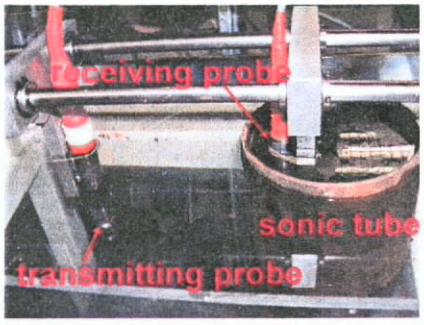

(c) The receiving probe at position X

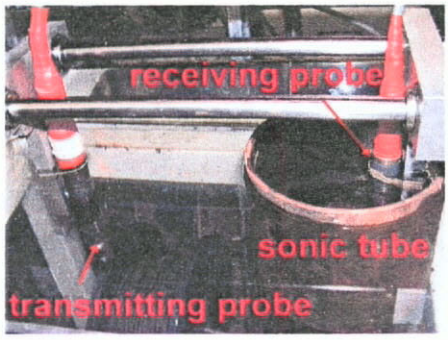

(d) The receiving probe at position X'

Figure 4.3.6. Three different positions of the receiving probe inside the Ø165mm sonic access tube

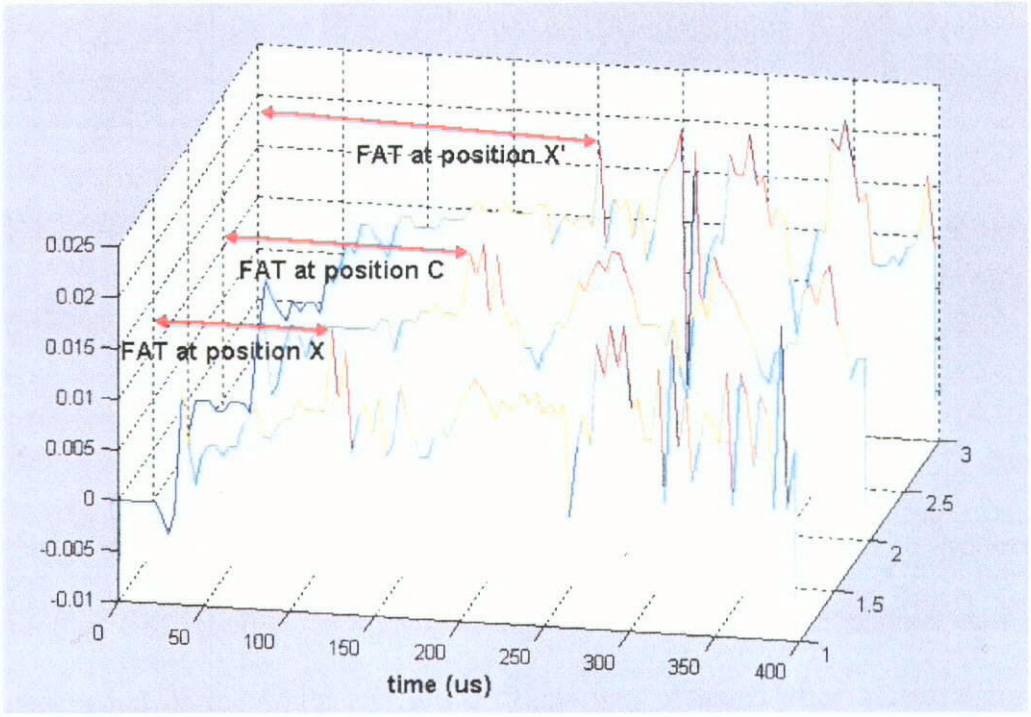

Figure 4.3.7. Variation of FAT at different positions of the receiving probe inside the larger sonic access tube

Figure 4.3.7 shows different FATs when the receiving probe was at positions X, C and X'. In fact, the receiving probe at position X was positioned comparatively closer (i.e. hence a smaller FAT) than that at positions C and X'. The use of a larger-diameter sonic access tube is not recommended as the probe may swing around more while being pulled up and down along the tube than when in a smaller diameter tube.

Inside sonic access tubes with a diameter more than twice the diameter of the probes, the probes shall be fitted with centralizers in accordance with ASTM D6760-02, as shown in Figure 4.3.8, to prevent undue movement inside the tubes during measurement.

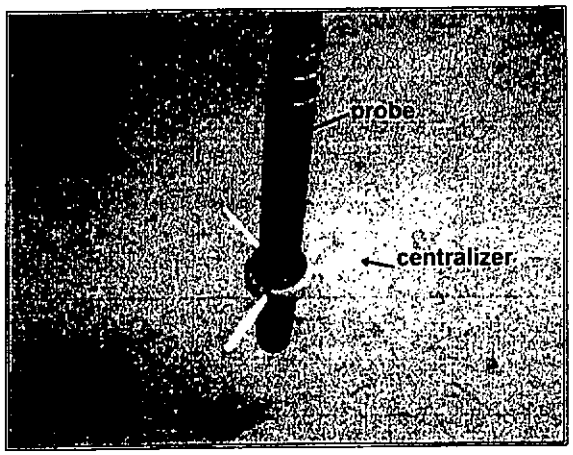

Figure 4.3.8. Photograph of the fitting of a centralizer to a probe

Figure 4.3.5 was tested again by the use of a centralizer to produce the regular CSL profiles as shown in Figure 4.3.9 in which a distinct and clear succession of the white and black stripes was obtained after a centralizer was fitted to the probes and the fuzzy stripes as depicted in Figure 4.3.5 disappeared.

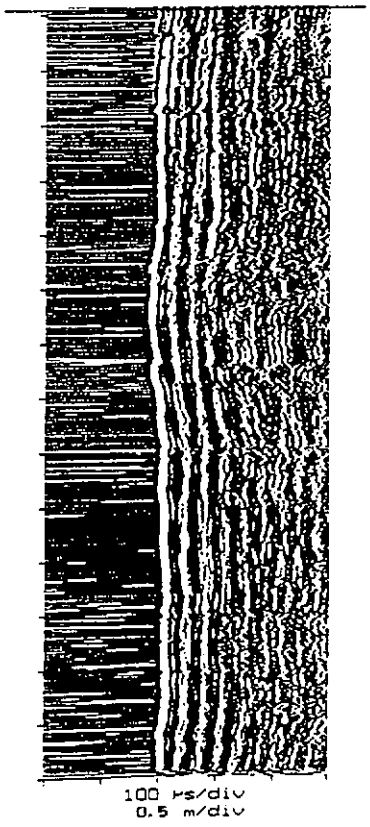

Figure 4.3.9. The sonic profile (using a centralizer) of the test bored pile in Figure 4.3.5

4.4. Summary of the effects of different materials of sonic access tubes on signal responses

Tests were conducted to determine the effects of different sonic access tube materials on the signal strength of ultrasonic waves. With the development of the in-house developed prototype MRS, the *apparent transmission velocity* and the signal strength of the waveforms were determined by the use of different sonic access tubes.

For each material, the signal strength increases with increasing sonic access tube diameter due to the effect of the curved surface wall of sonic access tubes. Greater signal strength is collected by the larger surface wall of a larger-diameter sonic access tube.

The signal strength when using PVC sonic access tubes are clearly larger than that when using steel tubes due to the smaller difference in acoustic impedance between PVC tubes and water. However, a risk of poor bonding between PVC tubes and concrete may result because of their smooth surfaces. In contrast, steel tubes bond well to the concrete, and steel tubes are therefore still preferable as sonic access tubes.

The experimental results produce a sonic profile with unclear and fuzzy successions of the white and black lines with the use of a larger-diameter (i.e. 150mm diameter) sonic access tube even though no defect is presented, as the

probes can move around inside the tube. In sonic access tubes with a diameter more than twice the diameter of the probes, the probes shall be fitted with centralizers in accordance with ASTM D6760-02 to prevent undue movement inside these tubes during measurement.

5.1. Introduction to the Field Investigation of the Ultrasonic Echo Sounding Technique

The in-house calibration and verification procedures are described in Sections 3.2 and 3.3 to ascertain the real performance and determine the limitations of the Ultrasonic Echo Sounding (UES) equipment in different working situations. And its applicability is demonstrated by performing field-testing investigations.

In this research work, extensive field investigations using UES were conducted on various Hong Kong construction sites including both public and private buildings projects to show the successful application of UES in the quality control of deep foundation drilling shafts. In this chapter, site descriptions, construction details, examples of typical results and the possible causes of the defects found by the UES testing technique, and the remedial works for unacceptable drilling shafts are discussed.

5.2. Site Descriptions and Construction Details

The tests of NDT were carried out by means of the UES technique on drilled shafts located in 16 different Hong Kong construction sites. In all of these investigations, the tests were performed under the author's leadership (as far as site work and further analysis is concerned).

Figure 5.2.1 shows the typical construction process of a cast-in-place concrete pile. The equipment Reverse Circulation Drill (RCD), Vibrator or Oscillator is used to construct the 'bell-out' in bedrock.

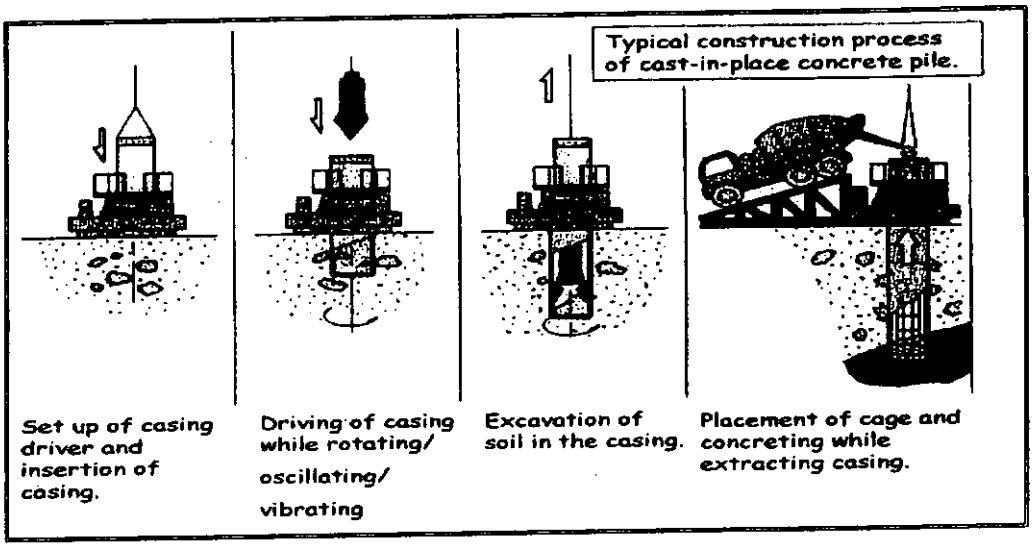

Figure 5.2.1. The typical construction process of a cast-in-place concrete pile (Source from Tysan Group)

In performing an UES test, the steel casings of drilled shafts are filled with water/bentonite slurry solutions in order to obtain a good coupling for ultrasonic wave propagation (Section 2.3.2).

In addition to the 'bell-out' and verticality checks using UES, some cases were involved for checking rock-socket construction at toes of the shafts in this research. Altogether the UES testing method was performed on a total number of 96 drilled shafts. The findings from these tests are related to:

- 3 construction sites connected with the construction of railways, with 29 piles (30% of total piles)
- 10 construction sites connected with the construction of residential buildings, with 58 piles (60 % of total piles)

- 1 construction site connected with the construction of hospitals, with 9 piles (10% of total piles)

Figure 5.2.2 shows some general characteristics of the test drilled shafts with respect to these three groups (shaft diameter and length, type of measurements).

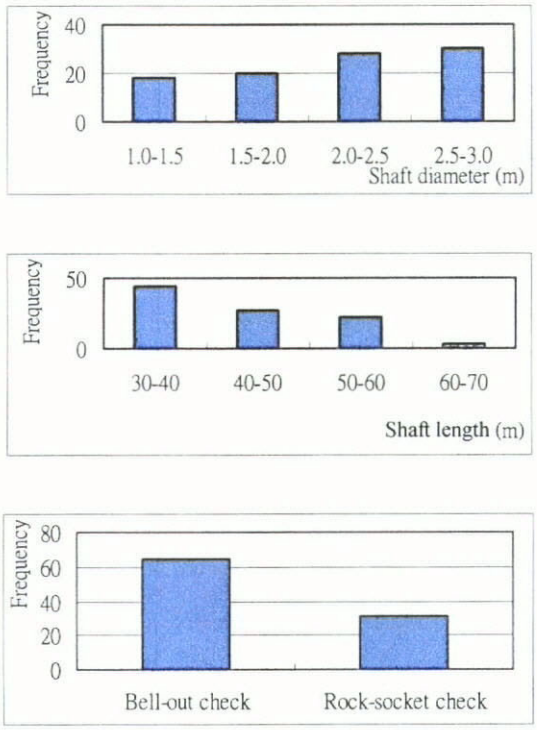

Figure 5.2.2. General characteristics of the test drilled shafts

5.3. Results and Discussion

Due to the design of the UES equipment applied in this project, only two directions of a drilled shaft are measured at any one time (Section 2.3.2). The signals recorded by the UES equipment are arranged into two separate UES

profiles for two different directions of a test drilled shaft (i.e. '*Channel 1 - Channel 2*' on an UES profile for *X-X' direction* and '*Channel 3 - Channel 4*' on an UES profile for *Y-Y' direction*). The scales used in the profiles are as follows:

- Horizontal scale: radius of a test drilled shaft = in a range between 0.5 and 1.0 meter per division
- Vertical scale: depth of a test drilled shaft = 1 meter per division

During the course of this investigation, 90% of the test drilled shafts were identified to be acceptable in terms of verticality and 'bell-out'/rock-socket dimensions. Of the remaining 10% with unacceptable features, the majority was slanted in one-direction with/without unacceptable 'bell-out' dimensions at the shaft toes (i.e. they could not meet the design requirements provided by the clients). The UES profiles obtained from the field investigation in this research are given in the internal test report (Chan 2003a). Examples and discussion of an acceptable drilled shaft and a slanted one are discussed below.

5.3.1. Example of an Ultrasonic Echo Sounding profile of an acceptable drilled shaft

Figures 5.3.1 and 5.3.2 show an example of the UES profiles (in *X-X' direction* and *Y-Y' direction*) of an acceptable drilled shaft. The shaft was cased, lined with a steel casing (from the ground level down to 45m below the ground level), and of nominal diameter 2.5m. The two thick black lines on both sides of the center line are the first received signals from the first reflecting surfaces (such

as steel casing or bedrock) on each side. The horizontal distances between these lines are the ranges (i.e. shaft diameter and 'bell-out' at a shaft toe within the bell-shaped region in Figure 5.3.1) of a drilled shaft. The signals behind each thick black line (i.e. first received signals) are the "ringing". The corresponding depths of the drilled shaft are shown in the center of the UES profile

Due to the design of the UES equipment applied in this investigation, the sensor head was firstly lowered downwards to record one direction (i.e. *X-X' direction*) and then lifted upwards to record the other direction (i.e. *Y-Y' direction*). As a result, the 'bell-out' dimension is calculated based on the portion of the UES profiles at the bottom of Figure 5.3.1 and on the top of Figure 5.3.2.

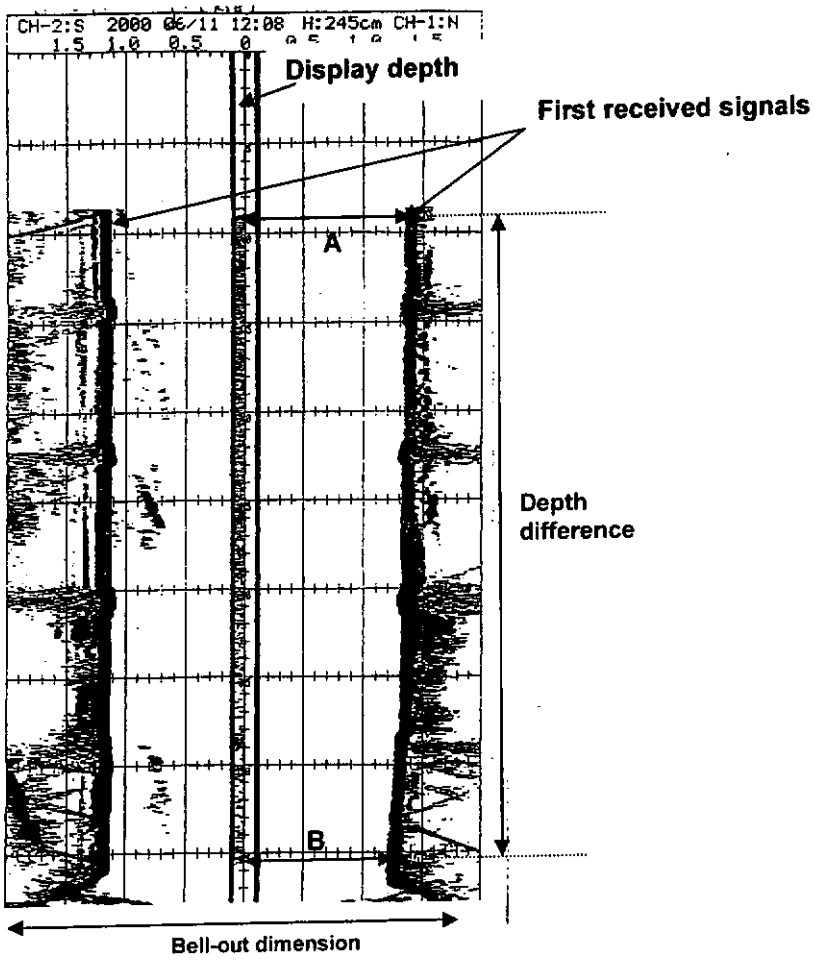

Figure 5.3.1. The UES profile of an acceptable drilled shaft in *X-X' direction*

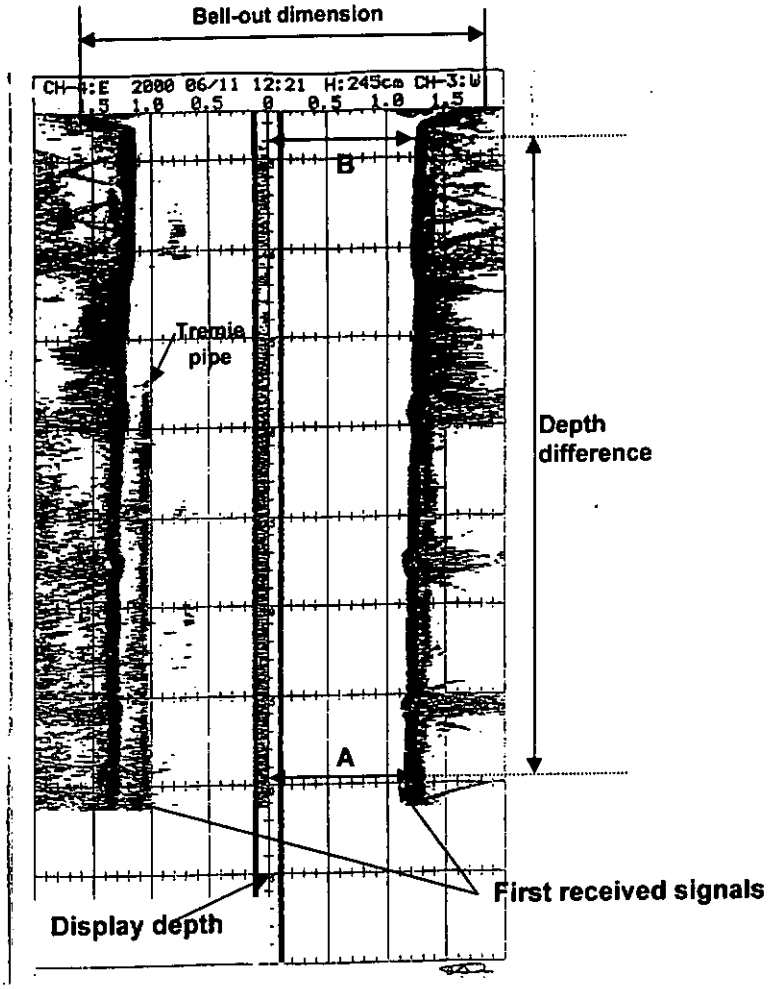

Figure 5.3.2. The UES profile of an acceptable drilled shaft in *Y-Y' direction*

In addition to the 'bell-out' dimension check, the verticality (V) of the test drilled shaft is calculated by the following equation:

$$V = \frac{(A - B)}{Depth\ difference} \qquad \text{--- (Equation 5.3.1)}$$

where A (unit: m) is the reading measured from the profiles near the top region of the first received signals.
B (unit: m) is the reading measured from the profiles near the bottom of the first received signals (but before a 'bell-out' region)
Depth difference (unit: m) is the depth difference between the depths at which the values of readings A and B are measured

The verticality is reported as a ratio (i.e. 1:V). The more the shafts slant in one direction, the smaller the value of V is. In this case, the design requirements of 'bell-out' and verticality are respectively 3.0m and 1:100. Table 5.3.1 shows the UES test results (in terms of 'bell-out' and verticality) of this test drilled shaft.

Table 5.3.1. The UES test results in terms of 'bell-out' dimension and verticality

	'Bell-out' dimension measured on the UES profiles (m)	**Verticality calculated from the UES profiles**
X-direction (Channel 1 - 2)	3.6	1 : 360
Y-direction (Channel 3 - 4)	3.6	1 : 360

Based on the above table, the calculated 'bell-out' dimensions and verticality values in both directions meet the design requirements such that this test drilled shaft is acceptable in terms of 'bell-out' and verticality parameters.

The ultrasonic waves reflected from the surfaces as a result of the changes of the acoustic impedance of different materials (Section 2.3.2). In Figure 5.3.3, the tremie pipe was still left inside the steel casing during the UES measurement, the ultrasonic waves were reflected firstly from the surface of the tremie pipe to produce the first received signals rather than from that of the steel casing. The profile in Figure 5.3.2 indicates the position of the tremie pipe inside the test drilled shaft. It is recommended that all the unnecessary accessories should be removed during the UES measurement in order not to produce a misleading UES profile.

Figure 5.3.3. Tremie pipe inside the test drilled shaft in *Y-Y' direction*

5.3.2. Example of an Ultrasonic Echo Sounding profile of rock-socket construction

The UES technique is typically applied to the check of 'bell-out' dimensions at a shaft toe. In this project, the measurements also focused on the rock-socket construction at the toes of concrete piles reinforced with an H beam (CPRH).

A CPRH was installed inside a steel tube and its cavity was filled with non-shrink cement grouting of a compressive strength not less than 30MPa. The details of CPRH are shown in Figures 5.3.4 and 5.3.5. Figure 5.3.6 shows the experimental set-up of the UES equipment in this project. At the bottom of this Figure, two beams were put on the test CPRH to support the UES equipment on the top. Then the UES test was carried out.

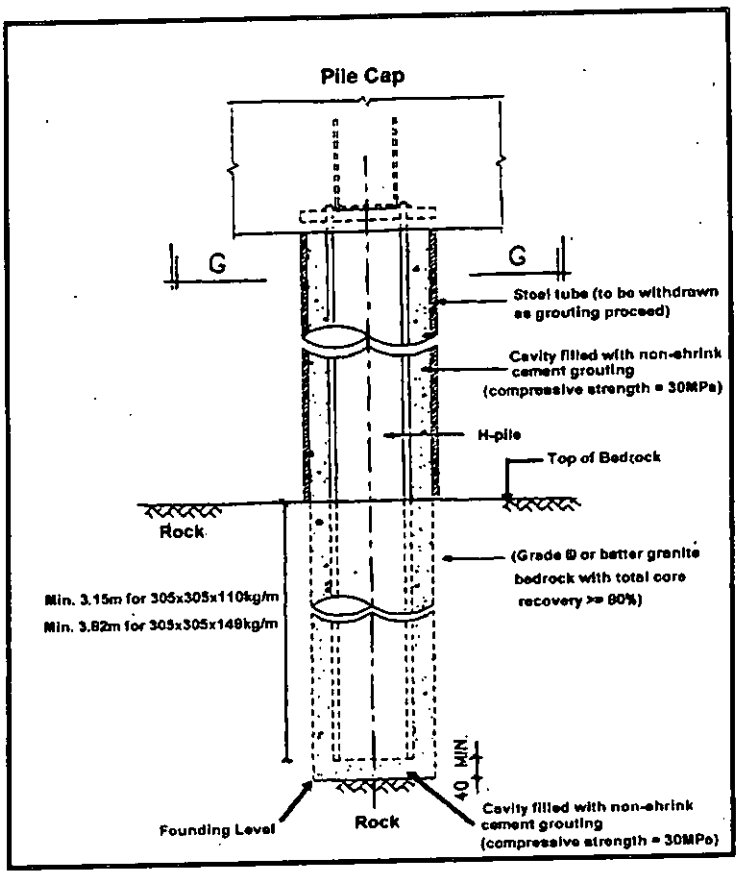

Figure 5.3.4. Schematic drawing of a concrete pile reinforced with an H beam

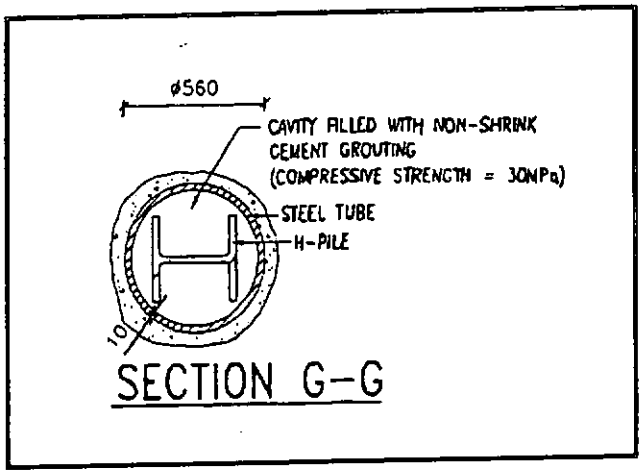

Figure 5.3.5. Schematic drawing in Section G-G of Figure 5.3.4

Figure 5.3.6. Test set-up of the UES test in which the UES equipment, being supported by two H-steels, was put on a concrete pile reinforced with an H beam.

In a test CPRH, the only lower section (about 4m from the base of the shafts) of a test CPRH was filled with water, and the signals were recorded within the water-filled zone. Two UES profiles (i.e. in *X-X' direction* and *Y-Y' direction*) were produced for each test CPRH. In Figure 5.3.7, the horizontal distances between the first received signals represent the rock-socket dimension at the toe of the CPRH. Based on the UES profiles obtained, all the signals reflected from the rock-socket region are irregular.

In some cases, not only the rock-socket regions were filled with water but also the sections of steel casings. Figure 5.3.8 shows the UES profiles reflected from both steel casings and rock-socket regions. Two patterns of receiving signals were obtained, one was within the rock-socket region and the other was within the

water-filled steel casing region.

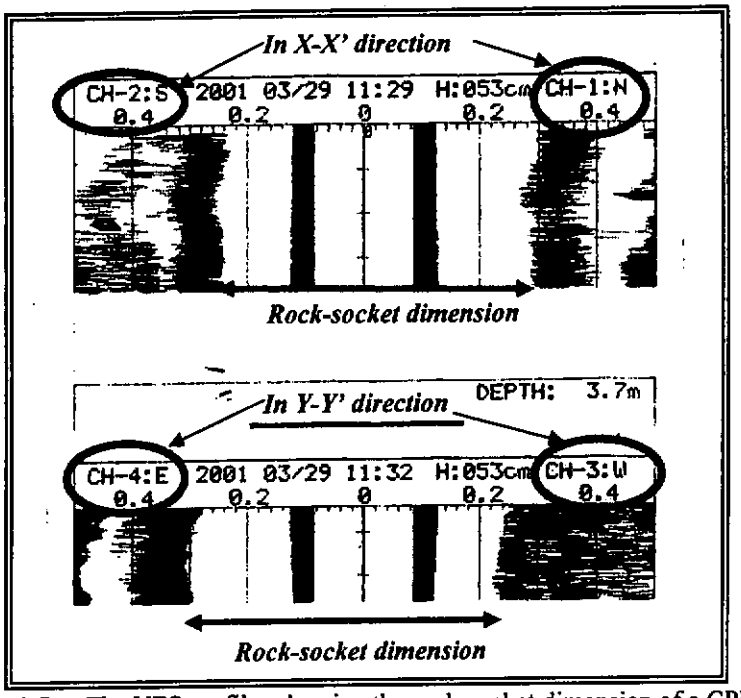

Figure 5.3.7. The UES profiles showing the rock-socket dimension of a CPRH

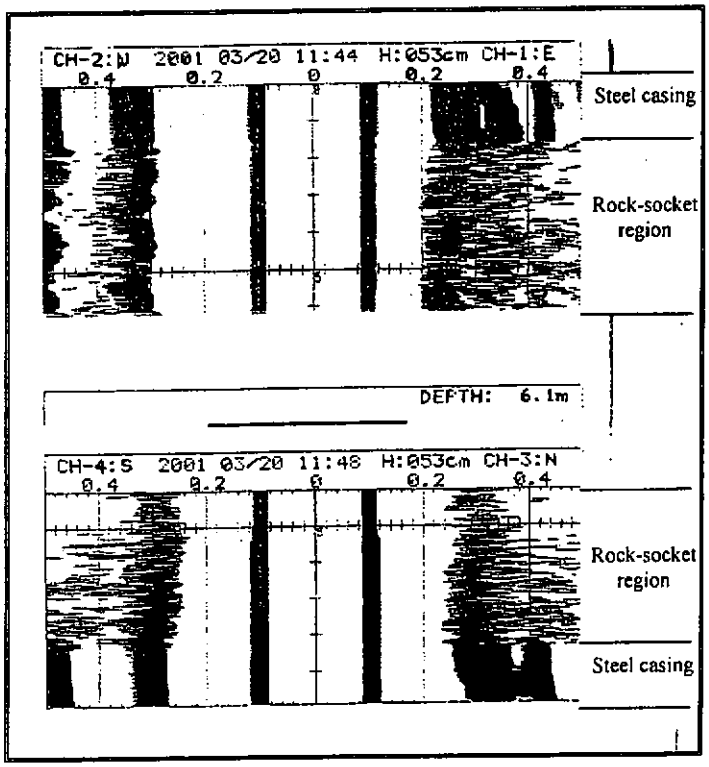

Figure 5.3.8. The UES profiles showing two patterns of the received signals reflected from a steel casing region and a rock-socket region

In the rock-socket region, the arrival times of the reflection and echoes are variable while that within the region of water-filled steel casing are quite regular. This phenomenon is attributed to the irregular surface of the rock-socket region and the perspective of acoustic impedance across the water/rock and water/steel interfaces. As a result, an ultrasonic beam partially transmits across the interface and partially reflects back towards the source (as shown in Figure 2.2.5). This discovery is a good foundation to distinguish between rock-socket and steel casing regions. Further research work should be carried out to verify the different patterns of receiving signals in order to distinguish the different kinds of materials (including steel casing, bedrock and soil layer) at different measurement levels.

5.3.3. Example of an Ultrasonic Echo Sounding profile of a slanted drilled shaft

Figures 5.3.9 and 5.3.10 show an example of the UES profiles (*X-X' direction* and *Y-Y' direction*) of a distinct slanted drilled shaft. As mentioned in previous section, the upper section of the UES profile in Figure 5.3.10 is corresponding to the lower section of that in Figure 5.3.9 and *vice versa*.

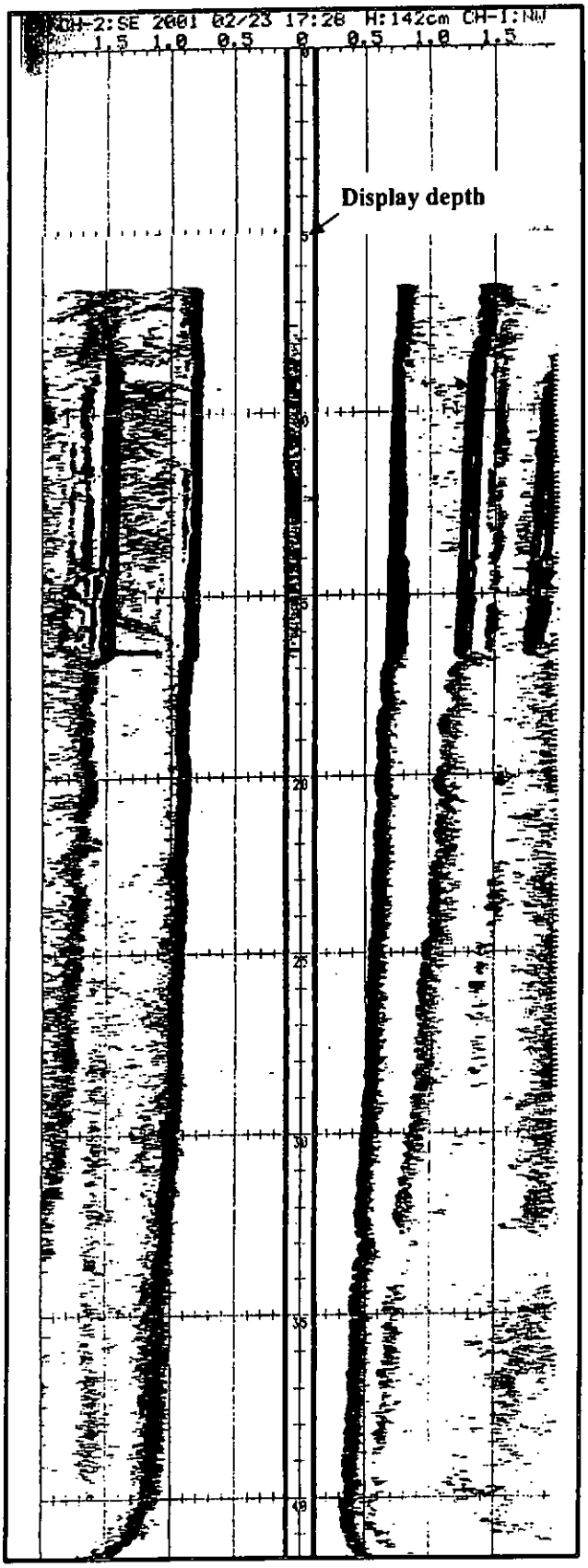

Figure 5.3.9. The UES profile of an unacceptable drilled shaft in *X-X' direction* (i.e. the sensors in *'Channel 1-Channel 2'*)

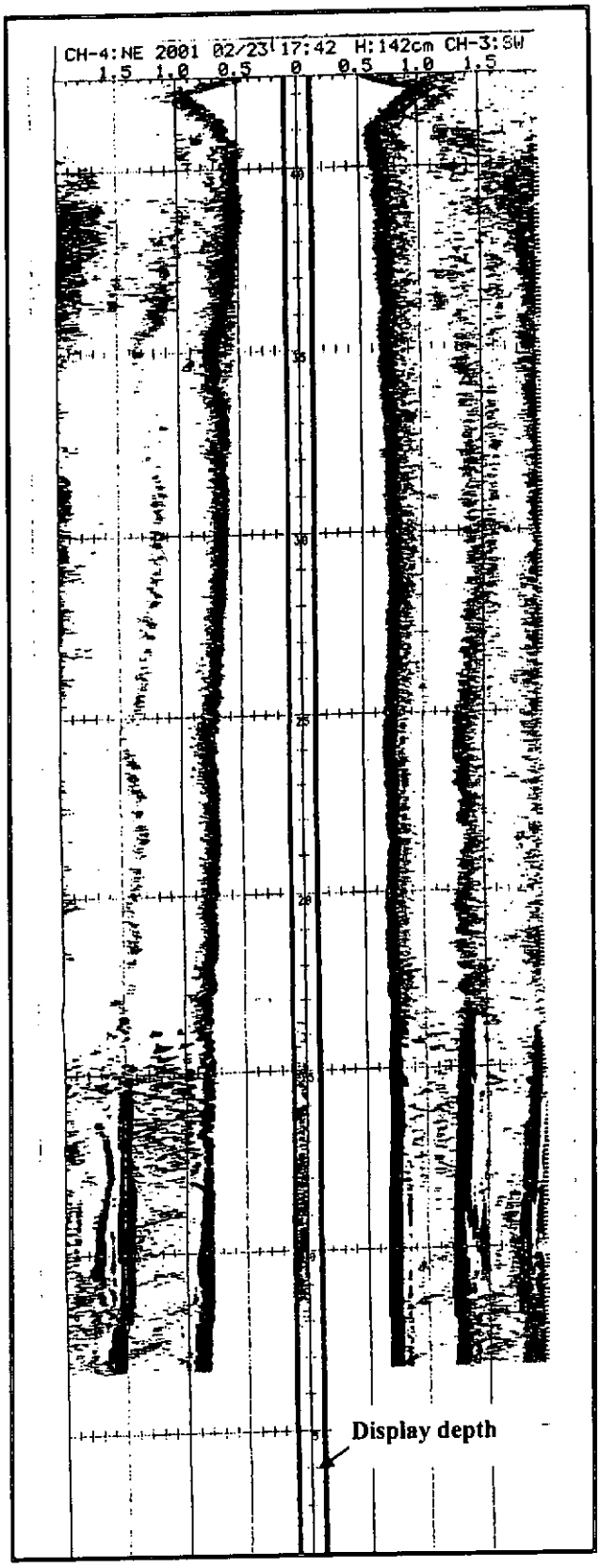

Figure 5.3.10. The UES profile of an unacceptable drilled shaft in *Y-Y' direction* (i.e. the sensors in *'Channel 3-Channel 4'*)

Based on the receiving signals in Figures 5.3.9 and 5.3.10 (i.e. displayed depth: 0 – 15m), the upper section of the drilled shaft was straight in vertical alignment. However, it is found that the shaft was slanted in the lower section especially near the shaft toe. In this case, the ranges (including shaft diameter and the 'bell-out' at the shaft toe) recorded at the lower measurement levels were smaller than the actual values due to the sensor head was laid on the chord of the shaft at the lower levels as shown in Figure 5.3.11.

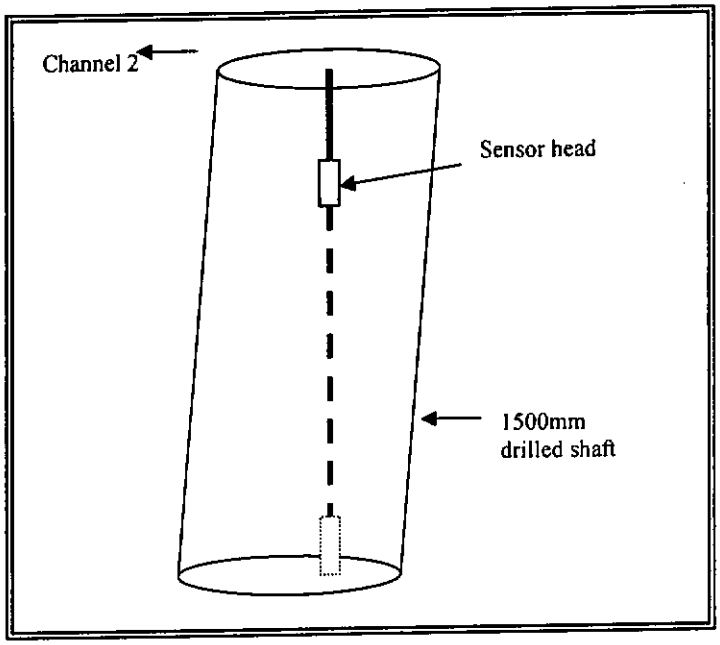

Figure 5.3.11. Schematic drawing of a slanted drilled shaft

For this slanted drilled shaft, another measurement was required in order to have an actual picture of the 'bell-out' at the toe. In the 2nd measurement, the UES equipment was moved 400mm towards '*Channel 2 & Channel 3*' as shown in Figure 5.3.12.

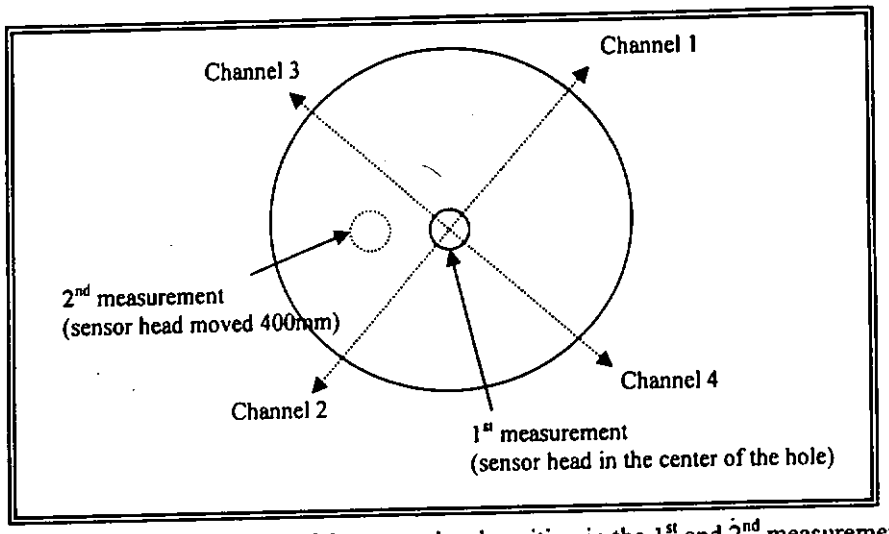

Figure 5.3.12. Schematic drawing of the sensor head position in the 1st and 2nd measurements

Figures 5.3.13 and 5.3.14 show the test results of the 2nd measurement in both *X-X' direction* and *Y-Y' direction*. In the *Y-Y' direction*, the measured 'bell-out' dimension was larger than that obtained from Figure 5.3.14 as the sensor head of the UES equipment was nearly in the center of the shaft in the lower measurement levels.

As a result, several UES measurements are recommended for slanted drilled shafts in order to obtain the actual picture of the construction of the drilled shafts especially the 'bell-out' at shaft toes.

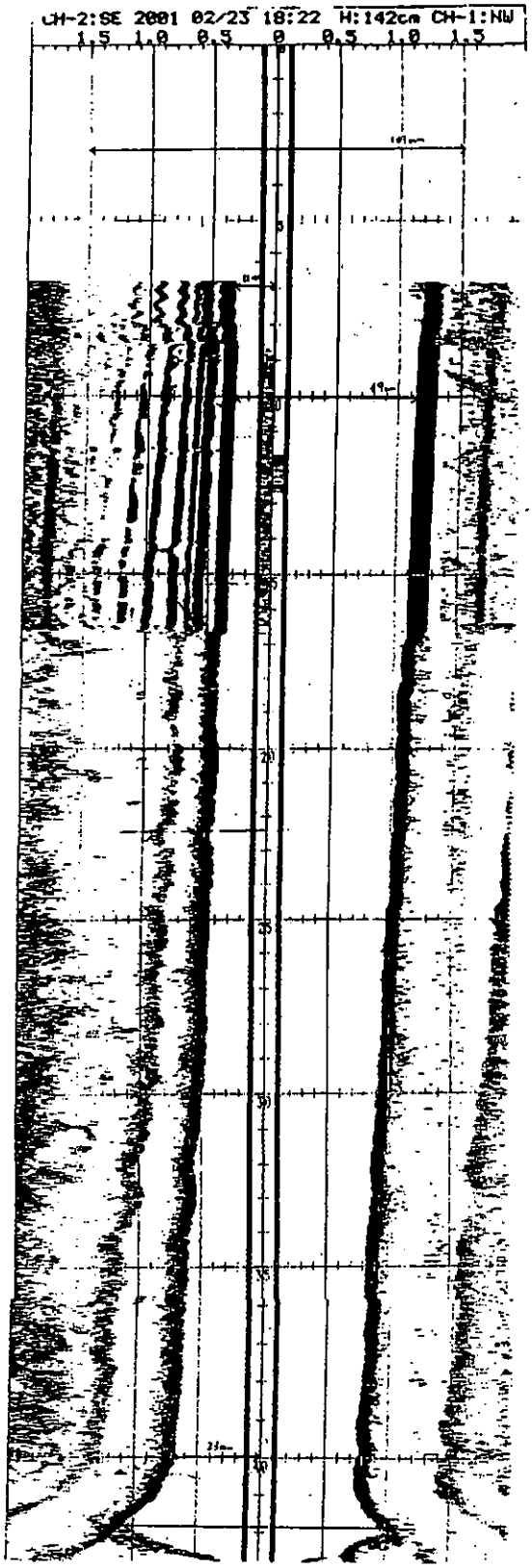

Figure 5.3.13. The UES profile showing the 2nd measurement of a slanted drilled shaft in *X-X' direction*

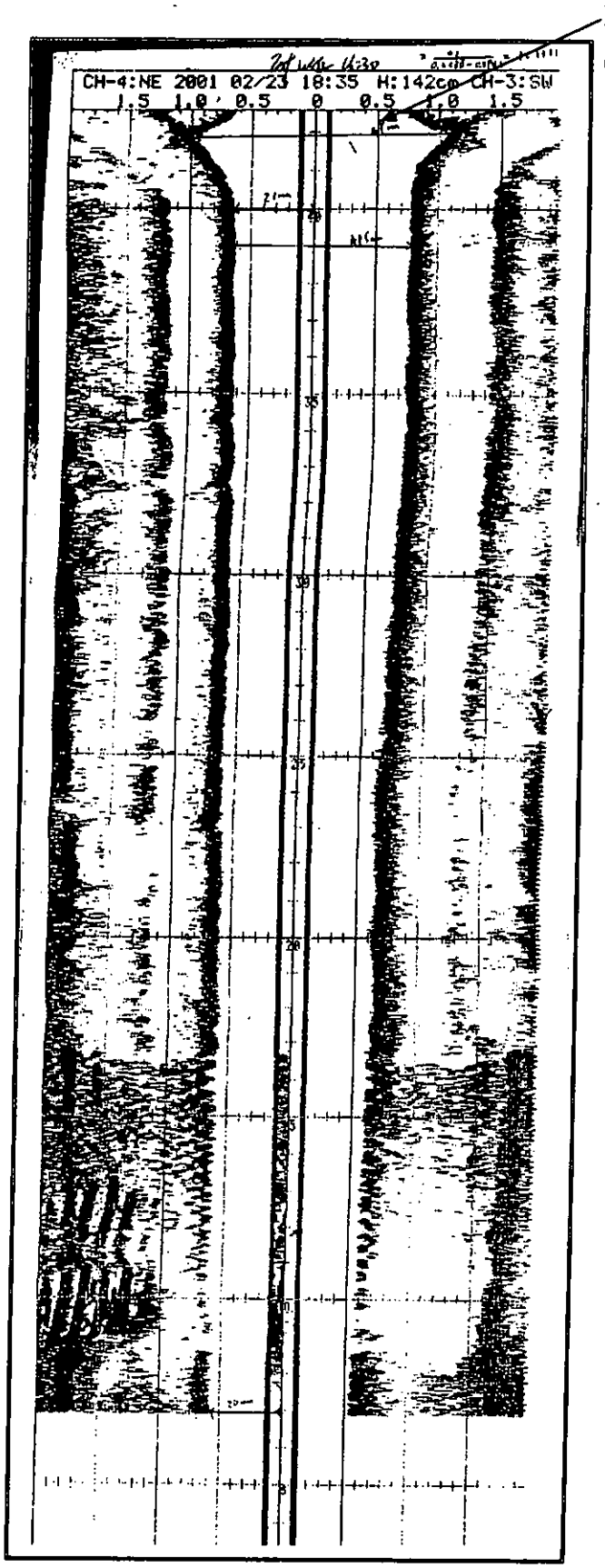

Figure 5.3.14. The UES profile showing the 2nd measurement of a slanted drilled shaft in *Y-Y' direction*

Remedial Works for Unacceptable Drilled Shafts

If a drilled shaft foundation does not meet the design requirements (such as 'bell-out' dimension at a shaft toe and shaft verticality), it is identified as an unacceptable shaft foundation using the UES test technique at an early stage.

When the measured 'bell-out' dimension (obtained from the UES profiles) is smaller than the pre-design one, extra drilling at the bedrock are required to enlarge the 'bell-out' size until it meets the design requirement. For slanted drilled shafts, some mini-piles may be constructed nearby in order to provide a better foundation to ascertain the load transfer safely from the superstructure to the foundation work.

5.4. Summary of the Field Investigation of the Ultrasonic Echo Sounding Technique

This chapter generally describes the sites and the construction details of the test shaft foundations. The equipment Reverse Circulation Drill, Vibrator or Oscillator was used to construct the 'bell-out' at a shaft toe in bedrock. Drilled shafts under testing are required to be filled with water/bentonite slurry solutions (as a propagation medium for the ultrasonic wave transmission) in performing an UES test. More than 90 shafts from a range of contexts including the deep foundations of railways, hospitals and residential buildings in various Hong Kong construction sites were tested by the UES testing technique (under the author's leadership), and the results are summarized in this chapter.

The UES technique has been proven a reliable and useful technique to assess the design of deep-drilled shaft foundations before the concreting stage. Its reliability is supported by the extensive tests carried out within the HKSAR territories presented here. The UES technique is effective to provide an early stage diagnosis and inspection of shafts characteristics such as shaft verticality, shaft diameter, shaft depth, and geometry and dimensions of the 'bell-out' at the shaft toes.

Measurement made with the UES technique helps in diagnosing the construction of shafts and deciding whether accept or reject the pile shafts concerned for the subsequent concreting operation after which failure is almost irreversible. Early detection of deviations from design allows timely correction of problems, minimization of construction time and reduction of overall construction cost.

The analysis of the UES test results show that 90% of the tested drilled shafts were identified to be acceptable in terms of verticality and 'bell-out'/rock-socket dimension. Of the remaining 10% with unacceptable features (i.e. they could not meet the design requirements provided by the clients), the majority was slanted in one direction with/without unacceptable 'bell-out' dimension at the shaft toe. Examples of the acceptable and slanted-drilled shafts, and the remedial works for the unacceptable drilled shafts are reported.

In addition to the check of 'bell-out' dimensions at shaft toes, the UES

test was also applied to the rock-socket construction at the toes of concrete piles reinforced with a H-beam (CPRH). The results show that the signals reflected from regions of steel casing and rock-socket are different. In rock-socket regions, the first received signals and the echoes are variable while that within water-filled steel casing regions are quite regular. This discovery provides a good foundation to carry out a further research regarding to the identification of different materials (including steel casings, soil layer and bedrock) in a drilled shaft.

6.1. Introduction of the Field Investigation of the Cross-hole Sonic Logging Technique

The need to check deep foundations before and after the concreting stage is equally important. The applications of two ultrasonic-based NDE techniques (i.e. the Ultrasonic Echo Sounding (UES) technique and the Cross-hole Sonic Logging (CSL) technique) provide a better picture regarding to the quality assurance of deep foundation concrete elements since UES and CSL are conducted respectively before and after the concreting stage.

The application of the UES technique identifies the suspected drilled shafts which can be taken into remediation works at an early stage (i.e. before the concreting stage). This minimizes the costs incurred and time taken during the construction project (Section 5.3).

For the quality control of deep foundation concrete elements after the concreting stage, extensive field investigations using CSL were conducted on various Hong Kong construction sites (including both public and private building projects) to show the effectiveness of the use of the CSL technique. In all of these investigations, the tests were performed under the author's leadership (as far as site work and further analysis is concerned).

In this chapter, site descriptions, construction details, examples of typical results and the possible causes of the defects found by the CSL testing technique are discussed.

6.2. Site Descriptions and Construction Details

More than 100 deep foundation concrete elements (i.e. bored piles, concrete barrette piles and diaphragm wall panels) in various construction sites were carried out. Figure 6.2.1 shows some general characteristics of the test deep foundation concrete elements with respect to these four groups (pile diameter and length, number of sonic access tubes, type of foundation concrete elements).

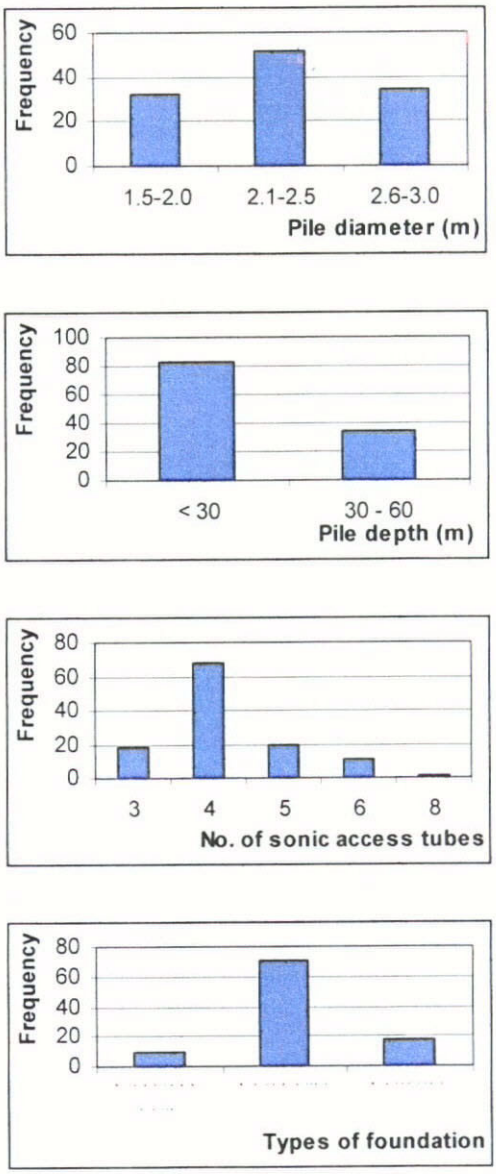

Figure 6.2.1. General characteristics of the test deep foundation concrete elements

The technical specifications regarding to the number, size, arrangement and material of sonic access tubes for performing an on-site CSL test are laid down in the published document ASTM D6760-02. The sonic access tubes are of about 50mm internal diameter. In some cases, when it is necessary to evaluate concrete of drilled shafts (i.e. concrete/rock interface) by mechanical coring, sonic tubes are of 150mm diameter. The details of performing a CSL test and a 'fan-shaped' test are presented in Section 2.4.3.

The tube top shall project approximately 300mm above pile cut-off level. The sonic access tubes are filled with water to provide a good coupling medium for ultrasonic wave transmission prior to concreting and during testing (Section 2.4.2). The sonic access tubes are usually denoted by letters. A profile is then named after the tubes between which ultrasonic waves pass, such as A-B or B-C.

6.3. Results and Discussion

The signals recorded during the CSL testing technique are arranged and shown in a propagation time versus depth plot. The horizontal axis is normally time in microseconds (i.e. μ s) unit whereas the vertical axis is depth in meter (i.e. m) unit. Figure 6.3.1 shows a typical CSL plot with a conventional '*propagation-time versus depth*' plot as well as a '*received-signal-energy versus depth*' plot. The received signal energy is expressed in percentage on the left column of each sonic profile.

- Horizontal axis: time of propagation (range from 100 to 150 μ s per division)

- Vertical axis: depth (range from 1m to 2m per division)

The CSL profiles obtained from the field-testing in the research are given in the internal test report (Chan 2003b). Further examples and discussions of acceptable foundation elements (without defects) as well as unacceptable ones (with defects) both along pile shafts and at pile toes follow.

6.3.1. Example of a CSL profile of an acceptable foundation element

Amongst the foundation elements tested, 80% of these elements have CSL profiles similar to the characteristics depicted from Figure 2.4.28 and were identified to be structurally sound with no significant defects detectable by CSL. In general, all acceptable foundation elements should have:

- regular CSL profiles (i.e. regular successions of white and black stripes) with minor variations of up to 30% of *first-arrival-time* (FAT);
- *apparent transmission velocity* above 3660m/s, as stipulated in Table 2.4.2;
- '*received-signal-energy versus depth*' profiles close to 100% in all places.

6.3.2. Example of a CSL profile of a foundation element with defects along a pile shaft

Figure 6.3.1 shows some irregularities near the middle section of the CSL profile. In general, most defective foundation elements tend to have:

- irregular CSL profiles (i.e. no clear succession of the white and black stripes and sometimes an outright discontinuity) with large variations of FAT;
- *apparent transmission velocity* below 3000m/s as stipulated in Table 2.4.2;
- '*received-signal-energy versus depth*' profiles of approximately 30% or less within the irregularities regions.

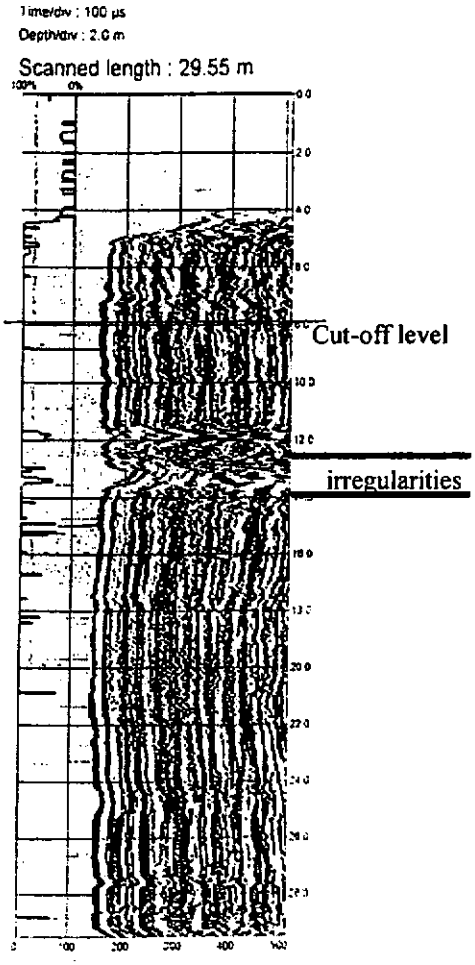

Figure 6.3.1. Example of CSL profile showing irregularities found along the pile shaft

In the case of total discontinuity, these are widely believed to be due to the cause of concrete defects itself or necking conjugated with soil inclusions etc. Concrete defects include low-grade concrete or/and honeycombed concrete. The

range of the total discontinuities could also be due to an error in the construction particularly in the concreting phase. For example, faulty procedures in keeping the tremie pipe fully immersed in fresh concrete at all times could cause the inclusion of foreign materials other than concrete within foundation elements. Likewise, faulty procedures in keeping the temporary casing for a sufficient amount of time are sometimes overlooked and the casings are prematurely extracted causing an undue collapse of surrounding soil into the concrete. Failure in using bentonite slurry as soil support for an uncased shaft produces similar consequences.

It is also possible that percussive piling in the vicinity of a freshly concreted foundation element will produce undesirable effects as far as concrete integrity is concerned. Disturbance of this kind (when coupled with the presence of weak surrounding soil strata) will produce an even larger problem.

Figure 6.3.2 illustrates a large attenuation of the received sonic signals producing fuzzy CSL traces between 5.0m and 6.0m below the pile cut-off level. This large attenuation is explained by the early extraction of the temporary casing causing an undue collapse of surrounding soil into the concrete, as ultrasonic waves do not propagate very well in soil when compared with concrete as illustrated in Figures 6.3.3 and 6.3.4.

Cross-hole sonic tests were conducted to obtain typical waveforms of ultrasonic transmission through soil and concrete as shown respectively in Figure 6.3.3 and 6.3.4. In carrying out these measurements, a typical set up (i.e. two

sonic access tubes separated by a fixed 300mm distance and filled with sound concrete and soil) was constructed.

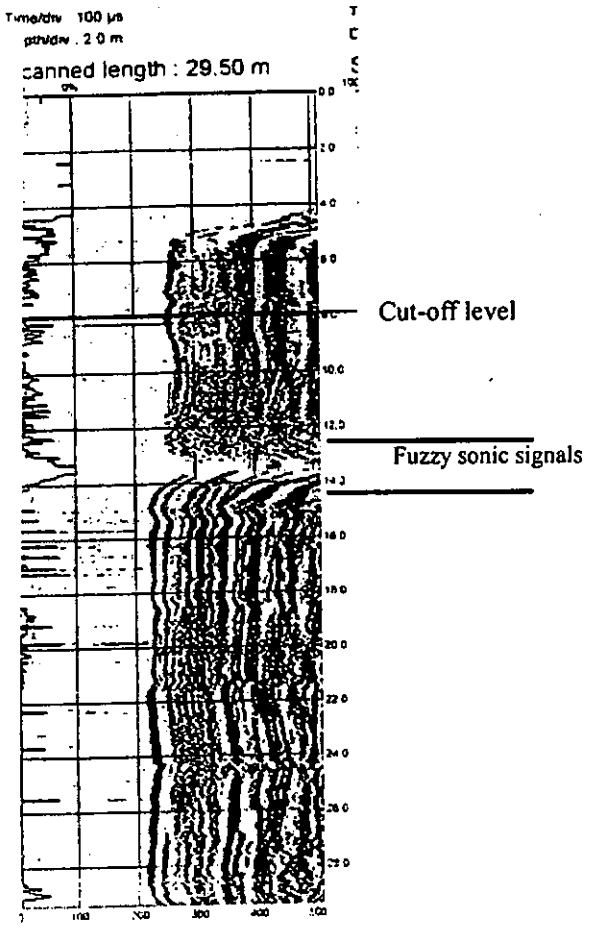

Figure 6.3.2. Example of CSL profile showing the presence of fuzzy sonic signals along the pile shaft

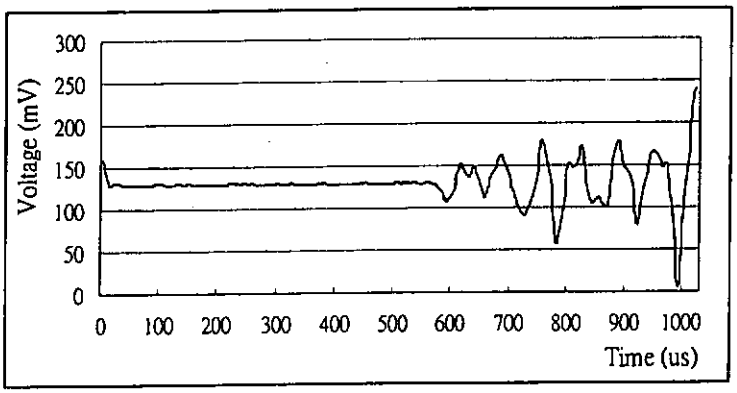

Figure 6.3.3. A typical time trace showing the ultrasonic waveform after propagation through 300mm soil.

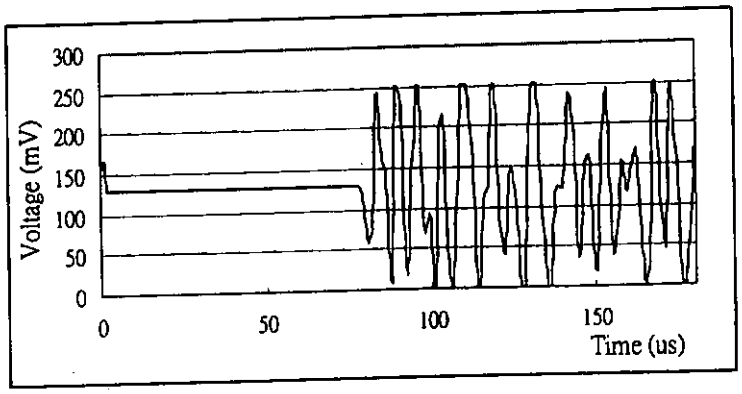

Figure 6.3.4. A typical time trace showing the ultrasonic waveform after propagation through 300mm concrete.

Figures 6.3.3 and 6.3.4 show the ultrasonic wave/pulse received through soil and concrete respectively. Close inspection of these figures reveals that the respective *peak-to-peak* signal amplitude and the FAT are different. In fact, the ultrasonic wave/pulse propagates better (with higher *peak-to-peak* signal amplitude and shorter FAT) when traveled through concrete than soil since soil is a highly attenuating material.

6.3.3. Example of a Cross-hole Sonic Logging profile of a foundation element with a defect at a pile toe (so called 'soft bottom')

Figure 6.3.5 shows a typical CSL profile with defects near the pile toe. These irregularities are explained partly by the presence of residue and sediment (i.e. mud/soil, water, bentonite slurry, etc.), partly due to the failure in the 'air-lifting' cleaning operation and partly by washing away of the cement from concrete (due to surrounding ground water) causing concrete honeycombing as shown in Figures 6.3.6 and 6.3.7.

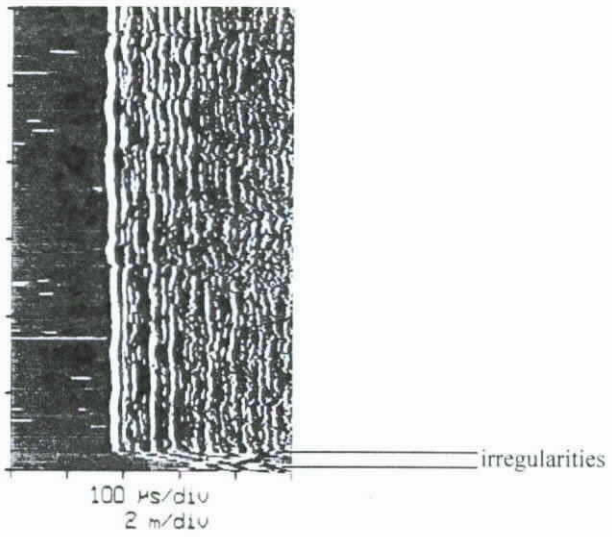

Figure 6.3.5. Example of CSL profile showing a 'soft bottom'

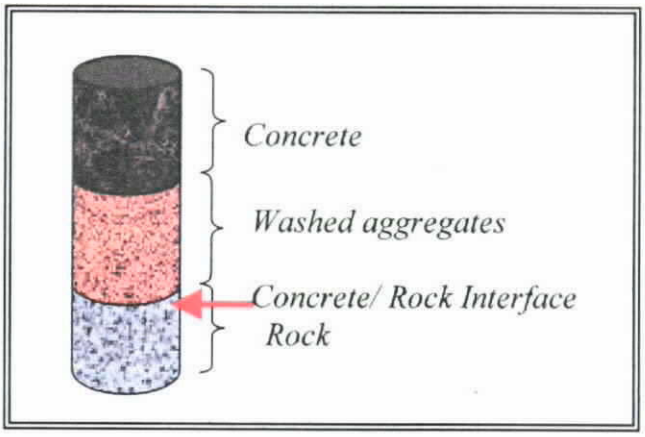

Figure 6.3.6. Schematic drawing showing the effect of cement washed-away at a pile toe

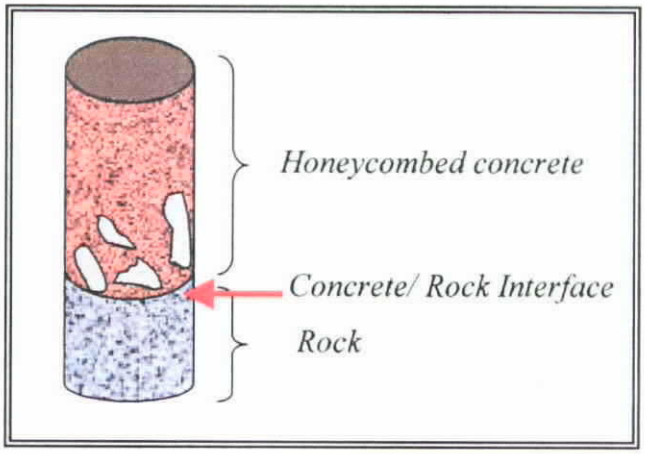

Figure 6.3.7. Schematic drawing showing the presence of honeycombed concrete at a pile toe

The presence of aggressive chemicals in the soil causes concrete quality to deteriorate gradually and compromise its integrity. If a pile is immersed in seawater as in offshore condition, wave action, water-freezing etc. also produces damaging effects.

6.3.4. Example of a Cross-hole Sonic Logging profile of an acceptable concrete/rock interface

A 'fan-shaped' test is typically performed to check the pile toe/rock interface. The two sonic probes are lowered respectively at the bottom of 50mm-diameter sonic access tube and the bored hole. The probe inside the bored hole is raised while the probe inside the 50mm-diameter sonic access tube is kept stationary. The details of performing this test were given in section 2.4.3.

Figure 6.3.8 shows a typical CSL profile of a sound concrete/rock interface. In general, a foundation element with a sound concrete/rock interface should have the following features in their profiles:

- clear and regular successions of white and black stripes across concrete/rock interface
- '*received-signal-energy versus depth*' profiles close to 100% across concrete/rock interface

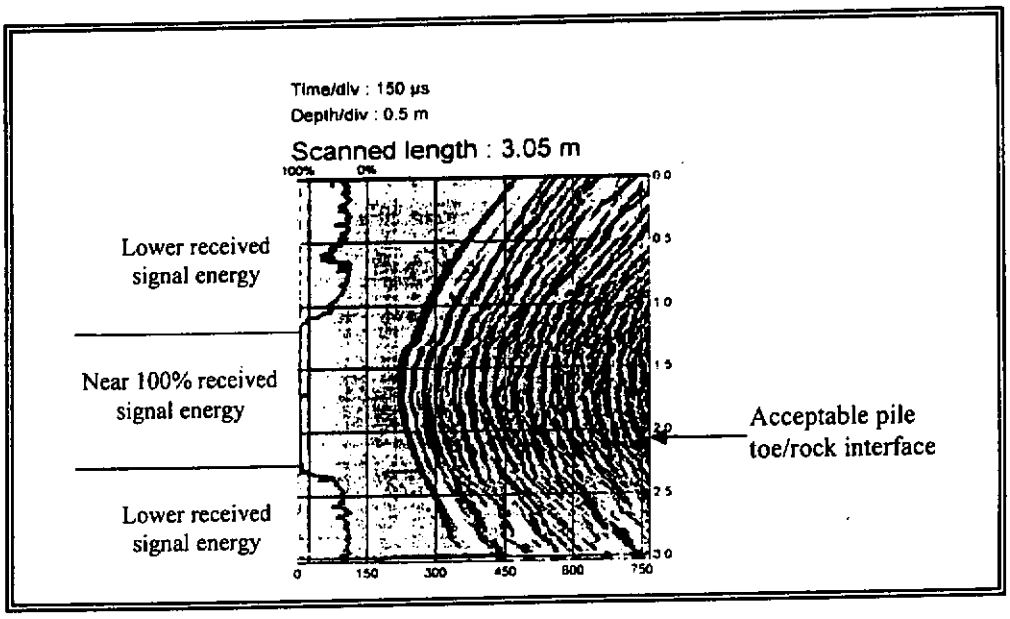

Figure 6.3.8. Example of CSL profile showing a sound concrete/rock interface

6.3.5. Example of a Cross-hole Sonic Logging profile of a suspected concrete/rock interface failure

Figure 6.3.9 shows an example of sonic profile of a suspected concrete/rock interface sonic profile. In general, CSL profiles for questionable concrete/rock interface show these features in their profiles:

- no clear succession of the white and black stripes and sometimes an outright total discontinuity of the concrete/rock interface
- '*received-signal-energy versus depth*' profiles show very low values at some regions near the questionable concrete/rock interface.

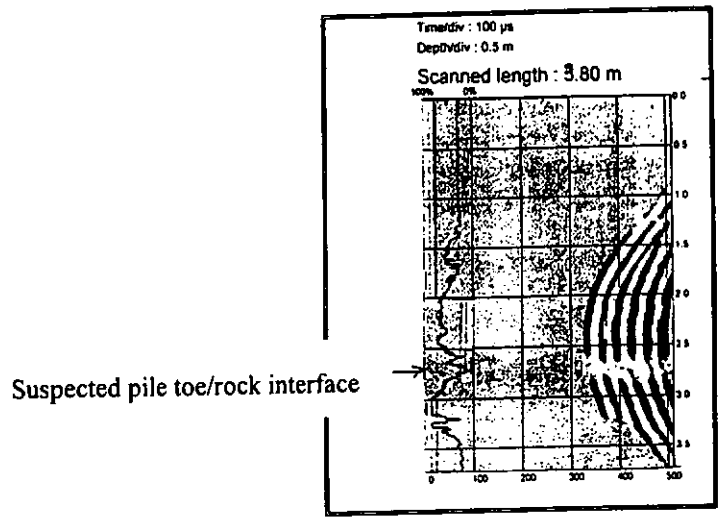

Figure 6.3.9. Example of CSL profile showing a suspected concrete/rock interface

These anomalies are explained by inappropriate '*air-lifting*' and cleaning operations which left behind the sediments and residues produced as a result of drilling by Reverse Circulation Drilling (RCD) at concrete/rock interface.

The presence of seams/joints (usually embedded with weaker grade material) in the founding bedrock is another possible reason (in additional to what has been described earlier) for causing the CSL irregular profile at the pile toe. Previous site investigation (SI) exercise may not be able to reveal this situation because of the small area covered by the SI bore hole. However, the author advocates the use of 'Ultrasonic Echo Sounding' technique to provide information in this regard. Details of this technique are reported in Sections 2.3 and 4.3. The traditional strategy to obtain concrete cores along the full length of piles down to bedrock is both expensive and time-consuming. The former adds substantial costs and the latter causes delays in the progress of a project.

6.4. Summary of the Field Investigation of the Cross-hole Sonic Logging Technique

This chapter generally describes the sites and the construction details of the test foundation concrete elements. The CSL technique was proven as a reliable and useful technique for assessing the quality of concrete and the integrity of deep foundation concrete elements. The proof of its applicability was achieved by the results obtained from the extensive tests carried out (within the HKSAR territories) and also examples shown in this chapter. Questionable/suspected defects found are reported and discussed thoroughly and classified into several categories.

The experience shows that CSL provides the precious information/feedback regarding the construction process of the final finished products (i.e. foundation elements in this case). This would not be possible otherwise without the help of ultrasonic evaluation technique in general and CSL in particular.

7.1. Introduction to the Instrumentation of the In-house Developed Prototype

The traditional instrumentation of the CSL technique involves two ultrasonic probes (i.e. one a transmitter and the other a receiver). They are used to measure the propagation time of a sonic/ultrasonic pulse traveling through concrete between two vertical sonic access tubes (Section 2.4.2). However, for some cases of sonic-tube-arrangement (i.e. more sonic access tubes), this traditional CSL system (i.e. a pair of probes) may be inadequate, and a more efficient instrumentation may be required to acquire several signals simultaneously in order to save time and cost. An adaptive, versatile and relatively low cost prototype was constructed and developed by the author to provide a more efficient way to conduct sonic tests.

The in-house multi-channel ultrasonic data acquisition prototype, called the 'Multiple Referencing System' (MRS), is especially designed for deep foundation concrete elements after installation. Two receivers rather than one in the traditional approach are put inside the two different sonic access tubes and capture output signals simultaneously during the sonic logging measurement.

Analysis of ultrasonic signals is typically limited to the measurement of the value of *first-arrival-time* (FAT). However, ultrasonic waveforms contain considerably more information regarding to the characteristics of test materials. A purposely-developed analysis graphical programming based on digital *virtual*

instrument was constructed to analyze the acquired waveforms in different parameters (i.e. signal strength in a time domain and signal energy spectral distribution in a frequency domain) in addition to the traditional parameter of FAT. The aim of this analysis is to increase the reliability of the testing method in evaluating test materials.

This chapter describes the construction and development of the hardware and software (based on digital *virtual instrument)* of the MRS. The verification (in terms of the transmission velocity and the possible transmission path) of the MRS is also investigated.

7.2. Description of the In-house Developed Prototype

The in-house developed prototype MRS consists of two major components, the high-voltage pulsing component and the data conditioning and processing component, as described in Figures 7.2.1 and 7.2.2. The MRS is designed to perform sonic tests in a bored pile with sonic tubes pre-installed. The high-voltage pulsing component excites an ultrasonic emission probe to transmit an ultrasonic pulse. The data conditioning and processing component serves the purpose of receiving ultrasonic pulses from the ultrasonic emission probe. The acquisition and analysis graphical programming in a Laboratory Virtual Instrument Engineering Workbench (LabVIEW) environment was constructed to further analyze the detected waveforms.

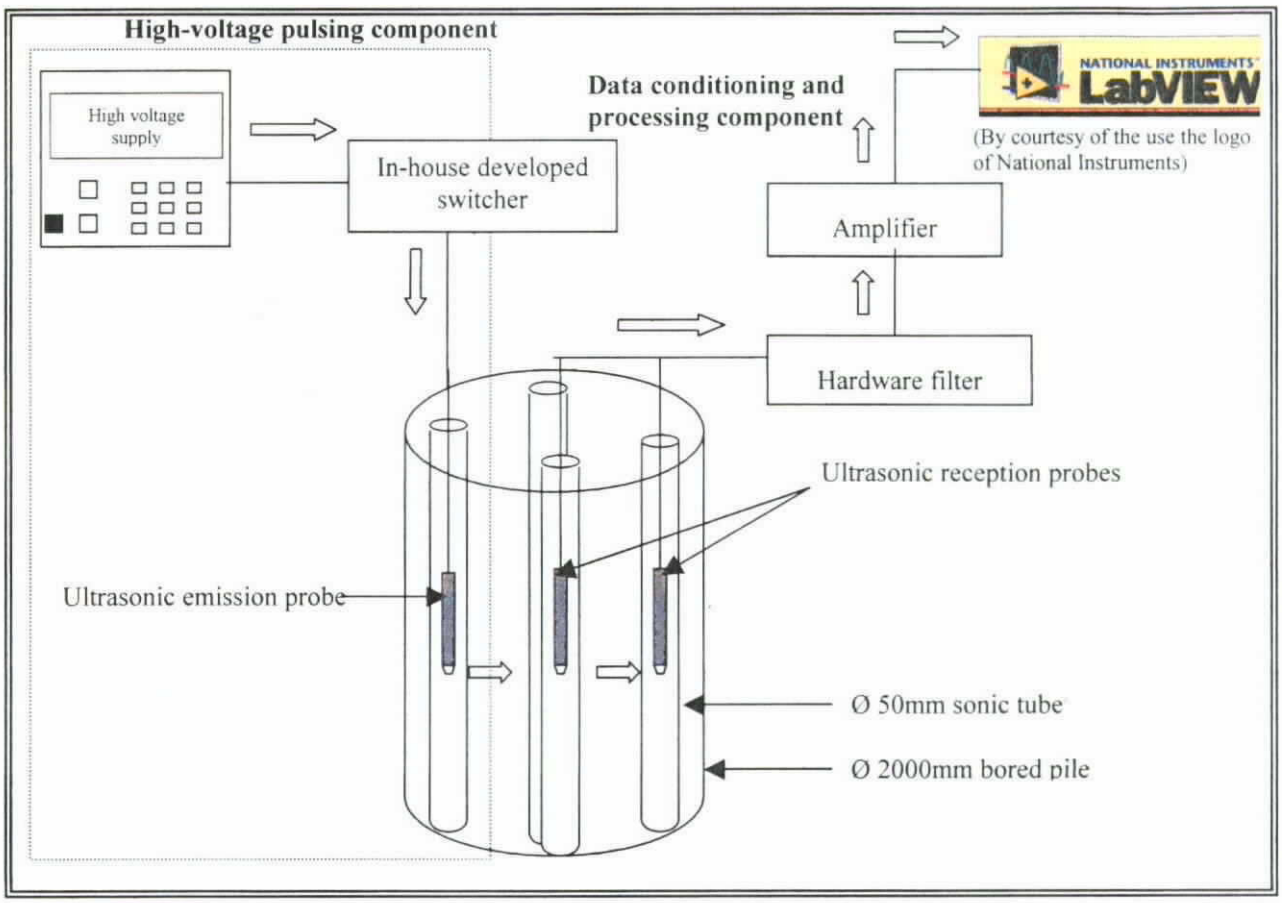

Figure 7.2.1. Schematic drawing of the In-house Developed Prototype

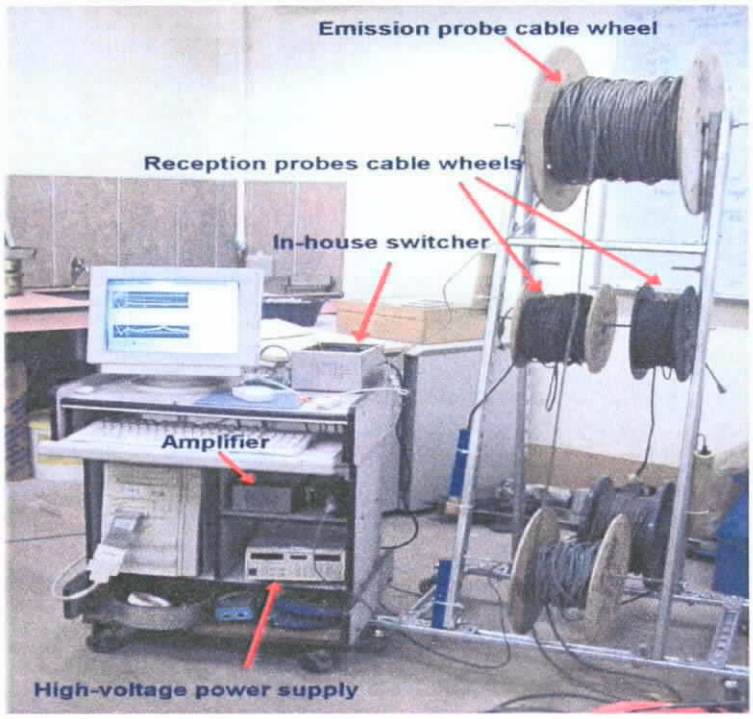

Figure 7.2.2. Photograph of the In-house Developed Prototype

7.2.1. The high-voltage pulsing component

The high-voltage pulsing component consists of an in-house developed ultrasound generator (including a high voltage supply and an in-house developed switcher) and an ultrasonic emission probe.

The high voltage supply

Figure 7.2.3 shows the high voltage supply applied in this project from Stanford Research Systems™ of model of PS310 with a range of 50~1250 volts direct current. By the control of the in-house developed switcher, the high voltage supply provides a sudden change of voltage to the piezoelectric materials for the ultrasonic pulse excitation.

Figure 7.2.3. Photograph of the high voltage supply

The in-house switcher

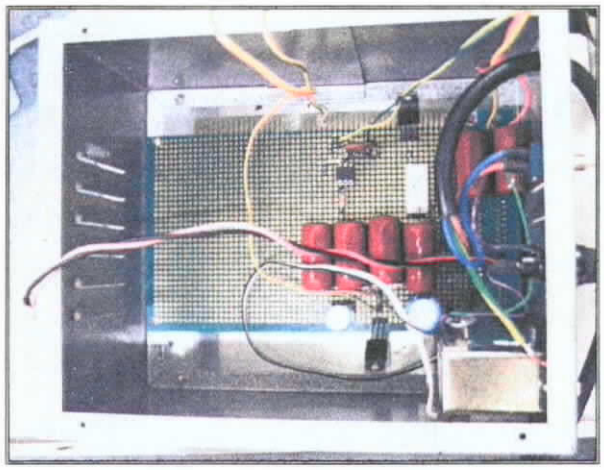

Figure 7.2.4. Photograph of the in-house developed switcher

If a high-voltage electrical pulse is applied to a piezoelectric material, a pulse of ultrasonic energy is generated in the material and propagates into the testing medium (Halmshaw 1987). The only application of the high voltage supply is that it cannot excite the emission probe to generate ultrasound. In this project, the in-house developed ultrasound generator, as shown in Figure 7.2.4, serves as a controller to the high voltage supply in the MRS to produce a high-voltage electrical pulse.

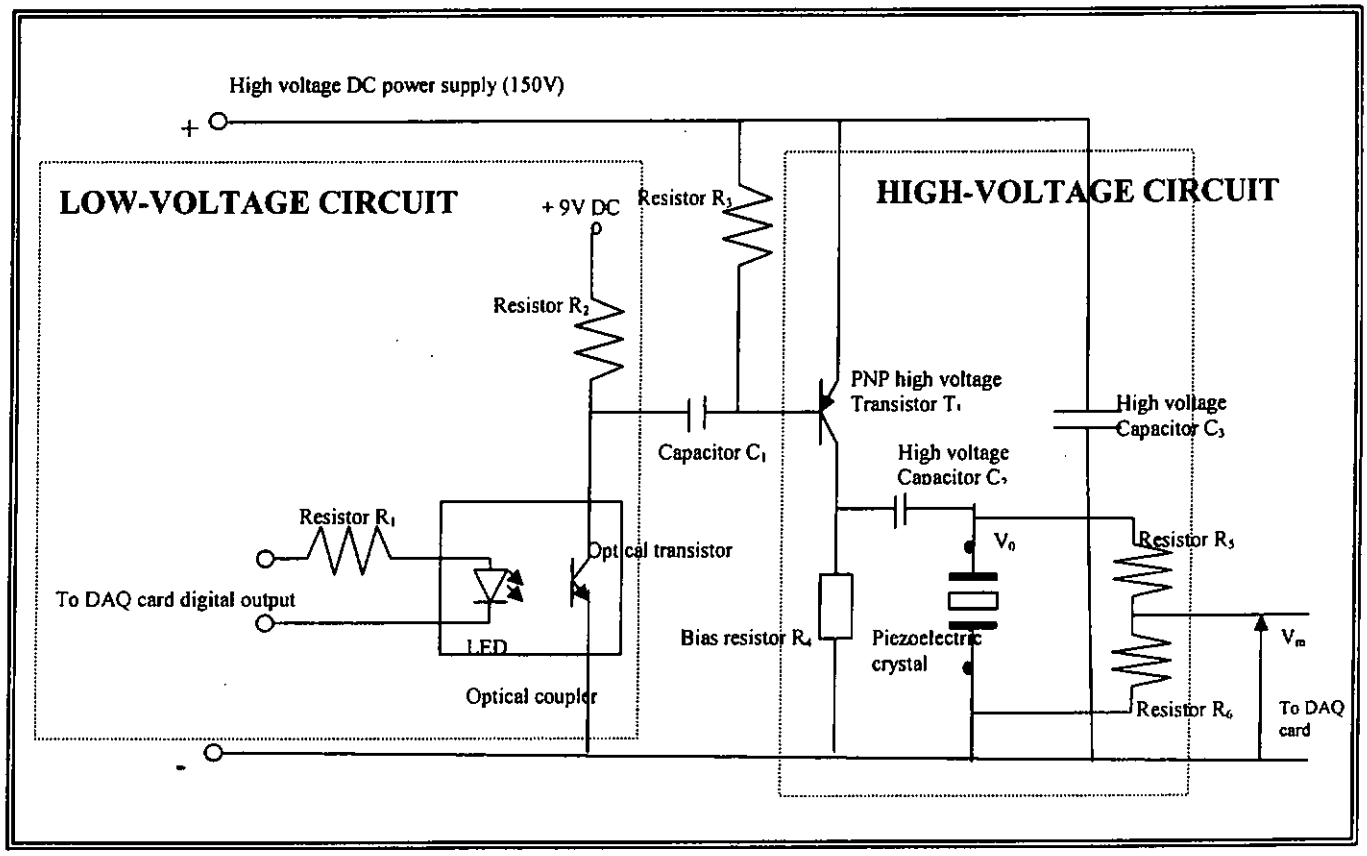

Figure 7.2.5. Circuit of the in-house developed ultrasound generator

Figure 7.2.5 shows the circuit of the in-house ultrasound generator and its operation is explained step-by-step as follows. In the low-voltage circuit, the programming controls the DAQ card to generate a 5V voltage pulse to the optical coupler. An optical coupler is used to isolate the DAQ card from the high-voltage circuit. The LED in the optical coupler controls the operation of the optical transistor. In a case of turning on the LED, the optical transistor will produce a 0V voltage drop. In another case of turning off the LED, the optical transistor will produce a 9V voltage signal. Repeating these two cases in a very short time can generate a square pulse.

The capacitor C_1 couples the square pulse from the low-voltage circuit to the high-voltage circuit, in which the square pulse is changed into a transient pulse. The width of a transient pulse depends on the value of the capacitor C_1 and the voltage of the square pulse.

In the high-voltage circuit, the bias resistor R_4 provides a minimum current to the high-voltage-transistor loop in order to keep the transistor T_1 turn on (i.e. following the transient pulses).

The PNP high voltage transistor T_1 amplifies the transient pulse by about 30 times. The high-voltage capacitor C_2 then couples the amplified transient pulse to the point V_0. In addition, the high-voltage capacitor C_3 saves the charges from the high-voltage DC supply (i.e. 150V), in which a large current can be produced in a very short time to the point V_0. At the point V_0, pulses of high voltage and high current (in a very short time) are transmitted to the emission probe. Pulses of ultrasonic energy are finally generated.

The resistors R_5 and R_6 act as voltage dividers and form a configuration named as an attenuator. With the aid of the attenuator, the voltage across the emission probe can be attenuated to form V_m. This can ensure the DAQ card measure the value of V_0 safely.

The ultrasonic emission probe

The ultrasonic emitting probe, as shown in Figure 7.2.6, is placed in a

water-filled tube and emits an ultrasonic pulse. The probe, typically 0.2m long and 25mm diameter, consists of ceramic transducers in a sealed tube. In concrete testing, ceramic transducers are normally chosen because of their mechanical impedance close to that of concrete (Finno et al. 1997).

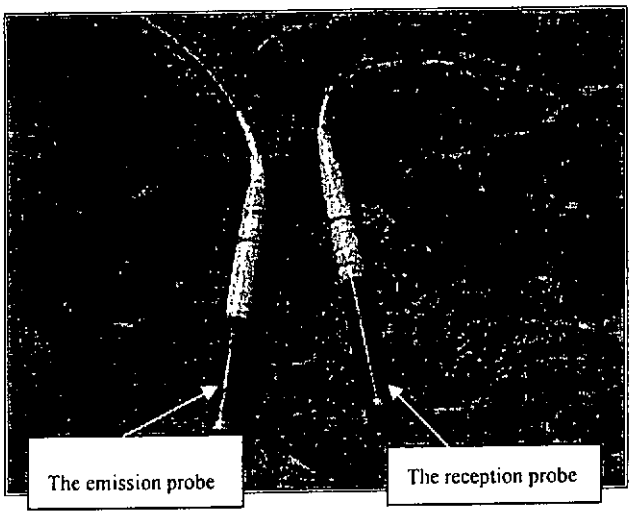

Figure 7.2.6. A pair of the emission and the reception probes

7.2.2. The Data Conditioning and Processing Component

The data conditioning and processing component consists of two ultrasonic reception probes, a filter, an amplifier, a National Instruments (NI) hardware interface, a NI data acquisition (DAQ) card and an acquisition and analysis programming in a LabVIEW environment.

The ultrasonic reception probes

The ultrasonic reception probes, as shown in Figure 7.2.6, are also ceramic in nature (same as the ultrasonic emission probe) and used to capture ultrasonic pulses transmitted from the ultrasonic emission probe. Before a

computer-based system can measure a physical signal, the reception probes convert the physical output signals into an electrical signal (i.e. voltage).

The filter

The use of filters is to remove unwanted noise from a signal. Depending on the frequency range of operation, filters either pass or attenuate input signal components. Figure 7.2.7 shows a high-pass filter applied in this project.

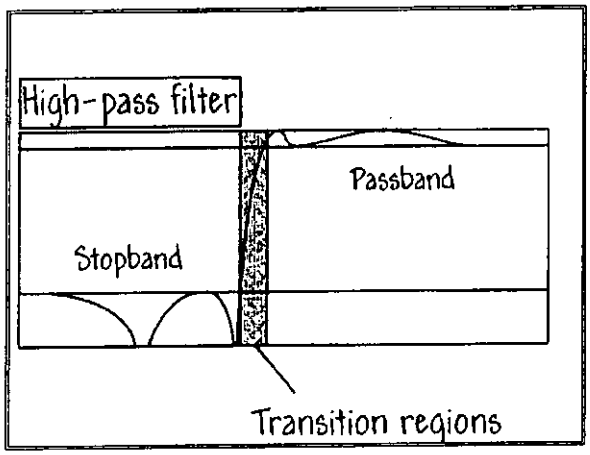

Figure 7.2.7. Schematic drawing of a high-pass filter

The amplifier

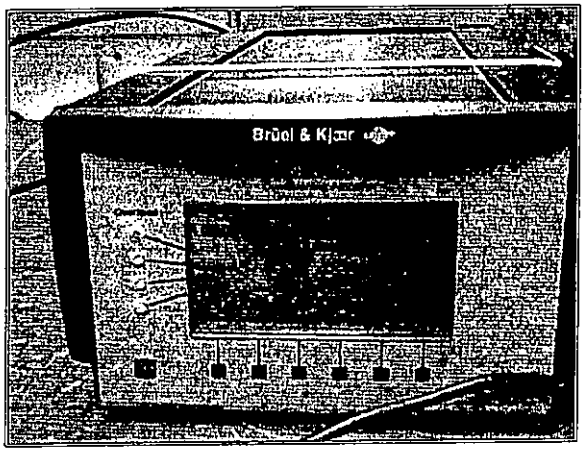

Figure 7.2.8. Photograph of the B & K model signal-conditioning amplifier

The B & K model signal-conditioning amplifier, as shown in Figure 7.2.8, is used to amplify the reception signals before conversion to a digital format for use in the computer. Amplification maximizes the use of the available voltage to increase the accuracy of the digitized signal and to increase the signal-to-noise ratio (SNR).

The National Instruments hardware interface and the data acquisition card

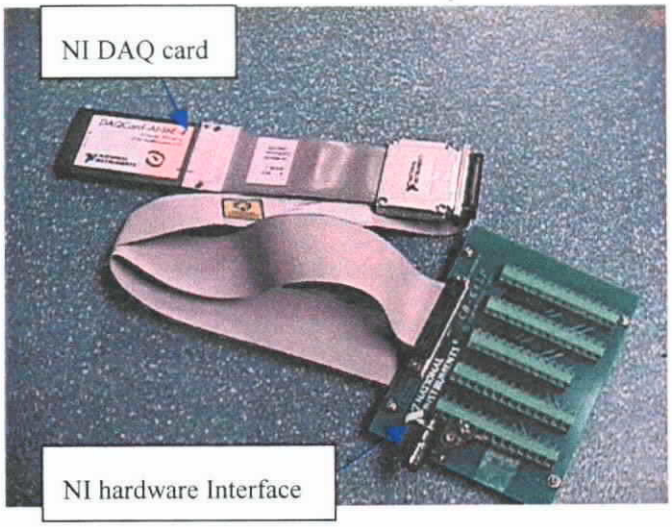

Figure 7.2.9. Photograph of the National Instruments (NI) hardware interface and the data acquisition (DAQ) card

The NI hardware interface and the DAQ card in Figure 7.2.9 serve as data acquisition interfaces between the reception probe and LabVIEW programming. The NI- DAQCard-AI-16E-4 card is installed on the same machine where the programming LabVIEW was located and collects the reception signals from the ultrasonic reception probes. This card allows 68 different I/O pin assignments (channels) and has a maximum scan rate of 500kS/s.

The data acquisition and analysis programming under a LabVIEW environment

The main program, LabVIEW (Laboratory Virtual Instrument Engineering Workbench) from NI, is a universal programming system based on the graphical programming language G. The characteristics (including ease of programming, higher flexibility and programming efficiency) of LabVIEW provide a powerful graphical programming development environment. LabVIEW is used for a wide variety of applications in many different fields (Ibrahim 2001)(Ruck et al. 2000)(Kraub et al. 1999)(Barrea et al. 2001).

The construction of a circuit diagram with a large number of graphical elements is typical for this programming language (Jamal et al. 1998). LabVIEW has two components, a graphical user interface ('Panel') and a graphical program code ('Diagram'). The 'Panel' is where the interactive controls and displays are located. The 'Diagram' is where the underlying logic and 'code' of the program is located. The 'Panel' and the 'Diagram' of this project are given in Figures 7.2.10 and 7.2.11 respectively.

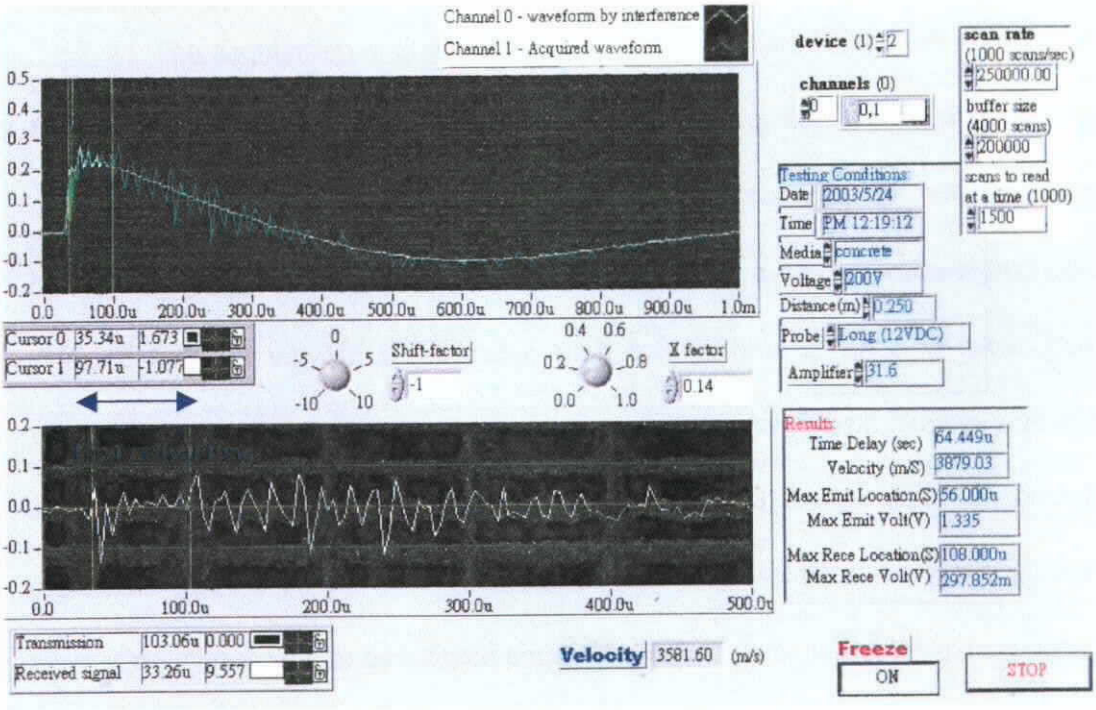

Figure 7.2.10. The 'Panel' of the MRS program. To the left is the instant graphical display of a total combined waveform and a true signal; to the right are the input windows (including a device number, number of channels, a scan rate, testing date, testing time, a testing medium, voltage applied, a transmission path and an amplification factor by the amplifier).

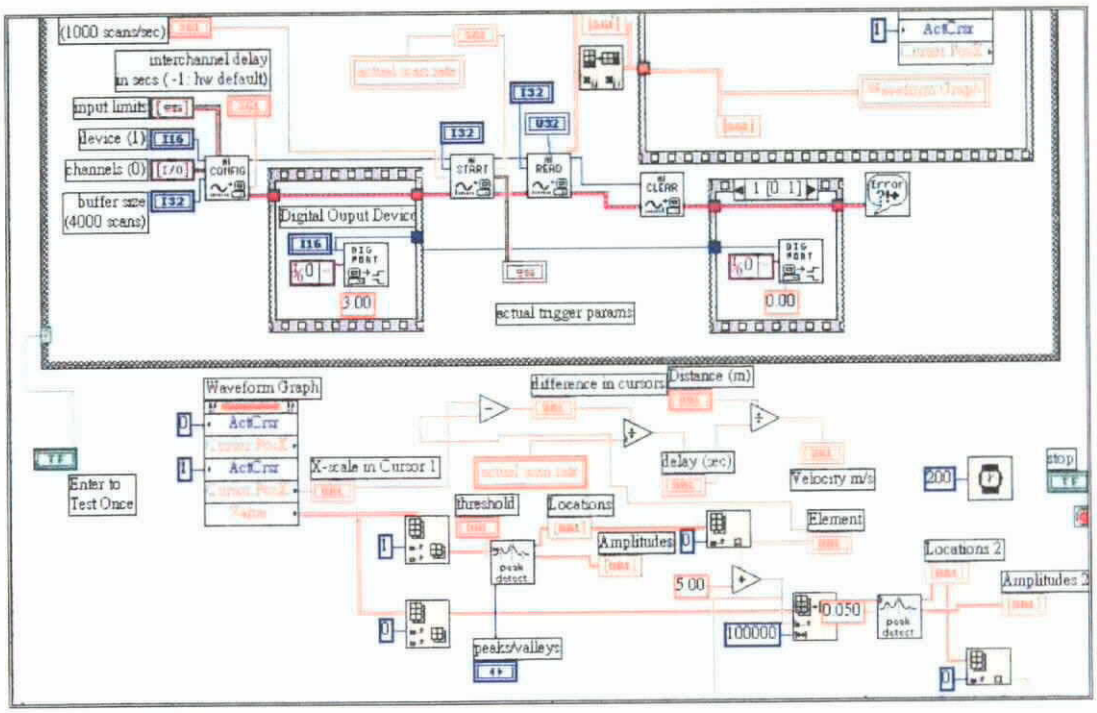

Figure 7.2.11. A portion of the 'Diagram' of the MRS programming of Figure 7.2.10. The graphical elements are wired to each other and visualize the dataflow.

The acquisition and analysis programming of the MRS was constructed for acquiring and manipulating the raw data, analyzing the data, and displaying the results. The useful information in analog time-domain signals was conveyed by the acquired data. The information associated with a time-domain signal (also referred to as a waveform) includes such information as time to peak, peak magnitude, time to settle, slope and the shape of peaks. The physical signal (i.e. discrete time samples) must be sampled and measured at a rate that adequately represents the shape of the signal. To deal with discrete time samples, care (including sampling rate and signal amplification) must be taken when converting from the analog, x(t), to the digital, x[n], domain.

Sampling rate

One of the most important parameters of an analog input system is the rate at which the DAQ board samples an incoming signal. A fast sampling rate acquires more points in a given time and can therefore often form a better representation of the original signal than a slow sampling rate. Sampling too slowly may result in a misrepresentation of the incoming analog signal. Figure 7.2.12 shows an adequately sampled signal, as well as the effect of under-sampling. The effect of under-sampling is that the signal appears as if it has a different frequency than it truly does. This misrepresentation of a signal is called an alias.

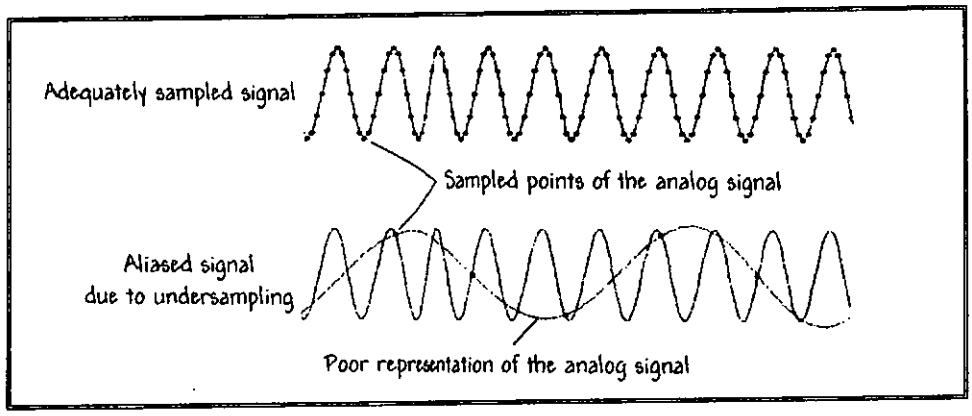

Figure 7.2.12. Poor representation of the analog signal due to a slow sampling rate

According to the *Nyquist Theorem* (Loertscher et al. 2000), the sampling rate must be at least twice the maximum frequency component in the signals in order to avoid aliasing. For a given sampling rate, the maximum frequency that can be represented accurately, without aliasing, is known as the Nyquist frequency. Signals with frequency components above the Nyquist frequency will appear aliased between direct current and the Nyquist frequency. In this research, the maximum frequency component in the signals is in the range of 40 to 50kHz. In order to have a truly representation of samples, the sampling rate was chosen to be at 250kHz which was more than twice of the maximum frequency component.

Signal amplification

Amplification by analog (a B & K signal-conditioning amplifier in this project) and digital means (a function of 'gain' in the DAQ programming) can amplify the reception signals (from the reception probes) before conversion to a digital format for use in the computer. Amplification maximizes the use of the available voltage to increase the accuracy of the digitized signals and to increase SNR.

7.3. Implementation of the In-house Developed Prototype Based on the Virtual Instrument Platform

The process to determine the *first-arrival-time* (FAT) is shown in Figure 7.3.1 and is explained step-by-step as follows. An acquired waveform was firstly frozen and then corrected by manipulating and controlling the two buttons (i.e. a *shift-factor* and an '*X-factor*' in the middle of the *virtual instrument* 'Panel' as in Figure 7.3.1). This correction/decoupling process is required to cancel the effect of inherent interference (i.e. induced by the in-house developed ultrasonic signal generator of the MRS) in order to obtain a true and meaning waveform.

The waveform captured in *Channel 0* is inherent within the system, even when no transmission is established. This waveform is labelled the inherent waveform (IWF) and it is believed to be induced by electronic interference within the in-house developed ultrasonic pulse generator of the MRS; while the waveform in *Channel 2* is a total combined waveform (i.e. a true signal combined with IWF). The true signal is recovered by subtracting IWF (i.e. *Channel 0*) from the total combined waveform (i.e. *Channel 2*). The end-product (i.e. a true signal) of this subtraction/decoupling process is then used for further processing on-line and off-line.

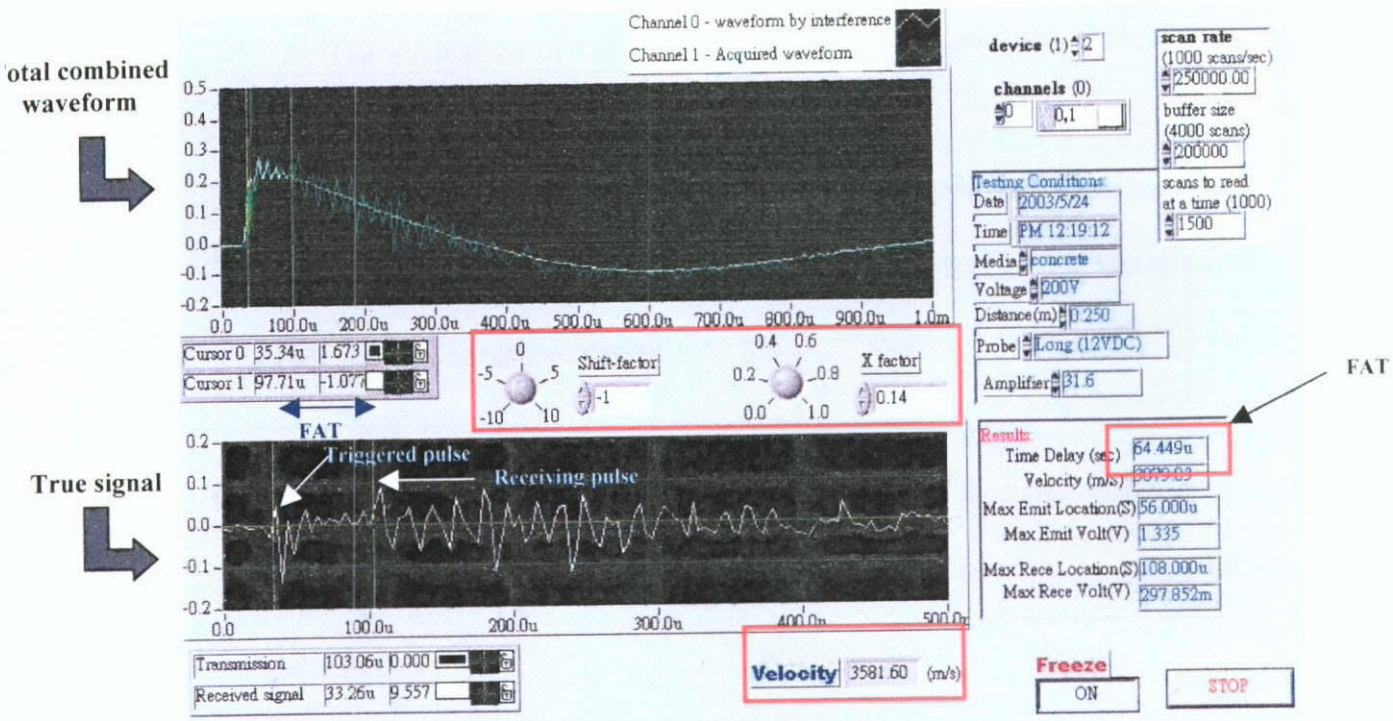

Figure 7.3.1. The 'Panel' of the MRS programming. To the top is the instant graphical display of a total combined waveform (i.e. a true signal combined with Inherent Waveform); to the middle is the control buttons of a '*shift-factor*' and an '*X-factor*'; to the bottom is a true and meaningful signal.

The FAT (which can be measured to a resolution of 0.001 μ sec) of the stress waves was determined as the time difference between the initiation time of the triggered pulse and the arrival time of the receiving pulse (as shown in a true signal in Figure 7.3.1). The transmission velocity of wave propagation in the test material was then calculated as the ratio of the travel path (i.e. the thickness of the specimen) to the FAT of the ultrasonic waves. Even though a single wave parameter (i.e. FAT or *apparent transmission velocity*) is sufficient to characterize test materials, evaluating more than one increases the reliability of the method (Ruck et al. 2000). Signal strength and signal energy spectral distribution of the true signals were also investigated by the Trapezoidal Rule of Integration and the *Fast Fourier Transform* (FFT) respectively.

The evaluation of the true signals comprises three phases as shown in Figure 7.3.2:

1. The *apparent transmission velocity* in a time domain (on-line data processing) is determined as the ratio of the travel path (i.e. the thickness of the specimen) to FAT of the ultrasonic waves.

2. The signal strength in a time domain (off-line data processing) is the summation of the successive partial evaluations of an acquired waveform as follows:

$$Signal\ strength = \int_{t_1}^{t_2} |f(t)| dt \approx \sum_j partial\ sums$$

where j is a range dependent on the number of points in an acquired waveform and the method of integration (i.e. the Trapezoidal Rule of Integration in this study).

3. The signal energy spectral distribution of the signals in a frequency domain is determined by the FFT which is one of the most powerful algorithms used for signal analysis and processing. It was developed by Jean Baptiste Joseph Fourier two centuries ago (Loertscher et al. 2000). A discrete FFT is applied to the raw ultrasonic waves when the samples are conveyed from the time domain representation to the frequency domain representation. In this project, the FFT was performed on the Hamming windowed waveforms.

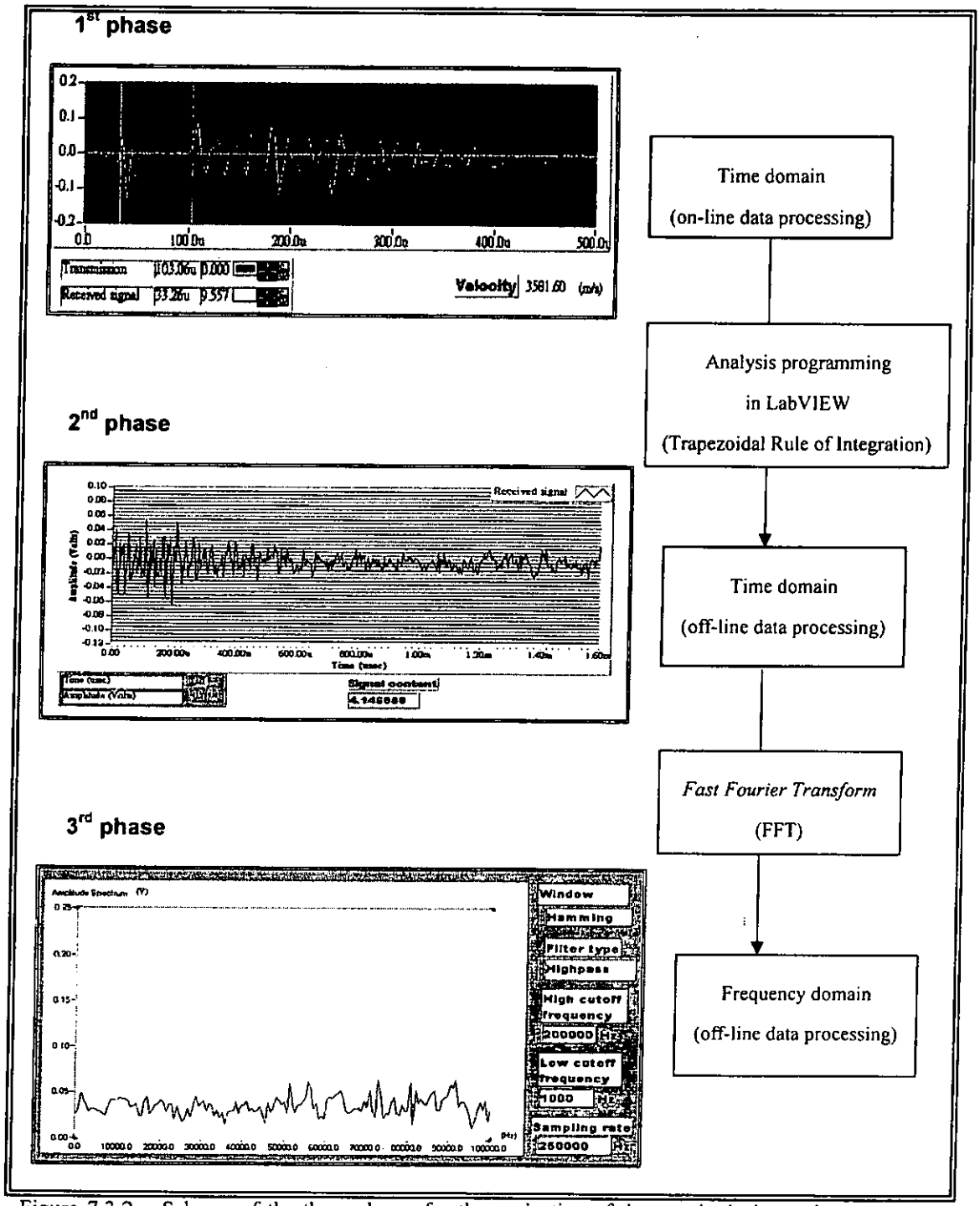

Figure 7.3.2. Scheme of the three phases for the evaluation of the acquired ultrasonic waves (on-line & off-line data processing)

7.4. Verification of the In-house Developed Prototype

Tests were conducted to verify the behavior of the pulses generated in the MRS. The verification included transmission velocities of the ultrasonic pulses (i.e. generated by the in-house developed ultrasound generator of the MRS) in different media (including water and concrete). The possible transmission path, especially in concrete, of the pulses generated was investigated in order to determine the working performance of the MRS in concrete testing.

7.4.1. Determination of the transmission velocity

Two ultrasonic probes (one an emission probe and the other a reception probe) were put inside a tank of water with a distance of 0.2m apart, as shown in Figure 7.4.1. In the verification, these probes were kept steady in order to get an average of 5 received waveforms. The FAT of a captured waveform in Figure 7.4.2 was automatically determined by the advanced analysis programming (Section 7.3). The *apparent transmission velocity* was computed by knowing the transmission path (i.e. distance between two probes).

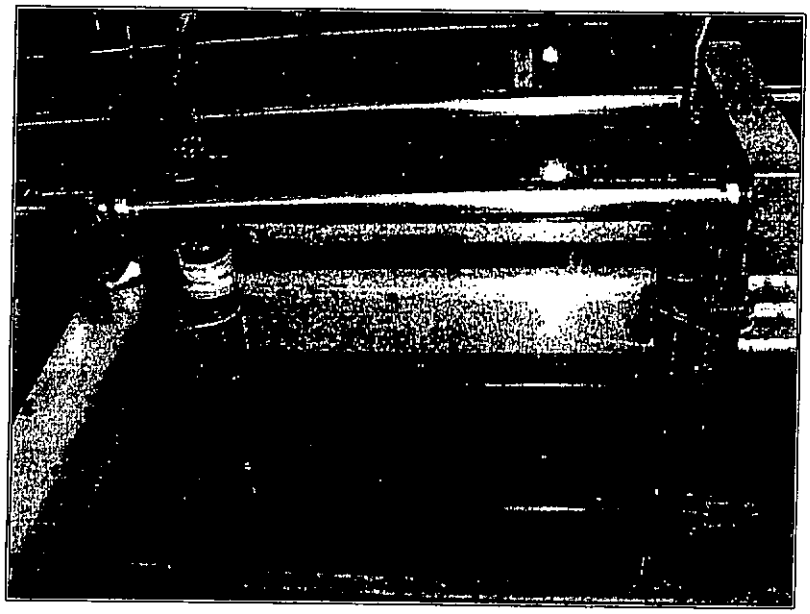

Figure 7.4.1. Experimental setup of the verification of the pulse in the water transmission

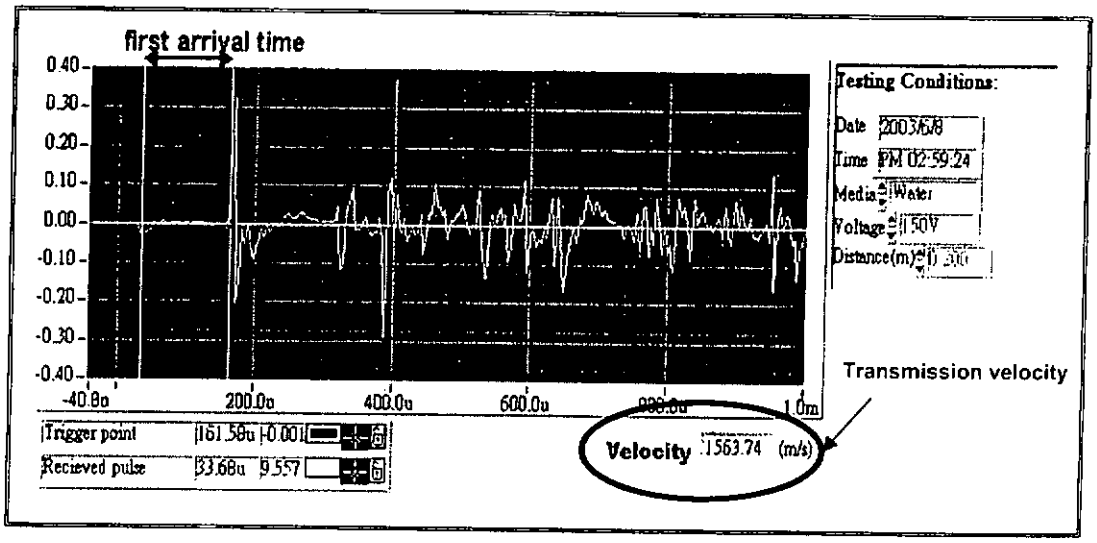

Figure 7.4.2. Determination of the *first-arrival-time* of the pulse in the water transmission

In addition to verify the MRS in water transmission, concrete testing is a prime interest in this research work, so that it is a need to verify the capability of the MRS in concrete transmission. A similar test was conducted in a test concrete specimen. Two probes were put at the bottom of two steel tubes with a distance of 0.25m apart in the concrete block as shown in Figure 7.4.3. The steel tubes were filled with water as a pulse transmission medium. Figure 7.4.4 shows the

determination of the FAT of the pulse in the concrete transmission.

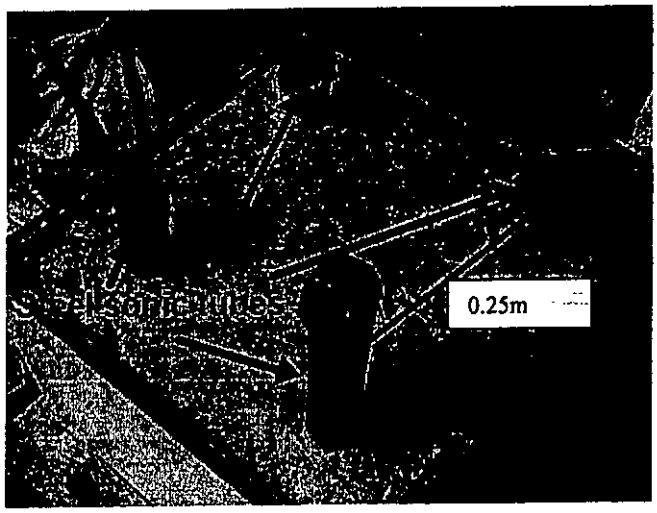

Figure 7.4.3. Specimen for the verification of the pulse in the concrete transmission

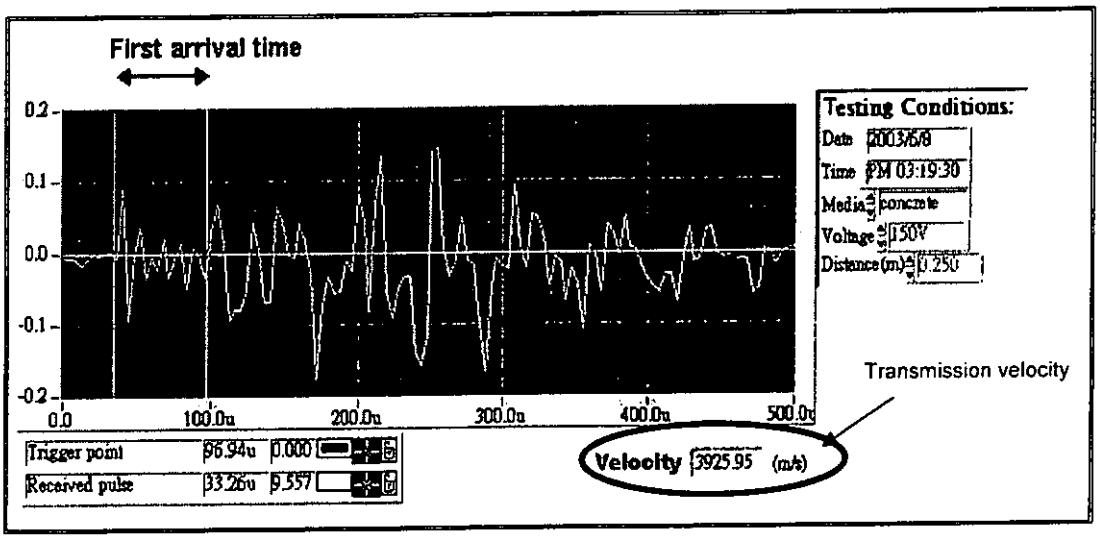

Figure 7.4.4. Determination of the *first-arrival-time* of the pulse in the concrete transmission

Table 7.4.1. Average transmission velocities in the water and concrete transmissions

	Verification in water			Verification in concrete		
	Transmission path (m)	First arrival time (FAT) (μs)	Transmission velocity (m/s)	Transmission path (m)	First arrival time (FAT) (μs)	Transmission velocity (m/s)
1st	0.20	127.88	1563.94	0.25	72.8	3925.95
2nd	0.20	129.88	1539.86	0.25	69.7	3886.80
3rd	0.20	127.06	1574.07	0.25	68.5	3949.64
4th	0.20	129.88	1539.86	0.25	72.6	3943.53
5th	0.20	130.18	1536.38	0.25	73.3	3910.64
		Average of transmission velocity in water =	1550.82 (m/s)		Average of transmission velocity in concrete =	3923.31 (m/s)

Table 7.4.1 shows the average transmission velocities in water and concrete. These computed transmission velocities are in good agreement with the values for ultrasonic transmission in both water and concrete (Sansalone et al. 1991).

7.4.2. Determination of the possible transmission path

Variation of transmission velocity with transmission path in a concrete medium was investigated in order to determine the working performance of the MRS in the concrete testing. In this experiment, six concrete blocks of different lengths (including 0.45m, 0.55m, 0.63m, 0.81m, 0.92m and 1.14m) without built-in defects were constructed as shown in Figure 7.4.5 and Table 7.4.2.

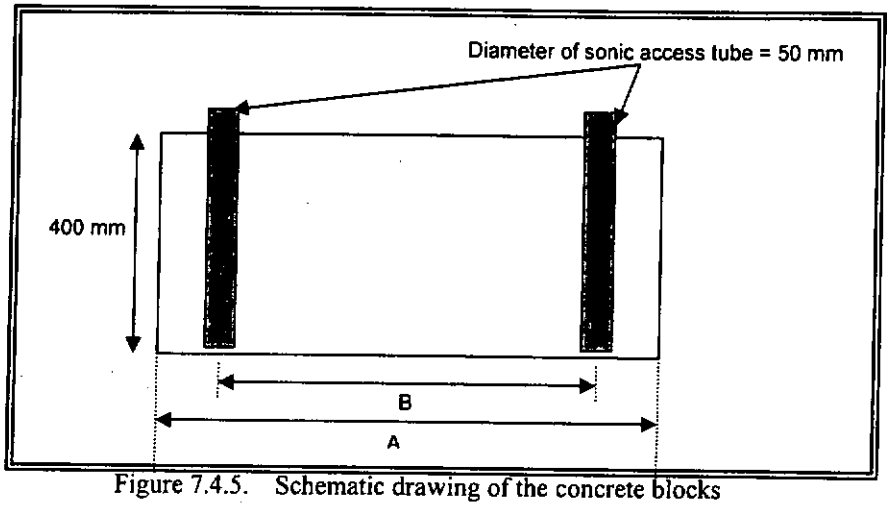

Figure 7.4.5. Schematic drawing of the concrete blocks

Table 7.4.2. Description of the concrete blocks

Test panel No.	Length of the concrete blocks (A, mm)	Length between two sonic access tubes (B, mm c/c)	Concrete strength (MPa)
1	450	250	35
2	550	350	35
3	630	430	35
4	810	610	35
5	920	720	35
6	1140	840	35

Before testing, all the sonic access tubes were filled with water to provide the necessary acoustic coupling. The probes were put at the bottom of the sonic access tubes and kept still while taking a measurement. Ultrasonic waves emitted from an ultrasonic emission probe traveling through the infilled material (i.e. concrete) and finally picked up by an ultrasonic receiving probe. The measured values of the FAT in these specimens are presented in Table 7.4.3 and Figure 7.4.6.

Table 7.4.3. FAT obtained from the MRS in the concrete specimens with different concrete transmission paths

Transmission path (m)	First arrival time (FAT) (μs)	Transmission velocity (m/s)
0.25	65	3832
0.35	93	3761
0.43	110	3896
0.61	158	3867
0.72	Signals received were too weak to be detected	
0.84	Signals received were too weak to be detected	

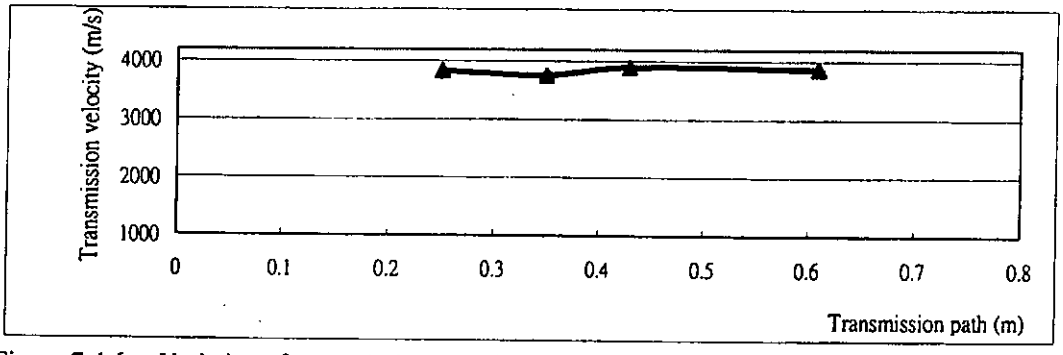

Figure 7.4.6. Variation of transmission velocity with transmission path in the concrete specimens tested

Figure 7.4.6 shows the computed transmission velocities ranging from 3760m/s to 3900m/s when the transmission paths are between 0.25m and 0.61m. This transmission velocity range is the category of the sound concrete by ultrasound transmission velocity identification. However, in a longer transmission path (i.e. longer than 0.61m), the ultrasonic transmission velocity is difficult to be determined. This is due to a low voltage supply to an ultrasonic emission probe so that a weaker pulse of ultrasonic energy generated, which is difficult to be detected in a longer transmission path. According to the above experimental results, the ultrasonic pulses generated in the MRS propagate well in a concrete medium up to a transmission path of 0.6m.

7.5. Summary of the Instrumentation of the In-house Developed Prototype

The construction and development of the hardware and software of the in-house multi-channel ultrasonic data acquisition prototype MRS are described. The MRS developed by the researcher is based on National Instruments hardware

and a LabVIEW environment. This prototype is capable of acquiring two or more channels of signals simultaneously in performing a sonic test in a bored pile with sonic-tube-installation. As a result, the prototype reduces the operation time and finally minimizes the overall project construction cost.

The data acquisition and analysis was facilitated by the use of a flexible graphical programming environment LabVIEW. It was designed for pre-programmed data acquisition, processing and visualizing. The evaluation of the ultrasonic signals is comprised of three phases both in the on-line and off-line processing.

The MRS of the pulses generated by the in-house developed ultrasound generator was verified in terms of the transmission velocity and possible transmission path, especially in a concrete medium. The *apparent transmission velocities* (obtained by the MRS) in both water and concrete media are in good agreement with the values for ultrasonic transmission in both media. By the experimental results, the ultrasonic pulses generated in the MRS are capable of propagating well in a concrete medium up to a transmission path of 0.6m.

8.1. Introduction to the Ultrasonic Assessment of Foundation Concrete by the In-house Developed Prototype

The in-house multi-channel ultrasonic data acquisition prototype MRS was constructed and developed (Sections 7.2 & 7.3) especially designed for deep foundation concrete elements after installation. To demonstrate the successful application of this prototype in assessment of foundation concrete elements, a sonic test was performed in a concrete specimen with built-in defects. The signals obtained from the MRS were analyzed in different approaches (including *apparent transmission velocity*, signal strength and spectral energy content). This provides more information about test materials.

8.2. Concrete Specimen Tested

The concrete Specimen I was constructed with artificial defects. The construction details of this specimen are shown in Figure 8.2.1. The Specimen I was made with the following sizes: 1m length, 0.26m width and 0.8m height, and embedded with four steel 50mm diameter sonic access tubes (namely A, B, C and D).

To introduce the artificial defects, pieces of polystyrene were put inside Specimen I between sonic access tubes A and B, and between sonic access tubes C and D. These pieces of polystyrene simulate typical concrete defects (such as low-grade concrete and inclusion of foreign materials other than concrete) along a

pile shaft. A void with size of 0.2m length, 0.26m width and 0.2m height was also created as shown in Figure 8.2.1.

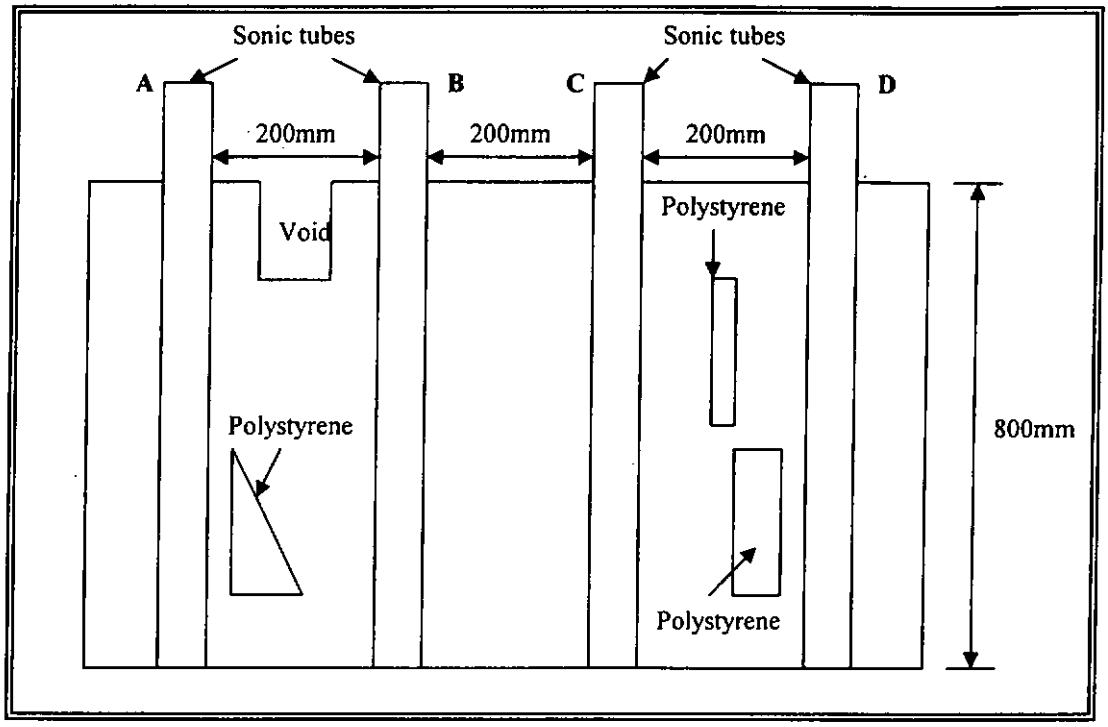

Figure 8.2.1. Details of artificial defects in Specimen 1

8.3. Hardware and Software Configuration of the In-house Developed Prototype

Table 8.3.1 shows the hardware and software configuration of the MRS in the concrete testing. The details of the construction and development of the MRS are described in Sections 7.2 and 7.3.

Table 8.3.1. Hardware and software configuration of the MRS in the concrete testing

The setup parameters in the hardware	
Power supply	150 V
Amplification factor of the hardware	316/volt
One emission probe and one reception probe	50 kHz (nominal frequency)
The setup parameters in the software	
Sampling rate	250 kHz samples/second
Sampling size	5000 samples

8.4. Experimental Procedures and Signal Processing

A sonic test using the MRS was carried out in this specimen, in which three probes (i.e. one transmitting probe and two receiving probes) were first lowered to the toe of the sonic access tubes (i.e. in tubes A, B and C, and another arrangement in tubes B, C and D) and slowly raised in unison (as shown in Figure 8.4.1). The details of carrying out a sonic test were given in Section 2.4.

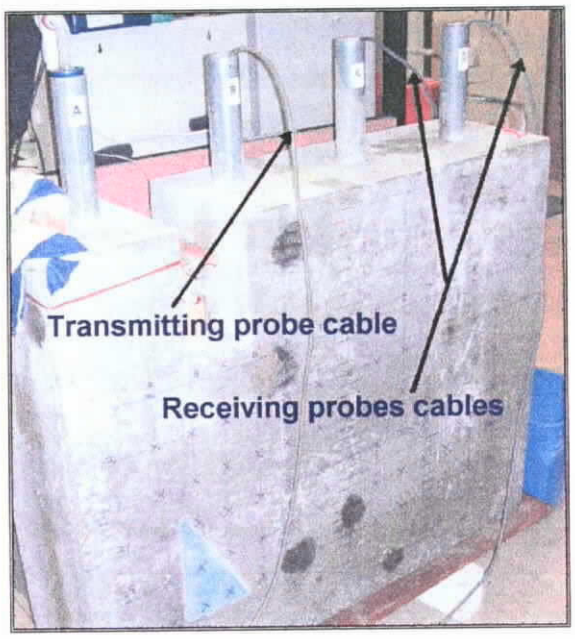

Figure 8.4.1. Photograph of the concrete Specimen I

With the use of the in-house developed MRS, acquisition of the ultrasonic signals at a very fine vertical interval (i.e. 0.02m) was performed. The *apparent transmission velocity* through concrete was determined at each measurement level. The accuracy of the method depended on the accuracies with which *first-arrival-time* (FAT) and the transmission path length between the probes have been determined. The distances (i.e. transmission path length) measured at the top of the sonic access tubes in Specimen I are shown in Table 8.4.1.

Table 8.4.1. Transmission path lengths between sonic access tubes in Specimen I

Specimen	Sonic access tubes	Transmission path length (m)
I	A-B	0.25
	B-C	0.25
	C-D	0.25

The determination of the transmission path length is also affected by the configuration of the transmitting and receiving probes. The highest accuracy is achieved with the probes on the same level to create a horizontal wave path. During the test the probes were lowered to the bottom of the tubes, and then withdrawn as pulses were recorded at regular depths (Finno et al. 1997). To know the precise depths of the transmitting probe and the receiving probes from the bottom of the tubes, and to make sure they were at the same depth, the length of each tube has been measured and is shown in Table 8.4.2.

Table 8.4.2. Length of sonic access sonic tubes in Specimen I

Specimen	Sonic access tubes	Length of access tube (m)
I	A	0.98
	B	0.98
	C	0.96
	D	0.98

Ultrasonic waves emitted from the transmitting probe passed through the concrete in Specimen I. The signals received by two receiving probes (as described earlier) were then digitized by the A/D converter in the MRS. These acquired signals (as shown in Figure 8.4.2) were processed and analyzed to obtain three parameters (i.e. ultrasonic transmission velocity, signal strength and signal energy spectral distribution) (as shown in Figure 7.3.2).

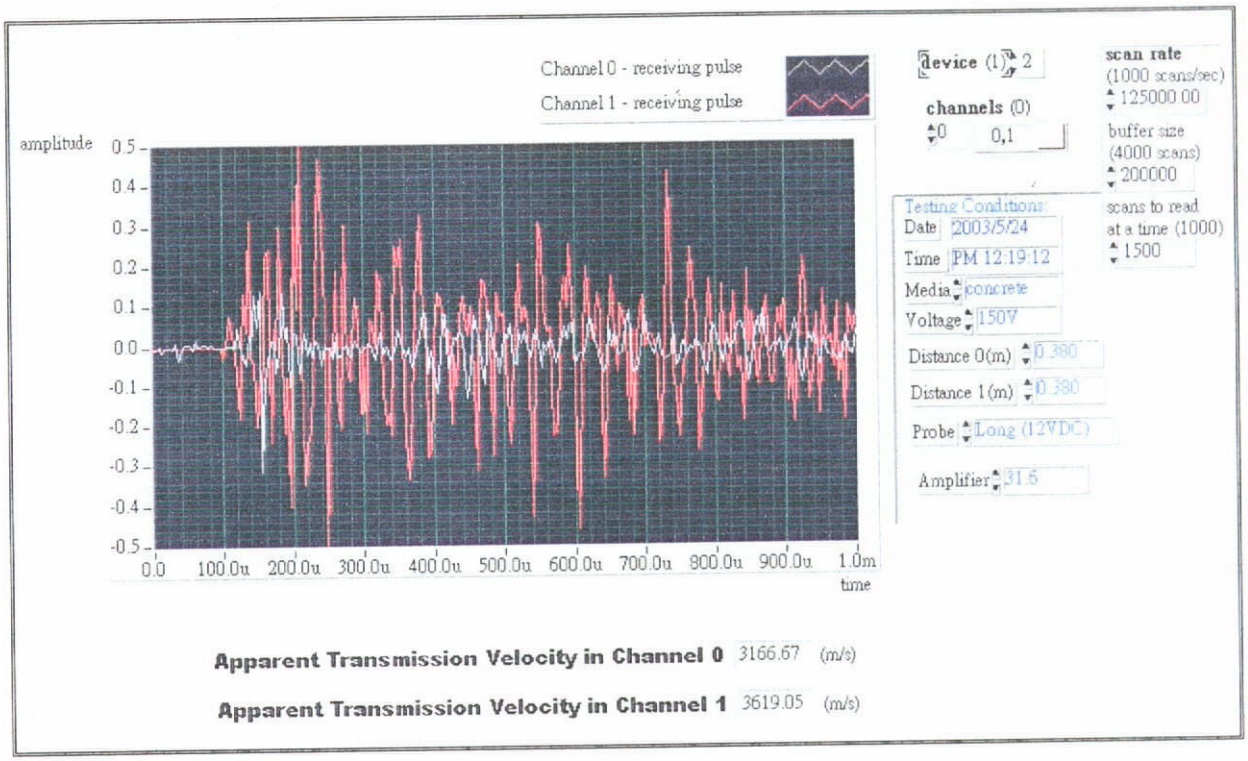

Figure 8.4.2. Diagram showing two acquired ultrasonic waveforms by the MRS

8.5. Results and Discussion

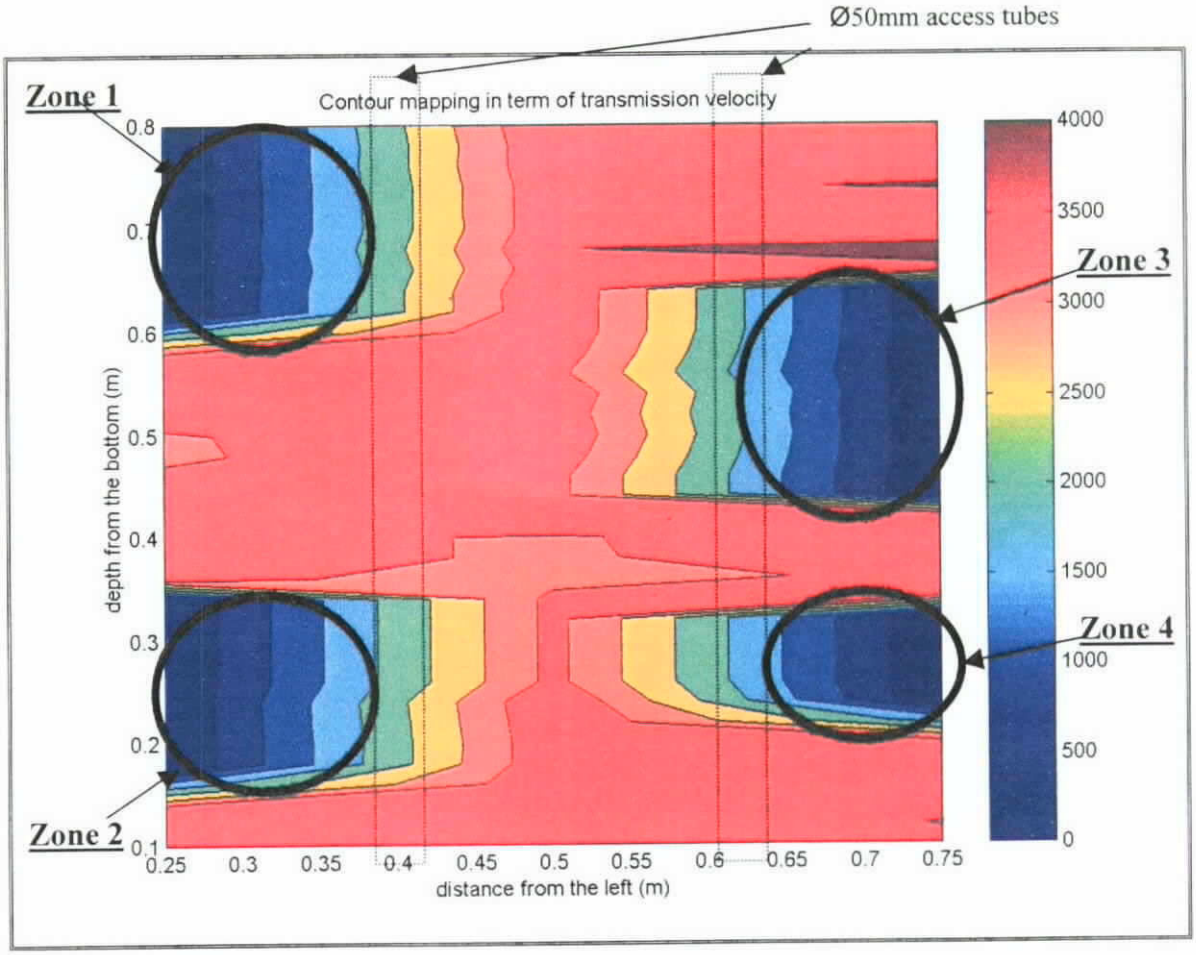

Figure 8.5.1. Contour mapping of the results in terms of *apparent transmission velocity*

Figure 8.5.1 shows the results obtained from the MRS and presented in the contour mapping in terms of *apparent transmission velocity*. The *apparent transmission velocities* of the highlighted regions, namely Zone 1 to Zone 4, are comparatively lower. This can be explained by the presence of the artificial defects inside the concrete block. The *apparent transmission velocities* (i.e. other than the highlighted zones) are found to be in the range of 3500m/s to 4000m/s which is in good agreement with the values for ultrasonic transmission velocity in sound concrete (as shown in Table 2.4.2).

Furthermore, Figure 8.5.2 shows the contour mapping in terms of the signal strength. Figure 8.5.2 shows similar results to Figure 8.5.1. The signal strengths in the highlighted regions, Zone 1 to Zone 4, are comparatively lower. This can also be explained by the presence of the artificial defects inside the concrete block.

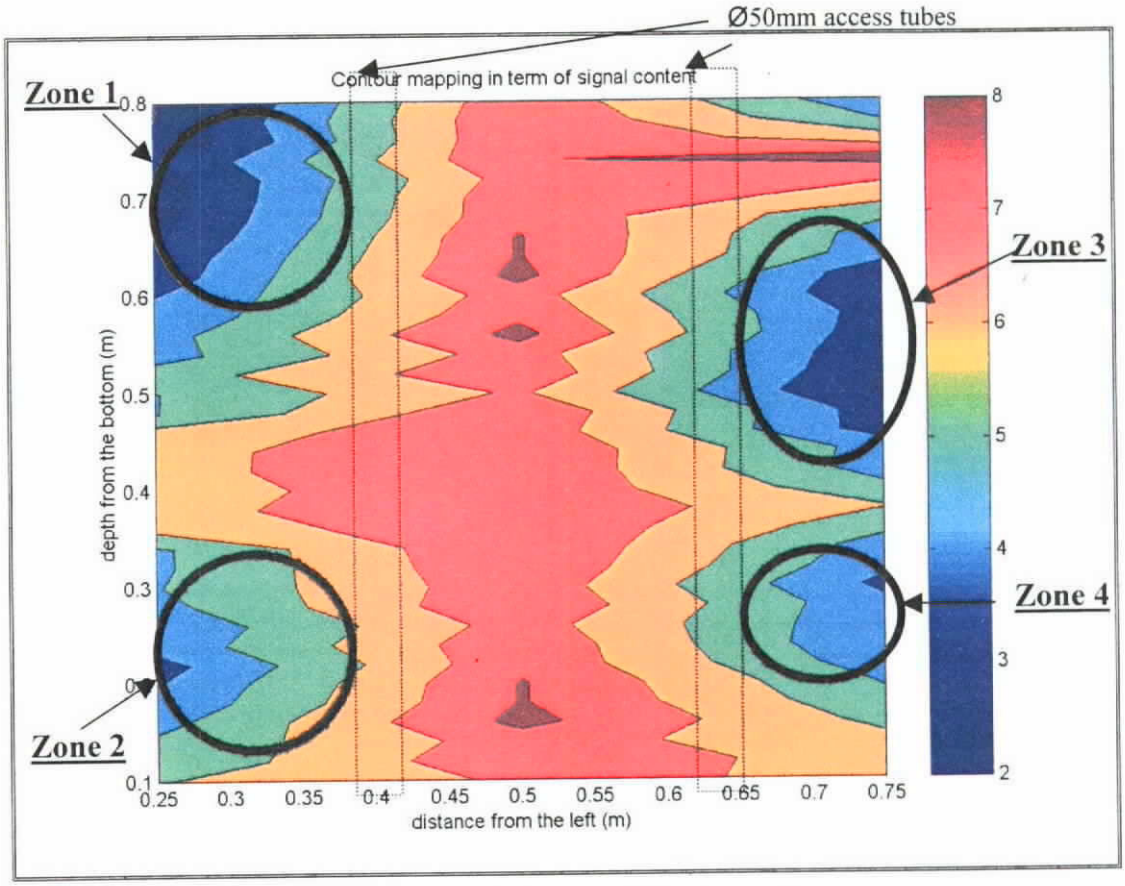

Figure 8.5.2. Contour mapping of the results in terms of signal strength

In addition to performing analysis in time domain, the signal energy spectral distribution across the analysis frequency span 0-100kHz of the signals was also investigated in a frequency domain (as shown in Figure 7.3.2). The signal spectral content represents the effectiveness of the propagation of mechanical energy of the ultrasonic waves through different transmission media.

Figure 8.5.3 shows different frequency spectra of ultrasonic waves obtained at different material media. It was observed that when the ultrasonic waves are propagating through sound concrete, the spectral energy content is always the greatest across the entire frequency span when compared with those transmitted through polystyrene and air (in descending order). This can be attributable to the signal attenuation imposed by the artificial defects (i.e. polystyrene and air). Air is known to be a very poor propagation medium of ultrasonic waves.

The different spectral energy content for ultrasonic transmission through different materials can be used for differentiating these different materials in addition to a differentiation technique based on transmission velocity criterion only.

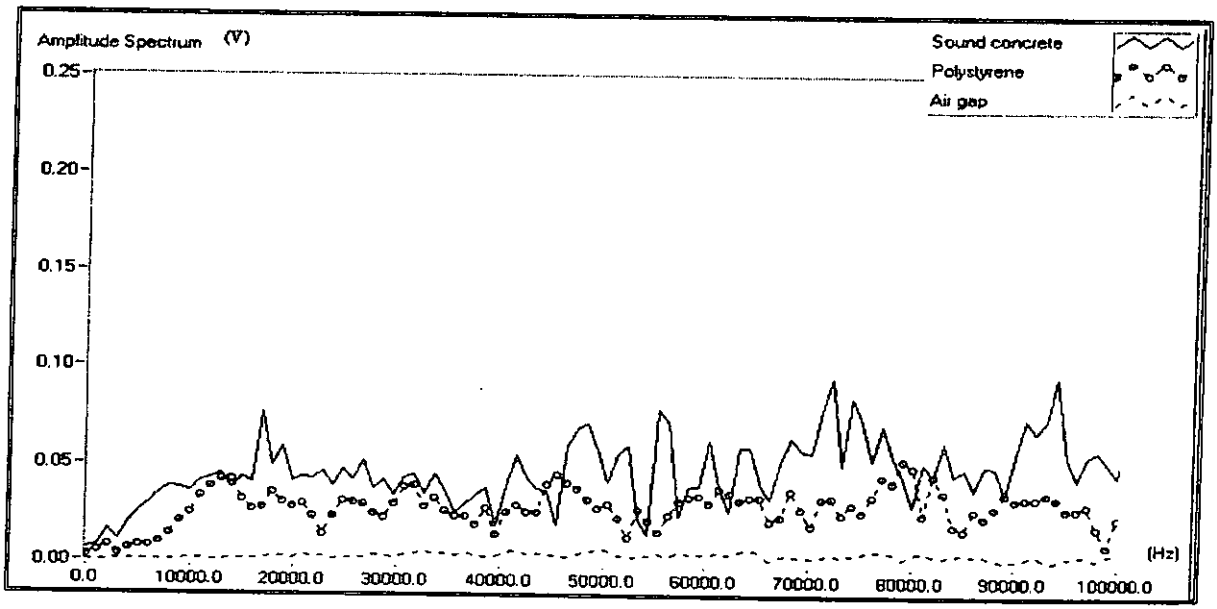

Figure 8.5.3. Signal energy spectral distribution of ultrasonic waves propagating through sound concrete, polystyrene and air.

8.6. Summary of the Ultrasonic Assessment of Foundation Concrete by the In-house Developed Prototype

This chapter generally describes the construction details about the artificial defects in Specimen I. The planned defects of Specimen I was constructed by putting pieces of polystyrene inside (as the simulation of concrete defects along a pile shaft) and leaving a hollow block near the top of Specimen I (as the simulation of void inside a pile shaft).

The successful application of the MRS in the concrete assessment was demonstrated by carrying out a sonic test in Specimen I with built-in defects. The signals acquired in two channels were displayed simultaneously during the measurement. The parameters (including *first-arrival-time/apparent transmission velocity*, signal strength and spectral content) of the signals were investigated, and they are found to be correlated to the properties of the materials. The consistent test results were obtained using the MRS.

Based on the experimental results, the computed *apparent transmission velocity*, signal strength and spectral content of the signals within the zones of the built-in defects are comparatively lower than that of sound concrete. This analysis approach is help to increase the reliability of the method in characterizing and evaluating test materials.

9.1. Introduction to the Ultrasonic Identification of Soil Strata by the In-house Developed Prototype

In soil characterization for civil and building engineering applications, drilling at a specific location is first conducted to obtain geological information about the soil, and laboratory tests using drilling cores are subsequently carried out. However, the information obtained at a particular drilling location is applicable only to that specific sampling point but not to soils between sampling points (Takahashi 2000).

Destructive methods (such as boring) are used to determine the properties and the behavior of the soil strata (Day 1999). Non-destructive test methods have shown to be fast, simple and useful approaches to characterize in-situ soils. Various geotechnical methods (for example the Seismic Refraction method, the Magnetic method and the Gravitational method) have been used to obtain geological information, not only at one specific point but also at various soil strata without changing the state of soils. Non-destructive ultrasonic testing technique is shown successful for evaluation of concrete foundation elements as discussed in Sections 2.4.1, 6.3 & 8.5.

This chapter demonstrates the application of an in-house developed MRS in characterizing soil strata (including very gravelly GRAVEL, sandy GRAVEL, gravelly SAND, very sandy SAND, silty clayey gravelly SAND and clayey gravelly sandy SILT as described in GEOGUIDE 3 and BS5930).

Variation of ultrasonic transmission velocity with degree of saturation and surcharge pressure are analyzed. A new method, called the '*X-factor*' technique, is proposed which is capable of characterizing soil strata based on the computed '*X-factor*'. The '*X-factor*' is found to be highly correlated to attenuation of ultrasonic signals.

9.2. Soil Specimen Tested

Tests were conducted on various types of soil (see Figure 9.2.1). The index properties of the soil are presented in Table 9.2.1. Laboratory testing methods were conducted to determine the geotechnical parameters of the soil. Particle size distribution and moisture content of each soil specimen were determined in accordance with Test 2.9.5b (Chen 1994) and Test 2.3.2a (GEO Chen 1994) respectively.

Figure 9.2.1. Photographs of the soil specimens

Table 9.2.1. Index properties of the soil specimens

		Specimen 1	Specimen 2	Specimen 3	Specimen 4	Specimen 5	Specimen 6
Classification*		very gravelly GRAVEL	sandy GRAVEL	gravelly SAND	very sandy SAND	silty clayey gravelly SAND	clayey gravelly sandy SILT
Particle Size (%)	Gravel	100	60	40	100	21	14
	Sand	0	40	60	0	38	31
	Silt	0	0	0	0	17	43
	Clay	0	0	0	0	24	12
Moisture Content (%)		0	2	6	9	3.8	6.8

(* In accordance with Table 15 in GEOGUIDE 3 by Hong Kong Geotechnical Control Office and BS5930:1999, Section 6)

9.3. Sample Preparation

Tests were conducted on the soil specimens to investigate the variations of ultrasonic signal parameters (i.e. *first-arrival-time* (FAT), transmission velocity and attenuation) with varying surcharge pressure at various degrees of saturation. Soil specimens were prepared in a rigid steel tank of 600mm long, 300mm wide and 300mm high as shown in Figure 9.3.1.

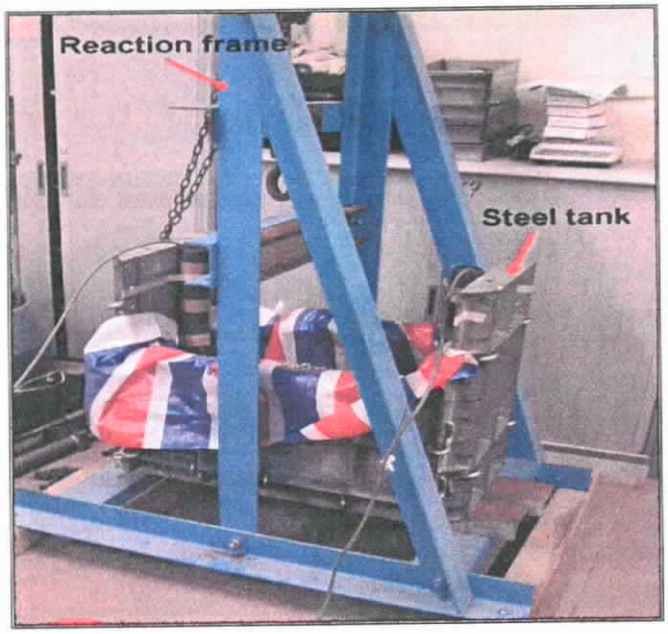

Figure 9.3.1. The steel tank in the soil testing

Soil specimens were prepared with water contents ranging from dry (0-23.3%) to a maximum degree of saturation (75-100%). A total of 30 samples were prepared. A pre-defined stepped increase of surcharge pressure as shown in Table 9.3.1 was applied on a soil specimen at each degree of saturation.

Table 9.3.1. A cycle of surcharge-pressure on a soil specimen at each degree of saturation

Applied surcharge pressure stage	Surcharge pressure (kPa)
1	0
2	10
3	50
4	100
5	150

9.4. Hardware and Software Configuration of the In-house Developed Prototype

The greater damping characteristic of soils causes a large attenuation of signals, which causes difficulty in defining the FAT of propagating waves. Soils are highly attenuating and absorptive materials, and the receiving signals are very weak and therefore dwarfed by noise. Therefore, when constructing a pulse transmission test apparatus, the amplitude of signal output must be high enough for the easy detection of propagating low amplitude elastic waves. To obtain a high level signal, it is necessary to apply a high voltage excitation pulse to excite a transducer, to increase the signal-to-noise ratio (SNR) of the transducer output, and to amplify a weak signal detected by a receiving transducer (Nakagawa 1996).

In soil testing using the MRS, the detected waves were amplified, before

post-processing, by one thousand times. The amplification factor required for soils was found to be, in general, three times greater than that for concrete (Table 8.3.1). Table 9.4.1 shows the hardware and software configuration of the MRS in soil testing. The construction and development of the MRS is described in greater detail in Section 7.2.

Table 9.4.1. Hardware and software configuration of the MRS in soil testing

The setup parameters in the hardware	
Power supply	150 V
Amplification factor of the hardware	1k/volt
An emission probe and a reception probe	50 kHz (nominal frequency)
The setup parameters in the software	
Sampling rate	250 kHz samples/second
Sampling size	1500 samples

9.5. Experimental Procedures and Signal Processing

In this experiment, two artificial tubes made of PVC, as shown in Figure 9.5.1, were pre-installed inside a soil specimen. A pre-defined stepped increase of surcharge pressure (as shown in Table 9.3.1) was applied on a soil specimen at each degree of saturation (as shown in Figure 9.5.2.

Tests were conducted using a through-transmission arrangement which is similar to that used for Cross-hole Sonic Logging (CSL) testing technique. The probes were first lowered to the toe of tubes and slowly raised in unison. The details of carrying out a sonic test were given in Section 2.4.

In this test, a pre-defined stepped increase of surcharge pressure was

applied on a soil specimen through a steel plate of 20mm thickness. A 12-ton capacity hydraulic jack was used to apply the surcharge pressure, and the force was monitored with a strain-gauge based load cell (of 12 tons capacity).

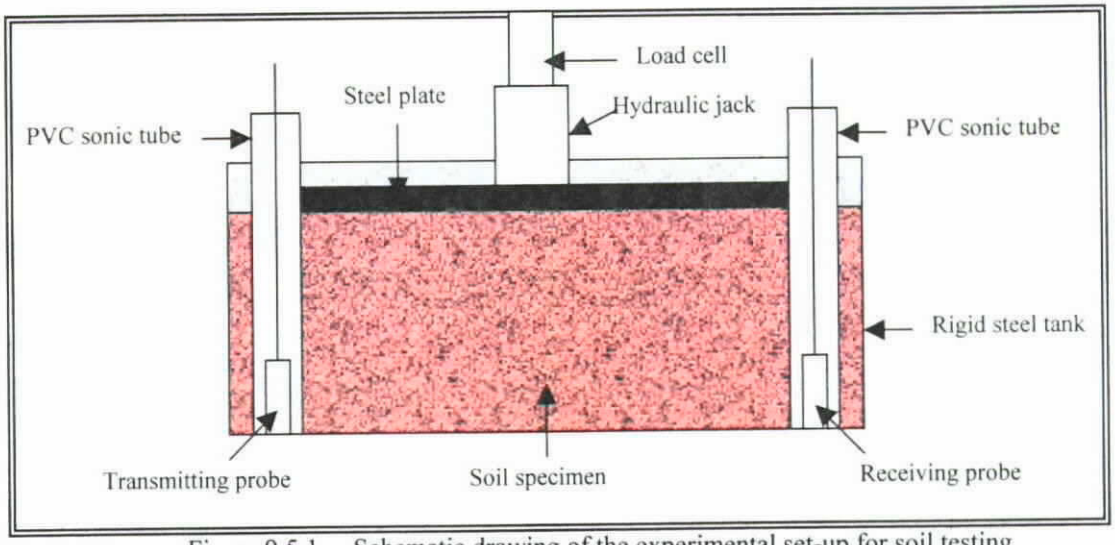

Figure 9.5.1. Schematic drawing of the experimental set-up for soil testing

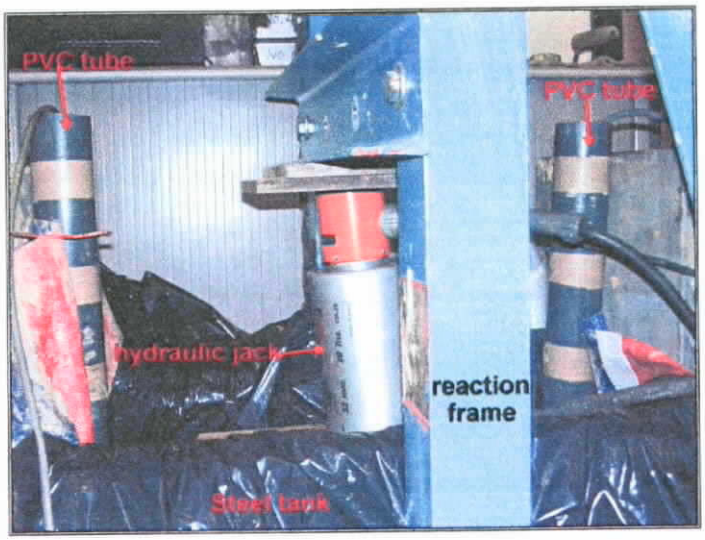

Figure 9.5.2. Photograph of the experimental set-up for soil testing

PVC tubes rather than steel tubes were chosen for the soil testing because steel tubes cause a higher attenuation of signals. The effects of different sonic access tube materials (i.e. steel and PVC tubes) on the signal strength in ultrasonic wave transmission are compared and discussed in Section 4.3. The amplitude of the received ultrasonic signals through PVC tubes is comparatively higher than that when steel tubes are used. The use of PVC tubes provides a higher SNR of the measured signals. This is particularly important for soils since they are highly attenuating materials and signals are inherently weak. The process to determine FAT is described in greater detail in Section 7.3. Figure 9.5.3 shows the control 'Panel' of the MRS programming for soil testing.

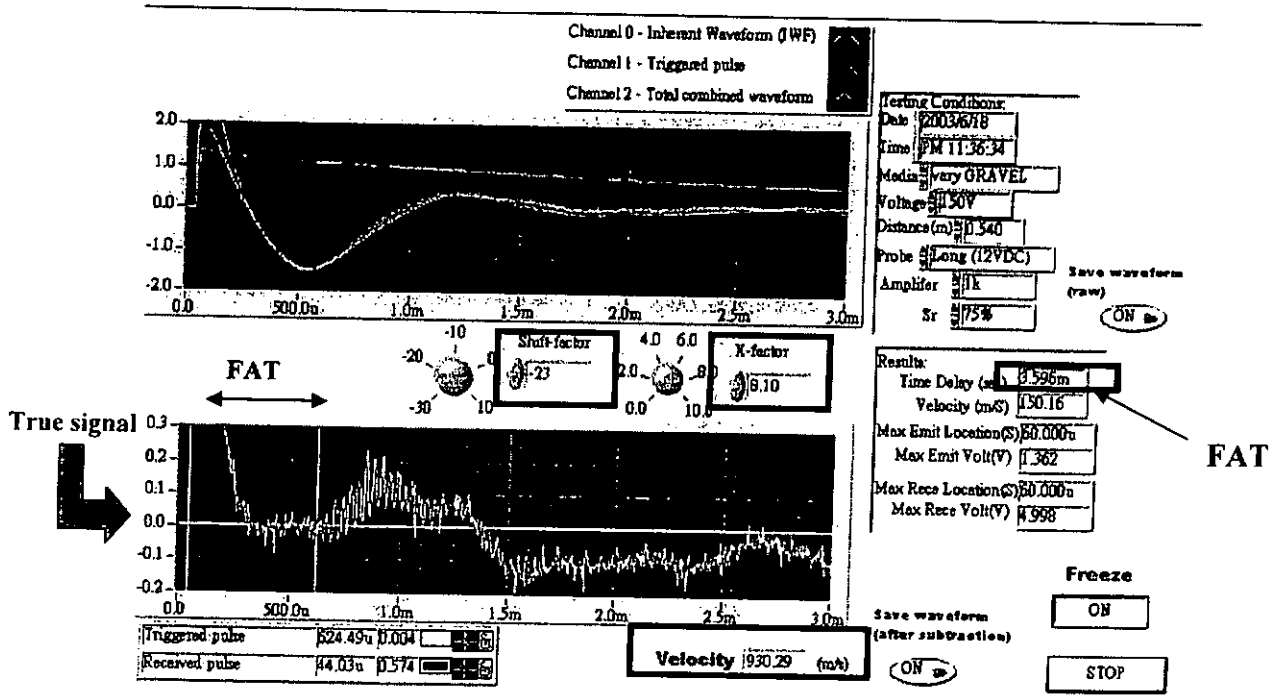

Figure 9.5.3. The control 'Panel' as in the graphical interface of the MRS program.
At the top is the instant graphical display of a total combined waveform (i.e. a true signal corrupted and coupled with Inherent Waveform).
In the middle are the control buttons of a '*shift-factor*' and an '*X-factor*'.
At the bottom is a decoupled waveform.

The characteristics of transmission of waves in a material are quantified, generally, using two parameters: transmission velocity and attenuation. Ultrasonic transmission velocity is governed by the elastic and mechanical properties of a material (such as Young's modulus, Poisson's ratio, etc.) whereas ultrasonic attenuation is related to the micro-structural properties of a material (McIntire 1991). With the developed MRS, the attenuation characteristics of a range of soils have been determined experimentally using the so-called '*X-factor*' technique (to be further explained in Section 9.6.3).

9.6. Results and Discussion

9.6.1. Variation of transmission velocity with degree of saturation

The relationship between transmission velocity and degree of saturation for Specimens 1 to 6 at different values of surcharge pressure are depicted in Figures 9.6.1 to 9.6.6 respectively. This relationship is found to be attributable to the variations in total unit weight and void ratio, as presented in Figures 9.6.1 to 9.6.6. According to the experimental results depicted in these figures, the velocity is found to increase with increasing total unit weight and decreasing void ratio of the specimens.

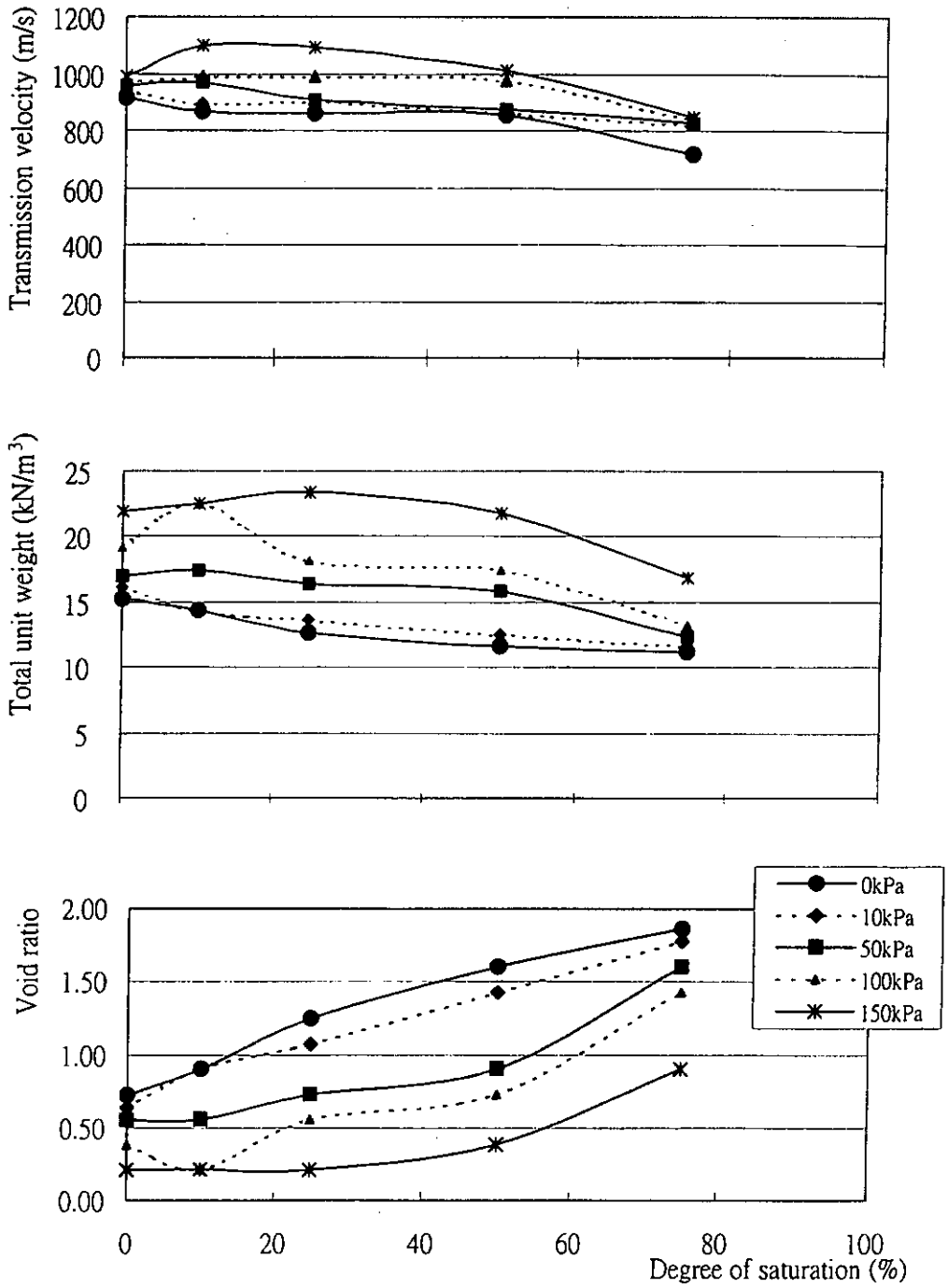

Figure 9.6.1. Variations of transmission velocity, total unit weight and void ratio with degree of saturation at each surcharge pressure for Specimen 1

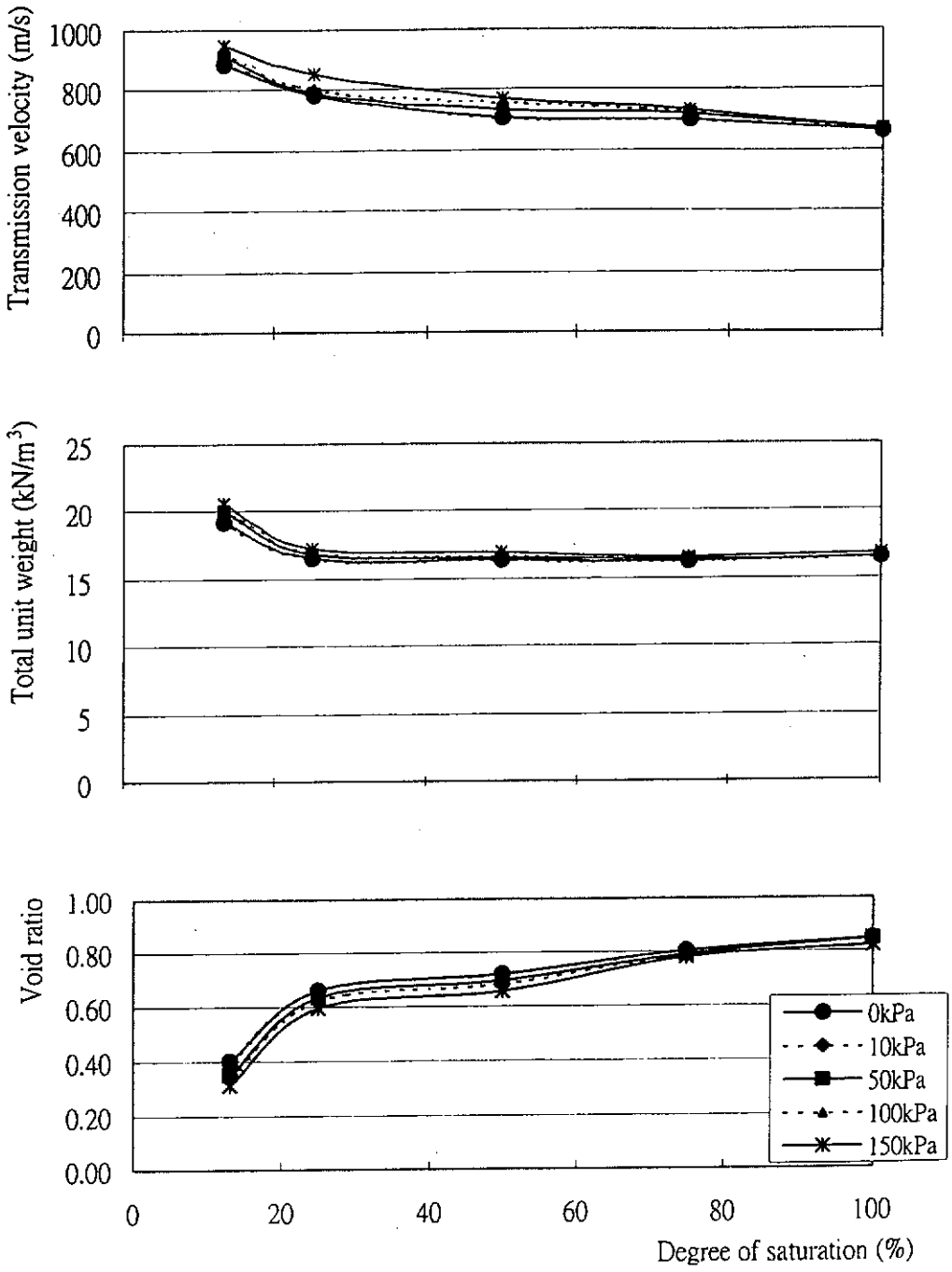

Figure 9.6.2. Variations of transmission velocity, total unit weight and void ratio with degree of saturation at each surcharge pressure for Specimen 2

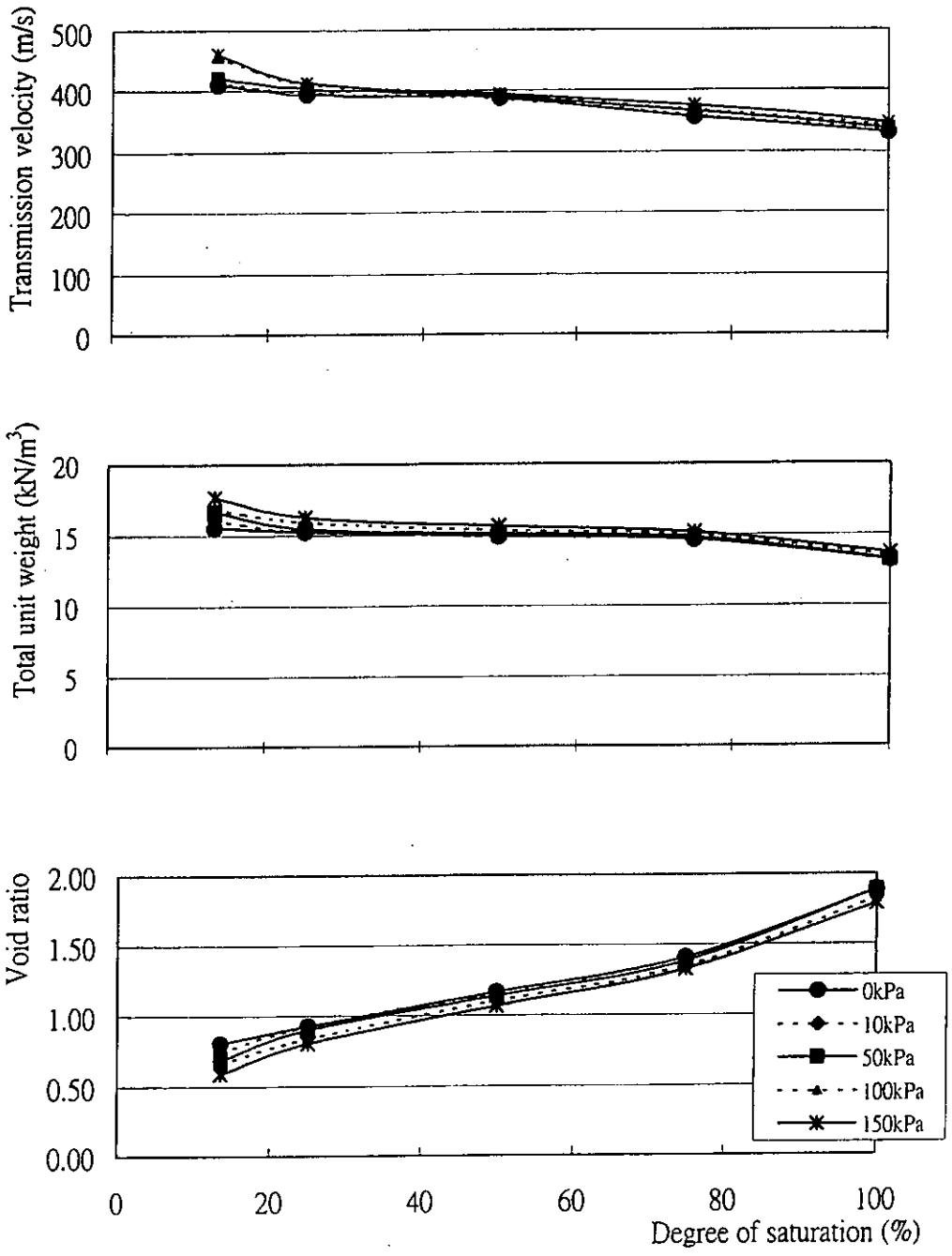

Figure 9.6.3. Variations of transmission velocity, total unit weight and void ratio with degree of saturation at each surcharge pressure for Specimen 3

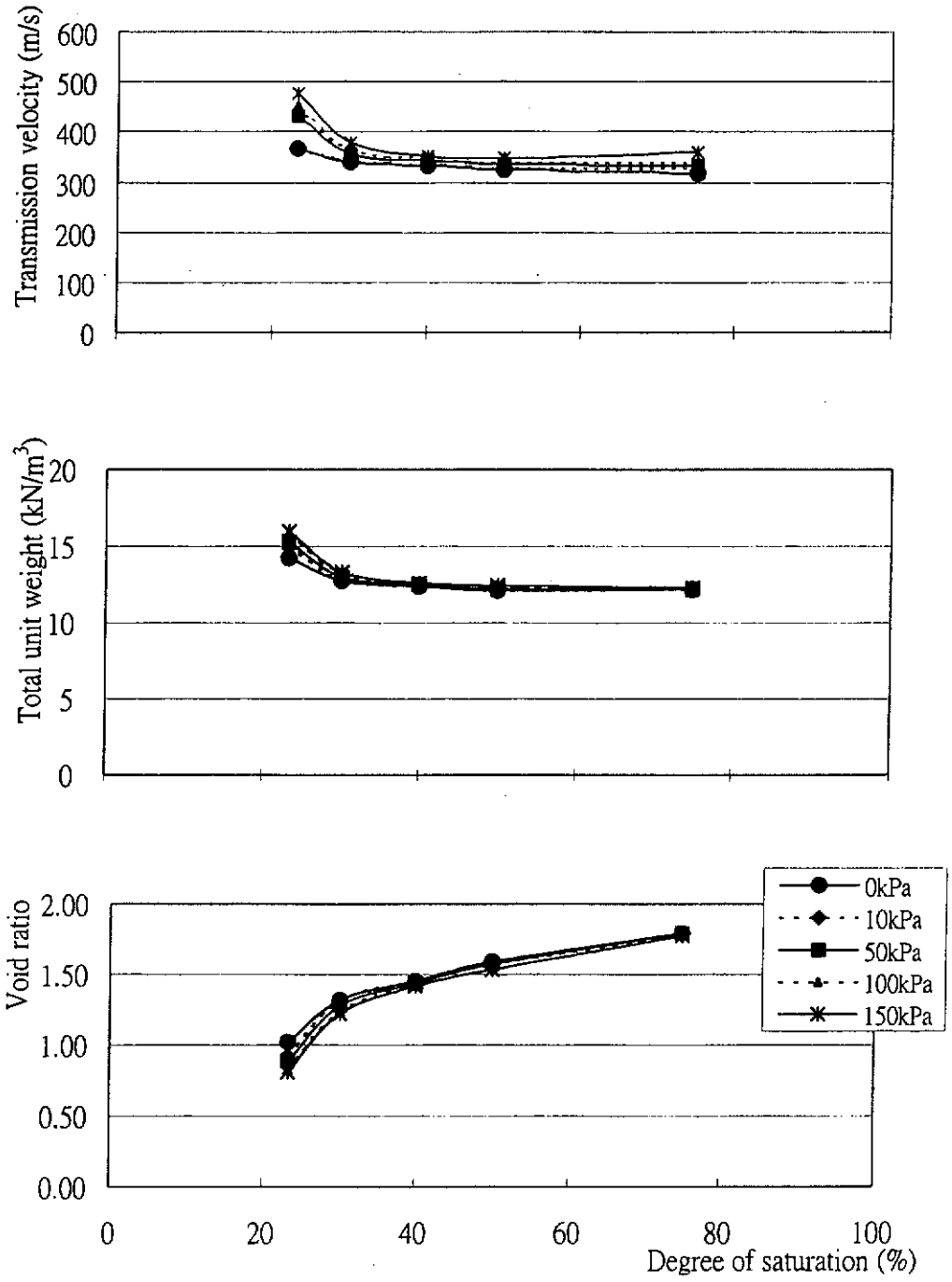

Figure 9.6.4. Variations of transmission velocity, total unit weight and void ratio with degree of saturation at each surcharge pressure for Specimen 4

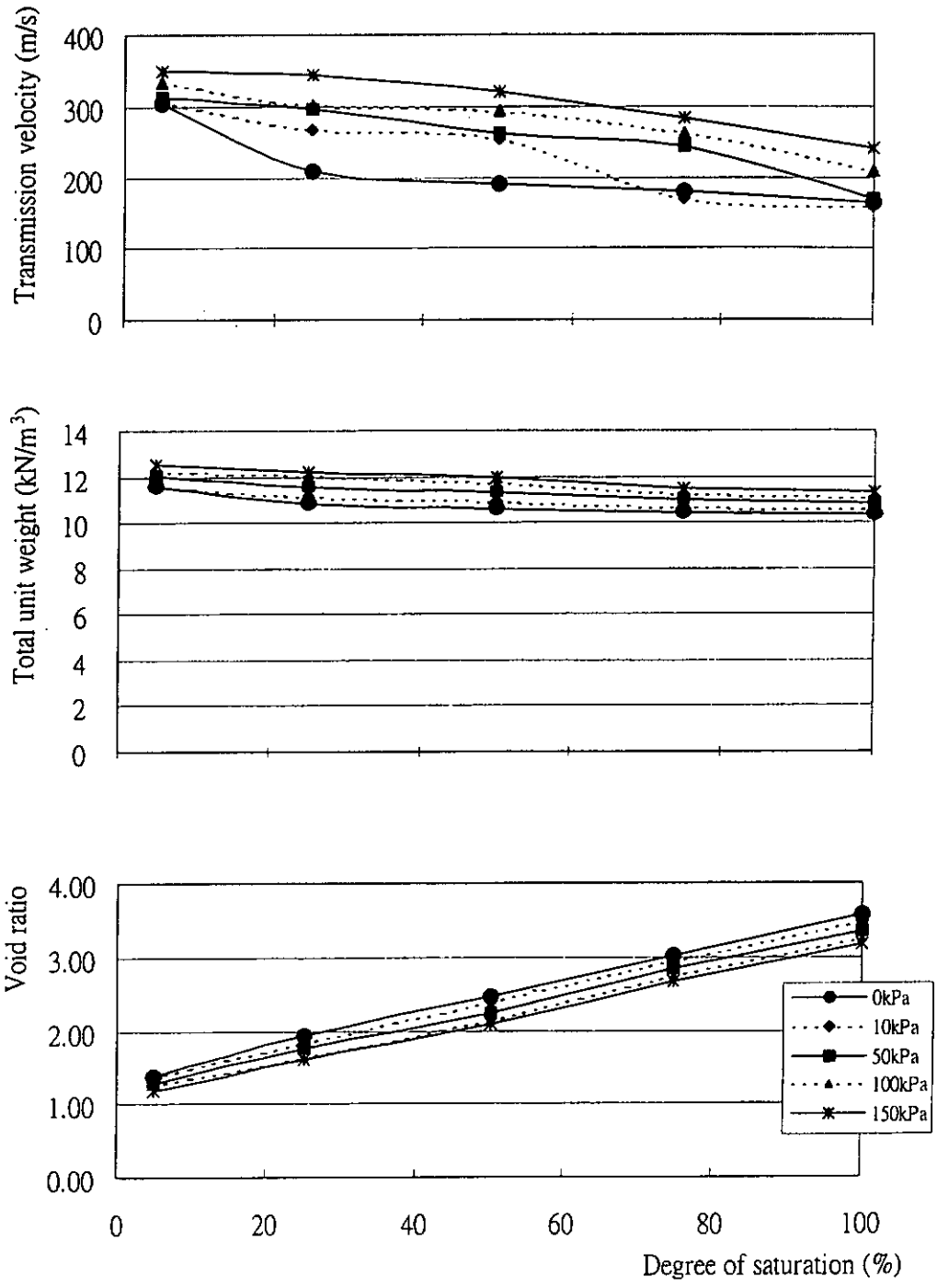

Figure 9.6.5. Variations of transmission velocity, total unit weight and void ratio with degree of saturation at each surcharge pressure for Specimen 5

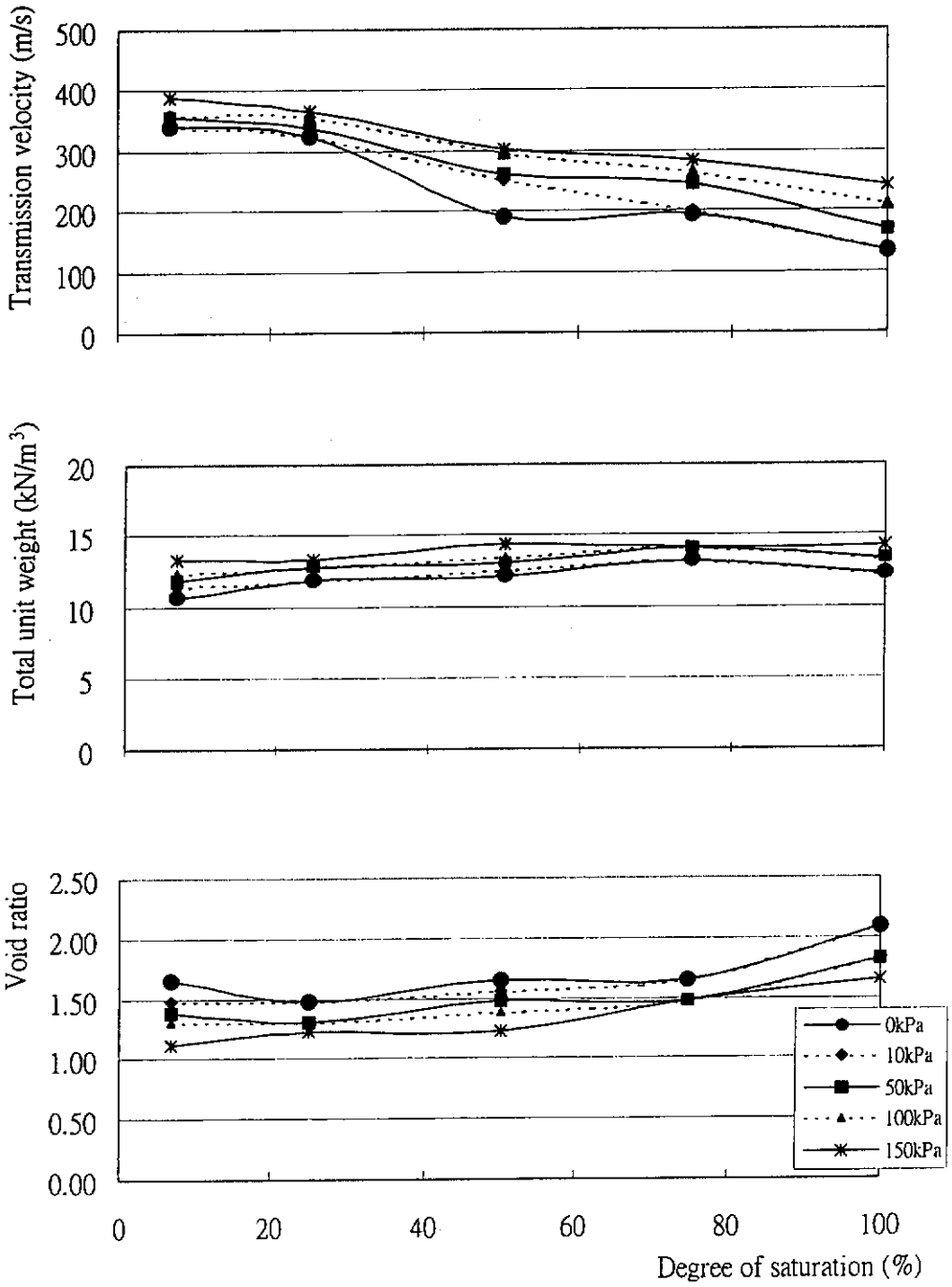

Figure 9.6.6. Variations of transmission velocity, total unit weight and void ratio with degree of saturation at each surcharge pressure for Specimen 6

For all the specimens, the variation of transmission velocity with degree of saturation is similar to the variation of total unit weight with degree of saturation but the inverse of the variation of void ratio with degree of saturation (Figures 9.6.1 to 9.6.6). In a three-phase system such as a compacted soil, wave transmission occurs through all of the phases. In general, velocities in solids are higher than velocities in liquids, which are higher than velocities in gases (McIntire 1991). Therefore, it is expected that high velocities occur at a high solid with low water and air contents.

Based on the experimental results, the transmission velocities decrease with increasing degree of saturation. The maximum velocities are observed at the lower degree of saturation (i.e. an initial degree of saturation) for all the specimens. Similar observation was made by Sheeran et al. (1967), in which velocities of P-waves were determined on three types of soils. It was observed that peak velocities increased with increasing dry density until the optimum water content. At water contents higher that the optimum water content, the velocities decreased with increasing dry density.

Highest solid and lowest void contents as indicated by maximum dry density and minimum void ratio occur at optimum water content in compacted soils (Inci 2002). Hence, maximum ultrasonic transmission velocity occurs at the optimum water content.

In this experiment, the specimens were not prepared from the dry water

content (i.e. a zero degree of saturation) and a trend of increasing transmission velocities from the zero to the optimum water content could not be investigated.

The highest maximum velocity is obtained for Specimen 1 and the lowest maximum velocity is obtained for Specimen 5 (Table 9.6.1). High densities (i.e. total unit weight in this case) and low air/water contents (i.e. void ratio in this case) result in high velocities, whereas low densities and high air/water contents result in low velocities. (Yesiller et al. 2000)

Table 9.6.1. Properties of the soil specimens under different surcharge pressures

	Specimen 1	Specimen 2	Specimen 3	Specimen 4	Specimen 5	Specimen 6
Classification*	very gravelly GRAVEL	sandy GRAVEL	gravelly SAND	very sandy SAND	silty clayey gravelly SAND	clayey gravelly sandy SILT
Maximum velocity (m/s)	1099.55	947.48	460.32	476.28	350.23	388.76
Maximum total unit weight (kN/m^3)	22.50	20.58	17.67	15.96	12.56	13.33
Minimum void ratio	0.21	0.31	0.59	0.81	1.19	1.12

(* In accordance with Table 15 in GEOGUIDE 3 by Hong Kong Geotechnical Control Office)

9.6.2. Variation of transmission velocity with surcharge pressure

Transmission velocities obtained for Specimens 1 to 6 at different surcharge pressure is presented in Figures 9.6.7 to 9.6.12 respectively. These figures show that transmission velocities increase with increasing surcharge pressure for all the specimens. Variation of transmission velocity with surcharge pressure can be attributed to variations in total unit weight and void ratio of the specimens as presented in Figures 9.6.7 to 9.6.12. Variation in transmission

velocity is similar to the variation of total unit weight and the inverse of void ratio.

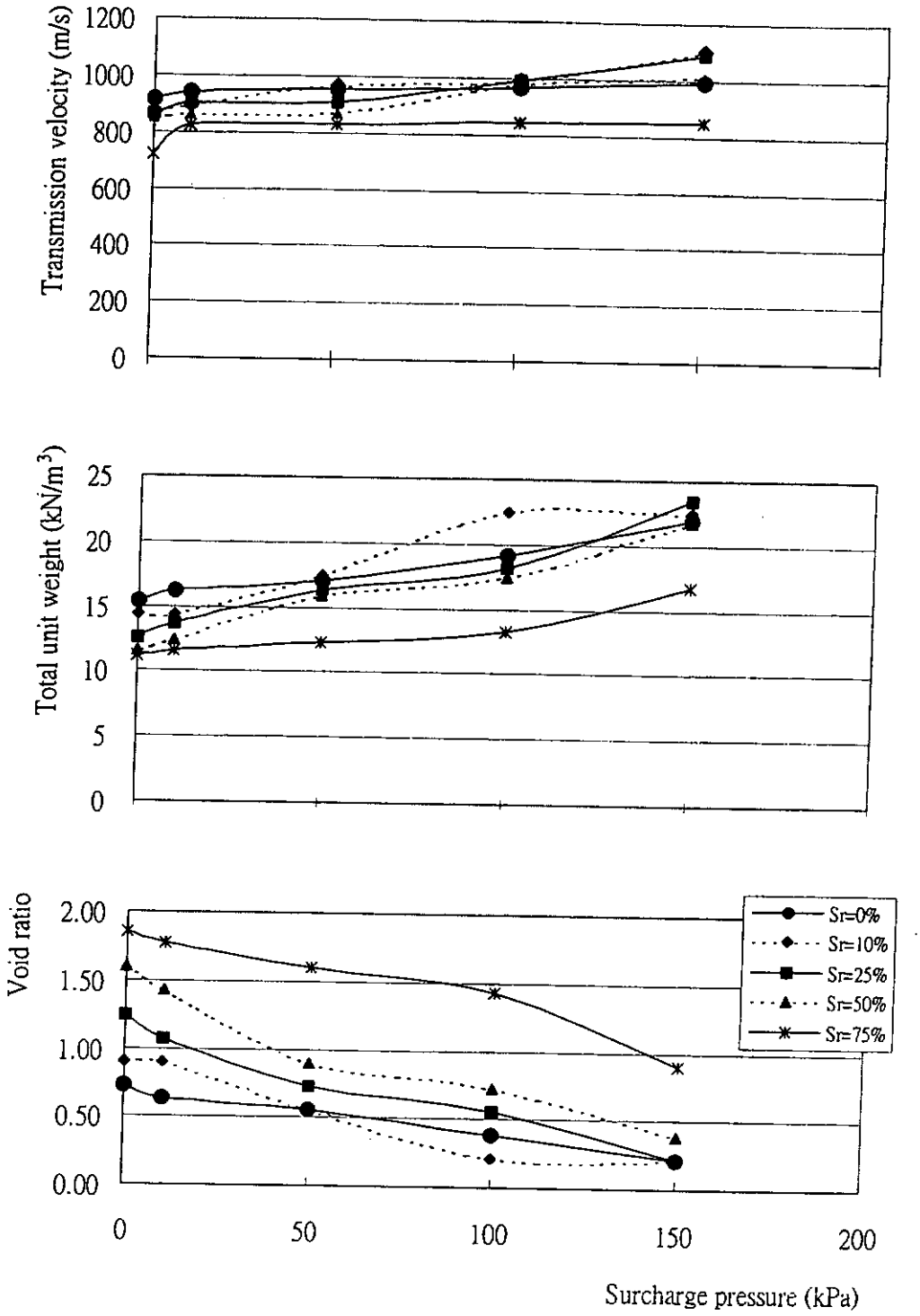

Figure 9.6.7. Variations of transmission velocity, total unit weight and void ratio with surcharge pressure at each degree of saturation for Specimen 1

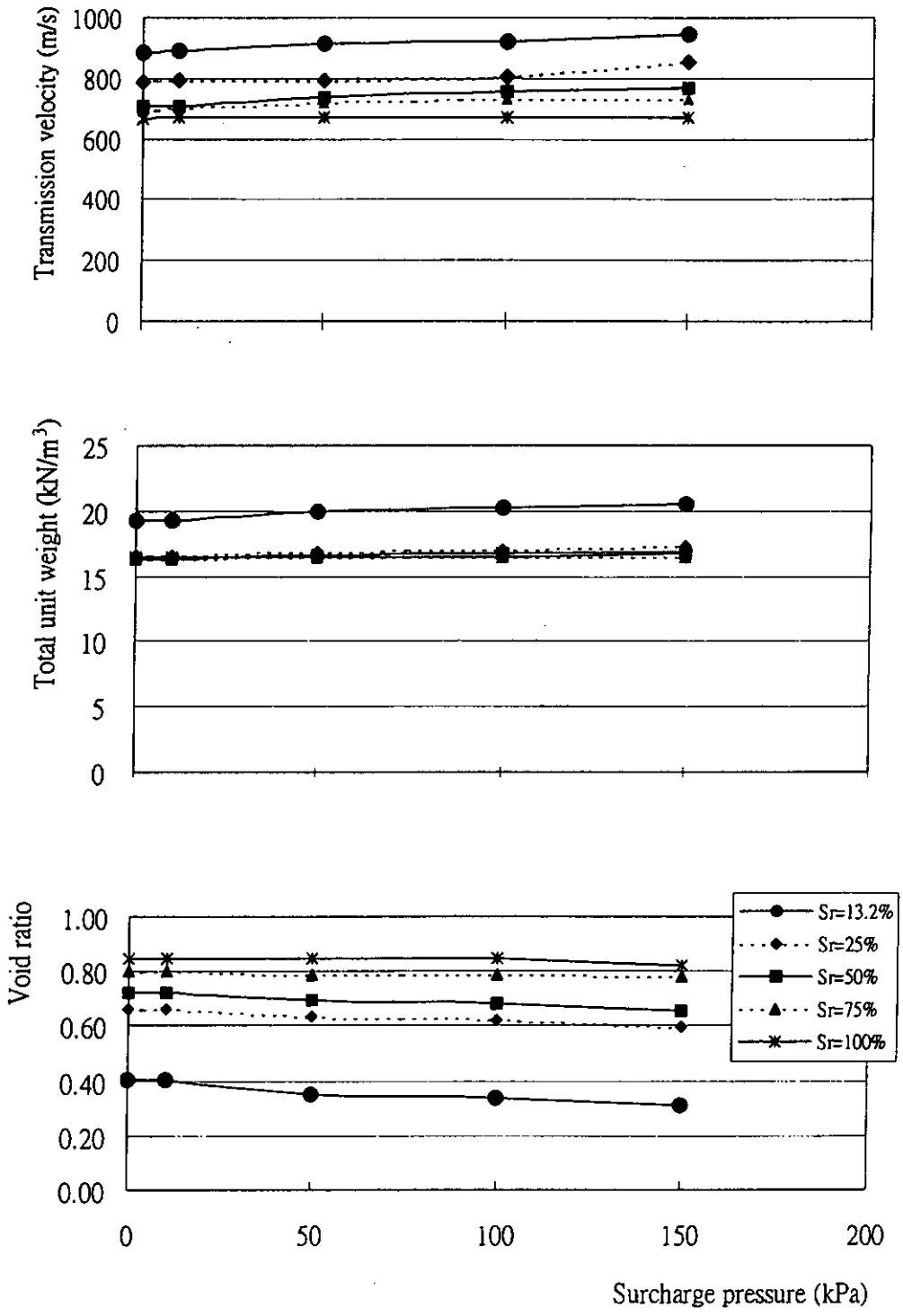

Figure 9.6.8. Variations of transmission velocity, total unit weight and void ratio with surcharge pressure at each degree of saturation for Specimen 2

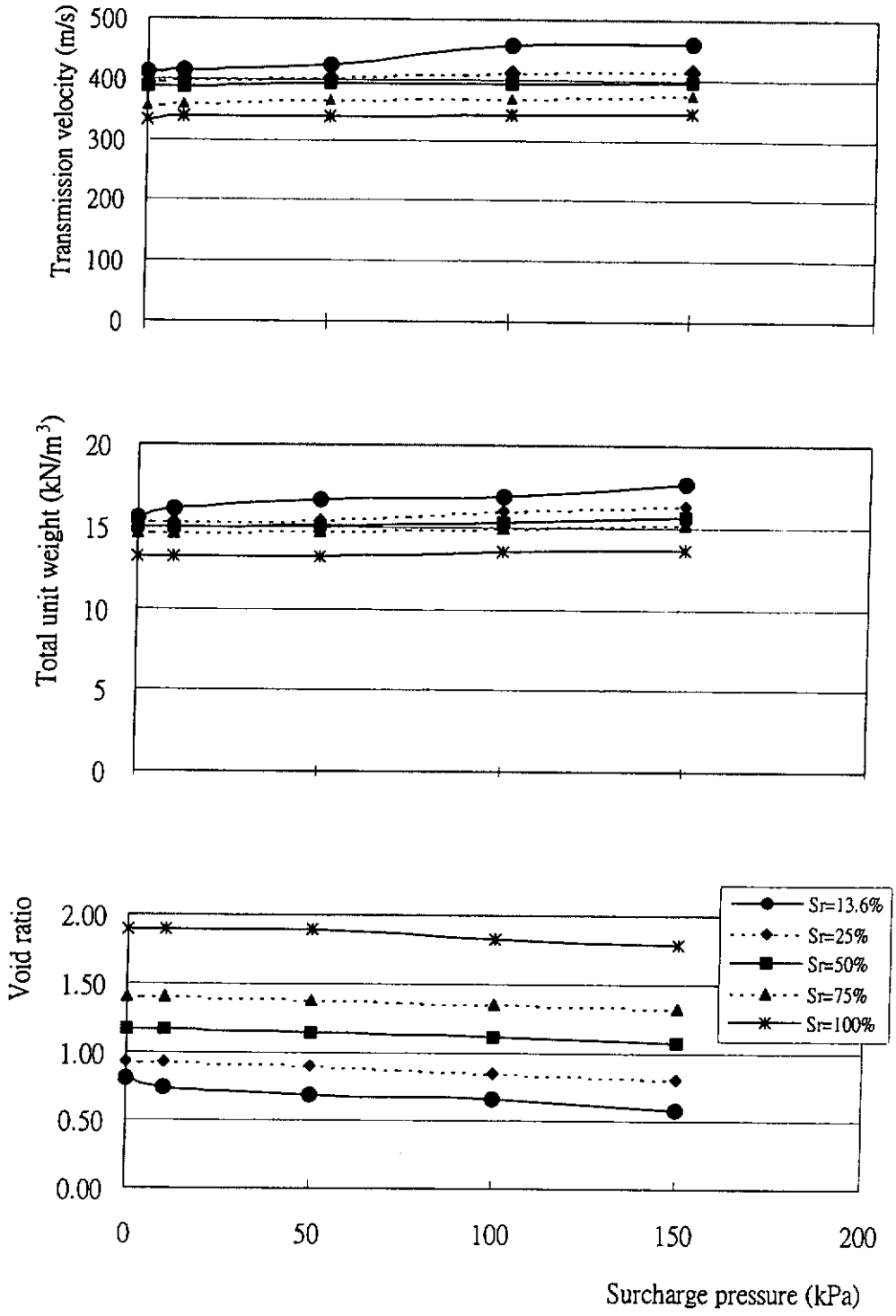

Figure 9.6.9. Variations of transmission velocity, total unit weight and void ratio with surcharge pressure at each degree of saturation for Specimen 3

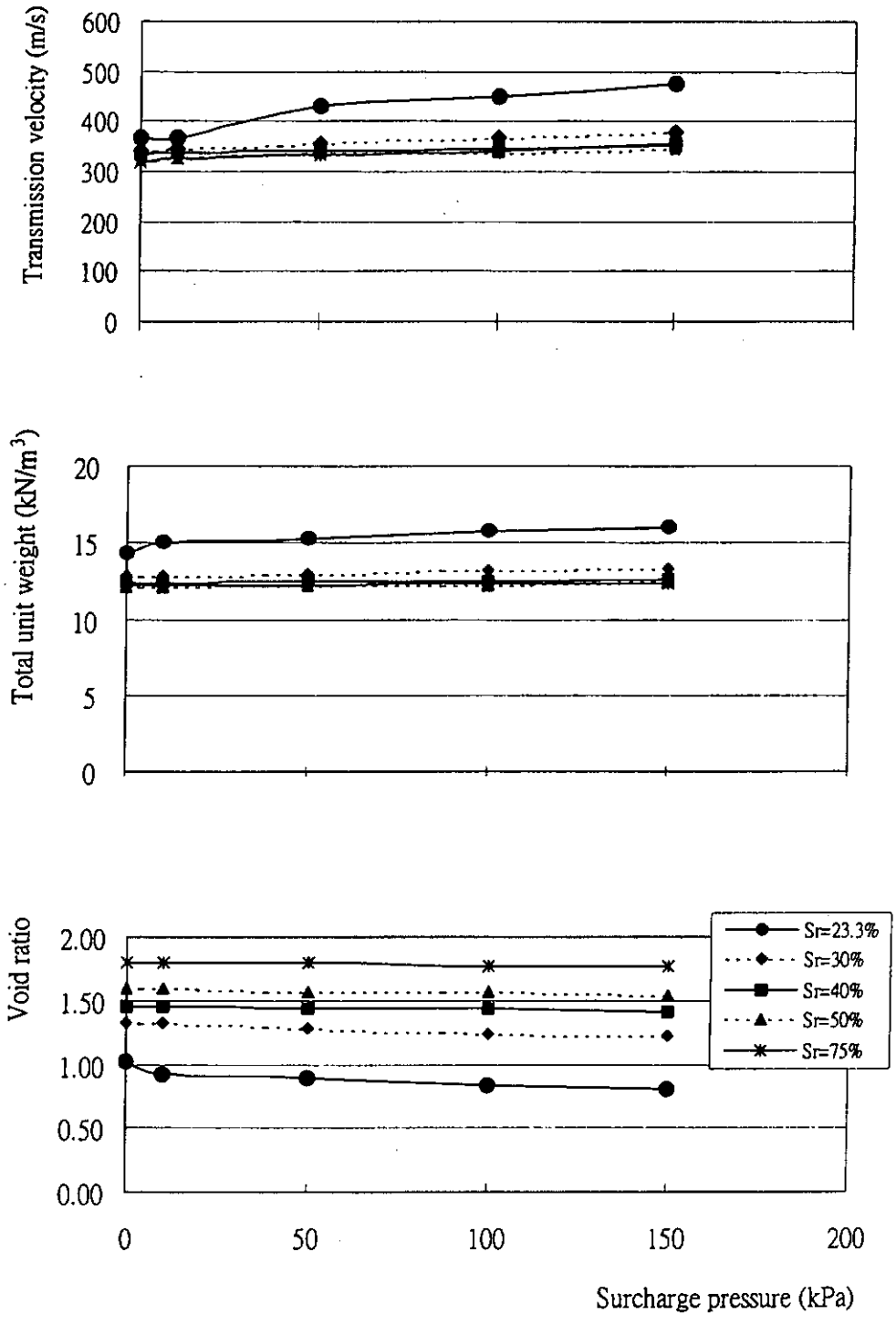

Figure 9.6.10. Variations of transmission velocity, total unit weight and void ratio with surcharge pressure at each degree of saturation for Specimen 4

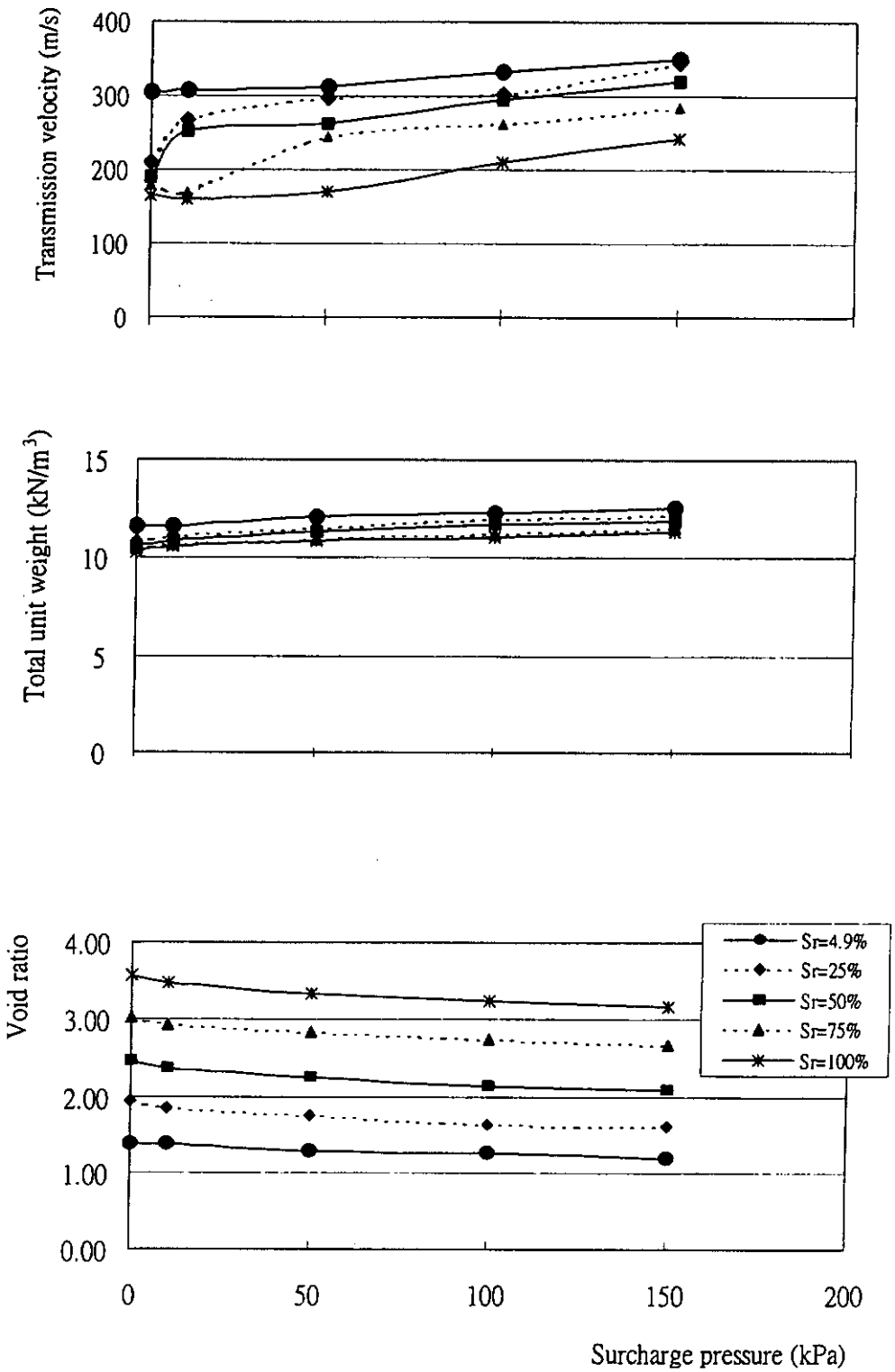

Figure 9.6.11. Variations of transmission velocity, total unit weight and void ratio with surcharge pressure at each degree of saturation for Specimen 5

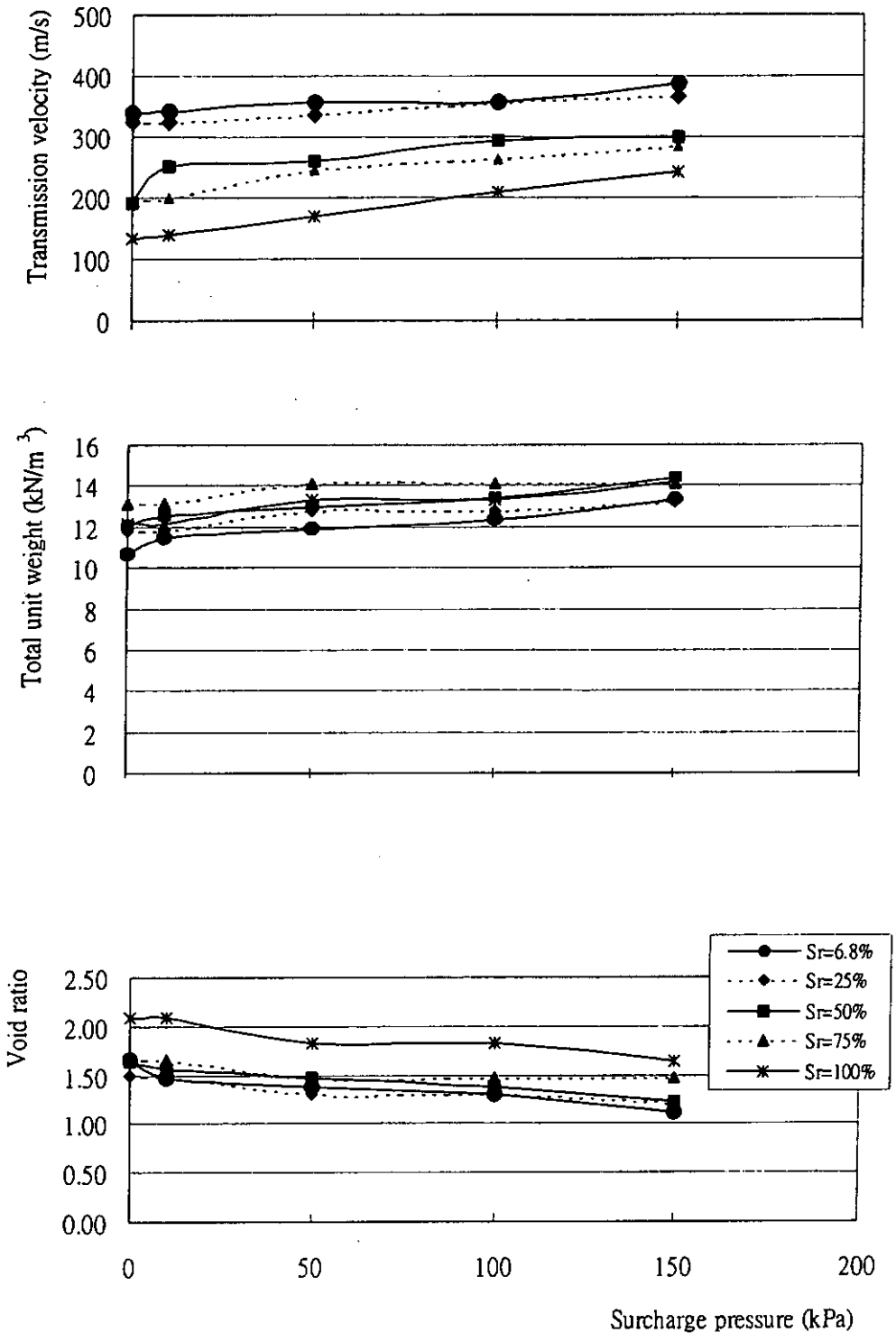

Figure 9.6.12. Variations of transmission velocity, total unit weight and void ratio with surcharge pressure at each degree of saturation for Specimen 6

For soils with the same degree of saturation, transmission velocities are found to increase with increasing surcharge pressure. This is true for all the specimens. The explanation of this behavior is believed to be due to the increasing total unit weight, lower void ratio (Figures 9.6.7 to 9.6.12), tighter packing and rearrangement of fabric. This observation is similar to that obtained by Yesiller et al. (2000), in which the velocity of wave-propagation increases as the solid contents in a soil mass (total unit weight) increases and the amount of voids filled with air and water (porosity) decreases. This phenomenon is particularly true at a high surcharge pressure (Wang et al. 1991).

9.6.3. Classification of soil strata by transmission velocity and the *'X-factor'* technique

Transmission velocity is found to be correlated with variations in microstructure (such as grain size and porosity), elastic constants, strength, toughness of materials, etc. (Vary 1977). Table 9.6.2 shows the representative ranges of transmission velocities for all the test specimens. The results show that the representative ranges of transmission velocities decrease from the top to the bottom (i.e. very gravelly GRAVEL to clayey gravelly sandy SILT). The highest-maximum velocity is obtained for Specimen 1 and the lowest-maximum velocities are obtained for Specimens 5 and 6 (Table 9.6.2).

Table 9.6.2. Representative ranges of transmission velocities for the soil specimens

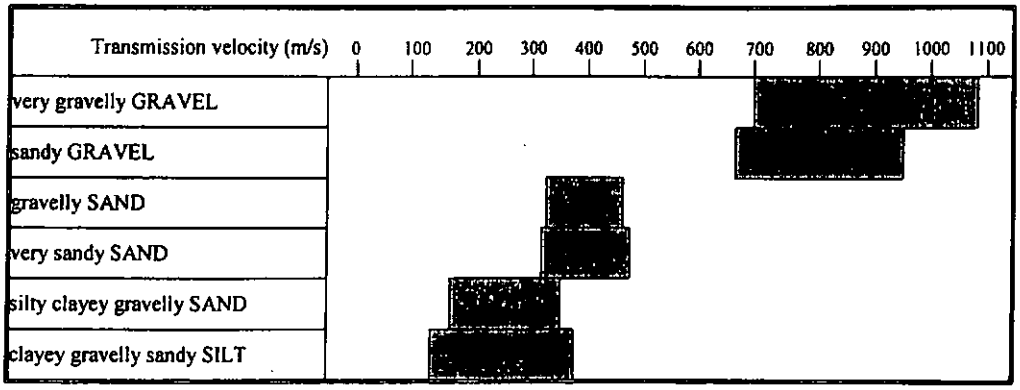

In addition to the relationships between transmission velocity, total unit weight and void ratio as depicted and discussed in Section 9.6.1, the results in Table 9.6.2 are found to be attributable to the low Young's moduli of materials in clay and silt (i.e. the contents in Specimens 5 and 6) compared to that in gravel (i.e. the contents in Specimen 1) as shown in Table 9.6.3.

Table 9.6.3. Young's Modulus and Poisson's ratio for gravel, sand and clay/silt

	Young's Modulus, E (MPa)	Poisson's ratio, ν
Gravel	180 (Everett 1994)	-
Sand	120 (Head 1998)	0.35 (Gazetas 1991)
Clay/Silt	15 - 30 (Yesiller 2001)	0.4 – 0.5 (Bowles 1988)

As discussed in Section 2.2.3, transmission velocity is a function of Young's modulus of elasticity, the mass density and Poisson's ratio of the medium of transmission. The Young's moduli represent the stiffness of the soil mass and hence are directly related to the velocity of wave propagation (Nazarian et al. 2001). Transmission velocity increases as the Young's modulus of the samples increases (Yesiller 2001). The variation of transmission velocity with the

mass density (i.e. total unit weight in this case) is presented in Sections 9.6.1 and 9.6.2.

According to the experimental results reported above, the transmission velocity has been shown to be very useful for identification of soils. However, more information and parameters can help to increase the reliability of this characterization of test materials. In this research, a novel method, called the *'X-factor'* technique, was developed. The value of the *'X-factor'* can be interpreted as amplification factors used in the decoupling process (Section 7.3). Table 9.6.4 shows the representative ranges of the '*X-factor*' for all the test specimens.

Table 9.6.4. Representative ranges of the '*X-factor*' for the soil specimens

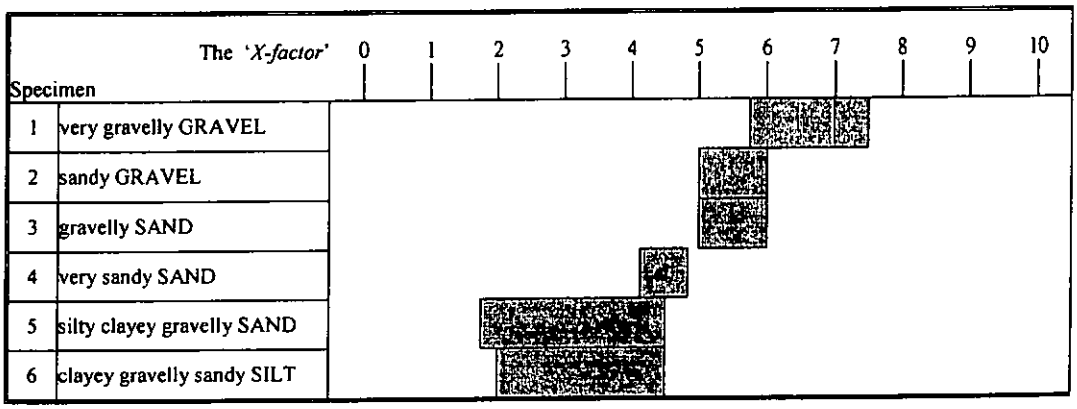

Table 9.6.4 shows that the values of the '*X-factor*' are found to decrease from Specimen 1 to Specimen 6 (i.e. very gravelly GRAVEL to clayey gravelly sandy SILT). This observation is similar to that obtained in Table 9.6.2. According to McIntire (1991), the material microstructure can be characterized by transmission velocity and attenuation measurements. The '*X-factor*' can be

correlated to attenuation property of the test materials.

Attenuation is a factor that describes the decrease in ultrasound intensity as discussed in Section 2.2.4. Attenuation is known to be more serious when the material is considered to be non-homogenous. Most material contains grain boundaries (especially concrete and soil) at which the acoustic impedance changes abruptly because two materials of different density or sound velocity meet at these interfaces. The soil specimens (i.e. Specimens 2, 3, 5 & 6) are consisted of mixtures of soil particles of different grains of materials, which have different acoustic impedances.

Larger attenuation as due to reflection/refraction across numerous grain boundaries happens in these soil materials (i.e. Specimens 2, 3, 5 & 6) when comparing to the pure materials relatively (i.e. Specimens 1 & 4).

Sand and clay are highly attenuating materials for ultrasonic waves due to their visco-elastic behavior. As a result, a higher attenuation due to absorption occurs in these soils (i.e. Specimens 2 to 6).

Scattering is an attenuation process in which the ultrasound beam interacts with material interfaces (i.e. grain size is smaller than the wavelength of the beam) causing the ultrasound beam energy to be dispersed in all directions (McDicken 1991). Table 9.6.5 shows the representative ranges of the distribution of grains for the soil specimens from larger to smaller grains. Higher scattering is

expected for smaller grain materials (i.e. Specimens 5 & 6).

Table 9.6.5. Particles sizes of the soil specimens

Soil specimen		Particle size (%)		
		Gravel (grain: 2 – 20 mm)*	Sand (grain: 0.06 – 2 mm)*	Silt/Clay (grain: 0.001 – 0.06 mm)*
1	very gravelly GRAVEL	100	0	0
2	sandy GRAVEL	60	40	0
3	gravelly SAND	40	60	0
4	very sandy SAND	0	100	0
5	silty clayey gravelly SAND	21	38	41
6	clayey gravelly sandy SILT	14	31	55

(* In accordance with Table A1 in GEOGUIDE 3 by Hong Kong Geotechnical Control Office)

Results also show that lower values of the *'X-factor'* are often associated with regions of higher attenuation (including absorption and scattering) and *vice versa.*

The usefulness of the *'X-factor'* technique in characterizing soil attenuation based on the *'X-factor'* was clearly demonstrated by the experiment carried out. In particular, the ability of using the *'X-factor'* in identifying the multiple-layer specimen such as in Figure 9.6.13 has been verified and confirmed experimentally.

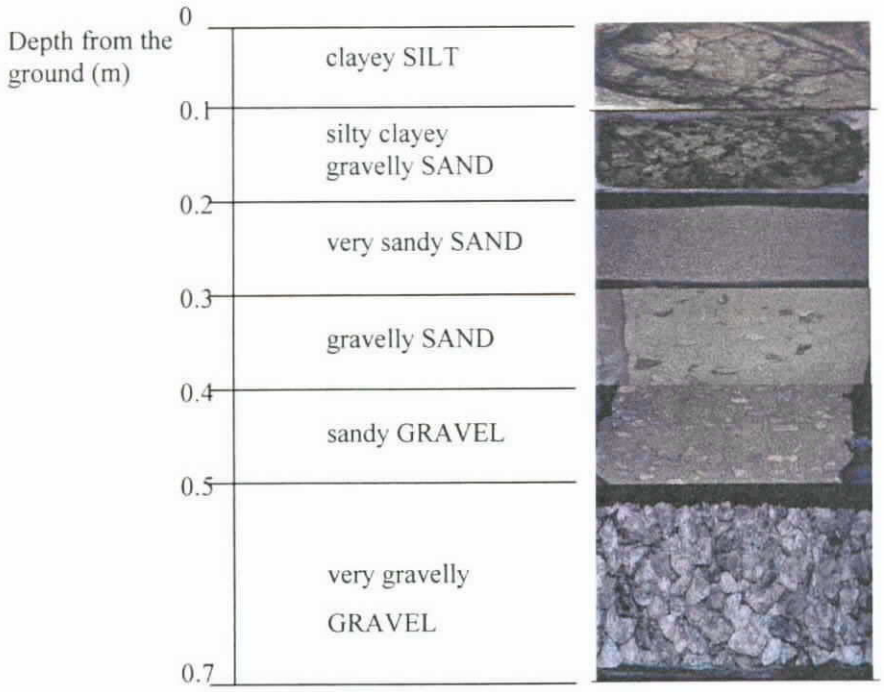

Figure 9.6.13. Properties of soils between the two artificial tubes in the multiple-layer soil specimen

In this experiment, two artificial tubes made of PVC, as shown in Figure 9.6.14, were pre-installed inside the multiple-layer soil specimen. A sonic test using the MRS was carried out, in which the probes were first lowered to the toe of two tubes and slowly raised in unison. The detail of carrying out a sonic test was discussed in Section 2.4.

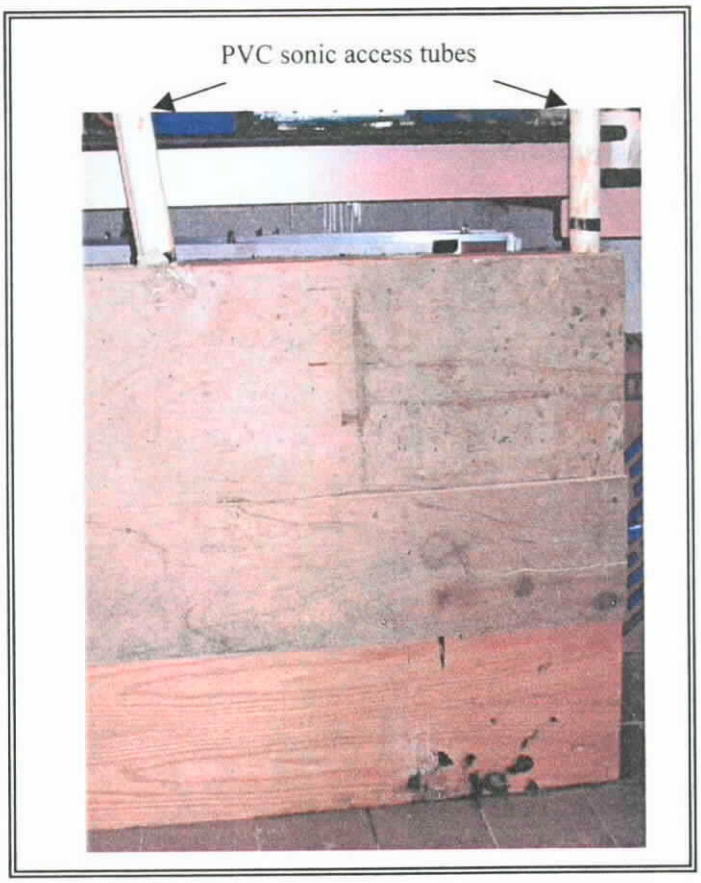

Figure 9.6.14. Photograph of the multiple-layer soil specimen

With the use of the in-house developed MRS, acquisition of the ultrasonic signals at a very fine vertical interval (i.e. 0.02m) was performed. Both the transmission velocity and '*X-factor*' were determined at each measurement interval. Three trials were carried out and the results are presented in Figures 9.6.15 and 9.6.16.

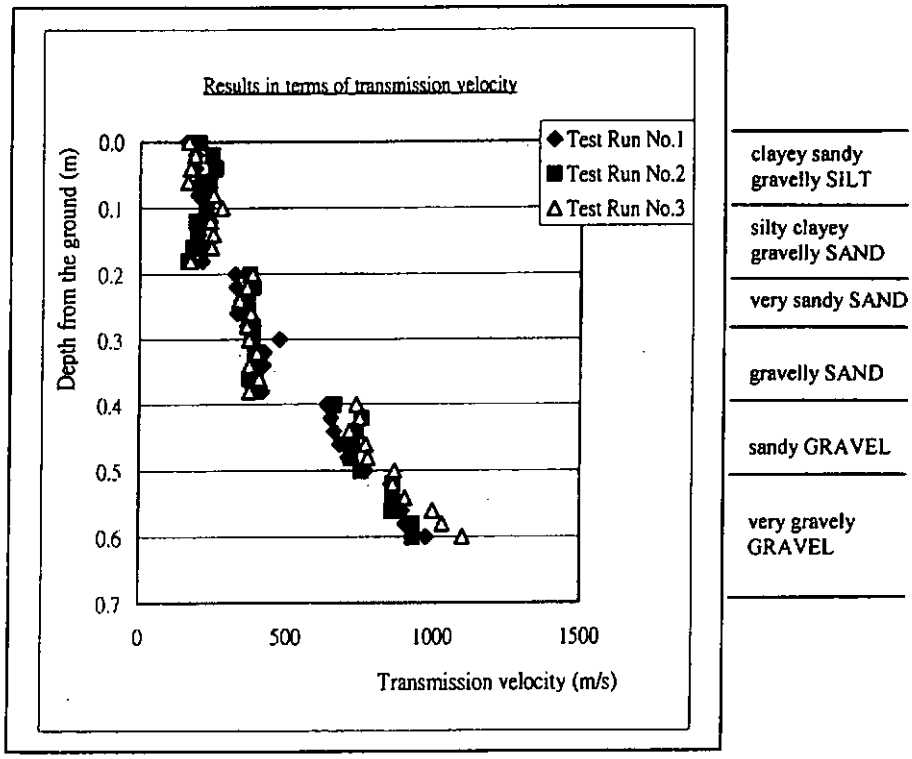

Figure 9.6.15. The results in terms of transmission velocity for the multiple-layer soil specimen

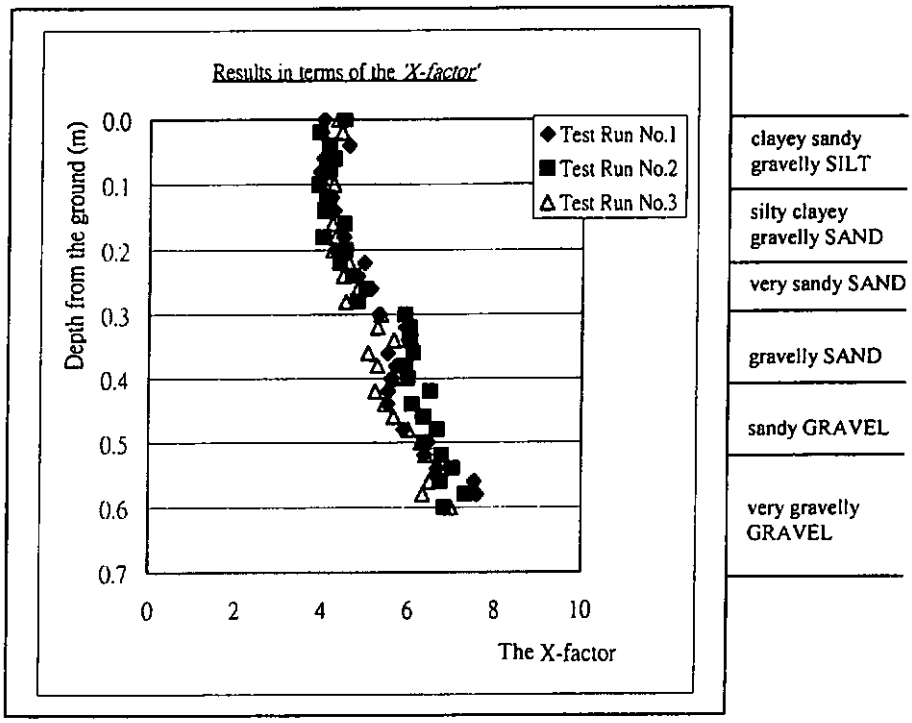

Figure 9.6.16. The results in terms of the *'X-factor'* for the multiple-layer soil specimen

Both Figures 9.6.15 and 9.6.16 show that the fine grain soil specimens (i.e. clayey sandy gravelly SILT and silty clayey gravelly SAND) possess lower transmission velocities as well as lower values for the '*X-factor*'. At the same time, the larger grain soil specimens (i.e. very gravelly GRAVEL and sandy GRAVEL) have higher transmission velocities as well as higher values for the '*X-factor*'. The ratio of transmission velocity can be as much as five times greater (200 to 1000m/s) from the larger grain materials to the smaller grain materials whereas the variation of the '*X-factor*' can be up to two times. Figure 9.6.16 also shows a continuous variation of the '*X-factor*' across a spectrum of different grains of soils, whereas, in Figure 9.6.15 the variation of transmission velocity is a stepped-distribution across soils of different grains.

The values of transmission velocities and '*X-factor*' are found to increase when the measurement depths are deeper. These values obtained at each type of soil layers in the multiple-layer soil specimen are consistent with the representative ranges (in terms of transmission velocity and '*X-factor*') as shown in Tables 9.6.2 and 9.6.4.

Materials with greater unit weight, a lower void ratio and a lower attenuation (i.e. very gravelly GRAVEL in the deepest layer) are identified by a higher transmission velocity and a higher *'X-factor'*. Conversely, materials with lower unit weight, a higher void ratio and a higher attenuation (i.e. silt/clay contents in the first two layers) are indicated by a lower transmission velocity and a lower *'X-factor'*.

9.7. Summary of the Ultrasonic Identification of Soil Strata by the In-house Developed Prototype

The success of the application of the MRS in the soil testing was demonstrated. Variation of transmission velocity with degree of saturation is found to be similar to the variation of total unit weight with degree of saturation but the inverse of the variation of void ratio with degree of saturation.

The classification of soils is achieved by transmission velocity. Different soil types have different representative ranges of transmission velocities. According to the experimental results, the transmission velocity increases as the modulus of the samples increases.

The proposed '*X-factor*' technique offers additional means of classifying in-situ soils: from classifying of soils based on transmission velocity alone to acoustic energy attenuation. It is clear that neither the transmission velocity based or *'X-factor'* based identification strategies are a direct substitute of each other, but rather, complementary to each other. As explained earlier, the '*X-factor*' provides additional information regarding the attenuation property of soils, which is not reflected in transmission velocity determination alone.

Materials with higher unit weight, a lower void ratio and a lower attenuation (i.e. gravel) are identified by a higher transmission velocity and a higher '*X-factor*'. Conversely, materials with lower unit weight, a higher void

ratio and a higher attenuation (i.e. silt/clay contents) are indicated by a lower transmission velocity and a lower '*X-factor*'.

10.1. Summary of the Research

The prime goal of this research is to apply ultrasonic Non-Destructive Evaluation (NDE) techniques to inspect and evaluate deep foundation elements without changing and damaging their properties during testing. This goal is achieved by further research and experimenting with two ultrasonic-based NDE techniques (i.e. the Ultrasonic Echo Sounding (UES) technique and the Cross-hole Sonic Logging (CSL) technique). The UES technique is often performed to assess the construction of drilled deep shaft foundations before concreting the shafts, whereas, the CSL technique is used to assess the homogeneity and integrity of in-situ concrete foundation elements. The pertinent literature related to the UES and the CSL testing techniques of deep foundations were reviewed.

The in-house developed calibration and verification procedures were developed to ascertain the real performance and behavior of the UES equipment under different testing conditions. The *range and depth* parameters (measured by the UES equipment) were investigated in the calibration work. The analysis of uncertainties in the calibration work was also discussed to assess the reliability of different measurement techniques. In the verification work, the effects of density of bentonite/slurry solutions, angles of reflection and roughness of reflecting surface on the measured ranges (obtained from UES profiles) of a shaft were quantified.

The effects of different sonic access tube materials (like PVC and steel)

on the signal strength of ultrasonic wave transmission were investigated by performing a series of experiments by the use of the in-house developed data acquisition prototype.

Extensive field investigations of the UES and the CSL testing methods have been performed on various Hong Kong construction sites under the author's leadership. The possible causes of different kinds of defects were identified using these techniques.

Furthermore, an adaptive, versatile and relatively low cost multi-channel ultrasonic data acquisition prototype called the 'Multiple Referencing System' (MRS) was constructed and developed. The in-house developed MRS enables ultrasonic tests be carried out efficiently and have enhanced the power of this technique via digital *virtual instrument* and control.

The successful application of the in-house developed MRS in concrete assessment was demonstrated by performing sonic logging tests in the concrete elements with sonic-tube-installation. A testing concrete block with built-in defects (including air-filled voids and pieces of polystyrene) was constructed and tested by the MRS. An efficient analysis graphical programming (based on *virtual instrument*) of the MRS was constructed to analyze the acquired data in different parameters (i.e. *first-arrival-time* (FAT)/*apparent transmission velocity* and signal strength in a time domain, and spectral energy content in a frequency domain). This analysis increases the reliability of the testing method of characterizing test

materials.

In addition to the concrete assessment, the MRS has also been used (as a geophysical technique) to identify various types of soil strata. The soil specimens were prepared at water contents ranging from dry to a maximum degree of saturation. A pre-defined stepped-increase of surcharge pressure was applied on a soil specimen at each degree of saturation. Variation of ultrasonic velocity with degree of saturation and surcharge pressure were analyzed. A new method, the '*X-factor*' technique, was developed to characterize soil strata.

10.2. Fulfillment of the Research Objectives

- The success of application of ultrasonic Non-Destructive Evaluation (NDE) for inspection and evaluation of deep foundation elements was clearly verified and demonstrated by the experimental tests both on laboratory specimens as well as field investigation on Hong Kong construction sites using the Ultrasonic Echo Sounding (UES) technique and the Cross-hole Sonic Logging (CSL) technique. The discussions on the possible causes of the different kinds of defects found in the UES and the CSL techniques were presented in Section 5.3 and 6.3 respectively.
- The real performance and behavior of the UES equipment were successfully verified by the in-house developed calibration and verification procedures under different testing conditions (i.e. different

density of bentonite/slurry solutions, different angles of reflection and different roughness of reflecting surface) which were presented in Sections 3.2 and 3.3.

- The effects of different sonic access tube materials (i.e. steel and PVC) on the signal strength of ultrasonic wave transmission were investigated (Sections 4.2 and 4.3) by the use of the in-house developed ultrasonic data acquisition prototype. The effects of these tubes is either not available in the past at all.
- An adaptive, versatile and relatively low cost multi-channel ultrasonic data acquisition prototype called the 'Multiple Referencing System' (MRS) was constructed and developed (Section 7.2) to conduct sonic tests in a more efficient way. The in-house developed MRS is based on the National Instruments hardware and a LabVIEW environment. The prototype is capable of acquiring two or more channels of ultrasonic signals simultaneously by using several receiving probes. The successful application of the MRS in concrete assessment was clearly demonstrated in carrying out a sonic test in the concrete panel block with built-in defects (Section 8.5).
- With the in-house MRS developed, the efficient analysis graphical programming based on the *virtual instrument* was constructed to analyze the ultrasonic waveforms in different approaches (i.e. signal content in a time domain and spectral energy content in a frequency domain) in addition to the traditional one (i.e. FAT/*apparent transmission velocity*) (Section 7.3).

- The effects of soil types on ultrasonic signal responses were successfully studied using the application of the in-house developed MRS. Variation of transmission velocity with degree of saturation and surcharge pressure were investigated and discussed in Sections 9.6.1 and 9.6.2. The *'X-factor'* technique was developed to classify different soil strata and presented in Section 9.6.3.

10.3. Contributions to the Knowledge of Non-Destructive Evaluation of Foundation Testing

- This research project has further enhanced the ultrasonic Non-Destructive Evaluation (NDE) techniques (including UES and CSL) for the inspection and evaluation of deep foundation elements.
- The pioneering work in the in-house developed calibration & verification procedures provides a means of verifying the real performance and behavior of UES equipment. These procedures have been already adopted by the Hong Kong Laboratory Accreditation Scheme (HOKLAS) as a basis for accreditation of a number of commercial laboratories specializing in UES tests.
- Numerous field investigations using UES and CSL have been conducted on various Hong Kong construction sites, which provide a valuable database of deep foundation elements (including drilled deep shafts, bored piles, concrete barrette piles and diaphragm wall panels). The examples and discussions on the possible causes of different kinds of

defects found in the corresponding testing techniques (i.e. UES and CSL) provide engineers/technologies a detailed picture of the interpretation of the test results using these testing techniques.

- The traditional instrumentation of CSL (involving a pair of probes) has been improved. An adaptive, versatile and relatively low cost multi-channel ultrasonic data acquisition prototype, called the 'Multiple Referencing System' (MRS), provides an efficient way to carry out sonic tests on concrete foundation elements with sonic-tube-arrangement. The system simultaneously acquires two or more channels of ultrasonic signals by using several receiving probes to save time and cost.
- The digital *virtual instrument* in the analysis graphical programming of the in-house developed MRS provides an efficient, environmental-friendly and successful means in signal processing and analysis. By only modification the icons of *virtual instrument* on the analysis programming, the ultrasonic signals are analyzed in different approaches (i.e. *first-arrival-time/apparent transmission velocity* and signal strength in a time domain, and spectral energy content in a frequency domain). These analysis approaches increase the reliability of testing methods to characterize test materials.
- The in-house developed MRS not only provides a means of assessing concrete foundation elements but also extends to soil strata identification. The latter is very useful to provide unknown soil strata information between boreholes.
- An innovative method, the *'X-factor'* technique, provides a fast and

simple alternative approach to analyze soil strata without changing their properties and disturbing their states. The *'X-factor'* is found to give information regarding the attenuation property of the test materials.

10.4. Conclusions about the Research

Following conclusions can be drawn from this research:

- Non-Destructive Evaluation (NDE) is an important and efficient tool to inspect and evaluate the deep foundation elements without changing and damaging their properties.
- The applications of two ultrasonic-based non-destructive testing techniques (i.e. UES and CSL) provide a better picture regarding to the quality assurance of deep foundation concrete elements since UES and CSL are conducted before and after the concreting stage respectively.
- The in-house developed calibration procedure provides a means to determine the real performance (including the *range and depth* concerns) of UES equipment. In the depth calibration, the measuring tape approach is more accurate than the theodolites approach by the calibration uncertainties determined.
- The in-house verification procedure ascertains the working performance of the UES equipment in different testing conditions. The UES equipment used in this research works properly in bentonite/slurry solutions with density not more than 1026(kg/m^3) and electrical conductivity up to 800(microsiemens/cm). The 'bell-out' measurement

by the UES equipment is limited to 30° with reference to the horizontal level. The horizontal measurement fineness of the UES equipment is limited to 25mm from a shaft wall.

- The signal strength when using PVC sonic access tubes are clearly greater than that when using steel tubes due to the smaller difference in acoustic impedance between PVC tubes and water. For each material, the signal strength increases with increasing sonic access tube diameter due to the effect of curved surface wall of sonic access tubes. Steel tubes bond well to the concrete so that steel tubes are still preferable as sonic access tubes.
- By the experimental results, the sonic profile with unclear and fuzzy successions of the white and black lines may be obtained by the use of a larger-diameter (i.e. 150mm diameter) sonic access tube, even though no defect is presented, as the probes can move around inside the tube. Inside sonic access tubes with a diameter more than twice the diameter of the probes, the probes shall be fitted with centralizers in accordance with ASTM D6760-02 to prevent undue movement during measurement.
- UES is a reliable and useful technique to assess the condition of deep-drilled shaft foundations before concreting the shafts. UES is effective to provide an early stage diagnosis and inspection of shafts characteristics such as shaft verticality, shaft diameter, shaft depth, and geometry and dimensions of 'bell-out' at the toe of shafts. The test results of the extensive field investigation show the effectiveness of the use of UES to reveal different kinds of failures (i.e. deviations from

design of drilled shafts before the concreting stage). Early detection of deviations from design allows timely correction of problems, minimization of construction time and reduction of overall construction cost.

- CSL provides the precious information/feedback regarding the construction process of the final finished foundation elements. The test results of the extensive field investigation show the effectiveness of the use of CSL to reveal different kinds of failures (i.e. honeycombing, voids or foreign materials embedded in drilled shafts after the concreting stage).
- The in-house developed prototype, called the 'Multiple Referencing System' (MRS), provides an efficient means of performing sonic tests in concrete elements with sonic-tube-installation. This prototype is capable of acquiring two or more channels of signals simultaneously. In addition to the transmission velocity measurement, the signal strength and spectral content are investigated by the use of the efficient analysis graphical programming of the MRS (based on the digital *virtual instrument*).
- The test results (obtained by the MRS) in concrete assessment show that the transmission velocities, signal strengths and spectral contents of the acquired signals within the zones of the built-in defects are comparatively lower than that of sound concrete.
- The success of application of the in-house developed MRS in soil strata testing was demonstrated. Variation of ultrasonic velocity with degree of

saturation and surcharge pressure were analyzed using the MRS. Variation of transmission velocity with degree of saturation is found to be similar to the variation of total unit weight with degree of saturation but opposite from the variation of void ratio with degree of saturation. At the same degree of saturation, velocities increase with increasing surcharge pressure for all the soil specimens.

- The innovative method, the *'X-factor'* technique, is found to have a high potential of identifying the types of soil strata. The values of the *'X-factor'* are found to be correlated to the attenuation of the test materials.

10.5. Suggestions for Future Research

- In performing an UES test, only two or four directions (depending on the type of machine) of the surface walls of the drilling shafts can be scanned/inspected at the same time and no data can be obtained beyond the coverage of this scanning. The operation mechanism of UES equipment should be improved to a 360-degree rotation scanning for measurement of the surface walls of the drilling shafts in all directions.
- UES is designed to check a 'bell-out' at a pile toe and the 'bell-out' should be laid in bedrock as usually required by the engineers' specification. A traditional instrument of UES equipment (i.e. analog output) should be improved to obtain digital output for further signal processing. The receiving signals (in digital format) reflected from different kinds of materials can be

investigated so that the locations of 'bell-out' of a test shaft can be identified within what type of layer, and even distinguish different reflecting layers (such as steel casing, soil layer and bedrock).

- The instrumentation of the in-house developed MRS should be improved especially the high-voltage pulsing component. A higher-voltage electrical pulse is required to be applied to an emission probe so that a stronger pulse of ultrasonic energy generated can propagate in a longer transmission path in test materials.
- More different kinds of soil strata in different transmission paths should be tested by the in-house developed MRS to establish a database to determine the effectiveness of the MRS in soil identification.
- The *'X-factor'* technique should be demonstrated by performing an on-site field investigation to ascertain the effectiveness of the *'X-factor'* technique on the classification of soil strata.

References

AASHTO *Standard Specifications for transportation materials and methods of sampling and testing, part II tests.* AASHTO, Washington, D.C (2000).

Amir, E.I. & Amir, J.M. "Recent advances in ultrasonic pile testing". *Proceedings of the 3rd International Geotechnical Seminar on Deep Foundations on Bored and Auger Piles,* Ghent, Belgium, p.p.181-185 (1998).

AS 2159 "Piling-Design and Installation". Australian Standard (1995).

ASTM *ASTM Standards on soil stabilization with admixtures.* ASTM, West Conshohocken, PA (1992).

ASTM D6760-02 "Standard Test Method for Integrity Testing of Concrete Deep Foundations by Ultrasonic Crosshole Testing". *Annual Book of ASTM Standards,* ASTM, West Conshohocken, PA, Vol. 04.08 (2002).

ASTM E664-93 "Standard Practice for the Measurement of the Apparent Attenuation of Longitudinal Ultrasonic Waves by Immersion Method". *Annual Book of ASTM Standards,* ASTM, West Conshohocken, PA, Vol. 03.03 (1993).

Banks, B., Oldfield, G., & Rawding, H. *Ultrasonic Flaw Detection in Metals.* Prentice-Hall, New Jersey (1962).

Barrera, G. et al. "Real time control of an 2 degree of freedom ultrasonic manipulator by means of a personal computer and virtual instrumentation." *Instrumentation and Development,* Vol.5, Nr.2, p.p.90-98 (2001).

Bobrowski, J., Bardhan-roy, B.K., Magiera, R.H. and Lowe, R.H. "The structural integrity of large diameter bored piles In: Proc. Conf., Instn. Civ. Engrs". *The Behaviour of Piles,* London 15-17 September, pp. 179-184 (1970).

Bowles, J. E. *Foundation Analysis and Design.* McGraw Hill, New York (1988).

Brettmann, T. & Olson, L. "Focus on Geotechnical Engineering Detect Detection". *Civil Engineering,* July, p.p.2A-6A (1996a).

Brettmann, T. & Frank, M. "Comparison of Cross Hole and Single Hole Sonic Integrity Logging Methods." *Proceedings of the 5th International Conference on the Application of Stress Wave Theory to Piles*, Orlando, Florida, September, p.p. 698-707 (1996b).

Bungey, J.H. "Validity of Ultrasonic Pulse Velocity Testing of In-Place Concrete for Strength". *Non-destructive Testing International*, Volume 13, No.6, December, p.p.296-300 (1980).

CEBTP "Integrity testing of piles by sonic coring". *Internal Test Report Ref. 1*, Centre Experimental de Recherches et d'Etudes du Batiment et des Travaux (1969).

CEBTP "Use of Sonic Coring in Structural Integrity of Large Integrity of Large Diameter Bored Piles". *Internal Test Report*, Centre Experimental de Recherches et d'Etudes du Batiment et des Travaux, France (1982).

Chan, W.Y. Internal Test Report of the Field-testing of the Ultrasonic Echo Sounding Technique, The Hong Kong Polytechnic University (2003a).

Chan, W.Y. Internal Test Report of the Field-testing of the Cross-hole Sonic Logging Technique, The Hong Kong Polytechnic University (2003b).

Chen, P.Y.M. *GEO Report 36 Methods of Test for Soils in Hong Kong for Civil Engineering Purposes (Phase I Tests)*, Geotechnical Engineering Office, Hong Kong (1994).

Chernauskas, L.R. & Paikowsky, G. P. "Defect Detection and Examination of Large Drilled Shafts Using a New Cross-Hole Sonic Logging System". A. J. Lutenegger and D. J. DeGroot, eds., *Performance confirmation of constructed geotechnical facilities : proceedings of sessions of ASCE Specialty Conference on Performance Confirmation of Constructed Geotechnical Facilities*, Amherst, Massachusetts, April 9-12, p.p.66-83 (2000).

Chernauskas, L.R. and Paikowsky, S.G. "Deep Foundations Integrity Testing: Techniques and Case Histories." *Civil Engineering Practice Spring/Summer 1999*, Vol. 14, no.1, Boston Society of Civil Engineers, Section/ASCE, p.p. 39-56 (1999).

Cockaerts, G. and De Cooman, P. "Measuring Wave Propagation Characteristics in

Artificial Sand-Clay Mixtures". *Surveys in Geophysics*, Vol. 15, No. 5, pp. 495-513 (1994).

Day, R.W. *Geotechnical and Foundation Engineering: Design and Construction.* McGraw-Hill, New York (1999).

Davis, A.G. and Hertlein, B.H. "A Comparison of the Efficiency of Drilled Shaft Down-Hole Integrity Tests". *Fawa Conference*, Orlando, Florida, p.p.1272-1286 (1994).

Everett, A. *Mitchell's Materials.* Longman Science & Technical, 5th Edition (1994).

Faiella, D. and Superbo, S. "Integrity non destructive tests of deep foundations by means of sonic methods – Analysis of the results collected on 37 sites in Italy". *Proceedings of the 3rd International Geotechnical Seminar on Deep Foundations on Bored and Auger Piles*, Ghent, Belgium, p.p.209-213 (1998).

Finno, R.J. and Champy, P. "Cross-Hole Sonic Logging Evaluation of Drilled Shafts at the Northwestern University National Geotechnical Experimentation Site". *Final Report to the Infrastructure Technology Institute*, Department of Civil Engineering Northwestern University, United States (1997).

Gassman, S.L. "Impulse Response Evaluation of Inaccessible Foundations". Evanston. Illinois (1997).

Gazetas, G. "Foundation Vibrations". H.Y. Fang, ed., *Foundation Engineering Handbook*, Van Nostrand Reinhold, New York, Ch.15, pp. 553-593 (1991).

Gross, H. et al. "Ultrasonic crosshole testing on large concrete piles". *The International Symposium Non-destructive Testing in Civil Engineering*, April 1997, Vol. 2, No.04 (1997).

Halmshaw, R. *Non-destructive Testing: Metallurgy and Materials Science Series*, London : Edward Arnold (1987).

Head, K.H. *Manual of Soil Laboratory Testing Volume 3: Effective Stress Tests.* Pentech Press, London (1998).

Herman, G.T. "Image Reconstruction from projections – The Fundamentals of Computerized Tomography". Academic Press, Inc., San Diego, California (1980).

HOKLAS "Construction Materials Test Category – Accreditation of Foundation Tests", HOKLAS Supplementary Criteria No.16, Hong Kong Laboratory Accreditation System (2001).

Hong Kong Geotechnical Control Office *Guide to Rock and Soil Descriptions GEOGUIDE 3*. Hong Kong Government Printer (1988).

Housing Department "Hong Kong SAR Government Housing Department Technical Specifications of Non-destructive Testing for Piles." *Non-Destructive Testing Report*, No.164/1998, Hong Kong (1998).

Ibrahim, M. "Development of Flexible Ultrasonic Waveform Analysis for NDE." *10th Asia Pacific Conference on Non-Destructive Testing* in Brisbane, Australia (2001).

Inci, G. "Nondestructive evaluation of compacted clayey soils". Ph.D. Thesis, Department of Wayne State University, Detroit, Michigan (2002).

ICE "Specification for Piling". Institution of Civil Engineers, Thomas Telford, London (1988).

JGJ94-94 "Technical Code for Building Pile Foundation Chapter 9: Inspection and Acceptance of Pile Foundation Engineering 9.1: Quality Inspection of Pile Installation", China (1994).

Jamal, R. and Krauss, P. "LabVIEW: Das Grundlagenbuch," Prentice Hall, München (1998).

Kissenpfennig, J.F., Motherwell, J.T. & LaFountain, L.J. "Integrity Testing of Bored Piles Using Sonic Logging". *Journal of Geotechnical Engineering*, Vol. 110, No.8, August, Paper No. 19052 (1984).

Krauß, A., Weimar, U. and Göpel, W. "LabVIEW™ for sensor data acquisition," *Trends in analytical chemistry*, Vol.18, no.5, p.p.312-318 (1999).

Lau, H.L. Zhuang ji gong cheng shou ce / "Zhuang ji gong cheng shou ce" bian xie wei yuan hui, Zhongguo jian zhu gong ye chu ban she, Beijing, p.p.786-799 (1995).

Lin, S.S. and Hoe, E. "Quality Control for Pile Foundations Using Nondestructive Testing: Case Studies in Taiwan". *Transportation Research Record* 1633, Sep. 1998, pp. 102 – 107 (1998).

Levy, J. F. "Sonic pulse method of testing cast-in-site concrete piles". *Ground Engineering*, Vol.3, No.3, 17-19 (1970).

Loertscher, H., Bartos, A. and Strycek, J. "Digital Signal Processing for Ultrasonic Testing." *15th World Conference on Non-Destructive Testing* in Rome (2000).

Malhotra, V.M. and Carino, N.J. *CRC Handbook on Nondestructive Testing of Concrete*, Boca Raton, Fla. : CRC Press (1991).

McDicken, W.N. *Diagnostic ultrasonics: Principles and use of instrumentation.* 3rd ed., Edinburgh [Scotland] : Churchill Livingstone (1991).

McIntire, P. et al. *Nondestructive testing handbook, volume seven ultrasonic testing.* American Society for Non-destructive Testing, Columbus, OH (1991).

Milsom, J. *Field Geophysics: The Geological Field Guide Series.* 3rd ed., John Wiley, Chichester (2003).

Members of the Pile Testing Sub Committee of the Association of Construction Materials Testing Laboratories Limited "Standard Test method for Ultrasonic Logging Test (Cross-Hole Method) for Integrity of Concrete Foundation Elements" Association of Construction Materials Testing Laboratories Limited, Hong Kong (2001).

Mor, G. "Fault Detecting in Foundation Piles and Sheet Walls with Ultrasonic Investigations". *4th International Conference on Piling and Deep Foundations*, Balkema of Rotterdam, Vol. 1, Stresa, p.p.625-626 (1991).

Naik, T.R., and Malhotra, V.M. "The ultrasonic pulse velocity". *V. M. Malhotra, N. J. Carino, eds., CRC Handbook on Nondestructive Testing of Concrete,* Boca Raton, Fla. : CRC Press, p.p.169-178 (1991).

Nakagawa, K., Soga, K., and Mitchell, J.K. "Pulse transmission system for measuring wave propagation in soils". *Journal of Geotechnical Engineering, ASCE*, Vol.122, No.4, pp. 302-308 (1996).

National Instruments Corporation, 11500 N Mopac Expwy, Austin TX USA. http://www.ni.com

Nazarian, S. et al. "Compaction Quality Control of Soils Using Wave Propagation Techniques". TRB-01-2670, Presented in 2001 Annual Transportation Research Board Meeting, Washington, DC (2001).

NFP94-160-1 "Auscultation d'un element de foudation". *Association Francoise de Mormalisation (AFNOR)*, Norme Francaise, Mai (1993).

Olson, L.D., Aouad, M.F. & Sack, D.A. "Nondestructive Diagnosis of Drilled Shaft Foundations". *Transportation Research Record 1633*, September, P120-127 (1998).

Olson, L.D., Lew, M., Phelps, G., Murthy, K.N. & Ghadiali, B.M. "Quality Assurance of Drilled Shaft Foundations with Nondestructive Testing". *Proceedings of the International Conference on Design and Construction of Deep Foundations*, Oriando, Volume III, Sessions 5 through 7, p.p.1231-1243 (1994).

Paquet, J. and Briard, M. "Controle non destructif des peiux en beton". *Annales de l'Institut Technique du batiment et des Travaux Publics Serie: Sols et Foundation*, No. 128, Supplement au No 337, Mars (1976).

Parasnis, D.S. *Principles of Applied Geophysics*. 5th ed., Chapman and Hall, New York, London (1997).

Robinson, E.S. & Coruh, C. *Basic Exploration Geophysics*. Wiley in New York (1988).

Ruck, H.J. et al. "FRESHCON 2.0 – Software for data acquisition and data analysis." *Otto-Graf-Journal*, Vol.11, p.p.49-57 (2000).

Sansalone, M. & Carino, N. J. "*Stress Wave Propagation Methods*". *V. M. Malhotra, N. J. Carino, eds., CRC Handbook on Nondestructive Testing of Concrete*, Boca Raton,

Fla. : CRC Press, p.p.275-304 (1991).

Sheeran, D. E., Baker, W. H., and Krizek, R. J. "Experimental Study of Pulse Velocities in Compacted Soils". *Highway Research Record No.177*, Highway Research Board, pp. 226-238 (1967).

Shi, Q. "Determination of the dynamic soil moduli by ultrasonic wave transmission method". Ph.D. Thesis, Arizona State University, United States (1998).

Sologyan, A. I. "Survey of Methods and Means for Determining Soil Density in the Field". *Soviet Journal of Nondestructive Testing*, Plenum Publishing Corp., Vol. 25, No. 7, pp. 480-486 (1990).

Stain, R.T. "Integrity Testing". *Civil Engineering (United Kingdom)*, April 1982, p.p.55-59 and May 1982, p.p.77-87 (1982).

Stain, R.T. & Williams, H. T. "Interpretation of Sonic Coring Results: A research project". *Proceedings of the 4th International DFI Conference*, Balkema, Rotterdam, p.p.633-640 (1991).

Stephens, R.W.B. "Ultrasonics International 1975 Conference Proceedings". *IPC Science & Technology Press*, Guildford, 1975, p.9 (1975).

Stephenson, R.W. "Ultrasonic Testing of Asphalt-Aggregate Mixtures". Ph.D. Thesis, Oklahoma State University, Norman (1968).

Stephenson, R. W. "Ultrasonic Testing for Determining Dynamic Soil Moduli". *Dynamic Geotechnical Testing*, ASTM STP 654, American Society for Testing and Materials, Philadelphia, ASTM, pp. 179-195 (1978).

Stokoe, K.H. and Woods, R.D. "In situ shear wave velocity by cross-hole method". *Journal of the Soil Mechanics and Foundations Division, Proceedings of the American Society of Civil Engineers*, Vol. 98, No.SM5, p.p.443-460 (1972).

Szilard, J. *Ultrasonic Testing*. John Wiley & Sons, Ltd., New York (1982).

Takahashi, T. "High-resolution geophysical methods as NDT for civil engineering

applications". Uomoto, T., ed., *Non-destructive testing in civil engineering*, Amsterdam ; New York : Elsevier, pp. 51-60 (2000).

Timoshenko, S.P. & Goodier, J. N. *Theory of Elasticity*. 3rd ed., McGraw-Hill, New York (1970).

Turner, M.J. *Integrity testing in piling practice Report 144*. Construction Industry Research and Information Association (1997).

Wang, R., Haibo, G., Ay, C., Schuler, R., Gunasekaran, S., and Shinners, K. "Ultrasonic Method to Evaluate Soil Moisture and Compaction". Presented at 1991 International Winter Meeting, Paper No. 91-1522, ASAE, St. Joseph, MI (1991).

Williams, H.T. & Stain, R.T. "Integrity Testing of Piles – Horses for Courses". *International Conference on Piling and Deep Foundations*, London, England (1987).

Wooh, S.C. "Development of ultrasonic nondestructive methods for defect and damage characterization in composite materials". Ph.D. Thesis, The Northwestern University , United States (1989).

Yesiller, N., Inci, G., and Miller, C.J. "Ultrasonic testing for compacted clayey soils". C. D. Shackelford, S. L. Houston, and N.-Y. Chang, Eds. *Advances in Unsaturated Geotechnics, ASCE GSP 99*, ASCE, pp. 54-68 (2000)

Yesiller, N., Hanson, J.L., and Usmen, M.A. "Ultrasonic Assessment of Stabilized Soils". J. L. Hanson, R. J. Termaat, and United Engineering Foundation, eds, *Soft Ground Technology, ASCE GSP 112*, ASCE, pp. 170-181 (2001).

Appendices

Appendix A	Results in the *Range* Calibration
Appendix B	Uncertainty calculation guidelines
Appendix C	Mathematical Model in the *Range* Calibration
Appendix D	Student's distribution in Statistics for 95% confidence level
Appendix E	Mathematical Model in the Depth Calibration (By the measuring tape approach)
Appendix F	Mathematical Model in the Depth Calibration (By the theodolite approach)
Appendix G	Verification results in different angles of reflections
Appendix H	Verification results in different rough reflecting surfaces

Appendix A

Results in the *Range* Calibration

Conditions of the calibration

Calibration level : 0.4 m

Measurement direction* : X / ~~Y~~

Scale* (m/mm) : 0.0074 / ~~0.0148 / 0.0296 / 0.0593~~

Sensitivity Setting : 0.3

Reference distance : 800mm

*Delete not necessary

esults

1. Original printout of result of profile ranging :

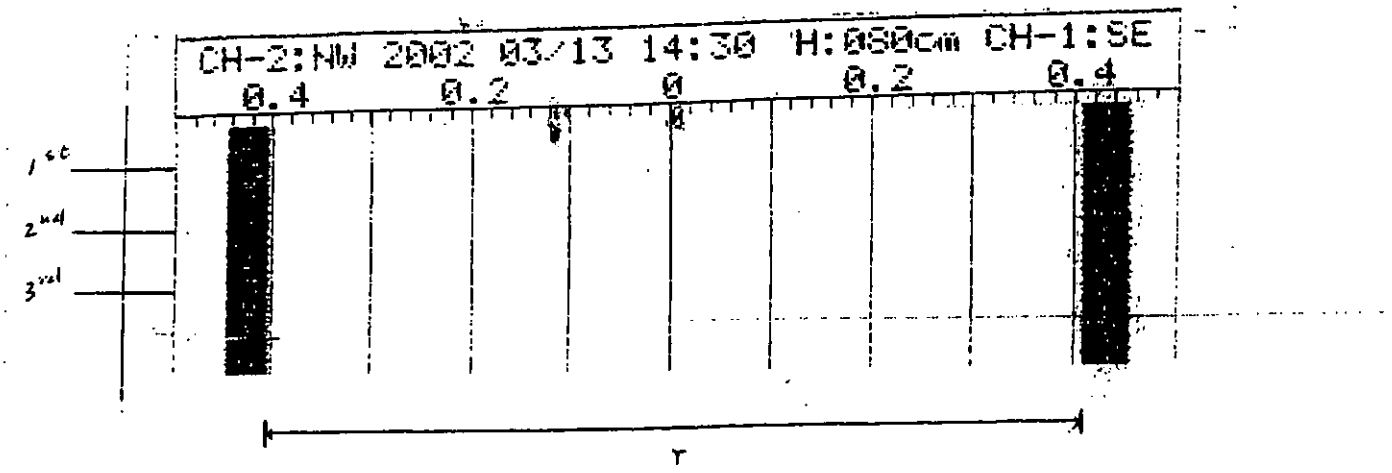

2. Distance deviation over the course of measurement is not greater than ± 1cm.

3. Distance between the first arrival echoes on the printout, measured by the caliper (r) :

Reference scale on trace (S) : 0.0074

	Reading on trace (r)	
1st reading	109.82	mm
2nd reading	109.75	mm
3rd reading	109.78	mm
Average	109.78	mm
Average figure corrected to actual scale (r*S)	0.81	m

Conditions of the calibration

Calibration level : 0.4 m

Measurement direction* : X / ~~Y~~

Scale* (m/mm) : ~~0.0074~~ / 0.0148 / ~~0.0296 / 0.0592~~

Sensitivity Setting : 0.3

*Delete not necessary

Reference distance : 1000mm

Results

1. Original printout of result of profile ranging :

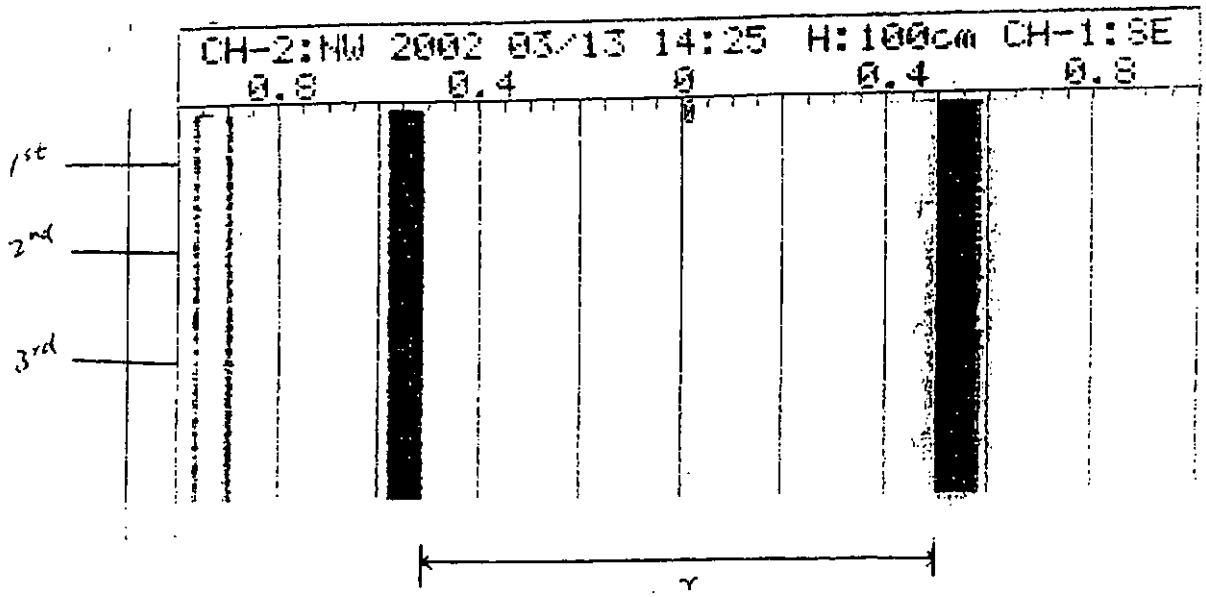

2. Distance deviation over the course of measurement is not greater than ± 1 cm.

3. Distance between the first arrival echoes on the printout, measured by the caliper (Y) :

Reference scale on trace (S) : 0.0148

	Reading on trace (Y)	
1st reading	67.86	mm
2nd reading	67.88	mm
3rd reading	67.98	mm
Average	67.91	mm
Average figure corrected to actual scale (Y*S)	1.01	m

Conditions of the calibration

Calibration level : 0.4 m

Measurement direction* : X / ~~Y~~

Scale* (m/mm) : ~~0.0074~~ / 0.0148 / ~~0.0296 / 0.0592~~

Sensitivity Setting : 0.3

Reference distance : 1500mm

*Delete not necessary

Results

1. Original printout of result of profile ranging :

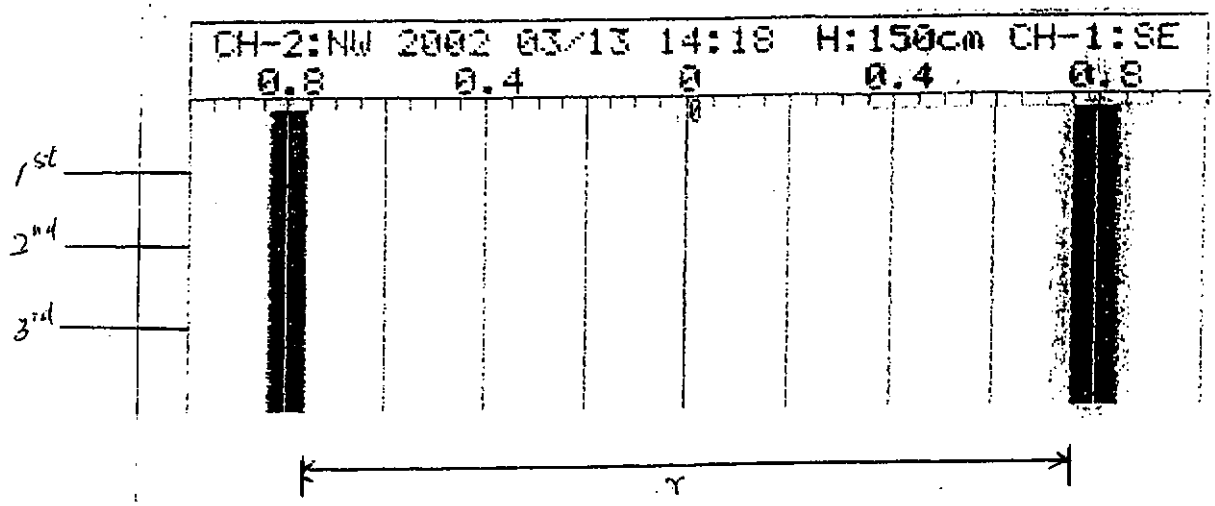

2. Distance deviation over the course of measurement is not greater than ± 1cm.

3. Distance between the first arrival echoes on the printout, measured by the caliper (Y) :

Reference scale on trace (S) : 0.0148

	Reading on trace (Y)	
1st reading	101.82	mm
2nd reading	101.90	mm
3rd reading	101.92	mm
Average	101.88	mm
Average figure corrected to actual scale (Y*S)	1.51	m

Conditions of the calibration

Calibration level	: 0.4 m	**Reference distance** : 2000mm
Measurement direction*	: X / ~~Y~~	
Scale* (m/mm)	: ~~0.0074 / 0.0148~~ / 0.0296 / ~~0.0592~~	
Sensitivity Setting	: 0.3	

*Delete not necessary

Results

1. **Original printout of result of profile ranging :**

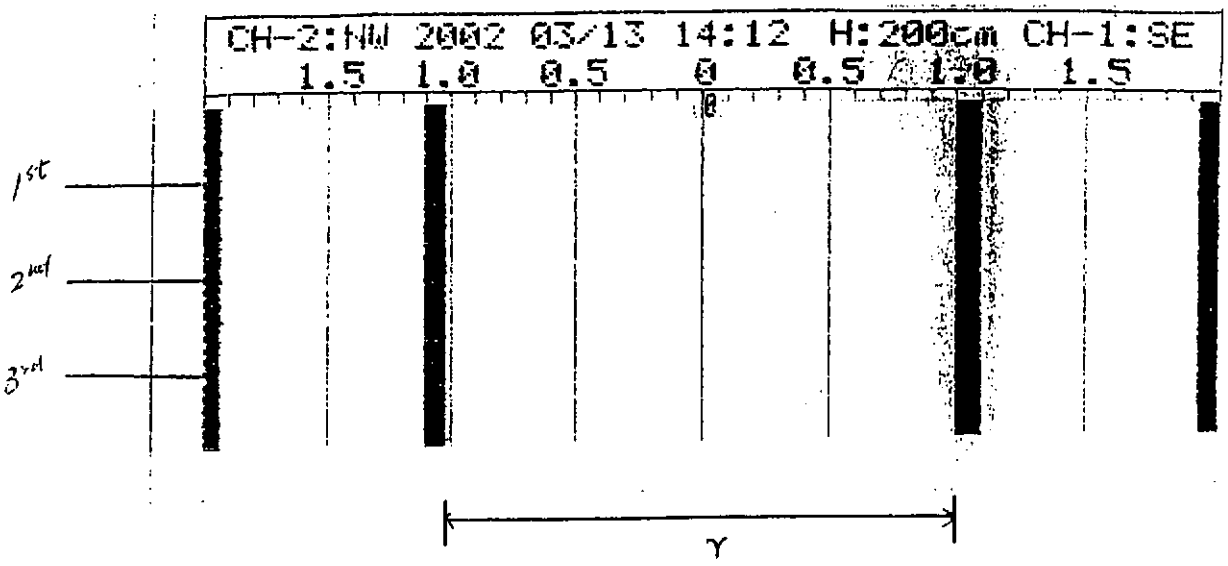

2. **Distance deviation over the course of measurement is not greater than ± 1cm.**

3. **Distance between the first arrival echoes on the printout, measured by the caliper (Y) :**

Reference scale on trace (S) : 0.0296

	Reading on trace (Y)	
1st reading	68.41	mm
2nd reading	68.32	mm
3rd reading	68.30	mm
Average	68.34	mm
Average figure corrected to actual scale (Y*S)	2.02	m

Conditions of the calibration

Calibration level : 0.4 m
Measurement direction* : X / ~~Y~~
Scale* (m/mm) : ~~0.0074 / 0.0148~~ / 0.0296 / ~~0.0592~~
Sensitivity Setting : 0.3

Reference distance : 2500mm

*Delete not necessary

Results

1. Original printout of result of profile ranging :

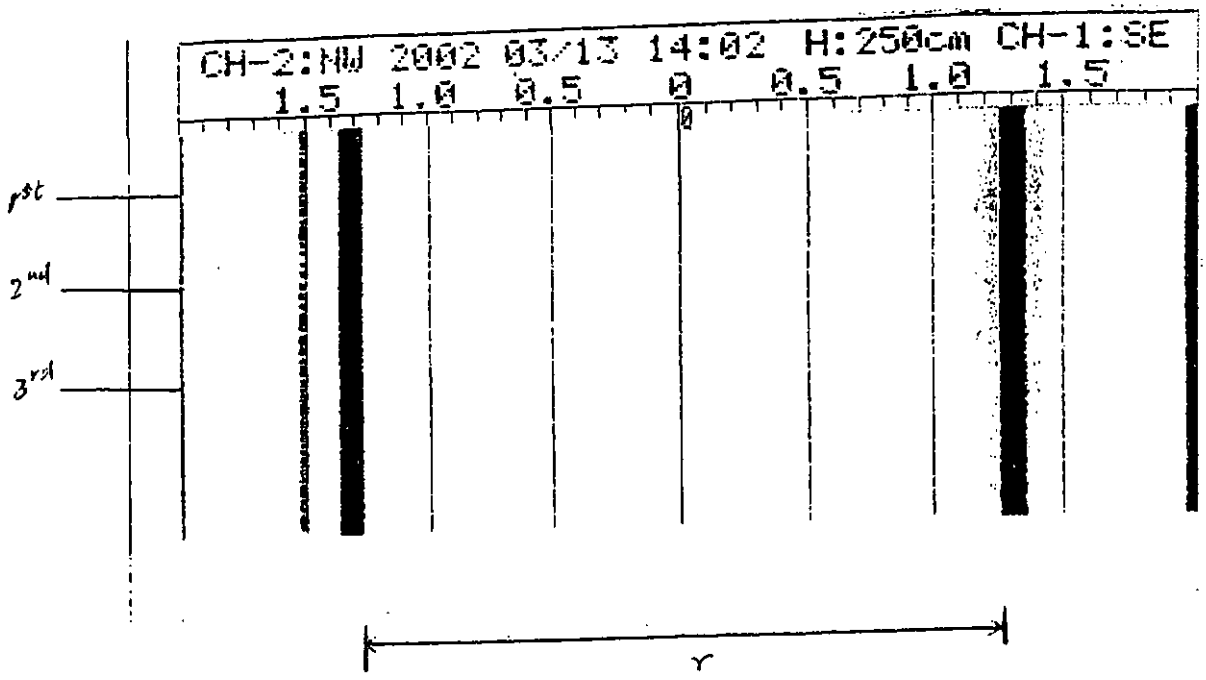

2. Distance deviation over the course of measurement is not greater than ± 1cm.

3. Distance between the first arrival echoes on the printout, measured by the caliper (r) :

Reference scale on trace (S) : 0.0296

	Reading on trace (r)	
1st reading	85.20	mm
2nd reading	85.16	mm
3rd reading	85.13	mm
Average	85.16	mm
Average figure corrected to actual scale (r*S)	2.52	m

Conditions of the calibration

Calibration level : 0.4 m

Reference distance : 3000mm

Measurement direction* : X / ~~Y~~

Scale* (m/mm) : ~~0.0074 / 0.0148~~ / 0.0296 / ~~0.0592~~

Sensitivity Setting : 0.3

*Delete not necessary

Results

1. Original printout of result of profile ranging :

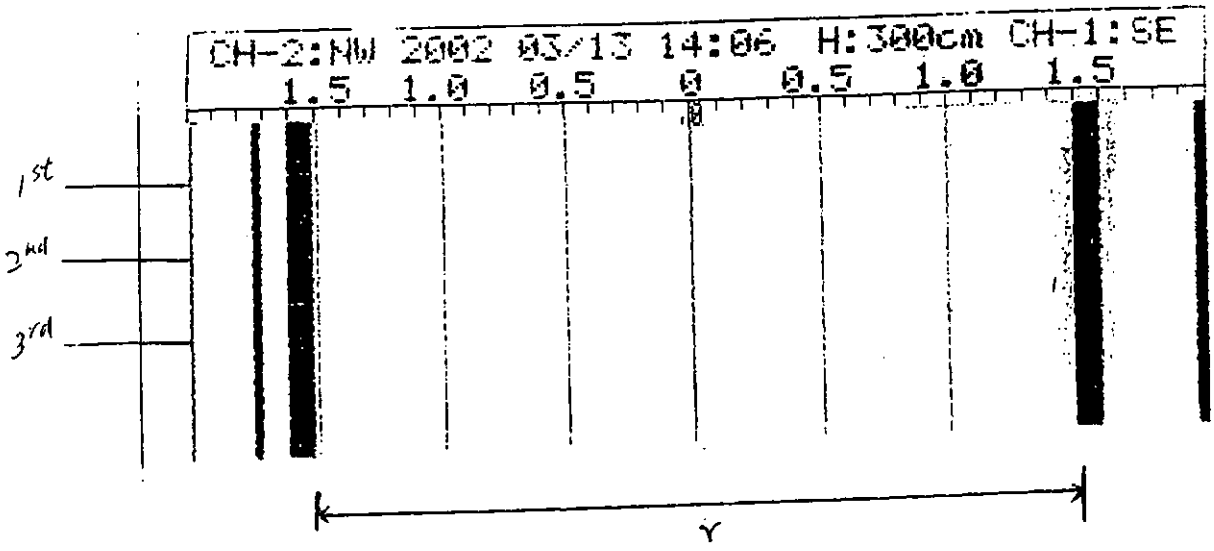

2. Distance deviation over the course of measurement is not greater than ± 1cm.

3. Distance between the first arrival echoes on the printout, measured by the caliper (Y) :

Reference scale on trace (S) : 0.0296

	Reading on trace (Y)	
1st reading	101.56	mm
2nd reading	101.73	mm
3rd reading	101.69	mm
Average	101.66	mm
Average figure corrected to actual scale (Y*S)	3.01	m

Conditions of the calibration

Calibration level : 0.4 m
Measurement direction* : X / ~~Y~~
Scale* (m/mm) : ~~0.0074 / 0.0148~~ / 0.0296 / ~~0.0592~~
Sensitivity Setting : 0.3
*Delete not necessary

Reference distance : 3500mm

Results

1. Original printout of result of profile ranging :

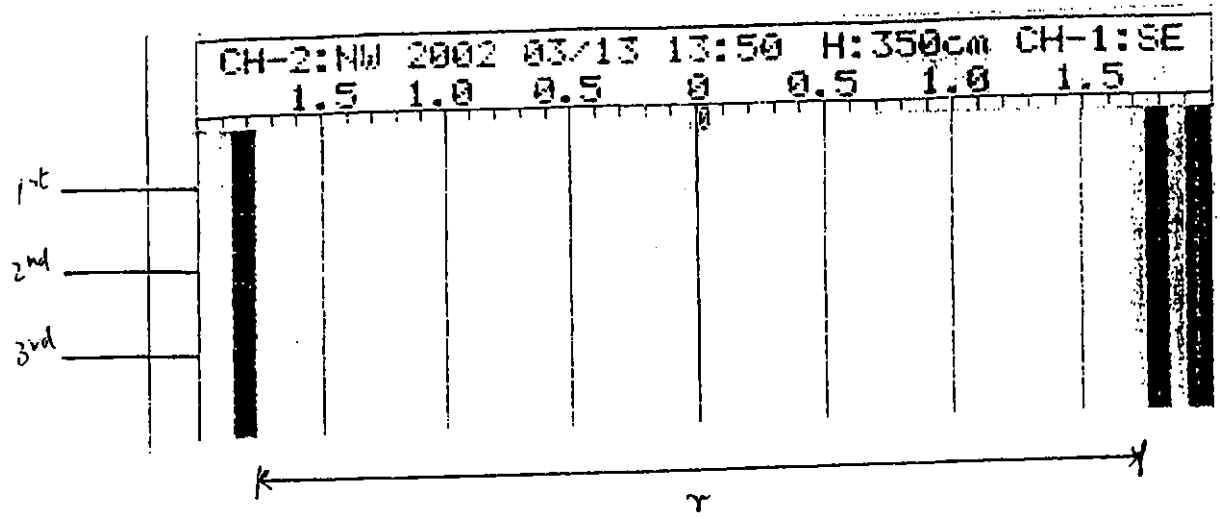

2. Distance deviation over the course of measurement is not greater than ± 1cm.

3. Distance between the first arrival echoes on the printout, measured by the caliper (Y) :

Reference scale on trace (S) : 0.0296

	Reading on trace (Y)	
1st reading	118.95	mm
2nd reading	118.90	mm
3rd reading	118.78	mm
Average	118.88	mm
Average figure corrected to actual scale (Y*S)	3.52	m

Conditions of the calibration

Reference distance : 3940mm

Calibration level : 0.4 m

Measurement direction* : X / ~~Y~~

Scale* (m/mm) : ~~0.0074 / 0.0148 / 0.0296~~ / 0.0592

Sensitivity Setting : 0.3

*Delete not necessary

Results

1. Original printout of result of profile ranging :

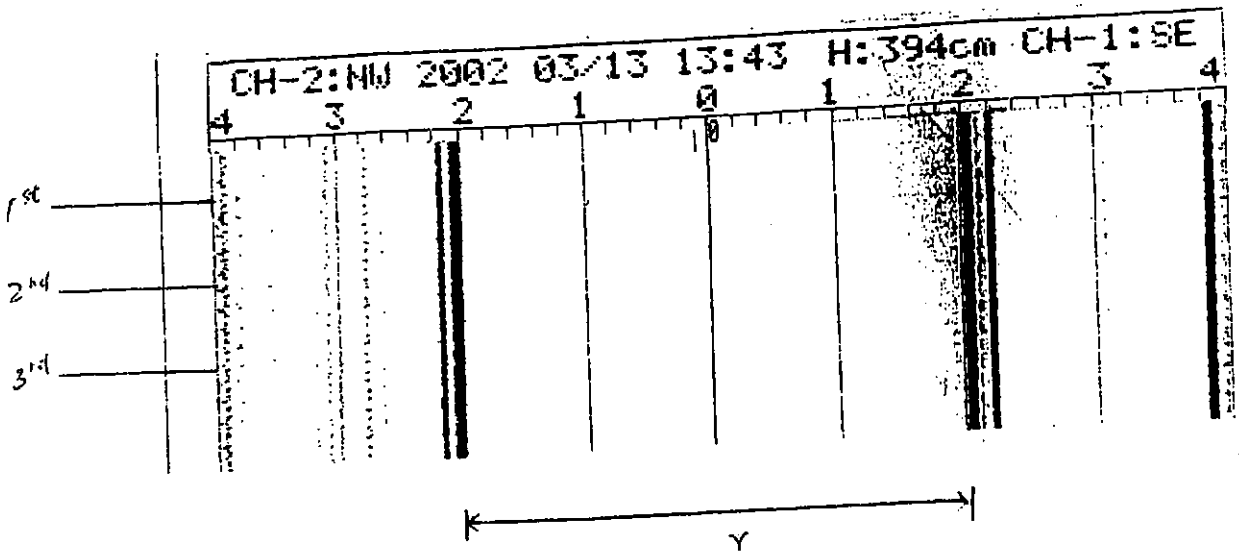

2. Distance deviation over the course of measurement is not greater than ± 1cm.

3. Distance between the first arrival echoes on the printout, measured by the caliper (Y) :

Reference scale on trace (S) : 0.0592

	Reading on trace (Y)	
1st reading	67.06	mm
2nd reading	67.03	mm
3rd reading	66.96	mm
Average	67.02	mm
Average figure corrected to actual scale (Y*S)	3.97	m

Conditions of the calibration

Calibration level : 0.4 m

Measurement direction* : ~~X~~ / Y

Scale* (m/mm) : 0.0074 / ~~0.0148 / 0.0296 / 0.0592~~

Sensitivity Setting : 0.3

*Delete not necessary

Reference distance : 800mm

Results

1. Original printout of result of profile ranging :

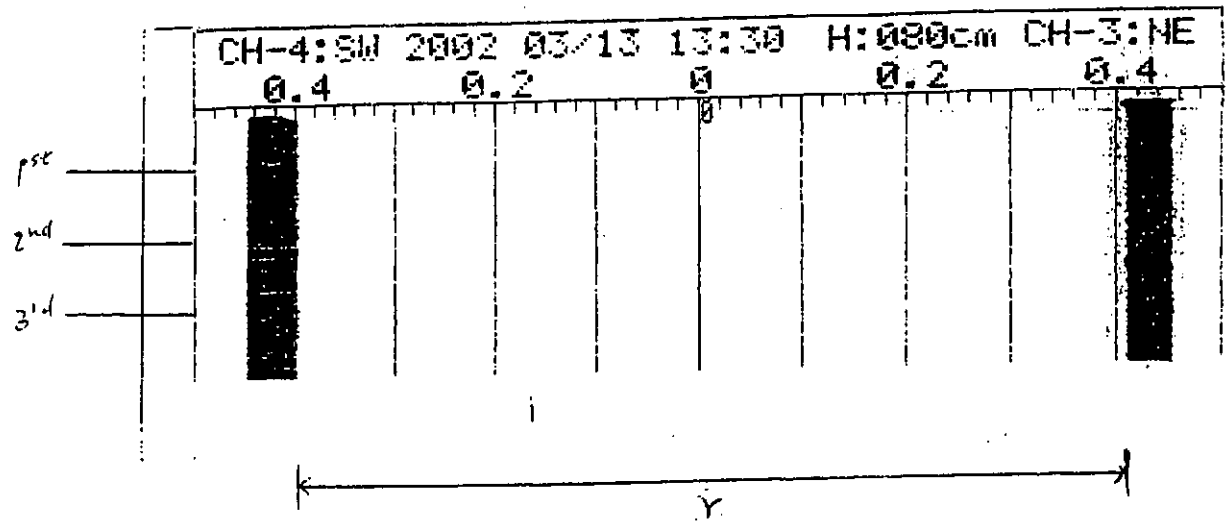

2. Distance deviation over the course of measurement is not greater than ± 1cm.

3. Distance between the first arrival echoes on the printout, measured by the caliper (r) :

Reference scale on trace (S) : 0.0074

	Reading on trace (r)	
1st reading	109.01	mm
2nd reading	109.25	mm
3rd reading	109.15	mm
Average	109.14	mm
Average figure corrected to actual scale (r*S)	0.81	m

Conditions of the calibration

Calibration level : 0.4 m

Reference distance : 1000mm

Measurement direction* : ~~X~~ / Y

Scale* (m/mm) : ~~0.0074~~ / 0.0148 / ~~0.0296~~ / ~~0.0592~~

Sensitivity Setting : 0.3

*Delete not necessary

Results

1, Original printout of result of profile ranging :

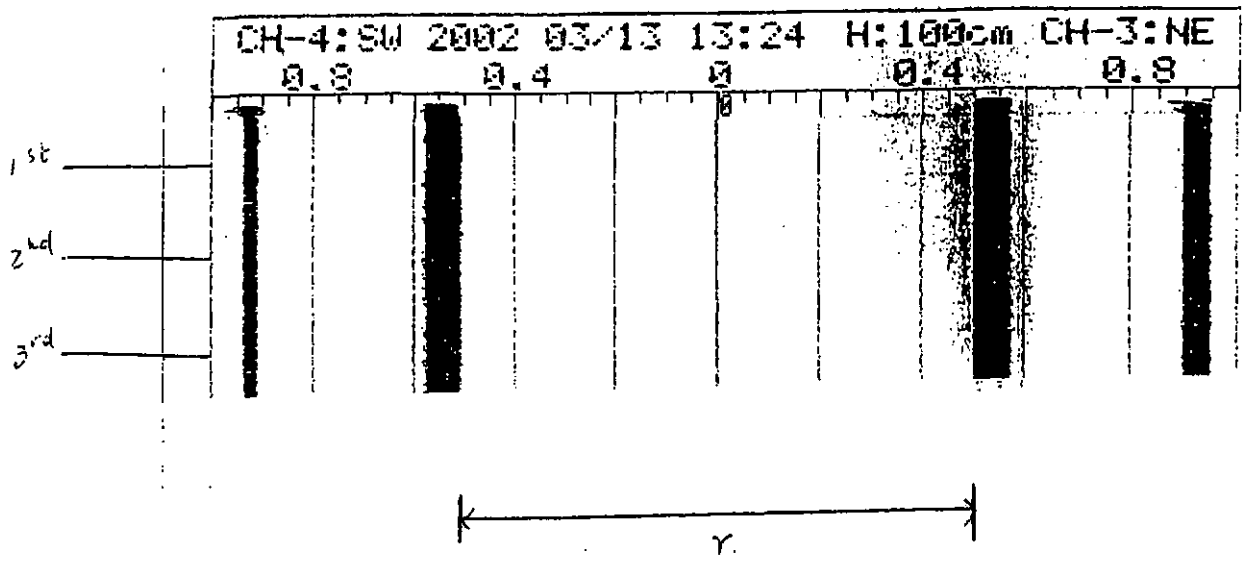

2. Distance deviation over the course of measurement is not greater than ± 1cm.

3. Distance between the first arrival echoes on the printout, measured by the caliper (Y) :

Reference scale on trace (S) : 0.0148

	Reading on trace (Y)	
1st reading	68.03	mm
2nd reading	68.05	mm
3rd reading	67.95	mm
Average	68.01	mm
Average figure corrected to actual scale (Y*S)	1.01	m

Conditions of the calibration

Reference distance : 1500mm

Calibration level	:	0.4 m
Measurement direction*	:	~~X~~ / Y
Scale* (m/mm)	:	~~0.0074~~ / 0.0148 / ~~0.0296~~ / ~~0.0592~~
Sensitivity Setting	:	0.3

*Delete not necessary

Results

1, Original printout of result of profile ranging :

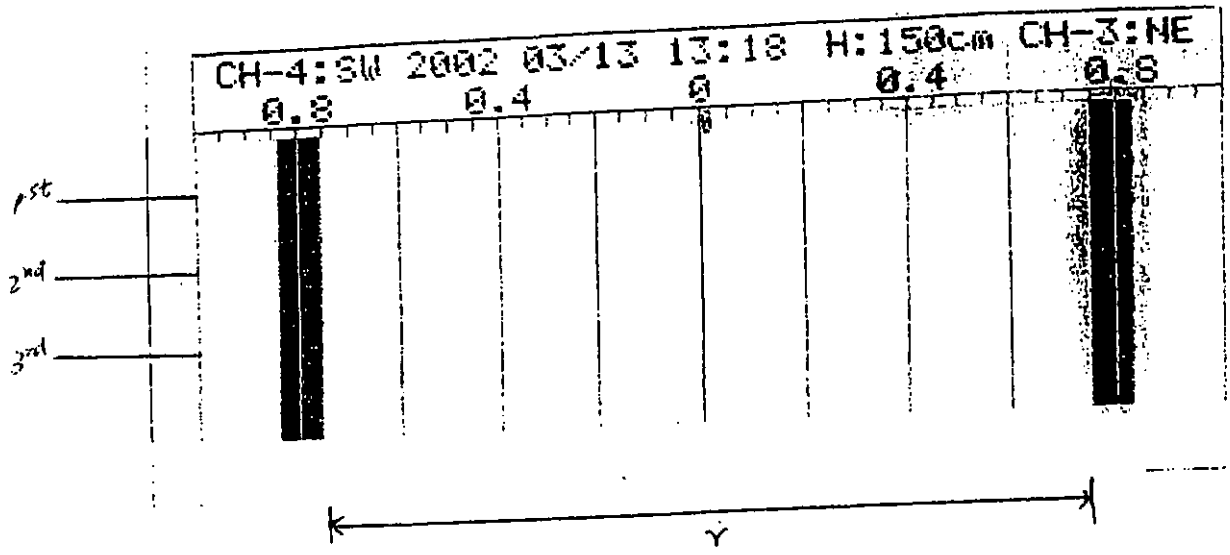

2. Distance deviation over the course of measurement is not greater than ± 1cm.

3. Distance between the first arrival echoes on the printout, measured by the caliper (Y) :

Reference scale on trace (S) : 0.0148

	Reading on trace (Y)	
1st reading	101.61	mm
2nd reading	101.59	mm
3rd reading	101.58	mm
Average	101.59	mm
Average figure corrected to actual scale (Y*S)	1.50	m

Conditions of the calibration

Calibration level : 0.4 m

Measurement direction* : ~~X~~ / Y

Scale* (m/mm) : ~~0.0074 / 0.0148~~ / 0.0296 / ~~0.0592~~

Sensitivity Setting : 0.3

*Delete not necessary

Reference distance : 2000mm

Results

1, Original printout of result of profile ranging :

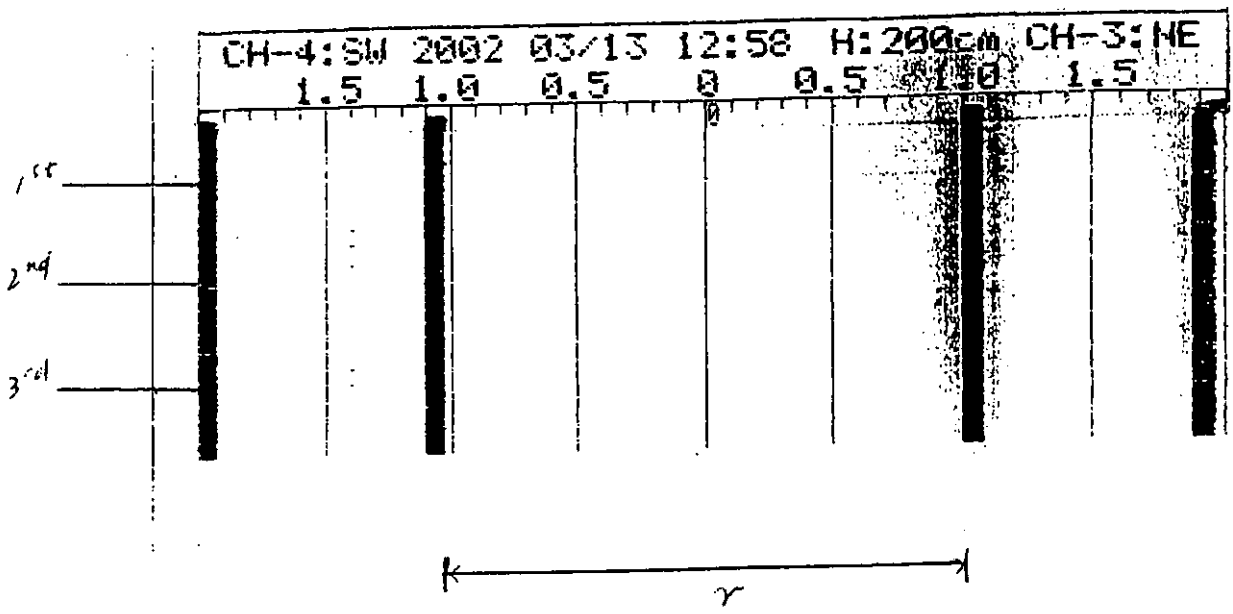

2, Distance deviation over the course of measurement is not greater than ± 1cm.

3, Distance between the first arrival echoes on the printout, measured by the caliper (r) :

Reference scale on trace (S) : 0.0296

	Reading on trace (r)	
1st reading	68.29	mm
2nd reading	68.42	mm
3rd reading	68.40	mm
Average	68.37	mm
Average figure corrected to actual scale (r*S)	2.02	m

Conditions of the calibration

Calibration level : 0.4 m

Measurement direction* : ~~X~~ / Y

Scale* **(m/mm)** : ~~0.0074 / 0.0148~~ / 0.0296 / ~~0.0592~~

Sensitivity Setting : 0.3

*Delete not necessary

Reference distance : 2500mm

Results

1. Original printout of result of profile ranging :

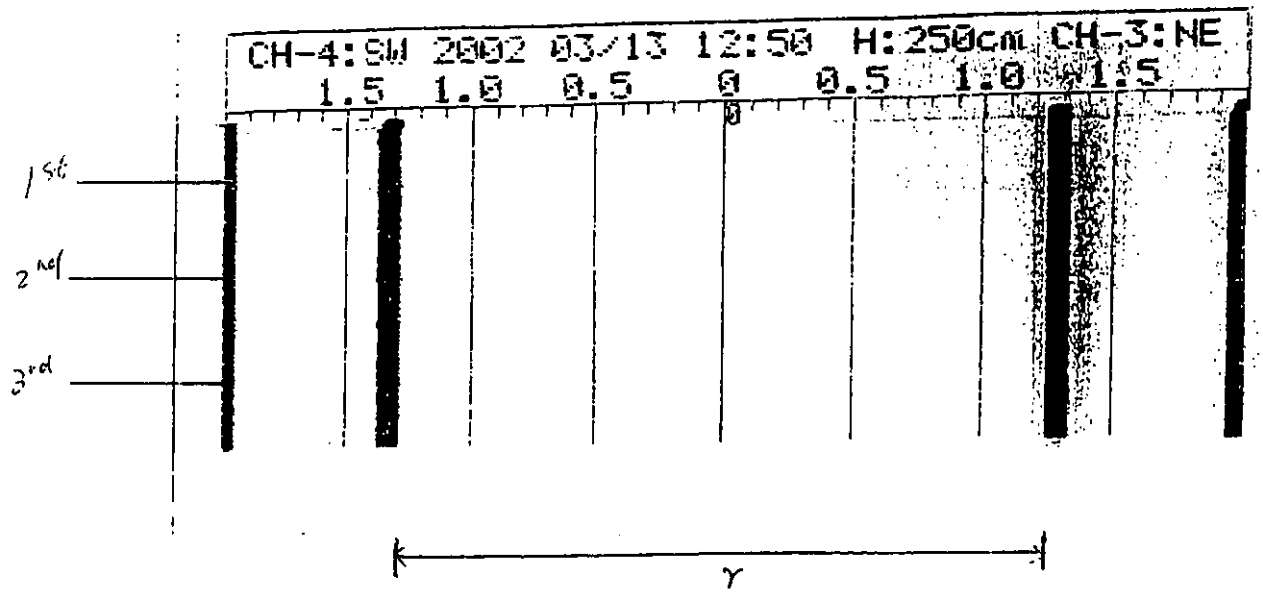

2. Distance deviation over the course of measurement is not greater than ± 1cm.

3. Distance between the first arrival echoes on the printout, measured by the caliper (Y) :

Reference scale on trace (S) : 0.0296

	Reading on trace (Y)	
1st reading	84.62	mm
2nd reading	84.80	mm
3rd reading	84.88	mm
Average	84.77	mm
Average figure corrected to actual scale (Y*S)	2.51	m

Conditions of the calibration

Calibration level : 0.4 m

Reference distance : 3000mm

Measurement direction* : ~~X~~ / Y

Scale* (m/mm) : ~~0.0074~~ / ~~0.0148~~ / 0.0296 / ~~0.0592~~

Sensitivity Setting : 0.3

*Delete not necessary

Results

1, Original printout of result of profile ranging :

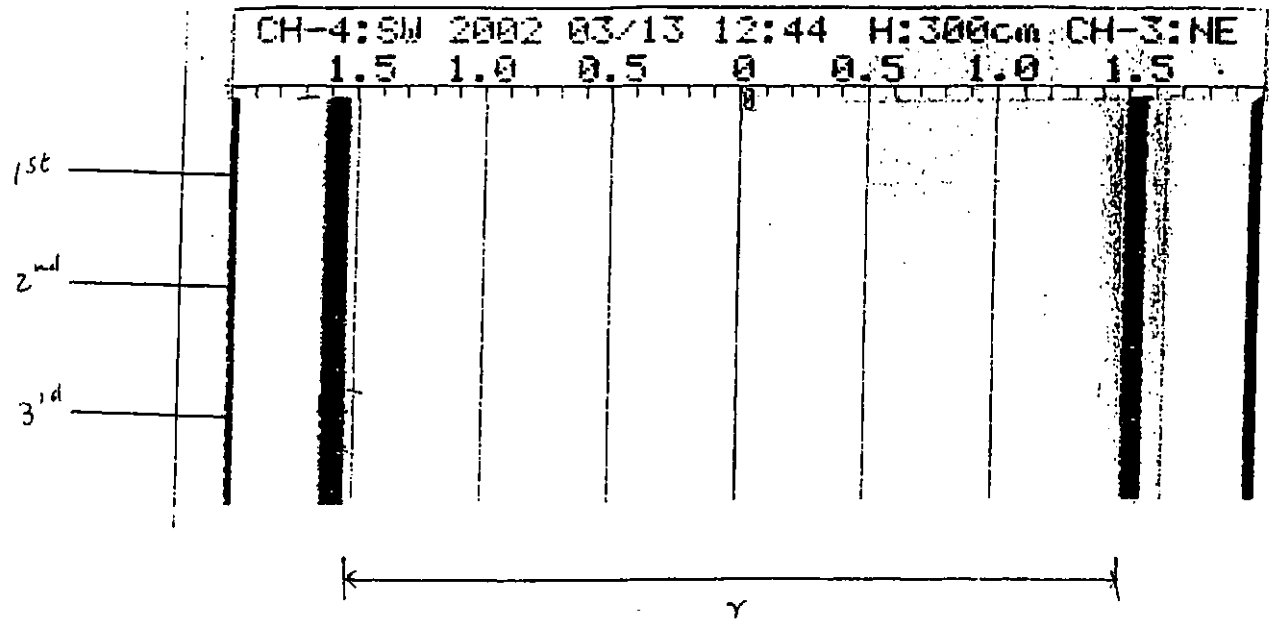

2, Distance deviation over the course of measurement is not greater than ± 1cm.

3, Distance between the first arrival echoes on the printout, measured by the caliper (Y) :

Reference scale on trace (S) : 0.0296

	Reading on trace (Y)	
1st reading	102.10	mm
2nd reading	101.95	mm
3rd reading	101.98	mm
Average	102.01	mm
Average figure corrected to actual scale (Y*S)	3.02	m

Conditions of the calibration

Calibration level : 0.4 m

Measurement direction* : ~~X~~ / Y

Scale* (m/mm) : ~~0.0074 / 0.0148~~ / 0.0296 / ~~0.0592~~

Sensitivity Setting : 0.3

Reference distance : 3500mm

*Delete not necessary

Results

1. Original printout of result of profile ranging :

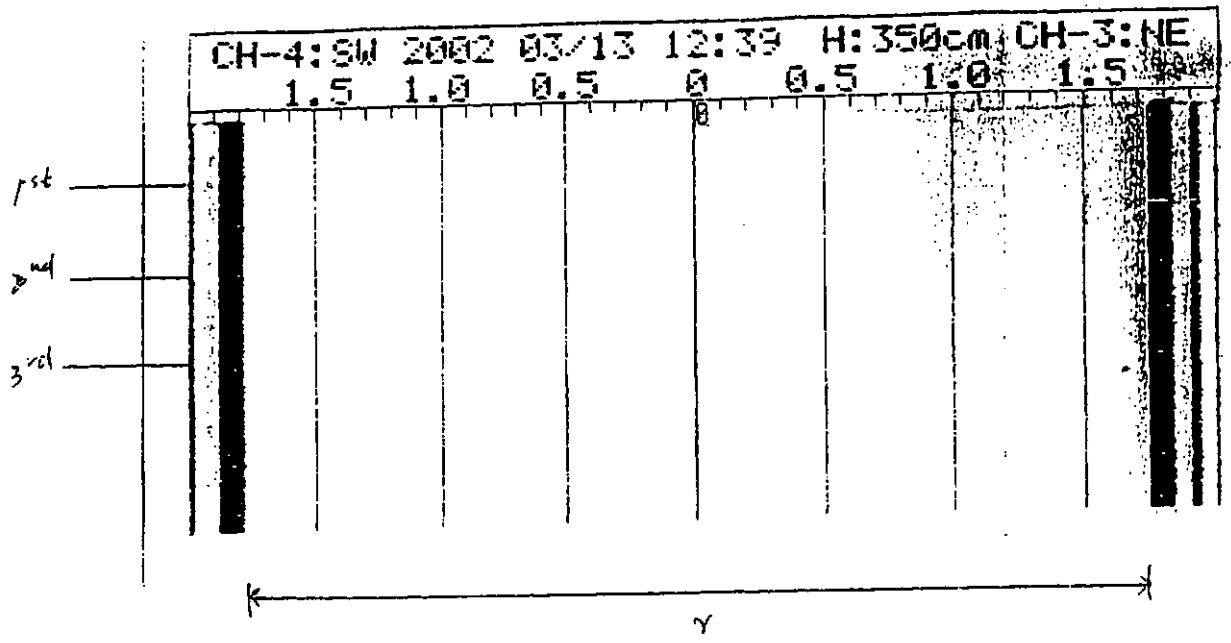

2. Distance deviation over the course of measurement is not greater than ± 1cm.

3. Distance between the first arrival echoes on the printout, measured by the caliper (Y) :

Reference scale on trace (S) : 0.0296

	Reading on trace (Y)	
1st reading	118.94	mm
2nd reading	118.90	mm
3rd reading	118.76	mm
Average	118.87	mm
Average figure corrected to actual scale (Y*S)	3.52	m

Conditions of the calibration

Calibration level	: 0.4 m	**Reference distance**	: 3940mm
Measurement direction*	: ~~X~~ / Y		
Scale* (m/mm)	: ~~0.0074 / 0.0148 / 0.0296~~ / 0.0592		
Sensitivity Setting	: 0.3		

*Delete not necessary

Results

1. **Original printout of result of profile ranging :**

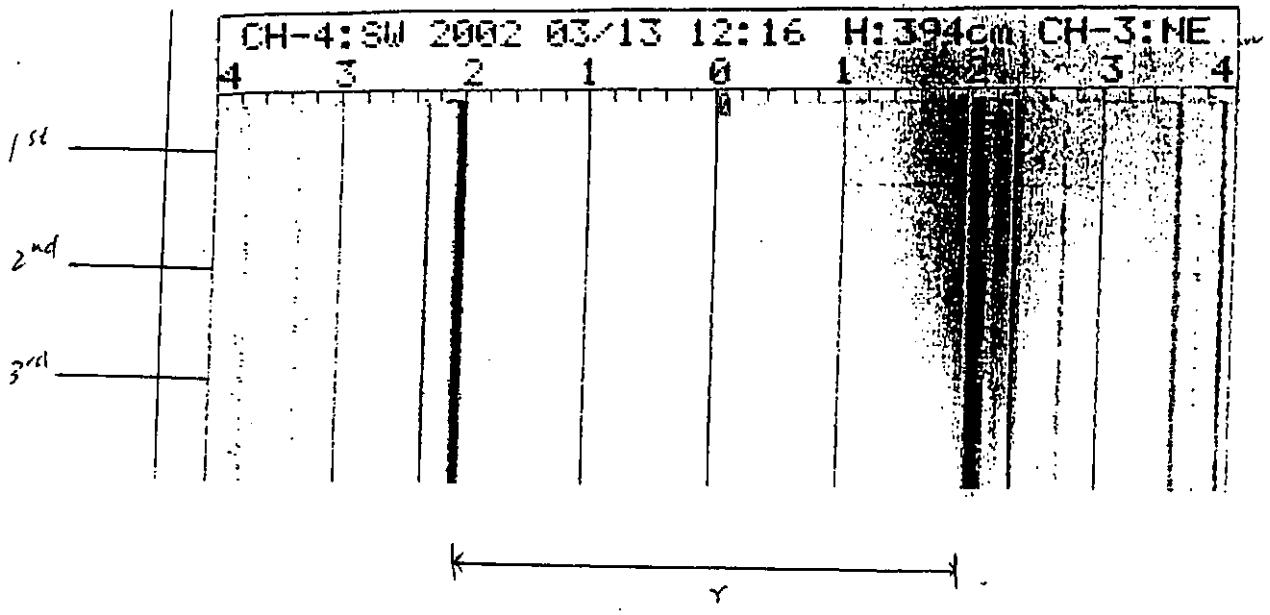

2. **Distance deviation over the course of measurement is not greater than ± 1cm.**

3. **Distance between the first arrival echoes on the printout, measured by the caliper (Y) :**

Reference scale on trace (S) : 0.0592

	Reading on trace (Y)	
1st reading	67.15	mm
2nd reading	67.10	mm
3rd reading	67.02	mm
Average	67.09	mm
Average figure corrected to actual scale (Y*S)	3.97	m

Appendix B

Uncertainty calculation guidelines

Flowchart for evaluating uncertainty of measurement

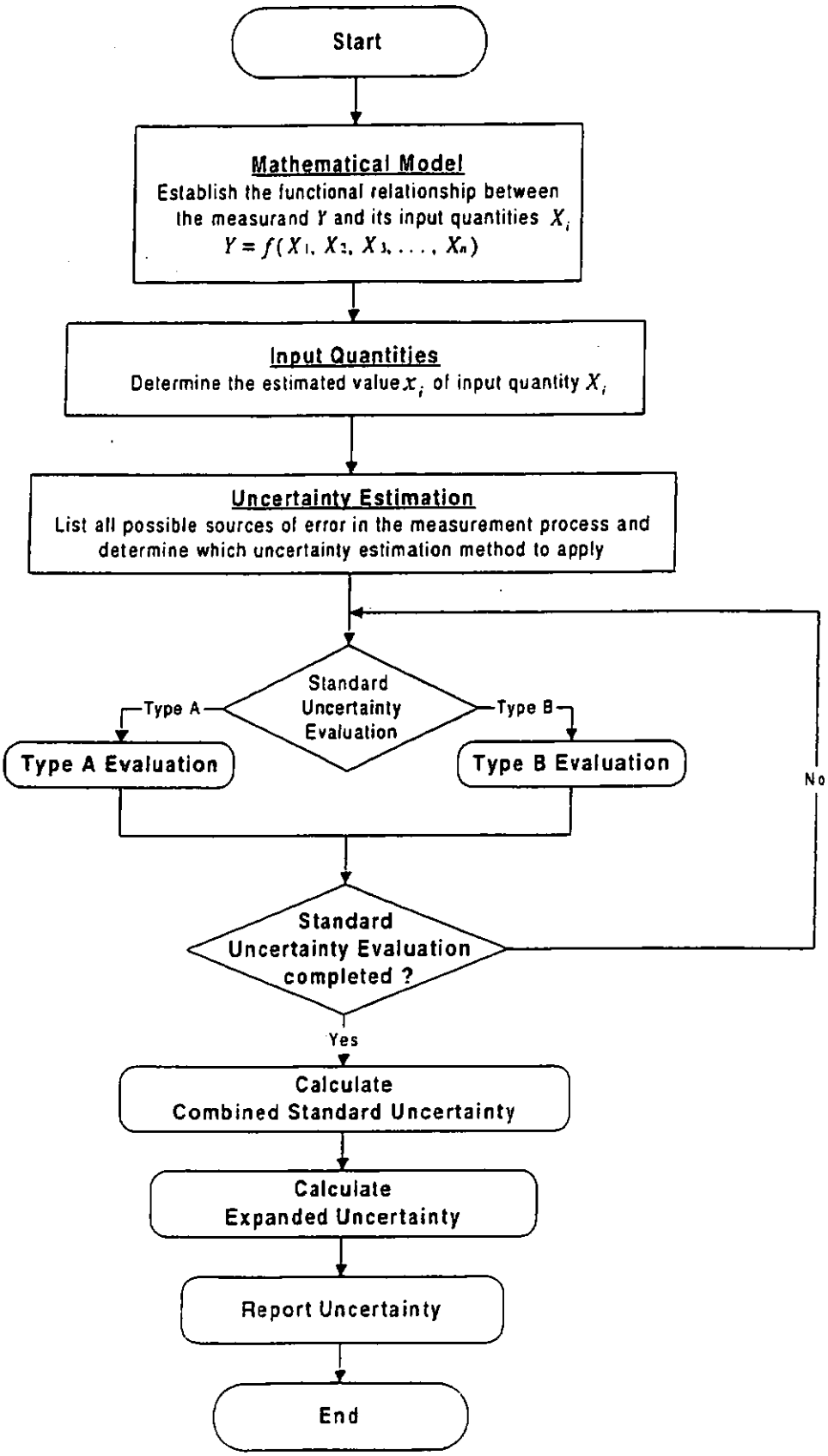

Chart - 1

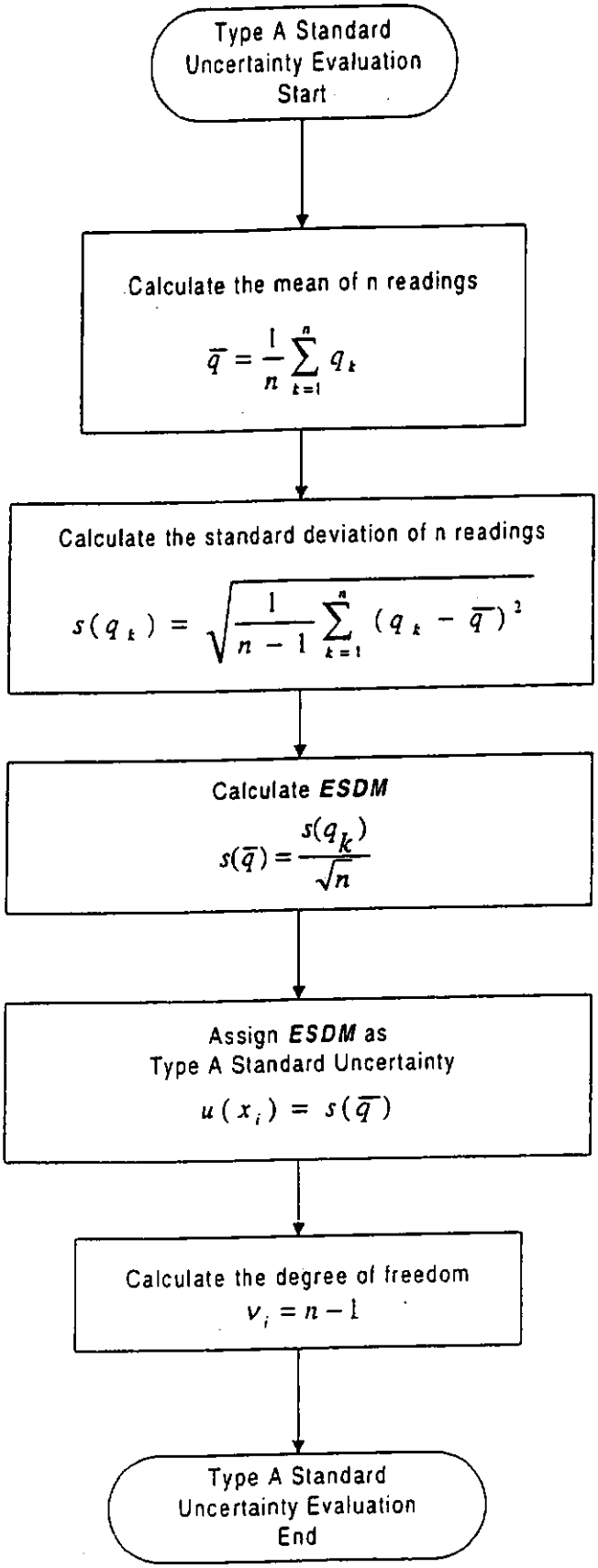
Type A Standard Uncertainty Evaluation Start
Calculate the mean of n readings
$\bar{q} = \frac{1}{n}\sum_{k=1}^{n} q_k$
Calculate the standard deviation of n readings
$s(q_k) = \sqrt{\frac{1}{n-1}\sum_{k=1}^{n}(q_k - \bar{q})^2}$
Calculate ESDM
$s(\bar{q}) = \frac{s(q_k)}{\sqrt{n}}$
Assign ESDM as Type A Standard Uncertainty
$u(x_i) = s(\bar{q})$
Calculate the degree of freedom
$v_i = n - 1$
Type A Standard Uncertainty Evaluation End

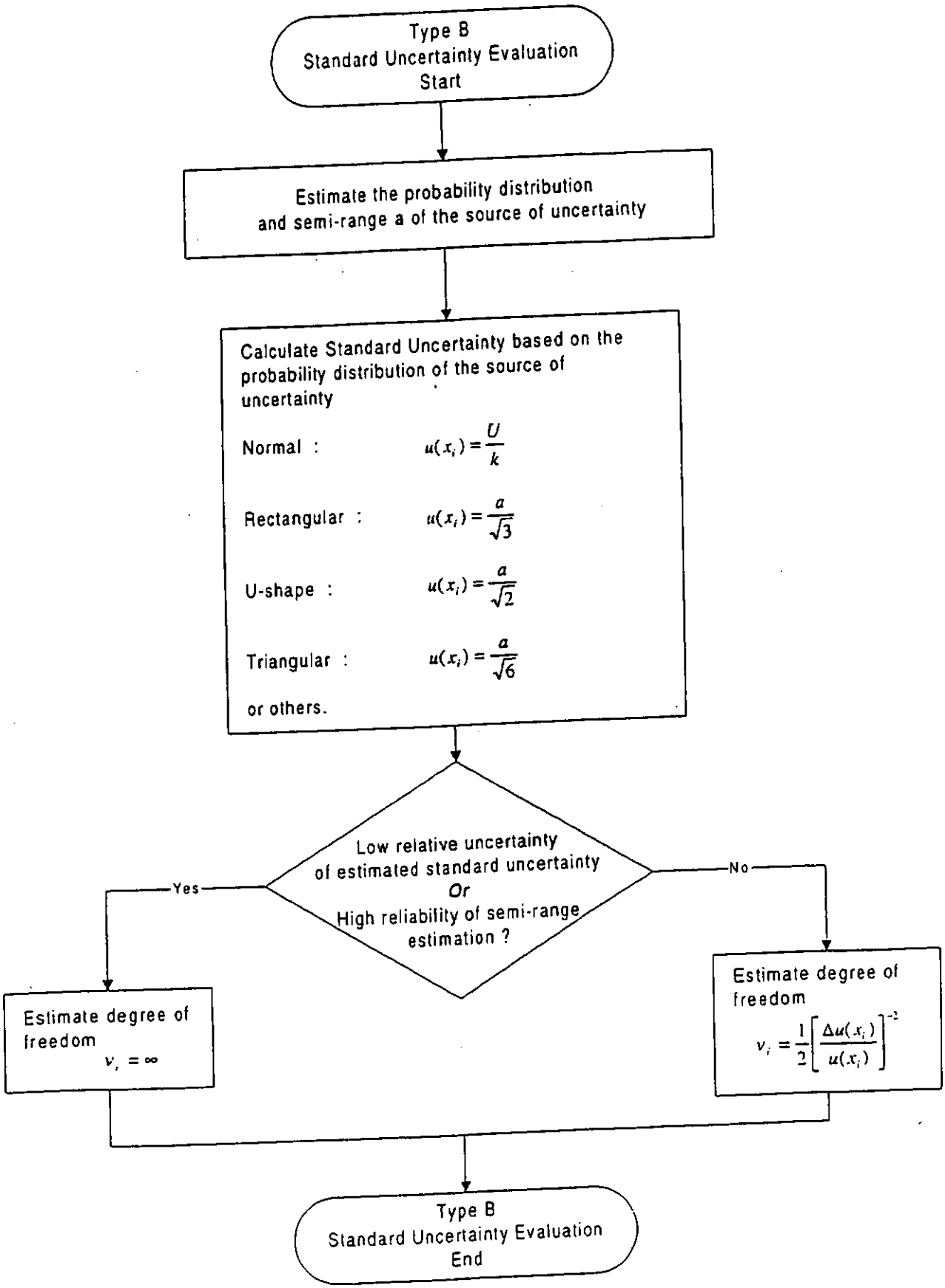
Type B
Standard Uncertainty Evaluation
Start
Estimate the probability distribution
and semi-range a of the source of uncertainty
Calculate Standard Uncertainty based on the probability distribution of the source of uncertainty
Normal : $u(x_i) = \frac{U}{k}$
Rectangular : $u(x_i) = \frac{a}{\sqrt{3}}$
U-shape : $u(x_i) = \frac{a}{\sqrt{2}}$
Triangular : $u(x_i) = \frac{a}{\sqrt{6}}$
or others.
Low relative uncertainty
of estimated standard uncertainty
Or
High reliability of semi-range
estimation ?
Yes
No
Estimate degree of freedom
$\nu_i = \infty$
Estimate degree of freedom
$\nu_i = \frac{1}{2}\left[\frac{\Delta u(x_i)}{u(x_i)}\right]^{-2}$
Type B
Standard Uncertainty Evaluation
End

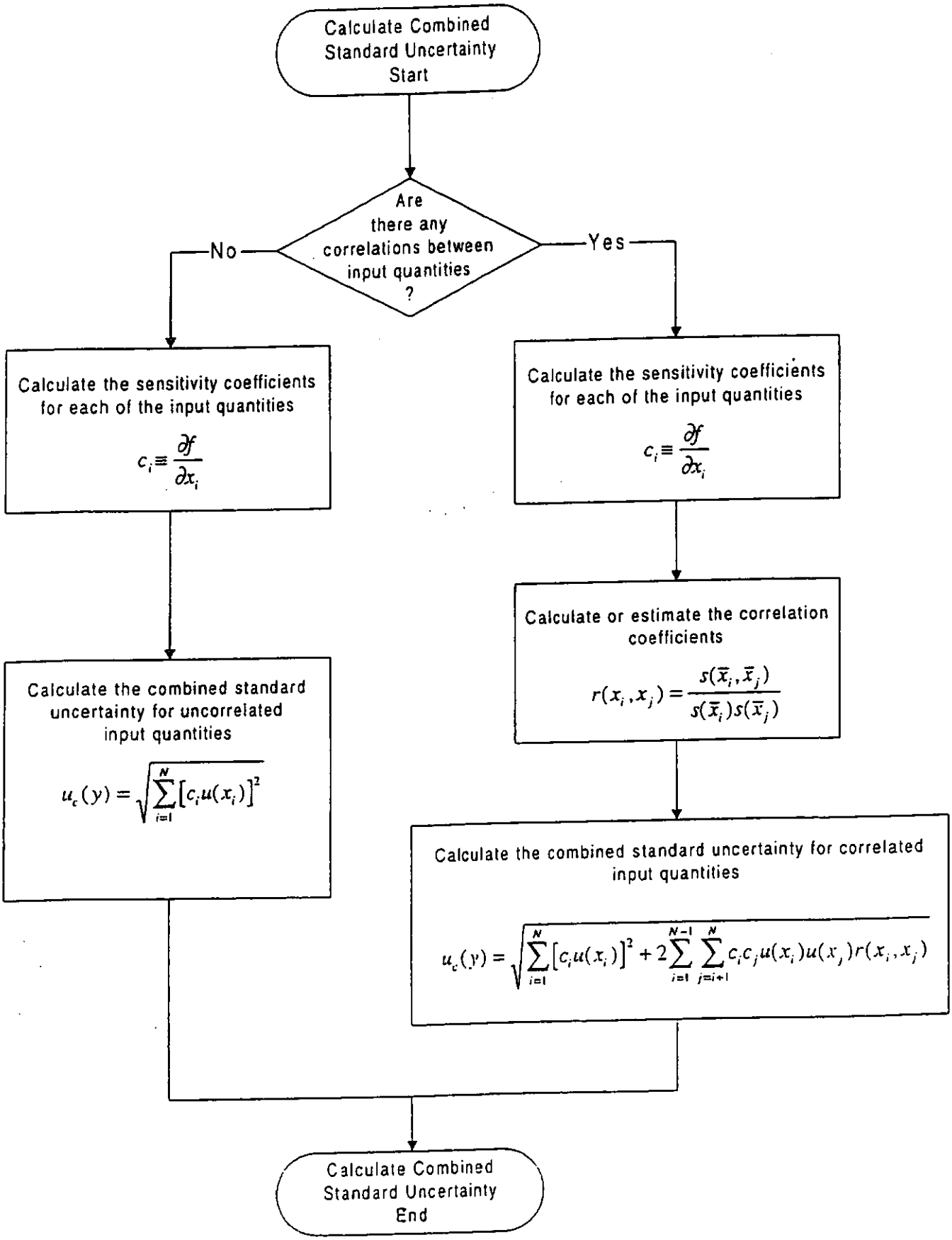
Calculate Combined Standard Uncertainty Start
Are there any correlations between input quantities ?
No
Yes
Calculate the sensitivity coefficients for each of the input quantities
$c_i \equiv \frac{\partial f}{\partial x_i}$
Calculate the combined standard uncertainty for uncorrelated input quantities
$u_c(y) = \sqrt{\sum_{i=1}^{N} [c_i u(x_i)]^2}$
Calculate the sensitivity coefficients for each of the input quantities
$c_i \equiv \frac{\partial f}{\partial x_i}$
Calculate or estimate the correlation coefficients
$r(x_i, x_j) = \frac{s(\bar{x}_i, \bar{x}_j)}{s(\bar{x}_i) s(\bar{x}_j)}$
Calculate the combined standard uncertainty for correlated input quantities
$u_c(y) = \sqrt{\sum_{i=1}^{N} [c_i u(x_i)]^2 + 2 \sum_{i=1}^{N-1} \sum_{j=i+1}^{N} c_i c_j u(x_i) u(x_j) r(x_i, x_j)}$
Calculate Combined Standard Uncertainty End

Chart - 4

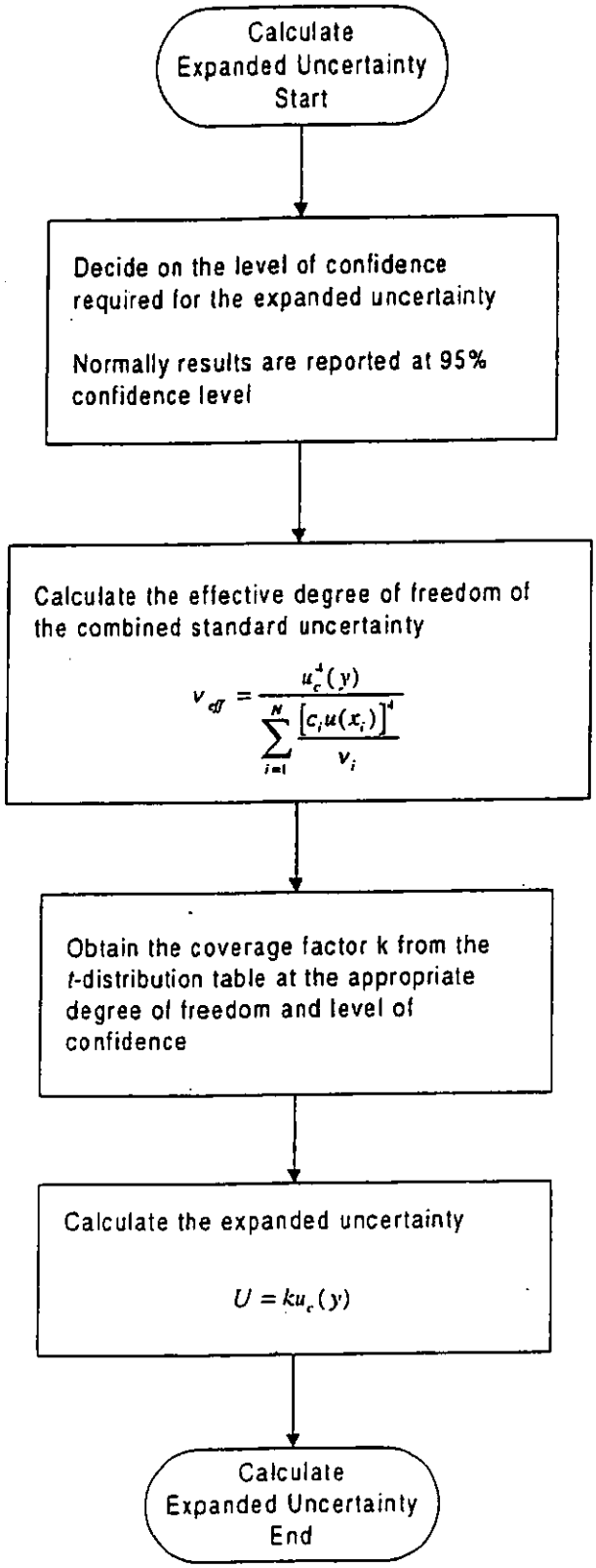
Calculate Expanded Uncertainty Start
Decide on the level of confidence required for the expanded uncertainty
Normally results are reported at 95% confidence level
Calculate the effective degree of freedom of the combined standard uncertainty
$v_{eff} = \frac{u_c^4(y)}{\sum_{i=1}^{N} \frac{[c_i u(x_i)]^4}{v_i}}$
Obtain the coverage factor k from the t-distribution table at the appropriate degree of freedom and level of confidence
Calculate the expanded uncertainty
$U = k u_c(y)$
Calculate Expanded Uncertainty End

Appendix C

Mathematical Model in the *Range* Calibration

Calibration Analysis in *Range* Calibration

Mathematical Model in Range Calibration

$$e = L_t - r_t * S \qquad \text{---------- Equation (1)}$$

where

e is the error;

L_t is the distance between two steel plates which is measured by a calibrated measuring tape at maximum temperature difference from 20°C;

r_t is the measured value on trace by a calibrated caliper at maximum temperature difference from 20 °C;

S is the scaling factor which is provided by the manufacturer.

And $L_t = L_{20}(1 + \alpha_L t)$ ---------- Equation (2)

$$r_t = r_{20}(1 + \alpha_r t) \qquad \text{---------- Equation (3)}$$

where

L_{20} is the measured value of distance between the two surface walls of the reference steel tank at 20°C;

r_{20} is the distance between two first arrival signals on printout echo traces by caliper at 20°C;

S_{20} is the reference scale provided by the manufacturer;

α_L is the thermal expansion coefficient of measuring tape, 1.5×10^{-4}/°C;

α_R & α_S are the thermal expansion coefficient of caliper, 11.5×10^{-6}/°C.

Substituting equations (2) and (3) into (1),

$$e = L_{20}(1 + \alpha_L t) - r_{20}(1 + \alpha_r t) * S$$

Uncertainty Components in Range Calibration

(i) Calibration uncertainty of the measuring tape, μ_{ta} [Type B]

$$\mu_{ta} = \frac{a_{ta}}{k_{ta}} \qquad \text{---------- Equation (4)}$$

where

a_{ta} is the uncertainty from the calibration certificate;

k_{ta} is the coverage factor applied in the calibration certificate.

(ii) Standard uncertainty of the measuring tape in error, μ_{te} [Type B]

$$\mu_{te} = \frac{a_{te}}{\sqrt{3}} \qquad \text{---------- Equation (5)}$$

where a_{te} is the error of the measuring tape.

(iii) Standard uncertainty of the measuring tape in resolution, μ_{tr} [Type B]

$$\mu_{tr} = \frac{a_{tr}}{\sqrt{3}} \qquad \text{---------- Equation (6)}$$

where a_{tr} is the semi-range of the measuring tape in resolution.

(iv) Experimental uncertainty in randomness of measurements L_{20}, μ_{LR} [Type A]

$$\mu_{LR} = \frac{L_{SD}}{\sqrt{n}} \qquad \text{---------- Equation (7)}$$

where

L_{SD} is the standard deviation of measurements L_{20};

n is the number of measurements for L_{20} in calibration.

(v) Standard uncertainty in thermal expansion of the measuring tape, $\mu_{\alpha t}$ [Type B]

$$\mu_{\alpha_L} = \frac{0.5x10^{-4}}{\sqrt{3}} \qquad \text{---------- Equation (8)}$$

Note: the interval for thermal expansion coefficient of the measuring tape, $\pm 0.5 \times 10^{-4}/^{\circ}C$.

(vi) Calibration uncertainty of the caliper, μ_{ca} [Type B]

$$\mu_{ca} = \frac{a_{ca}}{k_{ca}}$$ ---------- Equation (9)

where

a_{ca} is the uncertainty from the calibration certificate;

k_{ca} is the coverage factor applied in the calibration certificate.

(vii) Standard uncertainty of the caliper in resolution, μ_{cr} [Type B]

$$\mu_{cr} = \frac{a_{cr}}{\sqrt{3}}$$ ---------- Equation (10)

where a_{cr} is the semi-range of the caliper in resolution.

(viii) Standard uncertainty of the caliper error, μ_{ce} [Type B]

$$\mu_{ce} = \frac{a_{ce}}{\sqrt{3}}$$ ---------- Equation (11)

where a_{ce} is the error of the caliper.

(ix) Standard uncertainty in randomness of measurements r_{20}, μ_{rr} [Type A]

$$\mu_{rr} = \frac{r_{SD}}{\sqrt{n}}$$ ---------- Equation (12)

where

r_{SD} is the standard deviation of the measurements r_{20};

n is the number of measurements for r_{20} in calibration.

(x) Standard uncertainty in thermal expansion of the reference steel tank, μ_{a_S} [Type B]

$$\mu_{a_S} = \frac{0.5x10^{-6}}{\sqrt{3}}$$ ---------- Equation (13)

Note: the interval for thermal expansion coefficient of the reference steel tank, $\pm 0.5x10^{-6}$/°C.

The uncertainties of thermal expansion coefficients and temperature difference are negligible compared with other uncertainties, thus:

Combined Standard uncertainty of the measured value of distance between the sensor head and the wall of the reference steel tank, $\mu_{L_{20}}$

$$\mu_{L_{20}}^{\ 2} = \mu_{ta}^{\ 2} + \mu_{te}^{\ 2} + \mu_{tr}^{\ 2} + \mu_{LR}^{\ 2} \qquad \text{---------- Equation (14)}$$

Combined Standard uncertainty of the distance between two first arrival signals on printout echo traces by steel ruler, $\mu_{r_{20}}$

$$\mu_{r_{20}}^{\ 2} = \mu_{ca}^{\ 2} + \mu_{ce}^{\ 2} + \mu_{cr}^{\ 2} + \mu_{rr}^{\ 2} \qquad \text{---------- Equation (15)}$$

Sensitivity Coefficients in Range Calibration

$$\frac{\partial e}{\partial L_{20}} = 1 \qquad \text{---------- Equation (16)}$$

$$\frac{\partial e}{\partial r_{20}} = -S \qquad \text{---------- Equation (17)}$$

Combined Uncertainties, U_c, in Range Calibration

$$U_c = \sqrt{(\frac{\partial e}{\partial L}\mu_{L_{20}})^2 + (\frac{\partial e}{\partial r}\mu_{r_{20}})^2} \qquad \text{---------- Equation (18)}$$

where

U_c is the combined uncertainty;

$\mu_{L_{20}}$ is the combined standard uncertainty of dimension of the reference steel tank;

$\mu_{r_{20}}$ is the combined standard uncertainty of the distance between two first arrival signals on printout echo traces by caliper.

Effective degree of freedom, V_{eff} , in Range Calibration

$$V_{eff} = \frac{U_c^{\,4}}{\frac{(\frac{\partial e}{\partial L_{20}}\mu_{L_{20}})^4}{V_{L_{20}}} + \frac{(\frac{\partial e}{\partial r_{20}}\mu_{r_{20}})^4}{V_{r_{20}}}}$$

---------- Equation (19)

Expanded Uncertainties, U_e, in Range Calibration

From V_{eff} and students' t distribution in statistics for 95% confidence, determine the coverage factor k.

$$U_e = kU_c$$

---------- Equation (20)

where

U_e is the expanded uncertainty;

U_c is the combined uncertainty.

Appendix D

Student's distribution in Statistics for 95% confidence level

Table of student's t values for a 95% confidence interval

Effective Degrees of Freedom (ν_{eff})	t value (k)
1	12.7
2	4.30
3	3.18
4	2.78
5	2.57
6	2.45
7	2.36
8	2.31
9	2.26
10	2.23
11	2.20
12	2.18
13	2.16
14	2.14
15	2.13
16	2.12
17	2.11
18	2.10
19 to 24	2.09
25 to 29	2.06
30 to 34	2.04
35 to 39	2.03
40 to 44	2.02
45 to 59	2.01
60 to 69	2.00
70 to 99	1.99
100 to 120	1.98
infinite	1.96

Appendix E

Mathematical Model in the *Depth* Calibration (By the measuring tape approach)

Calibration Analysis in *Depth* Calibration (the measuring tape approach)

Mathematical Model in Depth Calibration (the measuring tape approach)

$$N = \mathrm{Re} - M_t \qquad \text{---------- Equation (1)}$$

where

N is the error between the readings from depth indicator and the measuring tape;

Re is the readings shown on the depth indicator of the logging unit;

M_t is the readings from the measuring tape at maximum temperature difference from 20°C.

$$\text{And } M_t = M_{20}(1 + \alpha_M t) \qquad \text{---------- Equation (2)}$$

where

M_{20} is the reading of the measuring tape at 20°C;

α_M is thermal expansion coefficient of measuring tape, 1.5×10^{-4};

t is the temperature difference.

Substituting equations (2) into (1),

$$N = \mathrm{Re} - M_{20}(1 + \alpha_M t) \qquad \text{---------- Equation (3)}$$

Uncertainty components in Depth Calibration (the measuring tape approach)

(i) Standard uncertainty of the resolution of the depth indicator of the control logging unit, μ_{SVa}

[Type B]

$$\mu_{SVa} = \frac{a_{SVa}}{\sqrt{3}} \qquad \text{---------- Equation (4)}$$

where a_{SVa} is the semi-range of the resolution of the depth indicator of the logging unit.

(ii) Calibration uncertainty of the measuring tape, μ_{ta} [Type B]

$$\mu_{ta} = \frac{a_{ta}}{k_{ta}} \qquad \text{---------- Equation (5)}$$

where

a_{ta} is the uncertainty from the calibration certificate;

k_{ta} is the coverage factor applied in the calibration certificate.

(iii) Standard uncertainty of the measuring tape error, μ_{te} [Type B]

$$\mu_{te} = \frac{a_{te}}{\sqrt{3}} \qquad \text{---------- Equation (6)}$$

where a_{te} is the error of the measuring tape.

(iv) Standard uncertainty of the measuring tape in resolution, μ_{tr} [Type B]

$$\mu_{tr} = \frac{a_{tr}}{\sqrt{3}} \qquad \text{---------- Equation (7)}$$

where a_{tr} is the semi-range of the measuring tape in resolution.

(v) Experimental uncertainty in randomness of measurements M_{20}, μ_{MR} [Type A]

$$\mu_{MR} = \frac{M_{SD}}{\sqrt{n}} \qquad \text{---------- Equation (8)}$$

where

M_{SD} is the standard deviation of measurements M_{20};

n is the number of measurements for M_{20} in calibration.

(vi) Standard uncertainty in thermal expansion of measuring tape, $\mu_{\alpha M}$ [Type B]

$$\mu_{\alpha M} = \frac{0.5x10^{-4}}{\sqrt{3}}$$ ---------- Equation (9)

Note: the interval for thermal expansion coefficient of measuring tape, $\pm 0.5x10^{-4}/^{\circ}C$.

The uncertainties of thermal expansion coefficients and temperature difference can be negligible compared with other uncertainties, thus :

Combined standard uncertainty of readings shown on the depth indicator of the logging unit, μ_{Re}

$$\mu_{\mathrm{Re}}{}^2 = \mu_{SVa}{}^2 + \mu_{RR}{}^2$$ ---------- Equation (10)

Combined standard uncertainty of readings from the measuring tape, μ_{M20}

$$\mu_{M_{20}}{}^2 = \mu_{ta}{}^2 + \mu_{te}{}^2 + \mu_{tr}{}^2 + \mu_{MR}{}^2$$ ---------- Equation (11)

Sensitivity coefficients

$$\frac{\partial N}{\partial \mathrm{Re}} = 1$$ ---------- Equation (12)

$$\frac{\partial N}{\partial M_{20}} = -1 - \alpha_M t = -1$$ ---------- Equation (13)

Combined Uncertainty, U_c, in Depth Calibration (the measuring tape approach)

$$U_c = \sqrt{(\frac{\partial N}{\partial \mathrm{Re}}\mu_{\mathrm{Re}})^2 + (\frac{\partial N}{\partial M_{20}}\mu_{M_{20}})^2}$$ ---------- Equation (14)

Degree of freedom, V_{eff}, in Depth Calibration (the measuring tape approach)

$$V_{eff} = \frac{U_c{}^4}{\frac{(\frac{\partial N}{\partial \mathrm{Re}}\mu_{\mathrm{Re}})^4}{V_{\mathrm{Re}}} + \frac{(\frac{\partial N}{\partial M_{20}}\mu_{M_{20}})^4}{V_{M_{20}}}}$$ ---------- Equation (15)

*Expanded Uncertainty, U_e, **in Depth Calibration (the measuring tape approach)***

From V_{eff} and students' t distribution in statistics for 95% confidence, determine the coverage factor k.

$$U_e = kU_c \qquad \text{---------- Equation (16)}$$

where

U_e is the expanded uncertainty,

U_c is the combined uncertainty.

Appendix F

Mathematical Model in the *Depth* Calibration (By the theodolite approach)

Calibration Analysis in Depth Calibration (the theodolites approach)

Mathematical Model in Depth Calibration (the theodolites Approach)

$$H = \left(\frac{x\tan\alpha_1 - \frac{h\tan\alpha_1}{\tan\beta_1}}{1-\frac{\tan\alpha_1}{\tan\beta_1}}\right) - \left(\frac{x\tan\alpha_2 - \frac{h\tan\alpha_2}{\tan\beta_2}}{1-\frac{\tan\alpha_2}{\tan\beta_2}}\right) \quad \text{---------- Equation (1)}$$

where

H is the length of cable of UES equipment,

$\alpha_1, \alpha_2, \beta_1, \beta_2$ are theodolites readings;

X is the distance difference between two theodolites;

h is the height difference between two theodolites.

Uncertainty components in Depth Calibration (the theodolites Approach)

(i) Calibration uncertainty of the measuring tape, μ_{ta} [Type B]

$$\mu_{ta} = \frac{a_{ta}}{k_{ta}} \quad \text{---------- Equation (2)}$$

where

a_t is the uncertainty from the calibration certificate;

k_{ta} is the coverage factor applied in the calibration certificate.

(ii) Standard uncertainty of the measuring tape in error, μ_{te} [Type B]

$$\mu_{te} = \frac{a_{te}}{\sqrt{3}} \quad \text{---------- Equation (3)}$$

where a_{te} is the error of the measuring tape.

(iii) Standard uncertainty of the measuring tape in resolution, μ_{tr} [Type B]

$$\mu_{tr} = \frac{a_{tr}}{\sqrt{3}} \quad \text{---------- Equation (4)}$$

where a_{tr} is the semi-range of the measuring tape in resolution.

(iv) Experimental uncertainty in randomness of measurements X, μ_{XR} [Type A]

$$\mu_{XR} = \frac{X_D}{\sqrt{n}} \qquad \text{---------- Equation (5)}$$

where

X_D is the standard deviations of measurements X;

n is the number of measurements for X in calibration.

(v) Experimental uncertainty in randomness of measurements h, μ_{hR} [Type A]

$$\mu_{hR} = \frac{h_D}{\sqrt{n}} \qquad \text{---------- Equation (6)}$$

where

h_D is the standard deviations of measurements S;

n is the number of measurements for S in calibration.

(vi) Calibration uncertainty of the theodolites, $\mu_{\theta C}$ [Type B]

$$\mu_{\theta C} = \frac{a_{\theta C}}{k_\theta} \qquad \text{---------- Equation (7)}$$

where

θ is either tan α_1, tan α_2, tan β_1 & tan β_2;

$a_{\theta C}$ is the calibration uncertainty of the theodolites in term of tangent;

k_θ is the coverage factor applied in the calibration certificate.

(vii) Standard uncertainty of the theodolites error, $\mu_{\theta E}$ [Type B]

$$\mu_{\theta E} = \frac{a_{\theta E}}{\sqrt{3}} \qquad \text{---------- Equation (8)}$$

where

θ is either tan α_1, tan α_2, tan β_1 & tan β_2;

$a_{\theta E}$ is the error of the theodolites in term of tangent.

(viii) Standard uncertainty of the theodolites resolution, $\mu_{\theta R}$ [Type B]

$$\mu_{\theta R} = \frac{a_{\theta R}}{\sqrt{3}} \qquad \text{---------- Equation (9)}$$

where

θ is either tan α_1, tan α_2, tan β_1 & tan β_2;

$a_{\theta R}$ is the error of the theodolites in term of tangent.

(ix) Experimental uncertainty in randomness of measurements θ, $\mu_{\theta M}$ [Type A]

$$\mu_{\theta M} = \frac{\theta_M}{\sqrt{n}} \qquad \text{---------- Equation (10)}$$

where

θ is either tan α_1, tan α_2, tan β_1 & tan β_2;

θ_M is the standard deviations of measurements θ;

n is the number of measurements for θ in calibration.

Combined standard uncertainty of the distance difference between two theodolites X, μ_X,

$$\mu_X^2 = \mu_{ta}^2 + \mu_{te}^2 + \mu_{tr}^2 + \mu_{XR}^2 \qquad \text{---------- Equation (11)}$$

Combined standard uncertainty of the height difference between two theodolites h, μ_h,

$$\mu_h^2 = \mu_{ta}^2 + \mu_{te}^2 + \mu_{tr}^2 + \mu_{hR}^2 \qquad \text{---------- Equation (12)}$$

Combined standard uncertainty of θ

(i.e. tan α_1, tan α_2, tan β_1 & tan β_2)

$$\mu_\theta^2 = \mu_{\theta C}^2 + \mu_{\theta E}^2 + \mu_{\theta R}^2 + \mu_{\theta M}^2 \qquad \text{---------- Equation (13)}$$

Sensitivity coefficients in Depth Calibration (the theodolites Approach)

$$\frac{\partial H}{\partial x} = \frac{(1-\frac{\tan\alpha_1}{\tan\beta_1})(\tan\alpha_1)}{(1-\frac{\tan\alpha_1}{\tan\beta_1})^2} - \frac{(1-\frac{\tan\alpha_2}{\tan\beta_2})(\tan\alpha_2)}{(1-\frac{\tan\alpha_2}{\tan\beta_2})^2}$$

$$\frac{\partial H}{\partial h} = \frac{(1-\frac{\tan\alpha_1}{\tan\beta_1})(\frac{\tan\alpha_1}{\tan^2\beta_1})}{(1-\frac{\tan\alpha_1}{\tan\beta_1})^2} - \frac{(1-\frac{\tan\alpha_2}{\tan\beta_2})(\frac{\tan\alpha_2}{\tan^2\beta_2})}{(1-\frac{\tan\alpha_2}{\tan\beta_2})^2}$$

$$\frac{\partial H}{\partial(\tan\alpha_1)} = \frac{(1-\frac{\tan\alpha_1}{\tan\beta_1})(x\sec^2\alpha_1 - \frac{h\tan\beta_1\sec^2\alpha_1}{\tan^2\beta_1})}{(1-\frac{\tan\alpha_1}{\tan\beta_1})^2} - \frac{(x\tan\alpha_1 - \frac{h\tan\alpha_1}{\tan\beta_1})(\frac{-\tan\beta_1\sec^2\alpha_1}{\tan^2\beta_1})}{(1-\frac{\tan\alpha_1}{\tan\beta_1})^2}$$

$$\frac{\partial H}{\partial(\tan\beta_1)} = \frac{(1-\frac{\tan\alpha_1}{\tan\beta_1})(\frac{h\tan\alpha_1\sec^2\beta_1}{\tan^2\beta_1})}{(1-\frac{\tan\alpha_1}{\tan\beta_1})^2} - \frac{(x\tan\alpha_1 - \frac{h\tan\alpha_1}{\tan\beta_1})(\frac{-\tan\alpha_1\sec^2\beta_1}{\tan^2\beta_1})}{(1-\frac{\tan\alpha_1}{\tan\beta_1})^2}$$

$$\frac{\partial H}{\partial(\tan\alpha_2)} = \frac{(x\tan\alpha_2 - \frac{h\tan\alpha_2}{\tan\beta_2})(\frac{-\tan\beta_2\sec^2\alpha_2}{\tan^2\beta_2})}{(1-\frac{\tan\alpha_2}{\tan\beta_2})^2} - \frac{(1-\frac{\tan\alpha_2}{\tan\beta_2})(x\sec^2\alpha_2 - \frac{h\tan\beta_2\sec^2\alpha_2}{\tan^2\beta_2})}{(1-\frac{\tan\alpha_2}{\tan\beta_2})^2}$$

$$\frac{\partial H}{\partial(\tan\beta_2)} = \frac{(x\tan\alpha_2 - \frac{h\tan\alpha_2}{\tan\beta_2})(\frac{-\tan\alpha_1\sec^2\beta_2}{\tan^2\beta_2})}{(1-\frac{\tan\alpha_2}{\tan\beta_2})^2} - \frac{(1-\frac{\tan\alpha_2}{\tan\beta_2})(\frac{h\tan\alpha_2\sec^2\beta_2}{\tan^2\beta_2})}{(1-\frac{\tan\alpha_2}{\tan\beta_2})^2}$$

Combined Uncertainty, U_c, in Depth Calibration (the theodolites Approach)

$$U_C = \sqrt{(\frac{\partial H}{\partial X}\mu_x)^2 + (\frac{\partial H}{\partial h}\mu_h)^2 + [\frac{\partial H}{\partial(\tan\alpha_1)}\mu_\theta]^2 + [\frac{\partial H}{\partial(\tan\beta_1)}\mu_\theta]^2 + [\frac{\partial H}{\partial(\tan\alpha_2)}\mu_\theta]^2 + [\frac{\partial H}{\partial(\tan\beta_2)}\mu_\theta]^2}$$

Degree of freedom, V_{eff}, in Depth Calibration (the theodolites Approach)

$$V_{eff} = \frac{U_C^4}{\left(\begin{array}{l} \frac{(\frac{\partial H}{\partial X}\mu_X)^4}{V_X} + \frac{(\frac{\partial H}{\partial h}\mu_h)^4}{V_h} + \frac{(\frac{\partial H}{\partial(\tan\alpha_1)}\mu_{\tan\alpha_1})^4}{V_{\tan\alpha_1}} \\ \qquad \frac{(\frac{\partial H}{\partial(\tan\beta_1)}\mu_{\tan\beta_1})^4}{V_{\tan\beta_1}} + \frac{(\frac{\partial H}{\partial(\tan\alpha_1)}\mu_{\tan\alpha_2})^4}{V_{\tan\alpha_2}} \\ \qquad\qquad + \frac{(\frac{\partial H}{\partial(\tan\beta_2)}\mu_{\tan\beta_2})^4}{V_{\tan\beta_2}} \end{array}\right)}$$

Expanded Uncertainty, U_e, in Depth Calibration (the theodolites Approach)

From V_{eff} and students' t distribution in statistics for 95% confidence, determine the coverage factor k.

$$U_e = kU_c \qquad \text{---- Equation (14)}$$

where

U_e is the expanded uncertainty,

U_c is the combined uncertainty.

Appendix H

Verification results in different rough reflecting surfaces

Roughness surface verification in Channel 1

Verification distance = 200mm
Sensitivity setting: *0.5*

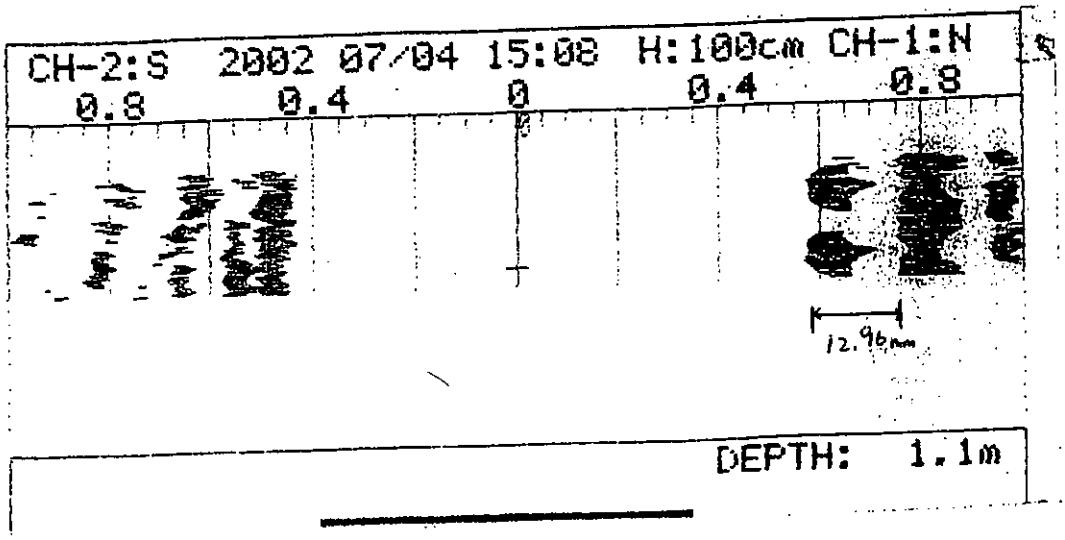

Verification distance = 150mm
Sensitivity setting: *0.5*

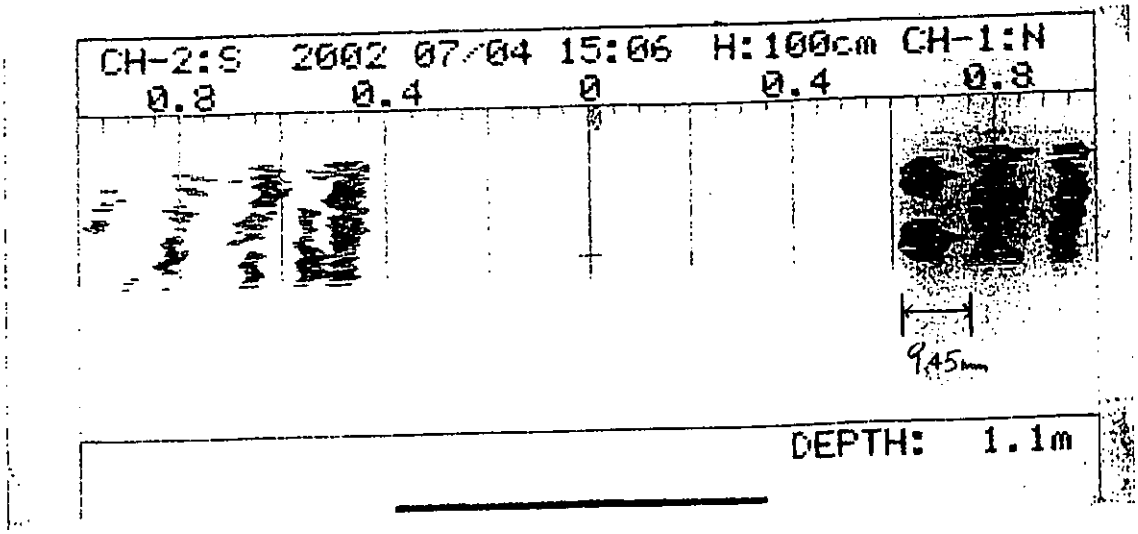

Roughness surface verification in Channel 1

Verification distance = 100mm
Sensitivity setting: a5

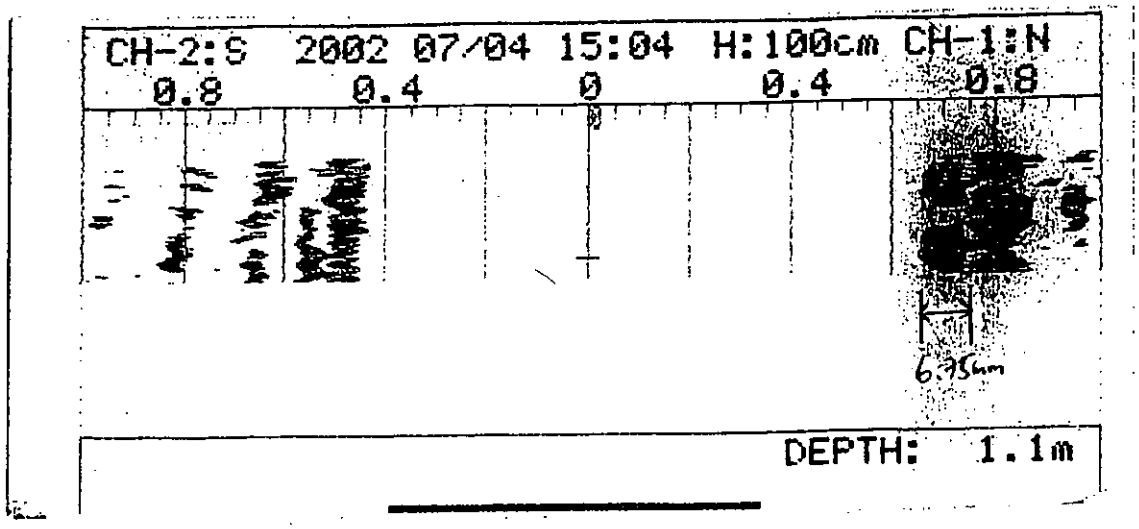

Verification distance = 50mm
Sensitivity setting: a5

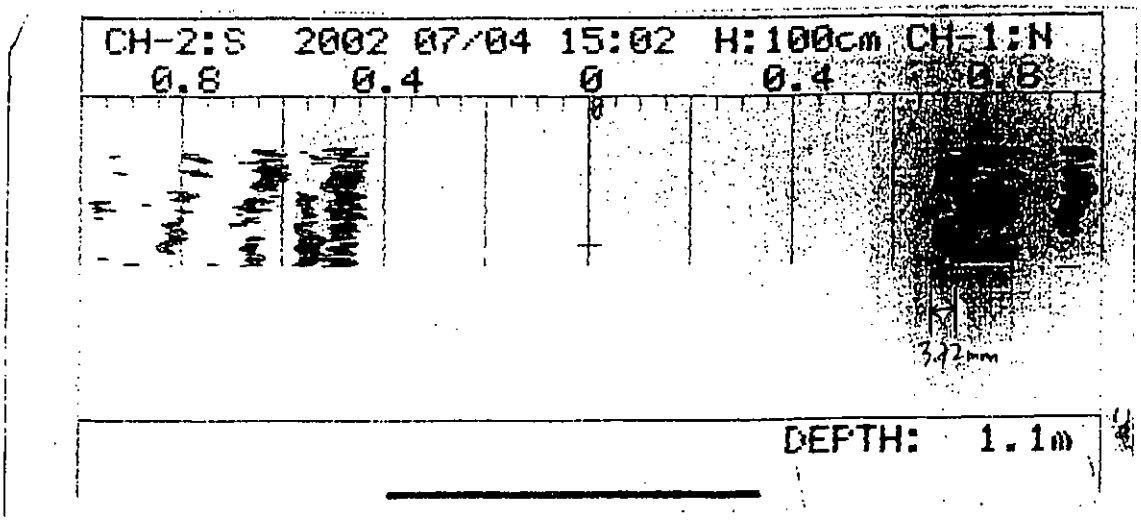

Roughness surface verification in Channel 1

Verification distance = 25mm
Sensitivity setting: 0.5

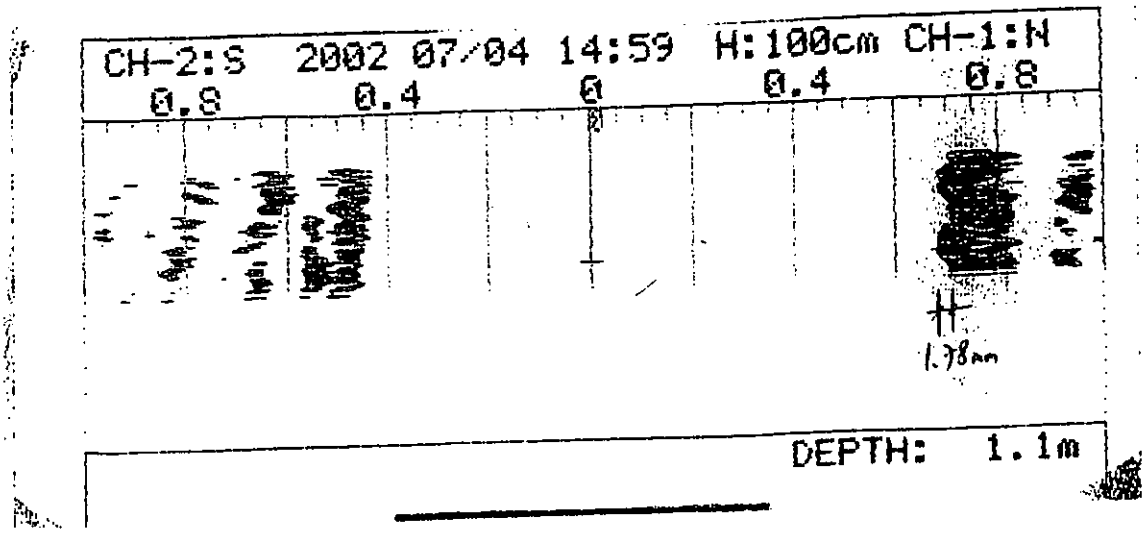

Roughness surface verification in Channel 2

Verification distance = 200mm
Sensitivity setting: 1.0

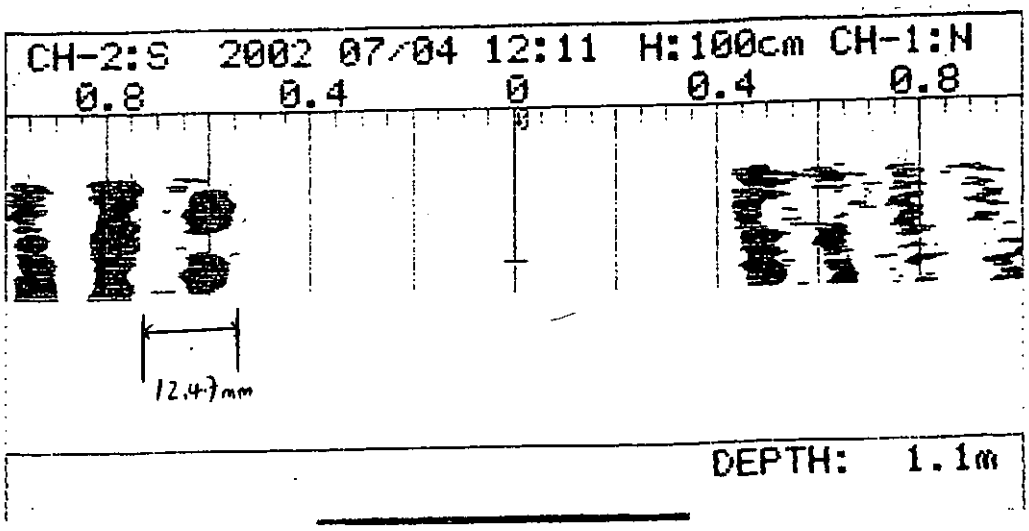

Verification distance = 150mm
Sensitivity setting: 0.5

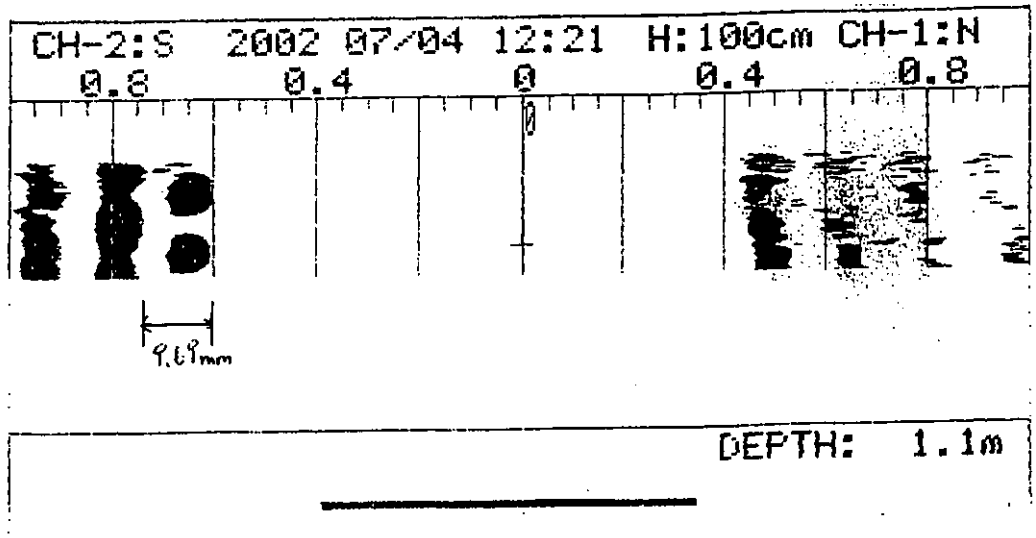

Roughness surface verification in Channel 2

Verification distance = 100mm
Sensitivity setting: 0.5

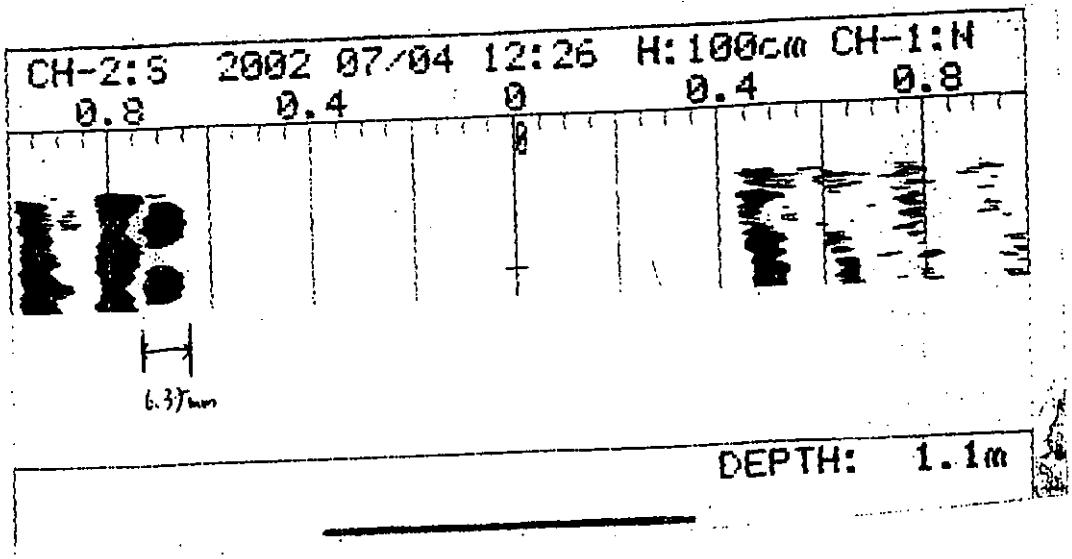

Verification distance = 50mm
Sensitivity setting: 0.3

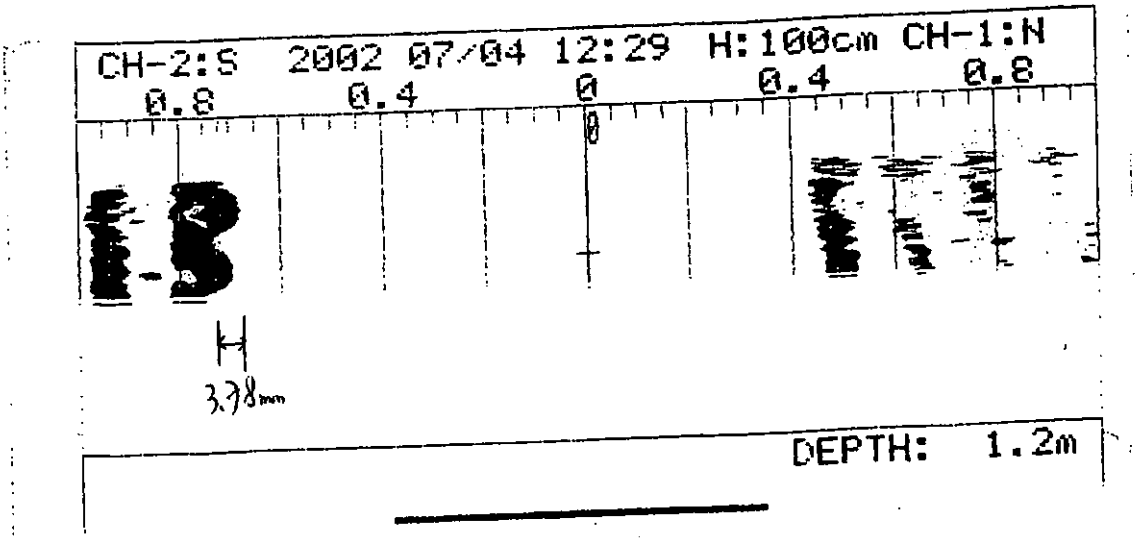

Roughness surface verification in Channel 2

Verification distance = 25mm
Sensitivity setting: 0.3

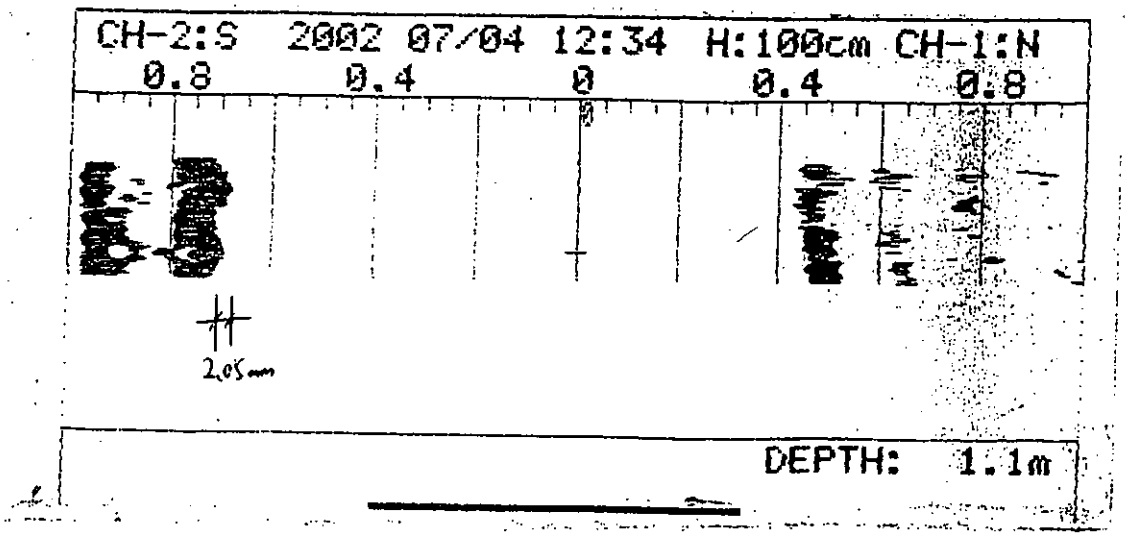

Roughness surface verification in Channel 3

Verification distance = 200mm
Sensitivity setting: 0.5

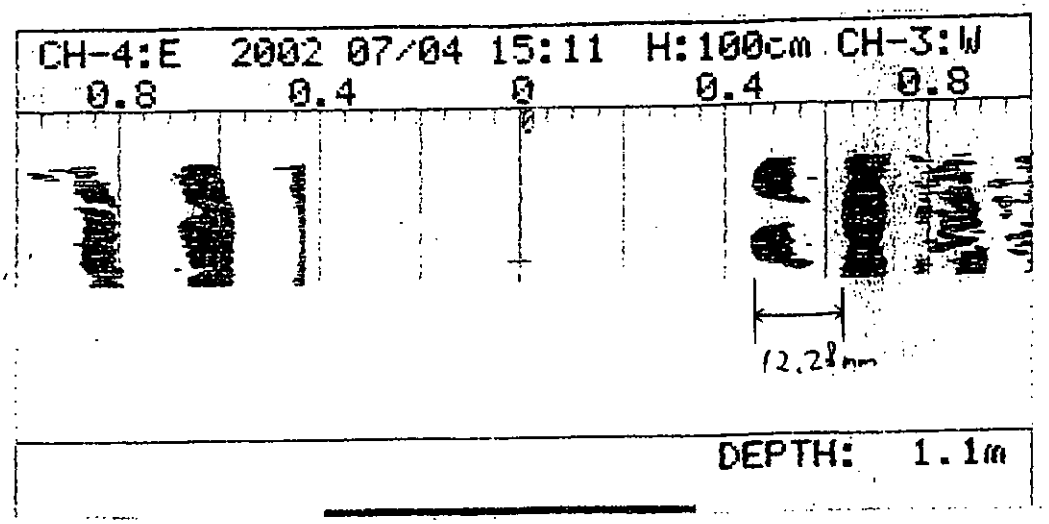

Verification distance = 150mm
Sensitivity setting: 0.5

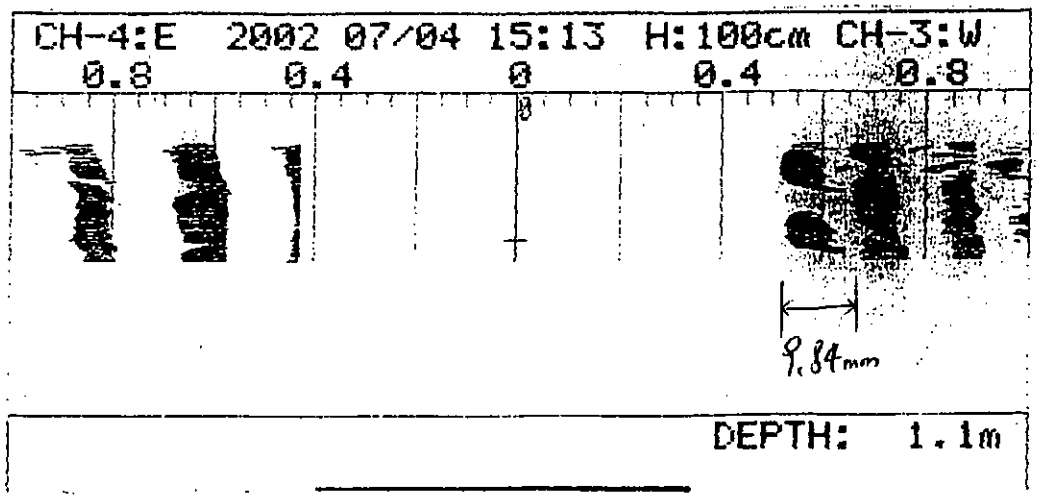

Roughness surface verification in Channel 3

Verification distance = 100mm
Sensitivity setting: 0.5

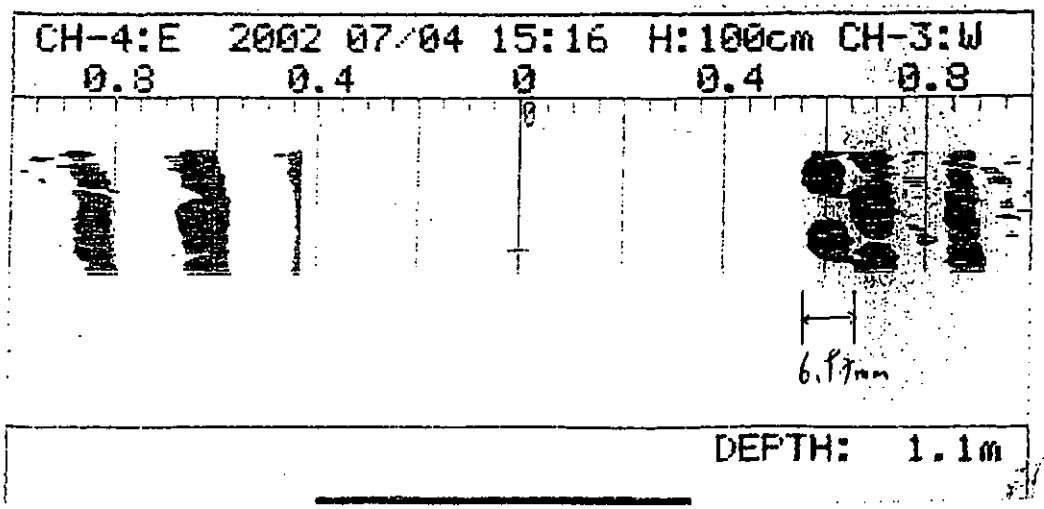

Verification distance = 50mm
Sensitivity setting: 0.5

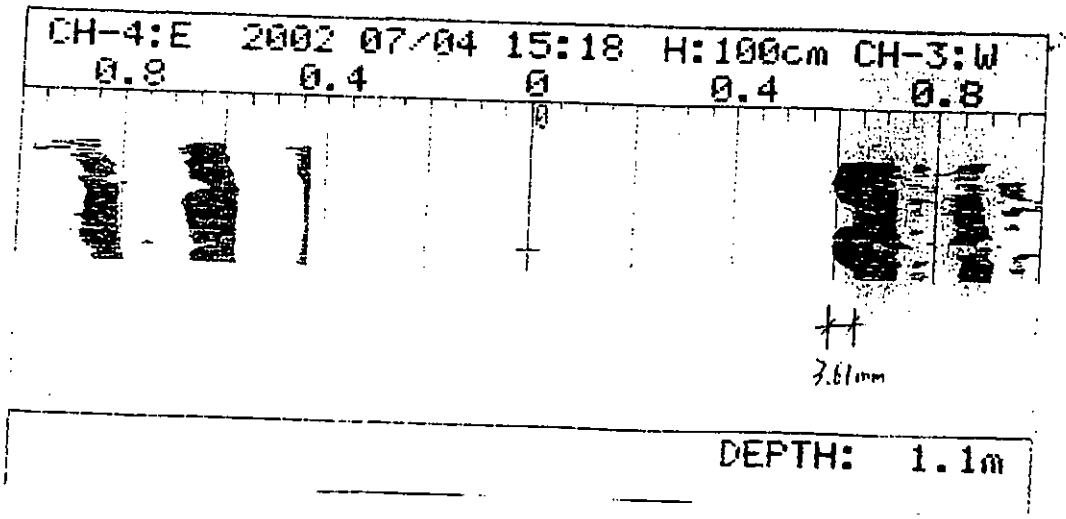

Roughness surface verification in Channel 3

Verification distance = 25mm
Sensitivity setting: 0.5

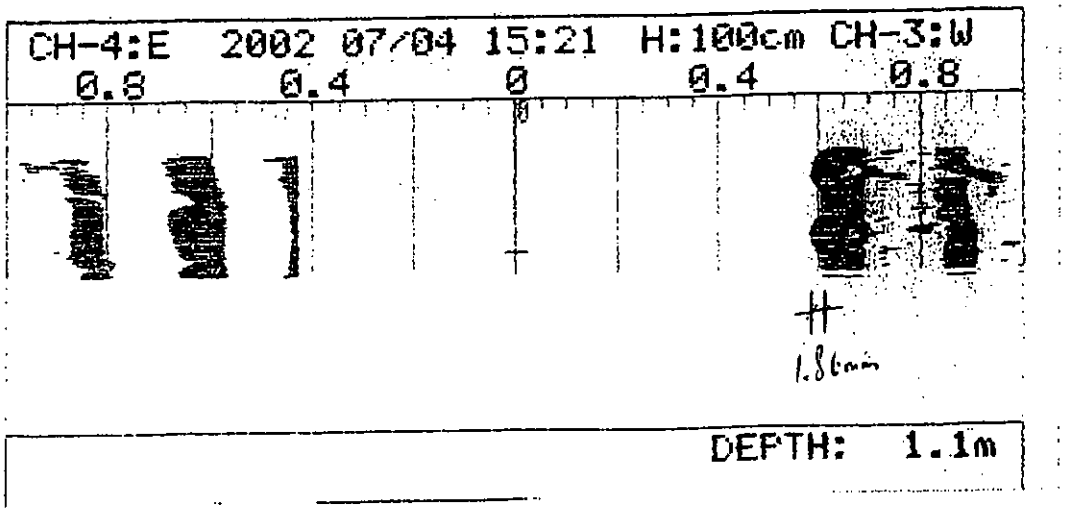

Roughness surface verification in Channel 4

Verification distance = 200mm
Sensitivity setting: 0.5

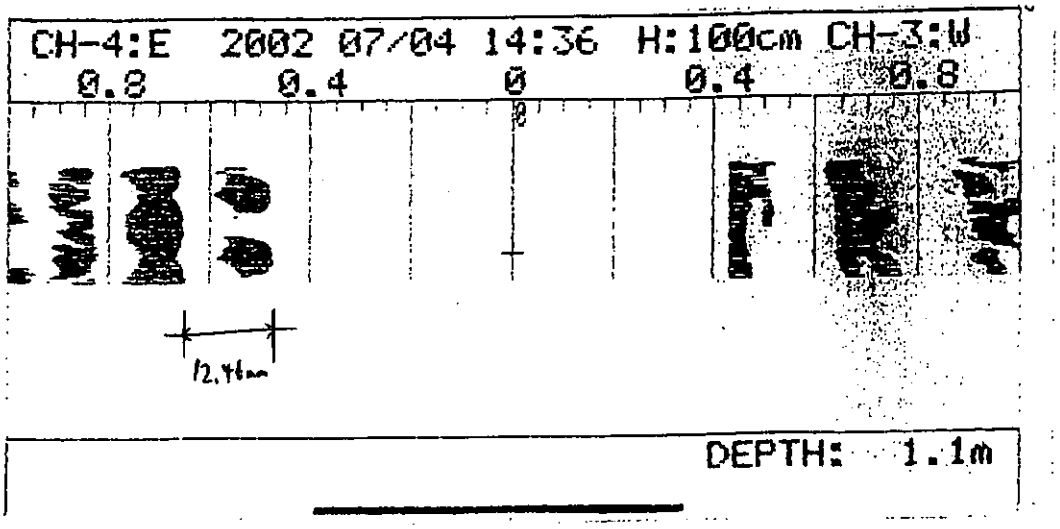

Verification distance = 150mm
Sensitivity setting: 0.5

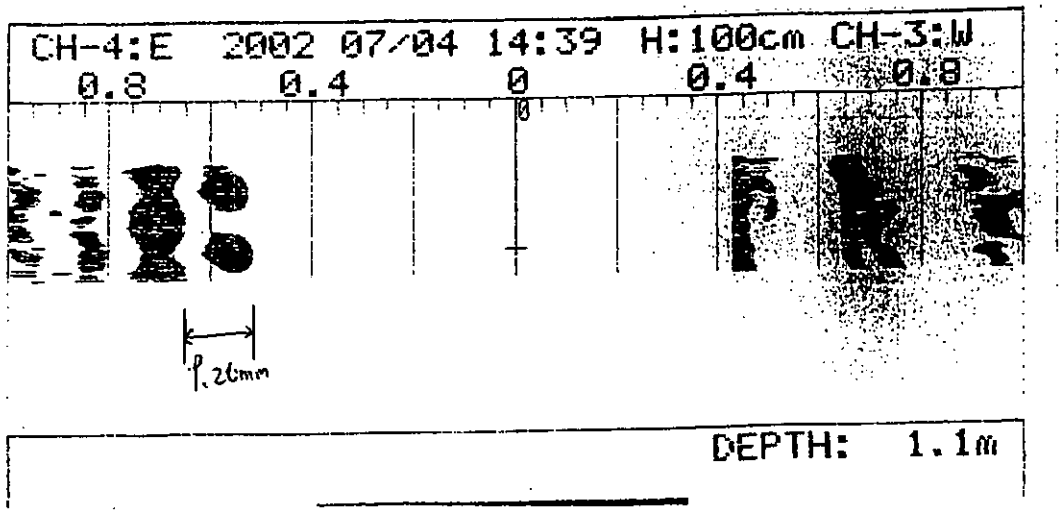

Roughness surface verification in Channel 4

Verification distance = 100mm
Sensitivity setting: 0.5

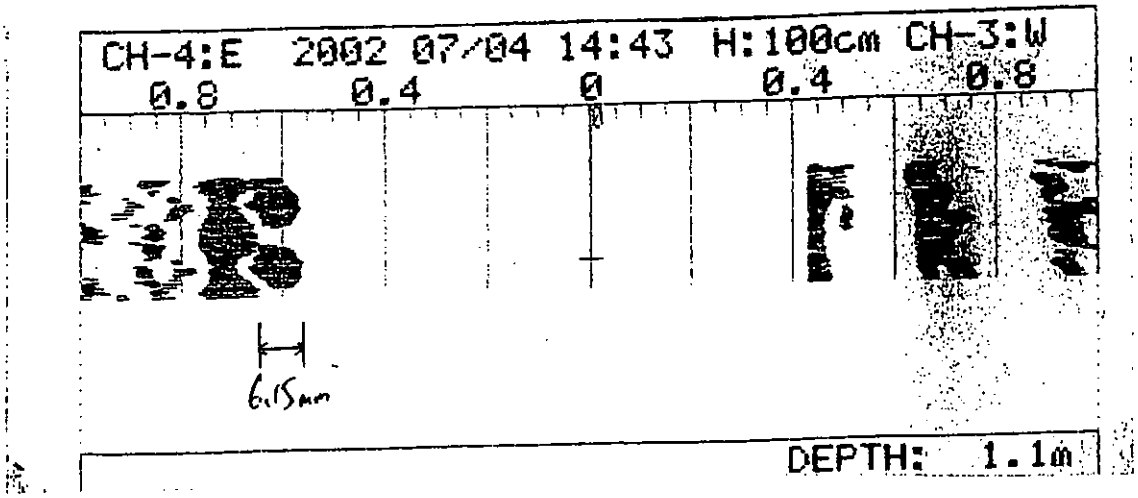

Verification distance = 50mm
Sensitivity setting: 0.5

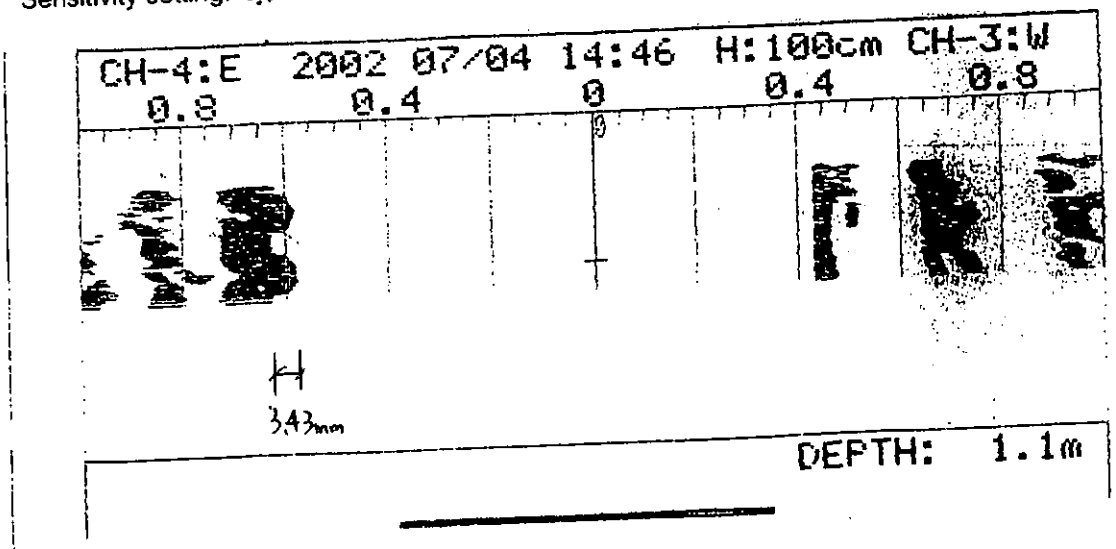

Roughness surface verification in Channel 4

Verification distance = 25mm
Sensitivity setting: 0.5

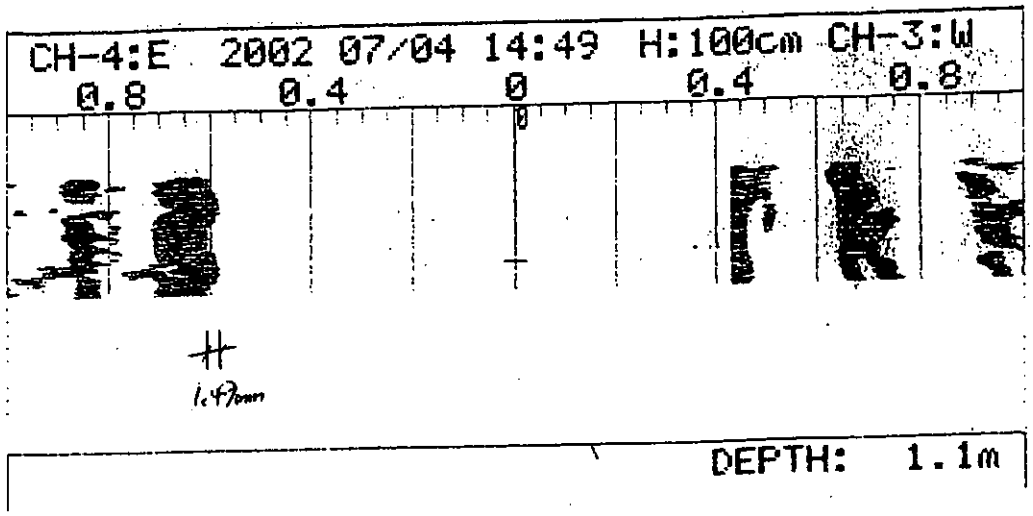

Appendix G

Verification results in different angles of reflections

Reflection from different angles verification in Channel 1

Reflection angle = 75°
Sensitivity setting: 1.0

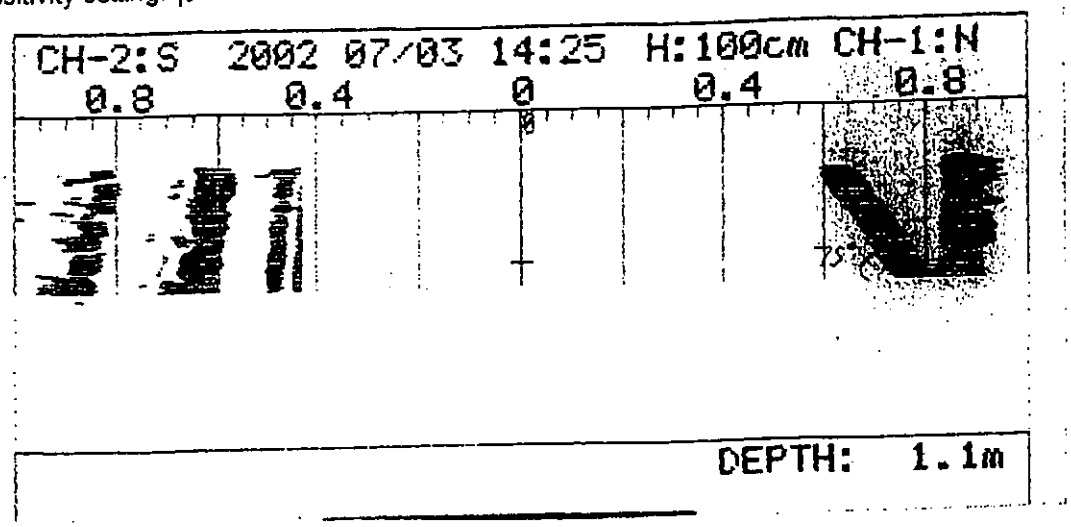

Reflection angle = 60°
Sensitivity setting: 3.0

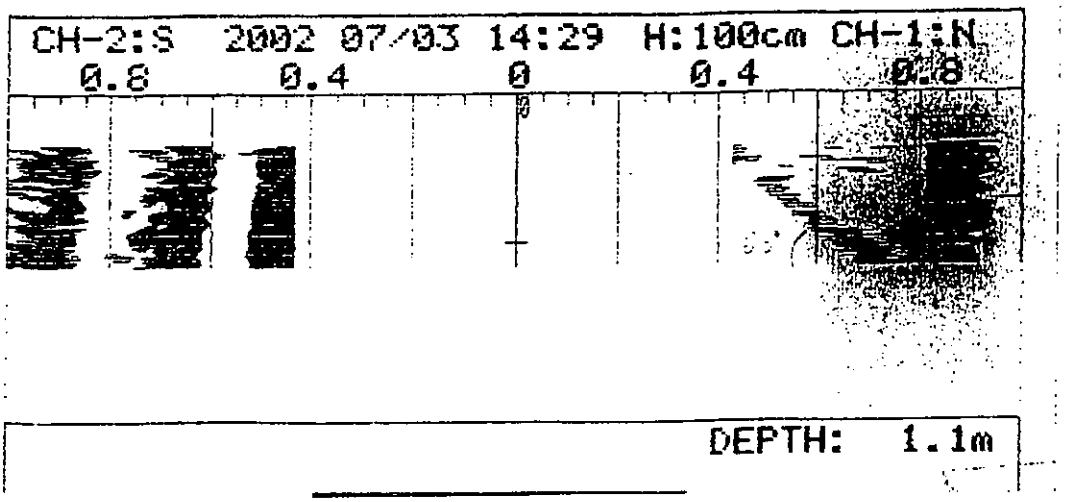

Reflection from different angles verification in Channel 1

Reflection angle = 45°
Sensitivity setting: 6.5

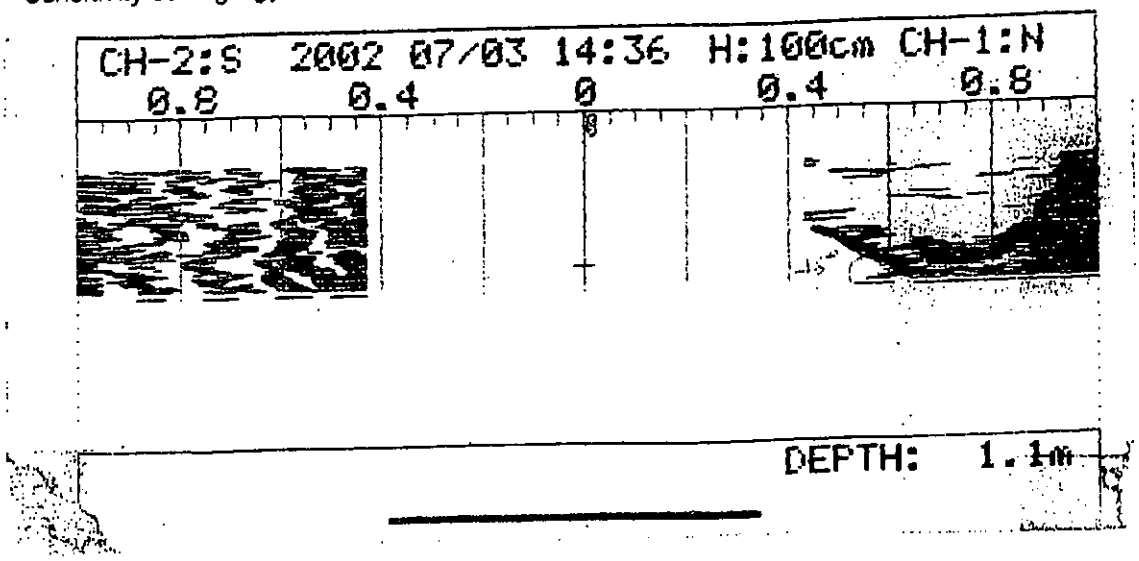

Reflection angle = 30°
Sensitivity setting: 7.0

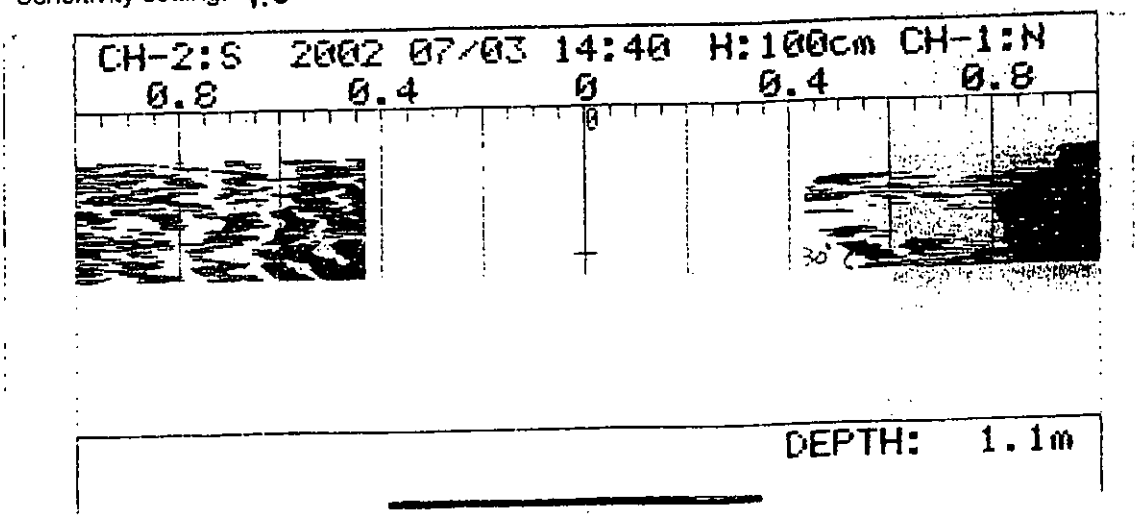

Reflection from different angles verification in Channel 2

Reflection angle = 75°
Sensitivity setting: 1.0

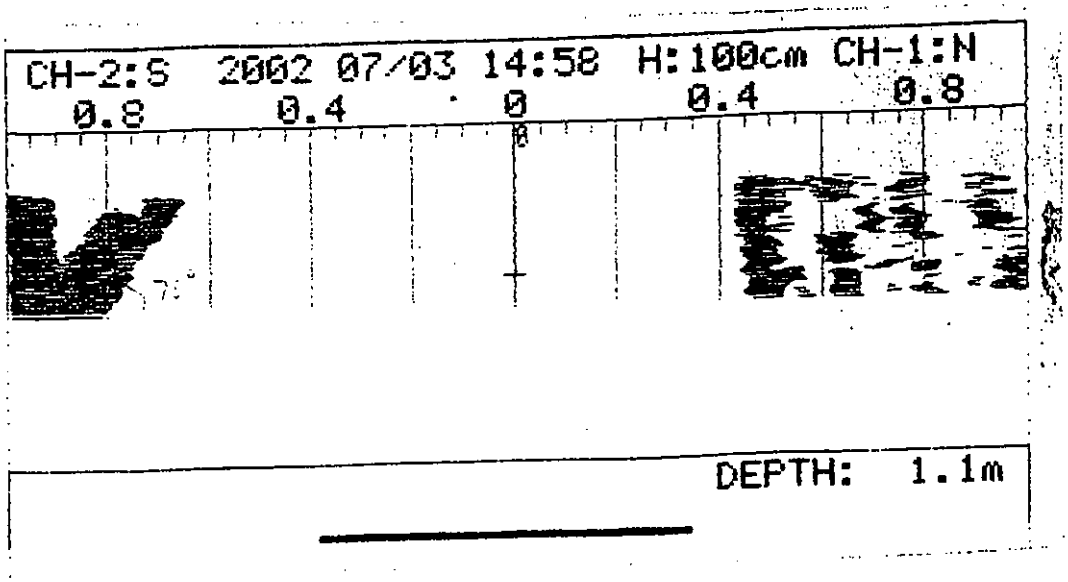

Reflection angle = 60°
Sensitivity setting: 3.0

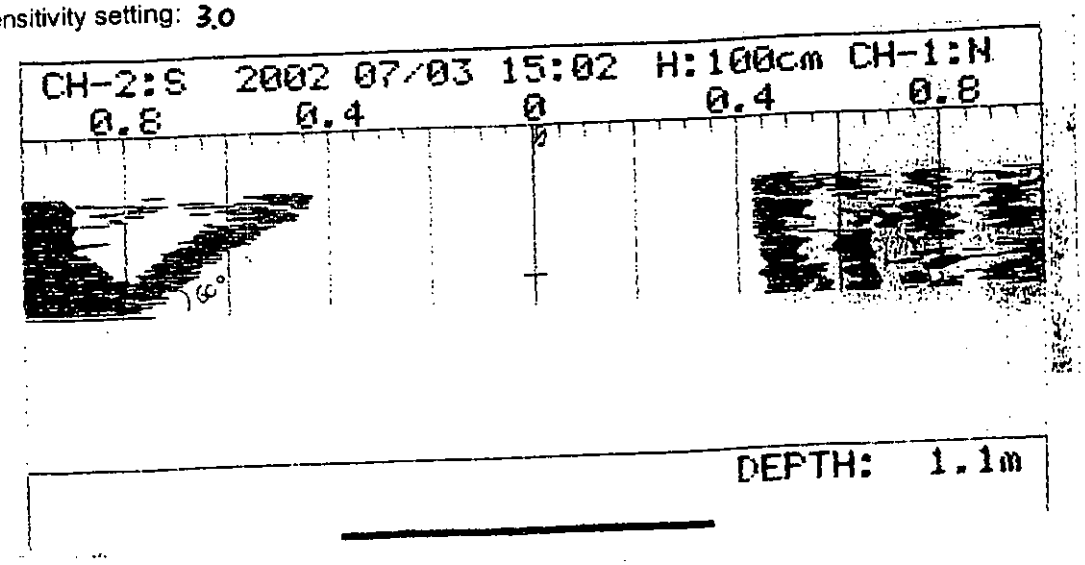

Reflection from different angles verification in Channel 2

Reflection angle = 45°
Sensitivity setting: 6.5

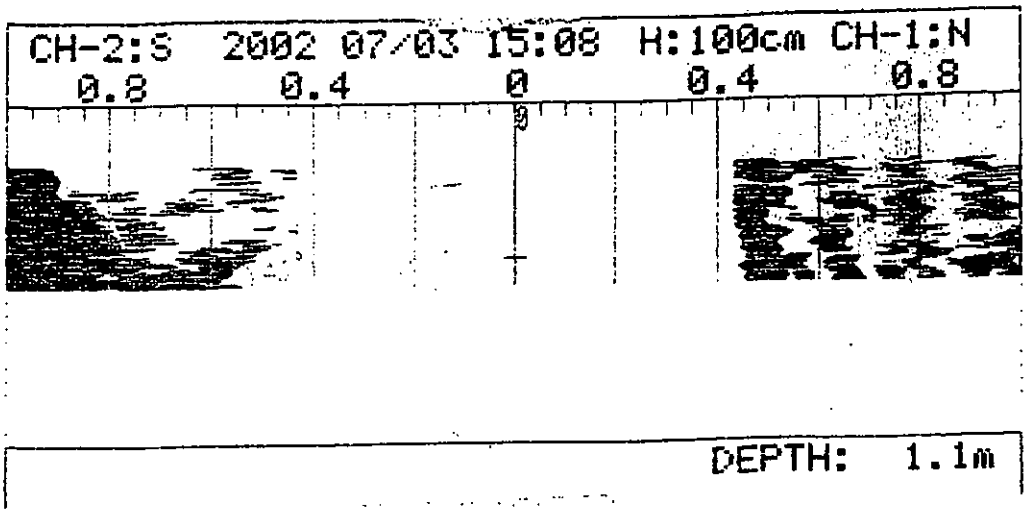

Reflection angle = 30°
Sensitivity setting: 7.0

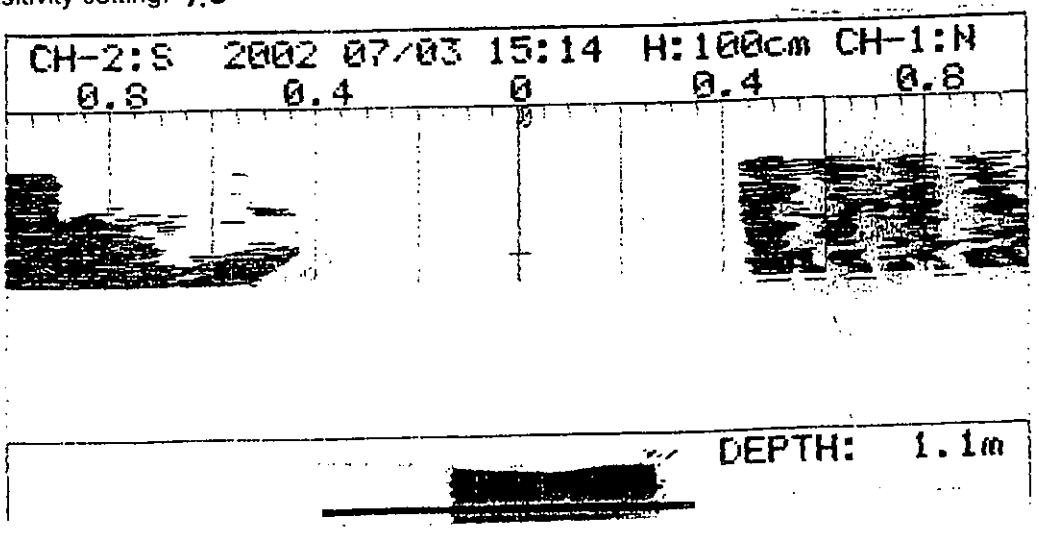

Reflection from different angles verification in Channel 3

Reflection angle = 75°
Sensitivity setting: 1.0

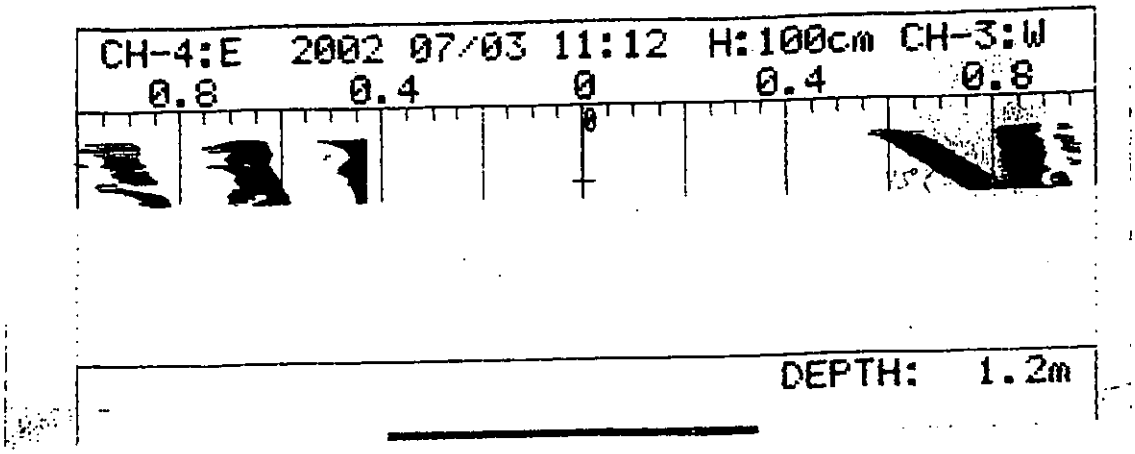

Reflection angle = 60°
Sensitivity setting: 4.0

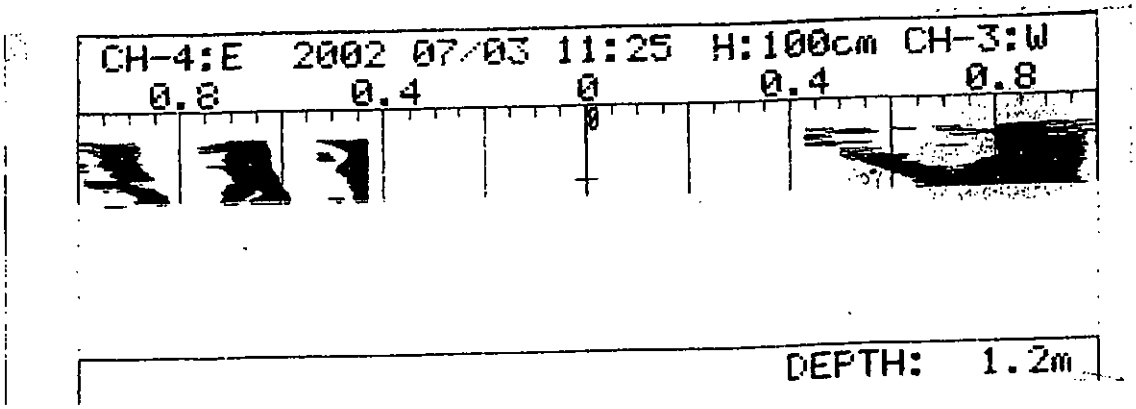

Reflection from different angles verification in Channel 3

Reflection angle = 45°
Sensitivity setting: 6.5

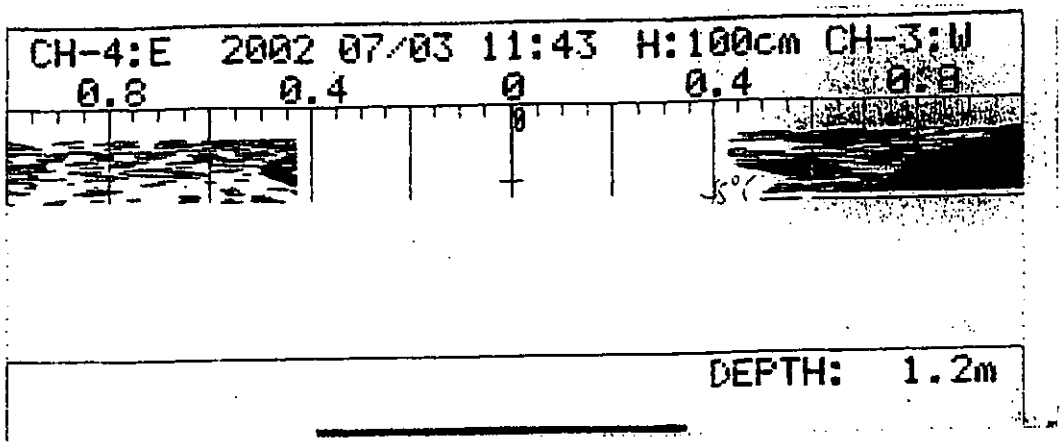

Reflection angle = 30°
Sensitivity setting: 7.0

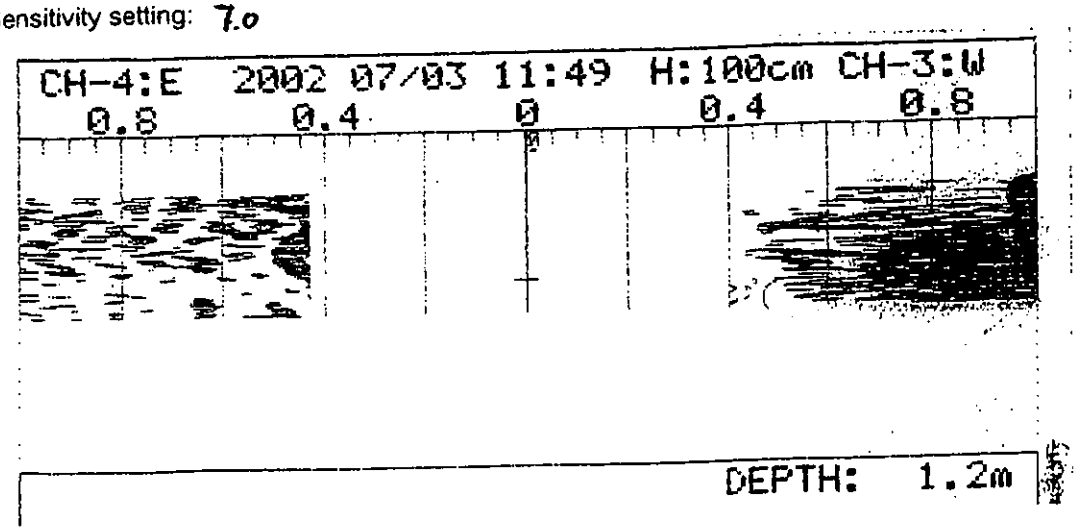

Reflection from different angles verification in Channel 4

Reflection angle = 75°
Sensitivity setting: 1.0

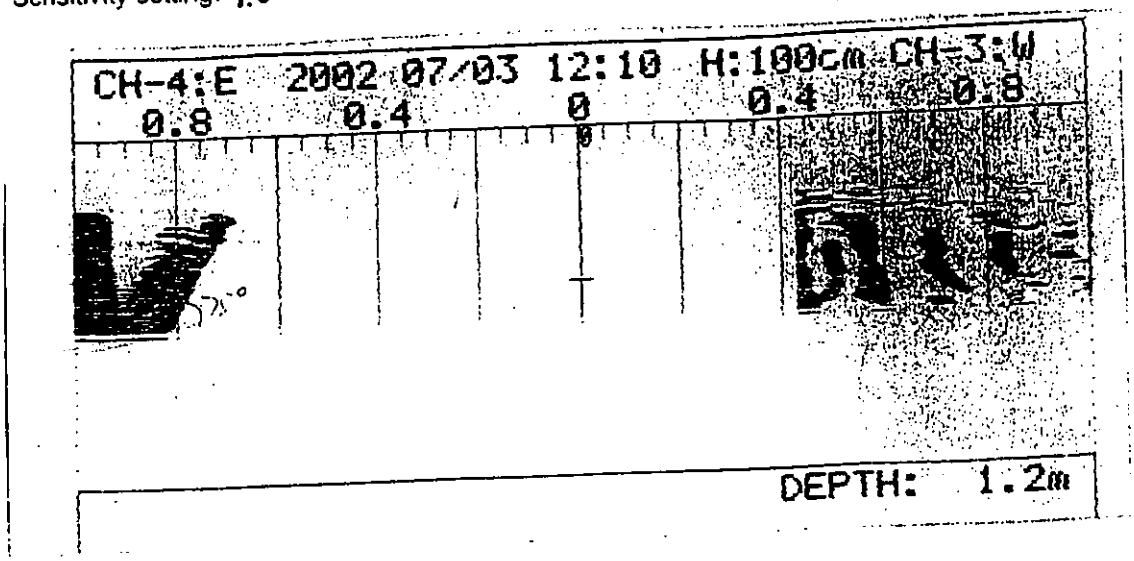

Reflection angle = 60°
Sensitivity setting: 3.0

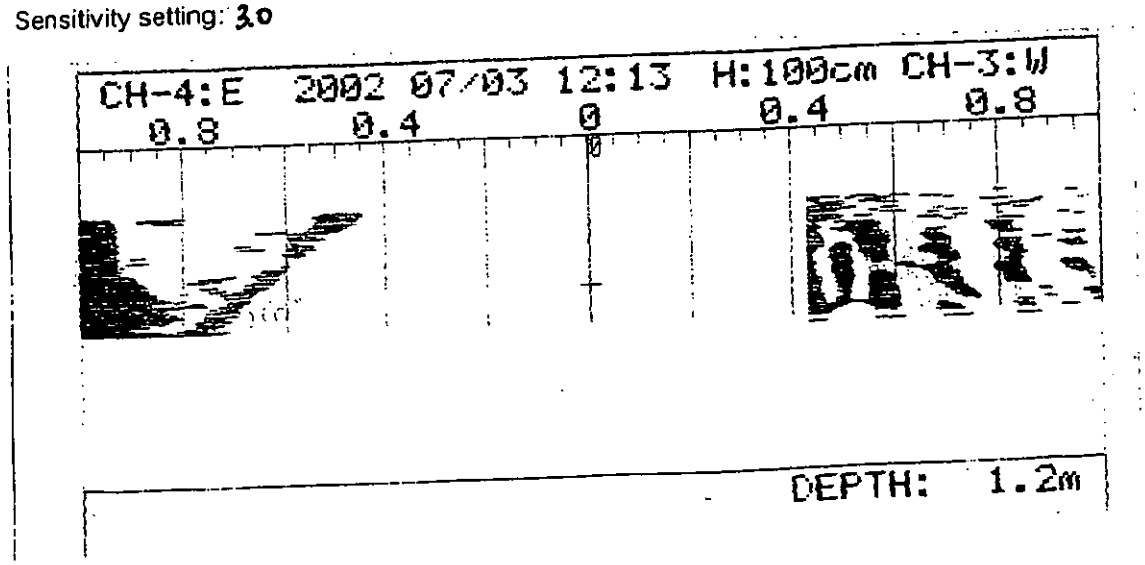

Reflection from different angles verification in Channel 4

Reflection angle = 45°
Sensitivity setting: 6.5

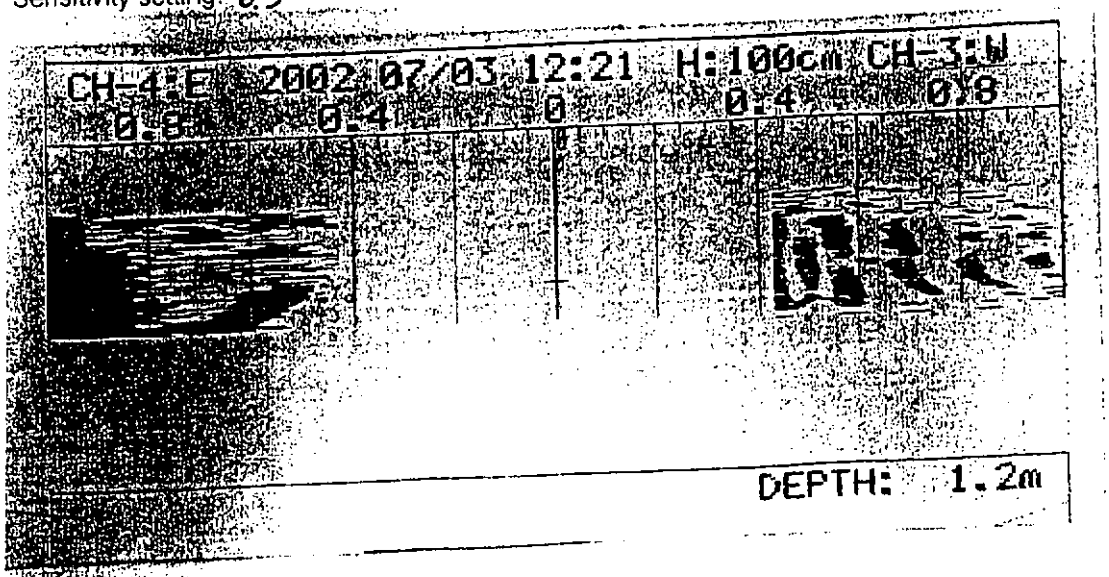

Reflection angle = 30°
Sensitivity setting: 7.0